

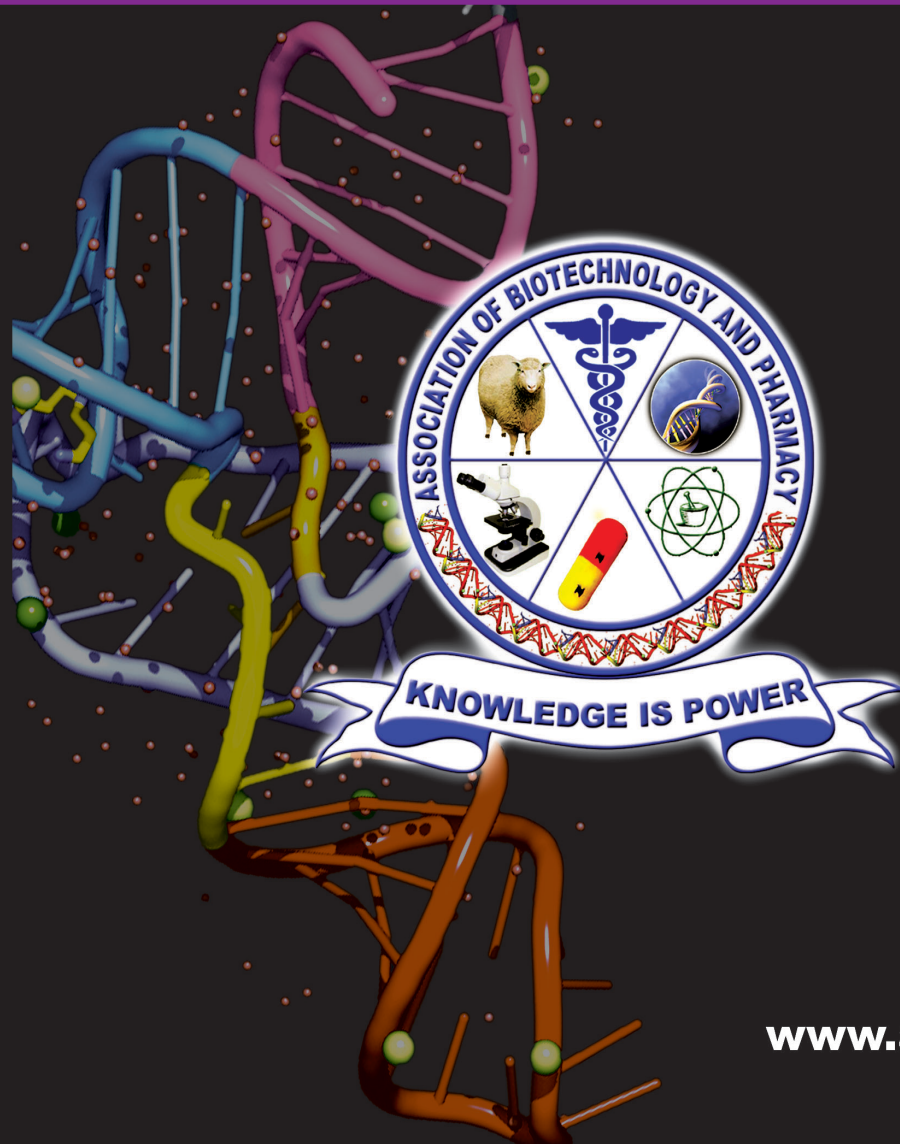
ISSN 0973-8916

Current Trends in Biotechnology and Pharmacy

Volume 5

Issue 2

April 2011



www.abap.co.in

Current Trends in Biotechnology and Pharmacy
ISSN 0973-8916 (Print), 2230-7303 (Online)

Editors

Prof. K.R.S. Sambasiva Rao, India
krssrao@abap.co.in

Prof. Karnam S. Murthy, USA
skarnam@vcu.edu

Editorial Board

Prof. Anil Kumar, India
Prof. Aswani Kumar, India
Prof. K.P.R. Chowdary, India
Dr. S.J.S. Flora, India
Prof. H.M. Heise, Germany
Prof. Jian-Jiang Zhong, China
Prof. Kanyaratt Supaibulwatana, Thailand
Dr. S.P.S. Khanuja, India
Prof. P. Kondaiah, India
Prof. Madhavan P.N Nair, USA
Prof. Mohammed Alzoghaibi, Saudi Arabia
Prof. T.V. Narayana, India
Dr. Prasada Rao S. Kodvanti, USA
Prof. T. Ramana, India
Dr. C. N. Ramchand, India
Prof. P. Reddanna, India
Dr. Samuel JK. Abraham, Japan
Dr. Shaji T George, USA
Dr. B. Srinivasulu, India
Prof. A. Subrahmanyam, India
Prof. B. Suresh, India
Prof. N. Udupa, India
Prof. Ursula Kuees, Germany
Dr. Urmila Kodavanti, USA
Prof. P. Appa Rao, India

Dr. P. Ananda Kumar, India
Prof. Chellu S. Chetty, USA
Dr. P.V.Diwan, India
Dr. Govinder S. Flora, USA
Prof. Huangxian Ju, China
Dr. K.S. Jagannatha Rao, India
Prof. Juergen Backhaus, Germany
Prof. P.B. Kavi Kishor, India
Prof. M. Krishnan, India
Prof. M.Lakshmi Narasu, India
Prof. Mahendra Rai, India
Prof. Milan Franek, Czech Republic
Prof. Mulchand S. Patel, USA
Dr. R.K. Patel, India
Prof. G. Raja Rami Reddy, India
Dr. Ramanjulu Sunkar, USA
Prof. B.J. Rao, India
Prof. Roman R. Ganta, USA
Prof. Sham S. Kakar, USA
Prof. Sehamuddin Galadari, UAE
Prof. Carola Severi, Italy
Dr. N. Sreenivasulu, Germany
Prof. Sung Soo Kim, Korea
Prof. Swami Mruthinti, USA
Dr. Vikas Dhingra, USA

Assistant Editors

Dr. Giridhar Mudduluru, Germany

Dr. Sridhar Kilaru, UK

Prof. Chitta Suresh Kumar, India
(Electronic Version)
www.abap.co.in

ISSN 0973-8916

Current Trends in Biotechnology and Pharmacy

(An International Scientific Journal)

Volume 5

Issue 2

April 2011



www.abap.co.in

Indexed in Chemical Abstracts, EMBASE, ProQuest, Academic Search™, DOAJ, CAB Abstracts, Index Copernicus, Ulrich's Periodicals Directory, Open J-Gate Pharmoinfonet.in Indianjournals.com and Indian Science Abstracts.

Association of Biotechnology and Pharmacy (Regn. No. 28 OF 2007)

The *Association of Biotechnology and Pharmacy (ABAP)* was established for promoting the science of Biotechnology and Pharmacy. The objective of the Association is to advance and disseminate the knowledge and information in the areas of Biotechnology and Pharmacy by organising annual scientific meetings, seminars and symposia.

Members

The persons involved in research, teaching and work can become members of Association by paying membership fees to Association.

The members of the Association are allowed to write the title **MABAP** (Member of the Association of Biotechnology and Pharmacy) with their names.

Fellows

Every year, the Association will award Fellowships to the limited number of members of the Association with a distinguished academic and scientific career to be as Fellows of the Association during annual convention. The fellows can write the title **FABAP** (Fellow of the Association of Biotechnology and Pharmacy) with their names.

Membership details

(Membership and Journal)		India	SAARC	Others
Individuals	- 1 year	Rs. 600	Rs. 1000	\$100
LifeMember		Rs. 4000	Rs. 6000	\$500
Institutions	- 1 year	Rs. 1500	Rs. 2000	\$200
(Journal only)	Life member	Rs. 10000	Rs.12000	\$1200

Individuals can pay in two instalments, however the membership certificate will be issued on payment of full amount. All the members and Fellows will receive a copy of the journal free

Association of Biotechnology and Pharmacy
(Regn. No. 28 OF 2007)
#5-69-64; 6/19, Brodipet
Guntur - 522 002, Andhra Pradesh, India

Current Trends in Biotechnology and Pharmacy

ISSN 0973-8916

Volume 5 (2)	CONTENTS	April - 2011
Research Papers		
	Integrity and Bioactivity of Insulin Loaded PLGA Nanoparticles Prepared by a Novel Aquesou Method and its Comparison to Emulsion Solvent Evaporation Method <i>Mahmoud M. Ibrahim, Omaina A. Sammour, Mohamed Hammad, Nagia A. Megrab, Xiaoling Li and Bhaskara Jasti</i>	1084-1097
	A Simple and Rapid Method for Isolation of Alternaric Acid from <i>Alternaria solani</i> <i>S.J. Patel, R.B. Subramanian and Y.S. Jha</i>	1098-1103
	Tool Development for Prediction of pIC ₅₀ Values - A pIC ₅₀ Values from the IC ₅₀ Value Calculator <i>Chandrabose Selvaraj, Sunil Kumar Tripathi, Karnati Konda Reddy and Sanjeev Kumar Singh</i>	1104-1109
	Formulation, Characterization and Pharmacokinetic Studies of Carvedilol Nanoemulsions <i>Koteswari Poluri, Ramakrishna Sistla, Prabhakar Reddy Veerareddy, Lakshmi M. Narasu, Amol A Raje and Sunder M. Hebsiba</i>	1110-1122
	Studies on Carrier State of <i>Chlamydomphila abortus</i> in Nnaturally Infected sheep <i>Rabia Abadía Elzlitne, Giuma Elaref Elhafí, Vijayan R. and Sateesh Kumar</i>	1123-1129
	Automated Synchronization of <i>P. falciparum</i> Using a Temperature Cycling Incubator <i>Alejandro Almanza, Lorena Coronado, Nicole Tayler Liuris Herrera and Carmenza Spadafora</i>	1130-1133
	Genome Analysis of Selected Foodborne Pathogens for Identification of Drug Targets <i>Sushil Kumar Shakyawar, Arun Goyal and Vikash Kumar Dubey</i>	1134-1148
	Targeted Integration of <i>Bacillus thuringiensis</i> δ -Endotoxin <i>cryIFaI</i> in Brinjal (<i>Solanum melongena</i> L.) <i>Dipty Shrivastava, Monika Dalal, Vikrant Nain, P. C. Sharma and P. Ananda Kumar</i>	1149 - 1156
	Effect of Dietary Alpha Glycine on Cocoon Production in the Silk Worm <i>Bombyx mori</i> <i>Biswaranjan Paital and Kalyani Bohidar</i>	1157 - 1162
	Molecular Identification and Development of Nuclear DNA ITS Sequence Based Marker to Distinguish <i>Cosciniium fenestratum</i> Gaertn. (Menispermaceae) from its Adulterants <i>S. P. Balasubramani and Padma Venkatasubramanian</i>	1163-1172
	Development of Matrix Type Transdermal Patches of Lacidipine: Evaluation of physicochemical, <i>in vitro</i> , <i>ex vivo</i> and mechanical Properties <i>Ramesh Gannu, Adukondalu Devandla, Madhav Burra and Madhusudan Rao Yamsani</i>	1173-1182
	Amplified Fragment Length Polymorphisms Reveals High Intraspecific Variability in Field Isolates of <i>Leishmania panamensis</i> <i>Carlos M. Restrepo, Efraín Pérez Lao, Carolina De La Guardia, Octavio E. Sousa, José E. Calzada and Ricardo Leonart</i>	1183-1192
	Calcium Addition Potentially Reverses Lead and Manganese Induced Enzymatic and Behavioral Alterations in Rats <i>M. Ram Kumar, K. Praveen Kumar, V. Kavitha and G. Rajarami Reddy</i>	1193- 1205
News Item		i - iii

Information to Authors

The *Current Trends in Biotechnology and Pharmacy* is an official international journal of *Association of Biotechnology and Pharmacy*. It is a peer reviewed quarterly journal dedicated to publish high quality original research articles in biotechnology and pharmacy. The journal will accept contributions from all areas of biotechnology and pharmacy including plant, animal, industrial, microbial, medical, pharmaceutical and analytical biotechnologies, immunology, proteomics, genomics, metabolomics, bioinformatics and different areas in pharmacy such as, pharmaceuticals, pharmacology, pharmaceutical chemistry, pharma analysis and pharmacognosy. In addition to the original research papers, review articles in the above mentioned fields will also be considered.

Call for papers

The Association is inviting original research or review papers in any of the above mentioned research areas for publication in *Current Trends in Biotechnology and Pharmacy*. The manuscripts should be concise, typed in double space in a general format containing a title page with a short running title and the names and addresses of the authors for correspondence followed by Abstract (350 words), 3 to 5 key words, Introduction, Materials and Methods, Results and Discussion, Conclusion, References, followed by the tables, figures and graphs on separate sheets. For quoting references in the text one has to follow the numbering of references in parentheses and full references with appropriate numbers at the end of the text in the same order. References have to be cited in the format below.

Mahavadi, S., Rao, R.S.S.K. and Murthy, K.S. (2007). Cross-regulation of VAPC2 receptor internalization by m2 receptors via c-Src-mediated phosphorylation of GRK2. *Regulatory Peptides*, 139: 109-114.

Lehninger, A.L., Nelson, D.L. and Cox, M.M. (2004). *Lehninger Principles of Biochemistry*, (4th edition), W.H. Freeman & Co., New York, USA, pp. 73-111.

Authors have to submit the figures, graphs in tiff with 300 resolution and with times new roman 11 font for the text in the figures and tables of the related research paper/article.

Authors can submit their papers and articles either to the editor or any of the editorial board members for onward transmission to the editorial office. Members of the editorial board are authorized to accept papers and can recommend for publication after the peer reviewing process. The email address of editorial board members are available in website www.abap.in. For submission of the articles directly, the authors are advised to submit by email to krssrao@abap.co.in or editor@abap.co.in

Authors are solely responsible for the data, presentation and conclusions made in their articles/ research papers. It is the responsibility of the advertisers for the statements made in the advertisements. No part of the journal can be reproduced without the permission of the editorial office.

Integrity and Bioactivity of Insulin Loaded PLGA Nanoparticles Prepared by a Novel Aquesou Method and its Comparison to Emulsion Solvent Evaporation Method

**Mahmoud M. Ibrahim,^{1,2} Omaima A.Sammour,³ Mohamed Hammad,²
Nagia A. Megrab², Xiaoling Li¹ and Bhaskara Jasti^{1*}**

¹Thomas J. Long School of Pharmacy and Health Sci, University of the Pacific, Stockton, CA, USA

²Dept. of Pharmaceutics, Faculty of Pharmacy, Zagazig University, Zagazig, Egypt

³Dept. of Drug Technology, Faculty of Pharmacy, Ain Shams University, Cairo, Egypt

*For Correspondence -bjasti@pacific.edu

Abstract

Poly lactic-coglycolic acid polymer nanoparticles of insulin were prepared by a novel aqueous based mixed micelle (MM) method and traditional emulsion solvent evaporation method that use organic solvents. The particle size and entrapment efficiency and insulin release from the nanoparticles were determined. The integrity of the entrapped insulin, bioactivity and immunogenicity were investigated using MALDI MS, cell viability assay, and ELISA tests. The pharmacodynamic activity of the entrapped insulin in nanoparticles was compared with its subcutaneous administration in diabetic rats. The nanoparticles released 50% of insulin immediately at pH 7.4, followed by slow release of the remaining entrapped insulin. At pH 1.2, complete release of insulin occurred within 5 minutes. At a pH closer to PI of insulin, the burst release decreased to 8%. The molecular mass, cell viability and Elisa test showed that insulin retained its integrity and activity. The blood glucose levels in rats showed sustained reduction following the administration of insulin loaded nanoparticles suggesting that insulin activity in nanoparticles prepared by MM and ESE methods has remained intact.

Keywords: Bioactivity, Immunogenicity, Insulin integrity, Mixed micelle, Nanoparticles

Introduction

Recently, considerable progress has been made in developing biodegradable nanoparticles as effective vehicles for the delivery of proteins and peptides (1). These polymer drug delivery systems offer many advantages as they can carry and deliver the drug to a target site, have the ability to deliver proteins, peptides and genes, increase the therapeutic benefits and minimize the side effects of the drug (2,3). Also, they can control the release of a pharmacologically active component at the therapeutically optimal rate and dose regimen and help to increase the stability of drugs and proteins (4,5). The PLGA polymers, being biocompatible, have been used as controlled release delivery systems for parenteral and implantable applications (6). A successful PLGA nanoparticulate system should have a high drug loading capacity as it allows a small quantity of the carrier during a single administration. Insulin is the most effective drug in the treatment of advanced-stage diabetes. Despite the significant advancement in the field of pharmaceutical research, development of a proper insulin delivery system remained a challenge (7). The biological half life of peptides is short and need frequent and multiple administrations. Their transport across biological barriers is also poor, due to poor diffusivity and lower partition coefficients. In this

respect, biodegradable nanoparticulate delivery systems have been proposed for the safe and controlled parenteral administration of peptides (8). PLGA polymers possess various unique properties for the design of sustained release drug delivery application (9-11). An aqueous dispersion of insulin loaded PLGA nanospheres showed complete bioactivity after pulmonary administration in guinea pigs (12). The bioactivity of the entrapped protein need to be ascertained, as high sheer force, organic solvents and surfactants used in the nanoparticle preparation have potential to inactivate them. Homogenization or sonication used to obtain a stable primary w/o emulsion in w/o/w method can provoke cavitation stress that may destroy proteins (13-14). Insulin encapsulated in various polyester and polyanhydride nanospheres was found to retain its bioactivity (15). A modified o/o solvent evaporation method used for the preparation of insulin loaded PLGA micro-particles using homogenous single phase in which insulin and PLGA are dissolved (16). This method also depends on volatile organic solvents which have harmful effects on both human and environment. So, it is important to avoid the w/o interface and organic volatile solvents during preparation of protein loaded nanoparticles. A novel aqueous based method (mixed micelle method- MM method) for the preparation of proteins entrapment in PLGA nanoparticles was developed in our laboratory (17). In this method, insulin is incorporated into mixed micelles of PEG/tween dissolving PLGA polymer then polymer precipitation in aqueous conditions. This method is similar to the nanoprecipitation technique but without the use of organic solvents(14). It has the advantage of avoiding organic solvents and easy to prepare at room temperature. However, the integrity and biological activity of protein nanoparticles prepared by MM method is not known. In this study, the bioactivity of insulin PLGA nanoparticles prepared by aqueous based

MM method and other organic solvent based methods were compared. The release profiles of insulin nanoparticles at different pH were also investigated. Additionally, the integrity, immunogenicity, and biological activity of insulin entrapped in nanoparticles prepared by different methods were evaluated.

Material and Methods

Poly (lactic-co-glycolic acid) (PLGA), 50:50 DL2A, M.W., 10 kDa was obtained from Alkermes, Inc. (Cincinnati, OH). Polyvinyl alcohol (PVA, M.W. 30-70 kDa), Bovine Insulin (M.W. 5.7335 kDa), and sulphorhodamine B (SRB) were purchased from Sigma-Aldrich (St. Louis, MO). Bicinchoninic acid (BCA) protein assay kit was purchased from Pierce Biotechnology Inc. (Rockford, IL). Dulbecco's Modified Eagle's Medium (DMEM) was obtained from Gibco BRL (Grand Island, NY). Streptozotocin purchased from Calbiochem, a division of EMD Biosciences, Inc. (La Jolla, CA). All other chemicals and solvents used were of analytical grade.

Nanoparticle preparation

ESE method: To 100 μ L of insulin suspension (100 mg/mL) in distilled water, 10 mL of PLGA solution in methylene chloride or ethyl acetate (4% w/v) was added. The first water/oil (W/O) and solid/oil (S/O) emulsions were generated by a high-speed homogenizer at 22,000 rpm for 1 min (Polytron® PT-MR 2100, Switzerland by Kinematica AG). This primary emulsion was added to 40 mL of ice cooled 1% w/v aqueous PVA solution and homogenized at 22,000 rpm for 15 minutes to form the multiple emulsions (both W1/O/W2 and S/O/W2). The emulsion was stirred at room temperature in a hood with a magnetic stirrer adjusted to 500 rpm overnight (Tekstir® 20, Tekpro/American Hospital supply corp., Evanston, IL), to remove the organic solvent.

MM technique: The PLGA polymer was dissolved into 10 mL of methoxy-PEG 350 in 4% w/v. A stabilizer such as Tween 20 was added as 1% v/v of the final volume (50 mL). One hundred microlitres of Insulin suspension (100 mg/mL) in distilled water were added while stirring at 500 rpm for one minute, and then about 40 mL of PVA solution (1% w/v) was poured while stirring at 500 rpm. Nanoparticles were formed at once and no further stirring was required. The procedure was performed at ambient room temperature.

Nanoparticles purification: The nanoparticles were collected and purified by centrifugation and washing by distilled water two times at 17,300 g for 20 minutes. The purified suspension of nanoparticles was then frozen and dried using freeze dryer (FTS systems, Corrosion resistant freeze dryer, Stone Ridge, New York, USA).

Protein entrapment efficiency: The amount of insulin loaded into nanoparticles was calculated indirectly as the difference between the total amount of initial insulin added and the amount of insulin determined in the supernatants obtained during the purification step (18). The results were confirmed by dissolving 5 mg of the dried nanoparticles into 3 mL of cold acetone and centrifuged at 6,000 rpm to separate the precipitated protein. The precipitated protein was dried under vacuum at room temperature for 3 hours and then dissolved into 1 mL of distilled water.

BCA protein assay kit was used to determine the amount of protein entrapped and the method termed as direct method of determining the EE%. A standard calibration curve was established using serial protein concentrations from 10 to 150 µg/mL and the color produced was estimated using UV-Visible spectrophotometer (UV-1601 – Shimadzu) at wave length of 562 nm. The protein entrapment efficiency (EE %) was defined as the percentage

of protein loaded relative to the initial amount of the insulin.

Particle size determination: Particle size was determined using a photon correlation spectroscopy (PCS) with a Zetasizer 3000HS (Malvern Instruments Ltd., UK). Each blank nanoparticle batch was appropriately diluted with double distilled water just after production and after freeze drying. Mean size was measured three times for each batch.

Zeta potential determination: Zeta potential of each nanoparticle composition was determined by Zetasizer 3000HS (Malvern Instruments Ltd., UK). Zeta potential was measured by diluting a sample of formulation 1:16, with phosphate buffer of different pH values (6.8, 7, and 7.4). An average of three readings was recorded.

Nanoparticle morphology: Nanoparticle shape and morphology were analyzed by scanning electron microscopy (SEM) (Hitachi 26100, Japan). Freeze dried nanoparticles were placed on a metal stub coated with gold under vacuum. Concentrated nanoparticle dispersions prepared by the MM method were finely spreading over the metal stub and left to dry under vacuum then coated with gold.

In vitro release studies: The freeze dried nanoparticles were suspended in phosphate buffer (pH 7.4 or 5.6) or in pH 1.2 buffer as 1mg/mL in 20 mL glass vials. The suspension was placed in a shaking water bath at 37°C in dark conditions. From this, 1 mL samples were withdrawn at 0.08, 0.5, 1, 6, and 24 h after incubation. Samples were centrifuged as mentioned before and supernatants were assayed by reversed phase HPLC. The percentage of insulin released was plotted as a function of time (19).

Quantitative analysis of insulin: The amount of insulin released into the medium was quantified using an HPLC equipped with UV detector (SPD-10A-UV-VIS- Shimadzu), waters TM 600 pump

and Waters™ 717 plus autosampler (Millipore, USA). The mobile phase consisted of distilled water (70%) and acetonitril (30%) with trifluoroacetic acid (0.1%) and 0.6 mmol sodium sulfate. Chromatography was performed using C18 reversed phase column (Nova-Pak C18, 3.9X150 mm, Waters™, Ireland) at a flow rate of 1.5 mL/min and the eluent was monitored at 220 nm. The concentration of the insulin was determined by integration of the peak area using the external standardization method. All measurements were conducted in triplicate.

Insulin Integrity: Insulin released from nanoparticles was characterized using MALDI-TOF MS to assess the molecular mass (20). Nanoparticles were dissolved in acetone, dried at room temperature under vacuum. These samples containing insulin were reconstituted in 1 mL of 0.01 N HCl. Reference insulin solution was also prepared the same way by dissolving into 0.01 NHCl. Aliquots of 2 μ L samples were then mixed with 8 μ L of the matrix (α -CHCA) in solution (10 mg/ml in 0.1% TFA and 50% acetonitrile solution) and 2 μ L of the mix was allowed to dry on a plate in a solid spot under vacuum. The plate was then inserted into the mass spectrometer.

MALDI-TOF MS experiments were conducted on a MALDI-TOF instrument (Shimadzu, Japan) using a 337-nm nitrogen laser. Spectra were acquired in positive ion linear mode (Acceleration voltage 33 kV).

Immunogenicity of insulin: The immunogenicity of insulin was assayed by an ELISA test (Merckodia, Uppsala, Sweden). Accurately weighed amounts of nanoparticles were dissolved into acetone and centrifuged to precipitate the protein and the supernatant containing PLGA polymer was discarded. Samples were washed twice by acetone and centrifuged to separate the pure insulin. Samples were then vacuum dried

and re-dissolved in distilled water in the concentration range of (1–200 mU/L) using the manufacture's protocol and its relative bioactivity was calculated by comparison with values obtained by BCA analysis of the same aliquots (21).

Cell viability assay: MCF-7 cells were grown into 96 well plates in 5,000 cells per well for 24 h at 37 °C, 5% CO₂ in DMEM + 5% heat inactivated fetal bovine serum, non-essential amino acids, and L- glutamine (200 mM). The cells were serum and insulin starved for another 24 h and then incubated with insulin or nanoparticles carrying insulin in concentrations of 7.5, 10, and 12 μ g/mL for 48 hours. Control wells were treated similarly and PBS of pH 7.4 was added instead of insulin. Cell viability was then estimated using SRB assay (22).

In vivo effects of insulin loaded nanoparticles

Animals / Conditioning: Male Sprague–Dawley (SD) rats, body weight ranging 160–200 g were used in the study. The animal protocol was approved by the Institutional Animal Care and Use Committee of the University of the Pacific. The animals were grouped in standard polypropylene cages and maintained under controlled room temperature (22 \pm 2 °C) and humidity (55 \pm 5% RH) with 12:12h light and dark cycle. All the rats are provided with commercially available rat normal pellet diet and water ad libitum. If the weight of the animals increases beyond 250 g, they were discontinued from the study.

Induction of Diabetes: Diabetes was induced in male rats (250 \pm 30g) by an intra-peritoneal injection of streptozotocin (65 mg/kg) in a 10 mM citrate buffer at pH 4.5 (23). Streptozotocin solutions were used within 30 min. Rats were considered diabetic when blood glucose level was higher than 300 mg/dL, a week after streptozotocin treatment (24).

Blood glucose levels after subcutaneous administration of insulin nanoparticles:

Insulin Loaded nanoparticles (10 IU/kg) prepared by the above different methods were injected to fed diabetic rats. Free insulin (10 IU/kg), unloaded nanoparticles and PBS (pH 7.4) were also administered in control animals. Samples of 1 drop of blood were withdrawn from the tail vein at different time intervals and evaluated for the glucose levels using OneTouch Ultra 2 glucometer before injection and 0.5, 1, 1.5, 2, 3, 6, 8, 10, 12, 24, 48, and 72 hour post injection. Rats were maintained fasted during the experiment up to 12 h and fed thereafter.

Statistical analysis: The mean and the standard errors were calculated for each group. For group comparisons a one-way analysis of variance followed by the least significant difference (LSD) as a post-hoc test was applied, using SPSS program version 9 software. When $P < 0.05$, the difference was considered significant.

Results

Nanoparticles size , morphology and insulin entrapment efficiency : In the present investigation, insulin nanoparticles were prepared by two different methods. An aqueous solvent based method (MM) was found to be easier and faster method for preparing PLGA nanoparticles.

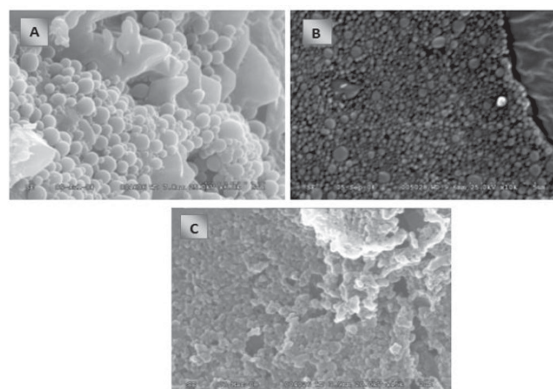


Fig. 1. Scanning electron micrographs of PLGA nanoparticles prepared by ESE method using DCM (A, PLGA 50:50; and Et-Ac (B), and mixed micelle method using methoxy Peg 350 as solvent (C).

As shown in Table 1, the size of the nanoparticles produced using MM method were smaller (247 nm) than those prepared by solvent evaporation method using dichloromethane (DCM) solvent (472.63 nm). ESE (Et-Ac) method produced nanoparticles of 257.9 nm which considered close to that produced by MM method. Morphological analysis of nanoparticles by SEM showed a homogenous distribution of spheroid particles with different particle sizes and no insulin crystals were observed. SEM photographs (Fig. 1) are clearly showing the difference in particle size according to the initial solvent used (each solvent corresponds a different method of preparation). All methods of preparation resulted in greater than

Table 1: Size, yield, and EE% of insulin nanoparticles prepared by different methods. (n=3).

Method of preparation	Before freeze drying Particle size (µm) (mean±SD)	Yield (%) (mean±SD)	EE (%) (mean±SD)	Zeta potential
ESE (DCM; PLGA 75:25)	863.90±11.50	72.93±2.80	99.22±0.10	N/A
ESE (DCM; PLGA 50:50)	472.63±22.92	67.58±3.50	87.67±8.85	-8.1± 5.00
MM (M-PEG- 350; PLGA 50:50)	247.00±5.30	51.23±1.20	84.75±0.75	-3.8± 4.3
ESE (Et-Ac; PLGA 50:50)	257.90±3.20	65.67±2.75	90.95±13.57	-1.3± 1.1
Nanoprecipitation (Acetone; PLGA 50:50)	248.40±2.20	56.67±4.25	89.00±1.83	-9.5± 7.4

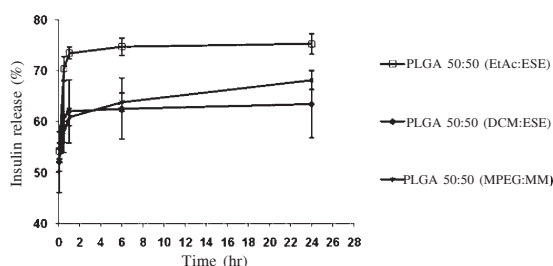


Fig. 2. Insulin release (%) from nanoparticles prepared by different methods in phosphate buffer pH 7.4 at 37° C Data represented as the mean±SD (n=3)

84% entrapment efficiency (EE) as shown in Table 1. Of the different methods of preparation, MM method resulted in lower EE%. However, there was no significant difference in Insulin EE% compared to nanoparticles prepared by ESE methods ($p>0.05$). All nanoparticles prepared by different methods showed negative zeta potential at pH 7.4.

Insulin Release from nanoparticles prepared by different methods : The release of insulin from nanoparticles prepared by different methods was found to be biphasic (Fig. 2). The initial rapid release (burst effect) was high, where, 52%, 52.4, and 54.2% of the entrapped insulin was released from nanoparticles prepared by ESE (DCM), MM, ESE (ET-AC), respectively. This burst release in the first 5 minutes was followed by about 8% release of insulin after 30 minutes in case of ESE (DCM) and MM methods. On the other hand, about 16% of insulin was released from nanoparticles of ESE (ET-AC) method following the burst release. After the first 30 minutes, very slow release of minute amounts of insulin was observed over 24 hours.

To use nanoparticles via the oral route, it is important to test the release of insulin at different pH range. Insulin release from nanoparticles of ESE (DCM) method was selected for the test as they show no significant differences in release compared to MM method ($P>0.05$). The release of insulin was significantly

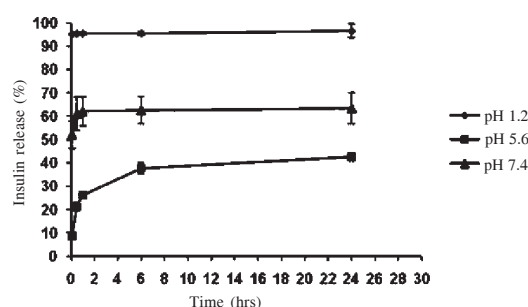


Fig. 3. Effect of release medium pH on insulin release from PLGA (50:50) nanoparticles prepared using ESE (DCM) method. Data represented as the mean± SD. (n=3).

affected by the external pH. Complete release of insulin occurred in 5 minutes at pH 1.2 as shown in Figure 3. However, the initial burst release was only 8% at pH 5.6 and 52% at pH 7.4. After 24 hours, only 42.5% of insulin was

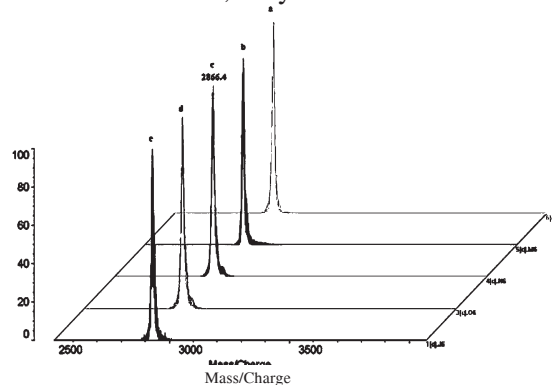


Fig. 4. MALDI-TOF Mass spectra of standrd insulin (a and e), insulin extracted from nanoparticles prepared using MM (b), ESE (ET-AC) (c), and ESE (DCM) (d) methods. Insulin concentration used was 0.2 mg/ml.

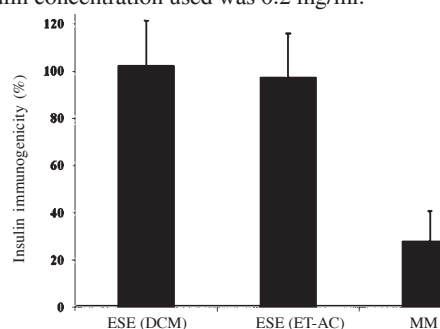


Fig. 5. Immunogenicity of insulin, determined as the ratio of insulin detected by ELISA test to insulin detected by BCA protein assay kit.

found released at pH 5.6, whereas 63.5% and 96% of insulin was released in pH 7.4 and 1.2 media, respectively.

Effect of Method of preparation on Insulin Integrity and Bioactivity : The integrity of insulin during the preparation of nanoparticles (organic solvent, homogenization, surfactants, freeze drying steps), was evaluated by extracting insulin from nanoparticles and analyzing the molecular weight by MALDI-TOF Mass Spectrometry. The mass spectra showed only a molecular peak at m/z 2866.4 (doubly charged, molecular weight of bovine insulin is 5733.5 Da) for samples prepared by both methods as well as the insulin solution (Fig. 4). This indicated that insulin retained its integrity and insulin was not degraded in the preparation process in all the methods evaluated.

The immunogenicity of insulin after encapsulation into nanoparticles by different methods was evaluated using ELISA test. The data showed that the antigen activity of insulin remained particularly unaffected by DCM

Table 2: Effect of tween 20 concentration on immunogenicity of insulin. Data represented as the mean±SD. (n=3).

Tween 20 Concentration (%)	0	1	2	4
Antigenicity (%)	23.11±0.02	29.51±0.72	27.61±0.16	28.18±13.38

(102.46% ± 19%), or ET-AC (97.63% ± 18.18%) in ESE method. However, only 28.18±13.38% insulin antigenicity was retained from nanoparticles prepared by MM method (Fig. 5).

Tween-20 and MPEG-350 were used in the preparation of insulin nanoparticles using MM method. To differentiate which of these two surfactants reduced antigenicity of insulin, ELISA assays were conducted using nanoparticles prepared at different Tween-20 concentrations. The antigenicity of insulin remained constant in the Tween-20 range of 1%-4% while it is

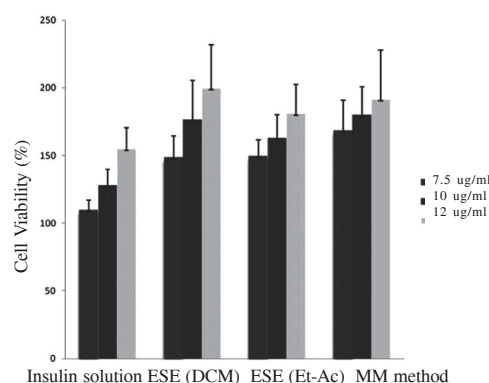


Fig. 6. Cell Viability (%) in the presence of insulin solution and insulin nanoparticles. Data presented as the mean±SD. (n=3).

significantly reduced ($P < 0.05$) when Tween-20 concentration was 0% suggesting the plausible reason for the reduced antigenicity of insulin nanoparticles is MPEG-350 and not Tween-20 as shown in Table 2.

Cell viability assay showed that all insulin carrying nanoparticles had increased the growth of MCF-7 cells, regardless of the method of preparation (Fig. 6). Increasing standard insulin concentration from 7.5 to 12 $\mu\text{g/mL}$ had increased cell viability from 110% to 154.85% compared to insulin starved cells. The nanoparticles carrying insulin prepared by ESE (DCM) method showed

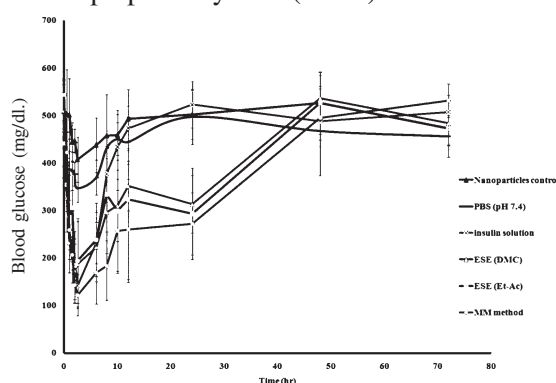


Fig. 7. Blood glucose concentrations following subcutaneous administration of insulin solution, insulin loaded nanoparticles prepared by different methods. PBS (pH 7.4) or empty nanoparticles of MM method (nanoparticles control). Insulin was administered at the concentration of 10IU/kg. Before the injection glycemia was 485.40±116.84 mg/dl. Results are expressed as means ±S.D. (n=6per group).

increased cell viability from 148.55% to 199.61% as the concentration of insulin increased from 7.5 to 12 µg/ml, respectively. The same behavior was observed when preparing nanoparticles by ESE (ET-Ac) technique. Also, Nanoparticles prepared by MM method increased cell viability from 168.56% to 191.4% as insulin content increased from 7.5 to 12 µg/ml, respectively.

***In vivo* effects of nanoparticles loaded with insulin on diabetic rats**

In contrast to the *in vitro* release results, where about 60% to 70% of insulin was released in the first 30 minutes, insulin nanoparticles have prolonged the hypoglycemic effect of the drug more than 24 hours compared to control insulin solution of the same dose (Figure 7). This clearly showed lack of *in vitro/in vivo* correlation for insulin containing nanoparticles. After the subcutaneous administration of 10 IU of insulin into diabetic rats as solution (in PBS, pH 7.4) and encapsulated in nanoparticles prepared by ESE (DCM), ESE (Et-Ac), and MM methods, the blood glucose levels decreased by 14.44%, 35.50%, 19.70% and 22.12%, respectively after 30 minutes. However, only nanoparticles of ESE (DCM) showed significantly lower blood levels compared to the remaining formulations and the controls ($p < 0.05$) except nanoparticles of MM method ($p > 0.05$). At 3 hours, blood glucose levels decreased by 69.30%, 63.81%, 56.33%, and 77.54% using insulin solution, nanoparticles of ESE (DCM), ESE (Et-Ac), and MM methods, respectively, and the differences between the groups are not statistically significant ($P > 0.05$). Blood glucose levels were significantly lower ($p < 0.05$) in rats injected with insulin containing preparations when compared to control preparations 6 hours post-administration. On the other hand, only insulin nanoparticles prepared by MM method provided of significantly lower blood glucose levels than insulin solution ($P < 0.05$). After 8 hours, all the insulin nanoparticle (except

ET-AC- ESE) exhibited significantly lower blood glucose levels when compared to insulin solution in rats ($P < 0.05$). All insulin loaded nanoparticles were effective in reducing the blood glucose levels even after 12 hours of administration when compared to insulin solution ($P < 0.05$). Insulin nanoparticles prepared by MM method resulted in significantly lower blood glucose levels ($P < 0.05$) compared to all insulin formulations and the controls except nanoparticles of ESE (DCM) method ($P > 0.05$). During the 12 hours post-administration, nanoparticles of ESE (DCM), ESE (ET-AC), and MM methods showed a plateau phase where blood glucose levels were constant (Figure 7). Statistical analysis showed a significant difference between insulin nanoparticles and solution forms 24 hours after administration ($P < 0.05$). After 48 and 72 hours of administration, the rats recovered completely from the insulin effect and there was no difference in blood glucose levels between the control and test groups ($P > 0.05$). The effect of insulin on the reduction of blood glucose levels lasted between 12-25 hours from nanoparticles preparation. However, only insulin nanoparticles prepared by MM method could keep blood glucose levels at $< 50\%$ of control group over the 24 hours.

Discussion

The data showed that the method of preparation affected both size and EE% for insulin (25-27). The ESE (DCM) method resulted in largest particle size nanoparticles due to water immiscibility of DCM and formation of larger emulsion globules. The partial water miscibility of Et-Ac and the complete water miscibility of MPEG-350 lead to the formation of much smaller nanoparticles. The thermodynamic parameters, such as diffusion coefficients (D_{sw} , D_{ws}), exchange ratio ($R = D_{sw}/D_{ws}$), and solvent-polymer interaction parameter (χ) were studied from PLGA nanoparticles prepared by emulsification-diffusion method. They have found

that R was proportional to the size of the PLGA nanoparticles, while χ was inversely proportional to it (28). The size distributions of the PLGA nanospheres prepared with different water immiscible, water miscible and partially water miscible solvents when PVA (1%) was used as the stabilizer were also studied (29). There was no significant difference in particle size between partially water soluble like ET-AC or fully water soluble solvent like acetone. Also, the study concluded that the larger particle size of nanoparticles prepared using DCM was due to its immiscibility with water causing significant aggregation of emulsion droplets.

The zeta potential results showed that insulin nanoparticles were negatively charged. It is well known that insulin above its PI (5.5) acquires a partial negative charge and because insulin's relatively smaller molecular size (6 kDa) when compared to other peptides, it might diffuse to the nanoparticle surface and impart negative charge to nanoparticles at the pH of 7.4 (30,31).

The drug present on the surface of the nanoparticles gets released quickly upon exposure to media, resulting in the initial burst of insulin (32). Previous studies have shown that the particle size of microparticle did not significantly affect the drug in-vitro release profiles (33). Hence, the variability in the release profiles may not be due to variability in the nanoparticle size.

The release of insulin was found to be similar from nanoparticles prepared by aqueous MM method and by ESE (DCM) method. Both methods showed lower burst release of insulin compared to ESE (ET-AC) method. A plausible explanation is that an increase in the hydrophilicity of ET-Ac enhanced the migration of insulin molecules to the surface of nanoparticles and insulin subsequently adsorbs to the nanoparticles surface after the evaporation of the solvent (34,35). On the other hand, higher viscosity of

MPEG, resulted in the accumulation of smaller insulin molecules on the nanoparticle surface by MM method. Thus, the drug release is largely controlled by the weak affinity between the insulin and the polymer, which resulted in a higher burst release (36).

The solubility of insulin varies at different pH conditions: >10 mg/ml, <1mg/mL, and about 5 mg/mL at pH 1.2, 5.6 (close to IP of insulin), and 7.4 (37). Insulin release from the nanoparticles was found to depend on the pH of the release media as insulin partitioning into the aqueous release depended on its solubility (38). This result suggested the nanoparticles are not useful for oral delivery.

Insulin fragments could be detected using MALDI TOF MS as a stability indicating assay (25). The mass spectra of insulin showed in Figure 4, exhibited only one identical monoisotopic peak corresponding to its molecular ion. No evidence of covalent aggregation or degradation peaks of disamido, dimmers, trimers or single chains insulin was noticed by MALDI TOF MS. The MALDI TOF MS analysis can prove unfolding of the C-terminal region of the α subunit in the folding intermediate (39). Also, this analysis was effectively used to prove the signal of insulin PEG conjugates and detect insulin degradation fragments. The resulting degradation products must exhibit two molecular weight distributions showing a shift in the MW distribution due to α and β chains of insulin (40). Figure 4 showed only a peak of 100% intensity which correspond insulin extracted from nanoparticles with no differences compared to ideal insulin solution. The result suggested extreme integrity of insulin molecule entrapped in nanoparticles by MM method and solvent evaporation technique.

ELISA method has very high sensitivity and specificity as the assay depends on the reaction of antigen with antibody. The method

was considered an appropriate means for detection of potential changes of the antigenic activity. It can confirm that the receptor binding epitopes on insulin were maintained after encapsulation (16). This could be true whenever the antigenicity is close to 100 %, however, in this study, reduction in antigenicity as tested by ELISA was not detrimental on receptor binding epitopes. Results showed that nanoparticles prepared by ESE method had 100% immunogenicity, whereas, nanoparticles prepared by MM method showed only 28.18% insulin immunogenicity based on ELISA testing. As shown in Table 2, the presence of minute amounts of methoxy PEG 350 after purification of nanoparticles was responsible for the reduced immunogenicity, while Tween-20 did not show any such effect. It is commonly known that PEGs could interfere with antibody antigen interaction. This effect is presumably the result of reduced exposure of hydrophobic parts of the protein in the presence of PEG (41). Low PEG residues on the nanoparticle surface, being more hydrophilic, decreased their opsonization, and reduced immune system recognition (42). This implied that the organic solvent/water interfaces, surfactants (PVA and Tween 20) and homogenization steps used in the preparation of nanoparticles did not alter insulin integrity. However, low immunogenicity did not result lower bioactivity obtained from cell viability assay.

The insulin present in the supplemented serum free medium seemed to be responsible for the enhanced cell growth (43). Insulin has potentiated lysophosphatidic acid to stimulate MCF-7 cell cycle progression and DNA synthesis (44). Hence, cell viability assay performed to elucidate the insulin bioactivity on growth of MCF-7 cells was studied using nanoparticles prepared by ESE and novel MM methods. Higher cell viability was evident from nanoparticles when compared to standard insulin solution at the same concentrations. The intimate contact of

nanoparticles to cells increased the concentration of insulin closure to cellular membranes enhancing cell viability. Since, the nanoparticles prepared by MM method exhibited good bioactivity while reducing the immunogenicity, this method of nanoparticle preparation seems to have advantages.

The biological effects of insulin encapsulated into nanoparticles were also proved by the *in vivo* studies. Nanoparticles preparation methods that involved organic solvents and surfactants showed prolonged reduction in blood glucose levels of diabetes induced rats, further suggesting that the biological activity of insulin is not affected by preparation methods. The blood glucose profiles of insulin nanoparticles showed 4 phases as shown in Figure 7. In the first phase a rapid reduction in blood glucose levels was observed that peaked at 3 hours, which correlated with insulin absorbed from the burst effect *in vitro* release media. In the second phase, blood glucose levels have increased as the absorbed insulin rapidly cleared from the rats between 3rd and 6th hours. The third plateau phase after 12 hours could be due to slow release of insulin from nanoparticles. A fourth phase of blood glucose levels recovery back to 100% and continued at that level at 48 and 72 hours revealed complete clearance of insulin from the rats. The reduced blood levels observed between 12 and 24 hours might from the insulin release due to the degradation of the polymer (19). On the other hand, insulin solution showed only first 2 phases shown by nanoparticles. This data clearly showed the unique advantages of nanoparticulate delivery systems, which include offering protection from degradation by enzymes in the body (44). A similar study showed lowered blood glucose levels in diabetic rats over 24 hours following intraperitoneal injection of PLGA nanoparticles (45). In that study, blood glucose level showed a minimum of 10 mmol/L at 1 hour after nanoparticle

administration which might be due to burst release of insulin, and a later prolonged hypoglycemic effect due to insulin continuous release from nanoparticles. In another study, the aqueous dispersion of PLGA nanospheres prepared by organic solvent based method and administered pulmonary route to guinea pig via nebulization have reduced the blood glucose level significantly for over 48 hours when compared to nebulized aqueous solution of insulin as a control (46). About 85% of insulin release from nanospheres was found to occur during the initial burst, followed by a prolonged release of the remaining drug in saline solution at 37 °C. Current study clearly indicated that encapsulation of insulin into biodegradable nanoparticles preserved its biological activity and prolonged its pharmacological activity over extended period of time. This might help to reduce the frequent multiple injections required to maintain blood glucose level at normal concentration and inhibit hyperglycemic side effects.

Conclusion

MM method is a promising technique for preparing PLGA nanoparticles of good physicochemical properties compared to conventional methods. MM method has better potential than existent methods as PLGA nanoparticles can be prepared using aqueous based solvent with low shear stress or energy at room temperature resulting in the retention of biological activity with lower immunogenicity. Finally, in vivo study results showed prolonged blood glucose reduction in diabetes induced rats suggesting that insulin bioactivity was retained.

References

1. Kumaresh, S. S., Tejraj, M. A., Anand Rao, R. K. and Walter, E. R. (2001). Biodegradable polymeric nanoparticles as drug delivery devices. *J. Controlled Release*, 70:1–20.
2. Langer, R. (2000). Biomaterials in drug delivery and tissue engineering: One laboratory's experience, *Accounts of Chemical Research*. 33: 94–101
3. Lanza, R.P., Langer, R. and Chick W.L. (1997). Principles of Tissue Engineering, in: Academic Press, Austin, TX, 405–427.
4. Kreuter, J. (1994). Nanoparticles, in: J. Kreuter (Ed.), *Colloidal Drug Delivery Systems*, Marcel Dekker, New York, pp.219–342.
5. Kumaresh, S. S., Tejraj, M. A., Anand Rao, R. K. and Walter, E. R. (2001). Biodegradable polymeric nanoparticles as drug delivery devices. *J. Controll. Rel.* 70:1–20.
6. Wise, D.L., Fellman, T.D., Sanderson, J.E. and Wentworth, R.L. (1979). Lactide / glycolide acid polymers, in: G. Geregoriadis (Ed.), *Drug Carriers in Biology and Medicine*, Academic, London, 237-270.
7. Sajeesh, S. and Sharma, C. P. (2006). Cyclodextrin–insulin complex encapsulated polymethacrylic acid based nanoparticles for oral insulin delivery. *Pharmaceutical Nanotechnology*, Int. j. Pharm., 325: (1-2), 147-154.
8. Couvreur, P. and Puisieux F. (1993). Nano- and microparticles for the delivery of peptides and proteins, *Adv. Drug Deliv. Rev.* 5: 141–162.
9. Yang, R., Chen, T., Chen, H. and Wang, W. (2005). Microfabrication of biodegradable (PLGA) honeycomb-structures and potential applications in implantable drug delivery. *Sensors and Actuators B* 106: 506–511.
10. Jin, C., Bai, L., Wu, H. and Teng, Z. (2008). Cellular uptake and radiosensitization of SR-

- 2508 loaded PLGA nanoparticles. *J. Nanoparticle Researc*, 10:1045-1052.
11. Cegnar, M., Premzl, A., Zavasnik-Bergant, V., Kristl, J. and Kos, J. (2004). Poly(lactide-co-glycolide) nanoparticles as a carrier system for delivering cysteine protease inhibitor cystatin into tumor cells. *Experimental Cell Research*, 301: 223-231.
 12. Kawashima, Y., Yamamoto, H., Takeuchi, H., Fujioka, S. and Hino T. (1999). Pulmonary delivery of insulin with nebulized DL- lactide / glycolide copolymer (PLGA) nanosphere to prolong hypoglycemic effect, *J. Control. Rel.* 62: 279-287.
 13. Bilati, U., Allemann, E. and Doelker, E. (2005). Strategic approaches for overcoming peptide and protein instability within biodegradable nano- and microparticles. *Eur. J. Pharm Biopharm.* 59: 375-388.
 14. Bilati, U., Allemann, E. and Doelker, E. (2005). Nanoprecipitation versus emulsion based techniques for the encapsulation of protein into biodegradable nanoparticles and process related stability issues. *AAPS Pharm Sci Tech* 6:E594-E604.
 15. Carino, G.P. and Jacob, J.S. (2000). Mathiowitz E., Nanosphere based oral insulin delivery, *J. Control. Rel.* 65: 261–269.
 16. Emami, J., Hamishehkar, H., Najafabadi, A. R., Gilani, K., Minaiyan, M., Mahdavi, H. and Nokhodochi, A. (2009). A novel approach to prepare insulin-loaded poly (lactic-co-glycolic acid) microcapsules and the protein stability study. *J. P. S.* 98 (5): 1712-1731.
 17. Ibrahim, M. M., Sammour, O. A., Hammad, M., Megrab, N. A., Li, X. and Jasti B. (2008). Novel Aqueous solvent based method for protein based nanoparticles. *Current Trends in Biotechnology and Pharmacy*, 2: (4) 575 -584.
 18. Rodrigues, J. S., Santos-Magalhães, N. S., Coelho, L. C. B. B., Couvreur, P., Ponchel, G. and Gref R. (2003). Novel core (polyester)-shell (polysaccharide) nanoparticles: protein loading and surface modification with lectins. *J. Controll. Rel.*, 92 (1-2):103-112.
 19. Sammour, O.A. and Hassan, H.M. (1996). Enhancement of the antibacterial activity of ampicillin by liposome encapsulation. *Drug Delivery*, 3: 273–278.
 20. Giuseppe, G., Enrico, R. and Giuseppe, S. (2007). AP/MALDI-MS complete characterization of the proteolytic fragments produced by the interaction of insulin degrading enzyme with bovine insulin. *J. Mass Spectrometry*, 42: 1590-1598.
 21. Sarmiento, B., Ribeiro, A., Veiga, F. and Ferreira, D. (2006). Development and characterization of new insulin containing polysaccharide nanoparticles. *Colloids and Surfaces B: Biointerfaces* 53: 193–202.
 22. Houghton, P., Fang, R., Techatanawat, I., Steventon, G., Hylands, P. J. and Lee C.C. (2007). The sulphorhodamine (SRB) assay and other approaches to testing plant extracts and derived compounds for activities related to reputed anticancer activity. *Methods*, 42: 377-387.
 23. Monica, A. V., Napoleon, A., Betts, A. C., Patrick, I. B. and Kenneth, R. (2006). Streptozotocin (STZ) diabetes enhances benzo(a)pyrene induced renal injury in Sprague Dawley rats. *Toxicology Letters*, 164 214–220.

24. Damge, C., Philipe, M. and Nathalie, U. (2007). Oral delivery of insulin associated to polymeric nanoparticles in diabetic rats. *J. Controll. Rel.*, 117: 163-170.
25. Jiang, G, Qiu, W. and Deluca, P. P. (2003). Preparation and in vitro / in vivo evaluation of insulin loaded poly (Acryloyl-hydroxyethyl starch) PLGA composite microspheres. *Pharmaceutical Research*, 20(3): 452-459.
26. Cohen, S., Yoshioka, T., Lucarelli, M., Hwang, L. H. and Langer R. (1991). Controlled delivery systems for proteins based on poly- (lactic/glycolic acid) microspheres. *Pharm. Res.* 8:713-720.
27. Igartua, M., Hernandez, R. M., Esquisabel, A., Gascon, A. R., Calvo, M. B., and Pedraz J. L. (1997). Influence of formulation variables on the in-vitro release of albumin from biodegradable microparticulate systems. *J. Microencapsul.* 14:349-356.
28. Choi, S.W., Kwon, H.Y., Kim, W.S. and Kim, J.H. (2002). Thermodynamic parameters on Poly (D,L-Lactide-Co-Glycolide) Particle size in Emulsification-Diffusion Process. *Colloids Surf. A: Physicochem. Eng. Aspects* 201: 283-289.
29. Song, K. C., Lee, H. S., Choung, I. Y., Cho, K. I., Ahn, Y. and Choi E. J. (2006). The effect of type of organic phase solvents on the particle size of poly(d,l-lactide-co-glycolide) nanoparticles. *Colloids and Surfaces A: Physicochem. Eng. Aspects* 276: 162-167.
30. Francine, K., Yvonne, H. L. and Damien, W. M. A. (2008). Electrochemical Study of Insulin at the Polarized Liquid-Liquid Interface. *Langmuir*, 24:(17), pp 9876-9882.
31. Zhao, Z. P., Wang, Z. and Wang, S. C. (2003). Formation, charged characteristic and BSA adsorption behavior of carboxymethyl chitosan/PES composite MF membrane. *J. Membrane Sci.* 217: 151-158.
32. Pillai, R. R., Somayaji, S. N, Rabinovich, M., Hudson, M. C. and Gonsalves, K. E. (2008). Nafcillinloaded PLGA nanoparticles for treatment of osteomyelitis. *Biomed. Mater.* 3:034114.
33. Nurhan, E. and Nevin, C. (1996). Factors influencing release of salbutamol sulphate from poly(lactide-co-glycolide) microspheres prepared by water-in-oil-in-water emulsion technique. *Int. J. Pharm.* 137: 57-66.
34. Brigger, I., Chaminade, P., Marsaud, V., Appel, M., Besnard, M., Gurny, R. and Renoir, M. (2001). Couvreur P. Tamoxifen encapsulation within polyethylene glycol-coated nanospheres. A new antiestrogen formulation, *Int. J. Pharm.* 214: 37-42.
35. Michael, C. , Ilia, F. , Haim, D. D. and Gershon, G. (2002). Lipophilic drug loaded nanospheres prepared by nanoprecipitation: effect of formulation variables on size, drug recovery and release kinetics. *J. Control. Rel.* 83: 389-400.
36. Fude, Cui, Kai Shi, Liqiang Zhang, Anjin Tao and Yoshiaki Kawashima. (2006). Biodegradable nanoparticles loaded with insulin-phospholipid complex for oral delivery: Preparation, in vitro characterization and in vivo evaluation. *Journal of Controlled Release* 114:242-250.
37. Larry, R. B., Elazer, R. E., Fariba, F. G. and Robert L. (1996). Characterization of Glucose-Mediated Insulin Release from

- Implantable Polymers. *J. Pharm. Sci.* 85(12): 1341-1345.
38. Joseph, K. (1990). Pulsed and Self-regulated Drug Delivery. CRC press.
39. Mendoza, V. L. and Vachet, R. W. (2009). Probing Protein Structure by Amino Acid-Specific Covalent Labeling and Mass Spectrometry. *Mass Spectrom Rev.* ; 28(5): 785–815.
40. Tuesca, A. D, Reiff, C., Joseph, J.I. and Lowman, A. M. (2009). Synthesis, Characterization and In Vivo Efficacy of PEGylated Insulin for Oral Delivery with Complexation Hydrogels. *Pharmaceutical Research*, 26 (3): 727-739.
41. Crommelin, D. J. A., Storm, G, Verrijck, R., Leede, L. D., Jiskoot, W. and Hennink, W. E. (2003). Shifting paradigms: biopharmaceuticals versus low molecular weight drugs. *Int. J. Pharm.* 266(1-2): 3-16.
42. Vasir, J. K., Reddy, M. K. and Labhassetwar, V. D. (2005). Nanosystems in Drug Targeting: Opportunities and Challenges. *Current Nanoscience*, 1: 47-64.
43. Chappell, J., Leitner, J. W., Solomon, S., Golovchenko, I., Goalstone, M. L. and Draznin B. (2001). Effect of insulin on cell cycle progression in MCF-7 breast cancer cells. *J. Biol. Chem.* 276(41): 38023-38028.
44. Kubik, T., Bogunia-Kubik, K. and Sugisaka, M. (2005). Nanotechnology on Duty in Medical Applications. *Current Pharmaceutical Biotechnology*, 6: 17-33.
45. Liu, J., Zhang, S. M., Chen, P. P., Cheng, L., Zhou, W., Tang, W. X., Chen, Z. W. and Ke, C. M. (2007). Controlled release of insulin from PLGA nanoparticles embedded within PVA hydrogels. *J Mater Sci: Mater Med* 18:2205–2210.
46. Kawashima, Y., Yamamoto, H., Takeuchi, H., Fujioka, S. and Hino T. (1999). Pulmonary delivery of insulin with nebulized DL- lactide / glycolide copolymer (PLGA) nanosphere to prolong hypoglycemic effect, *J. Control. Rel.* 62: 279-287.

A Simple and Rapid Method for Isolation of Alternaric Acid from *Alternaria solani*

S.J. Patel*, R.B. Subramanian and Y.S. Jha

B. R. Doshi School of Biosciences, Lab. No.103 B, Bakrol Vadtal Road, Satellite Campus,
Sardar Patel University, Vallabh Vidhyanagar 388120, India

*For correspondence - suchitapatel5@yahoo.com

Abstract

Alternaric acid is the major toxin of *Alternaria solani*, the causative agent of early blight of tomato. A simple and rapid method has been developed for the isolation of alternaric acid in crystalline form from the fungal culture filtrate (FCF) with ethanol and carbon tetrachloride. The crystalline form of alternaric acid obtained was subjected to High Performance Thin Layer Chromatography (HPTLC), spectrophotometric analysis and detached leaf assay to confirm the purity and biological activity of alternaric acid. This one step protocol is superior to earlier reported methods and also gives higher yield.

Keywords: Acid, Blight, Tomato, Toxin, TLC

Introduction

Tomato (*Lycopersicon esculentum* Mill.) belongs to the family Solanaceae. Worldwide, it is the second most consumed vegetable after potato (1). Early blight of tomato caused by the necrotrophic fungus *Alternaria solani* Sorauer is perhaps the most common foliar disease of tomatoes. In USA, Australia, Israel, UK, and India, significant reductions in yield (35 up to 78%) due to early blight (EB) have been observed (2, 3, 4). The symptoms occur on the leaves where circular and concentric lesions are produced. Early blight reduces the photosynthetic

area and, in severe cases, can defoliate plants. The fungus survives between crops as mycelia or conidia in soil, plant debris and seed (5). The spores are transported by water, wind, insects, other animals including man, and machinery. Eleven toxins have been identified in culture filtrates of *A. solani* (6). Among these, alternaric acid and solanapyrone A, B, and C are able to induce necrotic symptoms similar to EB symptoms (6). Out of these, alternaric acid is one of the major toxins found in the filtrates (7) which causes chlorosis and necrosis and therefore plays a major role in early blight symptoms and defoliation (8). Alternaric acid does not cause phytotoxicity when sprayed alone on tomato leaves, but it enhances the infection process and the development of necrotic symptoms when added to *A. solani* spore suspensions. Alternaric acid was previously crystallized by Brian *et al.* (9). Stoessl and Stothers (10) developed a method for extraction of alternaric acid from fungal culture filtrate.

Previously, Matern *et al.* (11) tried to isolate alternaric acid from crude FCF. The procedure is time consuming and the results were not reliable. Maiero *et al.* (12) made an attempt to isolate alternaric acid in bulk quantities for screening of resistant varieties, but were unsuccessful. Standard alternaric acid or alternaric acid in pure form are difficult to obtain

commercially. Isolation of alternaric acid by following the method proposed in this report offers better yield than the previous methods. Moreover, the time required for the process of isolation is less and there is a significant increase in the yield. By following this method a good quantity of purified form of alternaric acid can be obtained. The aim of this study is to develop a simple and rapid method which facilitates isolation of alternaric acid for use in various aspects of plant pathology.

Materials and methods

Fungal culture and its maintenance: *Alternaria solani* isolate was grown on potato-dextrose agar (PDA) plates and these plates were incubated at $25^{\circ}\text{C} \pm 1^{\circ}\text{C}$. After sporulation these plates were maintained at 4°C until use.

Fungal Culture Filtrate (FCF) production and its analysis: An 8 mm mycelial mat was cut with a sterile cork borer from 1 month old *A. solani*, grown on a PDA plate and transferred into a 250 mL Erlenmeyer flask containing 100 mL of autoclaved potato-dextrose broth (PDB). Flasks were incubated from 21 days at $25^{\circ}\text{C} \pm 1^{\circ}\text{C}$ in static submerged condition. Thereafter, the broth was filtered using Whatman filter paper No. 1. Fungal culture filtrate from 7th to 21st days was collected and subjected for HPTLC analysis.

Isolation of Alternaric acid : For development of crystals an 8mm mycelial mat was cut with a sterile cork borer from 1 month old *A. solani*, grown on a PDA plate and transferred into a 250mL Erlenmeyer flask containing 100mL of PDB. Flasks were incubated for 18 days at $25^{\circ}\text{C} \pm 1^{\circ}\text{C}$ in static submerged condition. Mycelial mat from 18 days old culture grown on PDB was removed and the broth was filtered using Whatman filter paper No. 1. The pH of the filtrate was adjusted between 3.0-3.5 by 1N HCl and extracted with equal volume of ethanol. The colorless solution obtained was dissolved by

adding drop by drop boiling carbon tetrachloride (2mL) using a glass dropper. Residual ethanol was removed by evaporation and crystalline alternaric acid appeared on cooling.

Characterization of alternaric acid: The isolated compound is alternaric acid was confirmed by the following analytical techniques and assay.

i. Microscopic analysis: A small drop of crystalline alternaric acid was taken on a clean concavity glass slide. Cover slip was gently put onto the drop and the slide was observed under microscope (Axioplan, Image Analyzer) at 10X and 40X magnifications.

ii. HPTLC (High Performance Thin Layer Chromatography): Purification of alternaric acid was carried out by HPTLC technique. Aluminum-backed silica gel 60 F₂₅₄ TLC foils (10X10cm) of 0.25mm thickness (Merck, Dramstadt, Germany) were run with methanol as the mobile phase and then dried in an oven at 120°C for 15-20 minutes before sample loading. Sample loading onto TLC foils were performed with a Linomat 5 applicator (CAMAG, Muttenez, Germany) using a 100 μ l Hamilton syringe. The TLC foils were developed in a solvent system of isopropanol:ammonia:water (5:1:5). After running the foils were dried in an oven at 120°C for 5mins and the developed plates were observed under a UV source at 254 and 366nm. Rf values were calculated for the observed metabolite. The presence of alternaric acid was further confirmed by scanning the developed TLC foils. The scanning of foils in which crystalline alternaric acid was separated were scanned in Scanner 3 at 254 and 366nm and observed for the presence of peak.

iii. Spectrophotometric analysis: The observed band was scraped and subjected to spectral scanning (Unicam Alpha) from 190 to 400nm to find out its absorbance maxima. The scanning of

undiluted and diluted samples was done. Dilutions were carried out using ethanol. The sample was diluted with ethanol. Thus, 50 μ l of sample and 2ml of ethanol was taken in a quartz cuvette. 3 ml of ethanol was taken as a blank.

iv. Detached leaf bioassay: Tomato leaves were washed in tap water. The leaves were surface sterilized with a cotton swab dipped in 4% Sodium hypochlorite solution for 10-15 seconds. They were then washed thoroughly in sterile water and placed in sterile Petri plates containing Whatman No. 1 paper. 100 μ l of crystals along with water was applied gently on leaf surface using a micropipette and 100 μ l of water was applied on control leaves. These plates were allowed to incubate at 25°C \pm 1°C for 1 to 2 days and the moisture in dishes was maintained throughout the experiment. The results were recorded after 24 hours. The experiment was carried out in triplicates.

v. Comparison of bands and Rf values: Aluminum-backed silica gel 60 F₂₅₄ TLC foils (10X20cm) of 0.25mm thickness (Merck, Dramstadt, Germany) were run with methanol as the mobile phase and then dried in an oven at 120°C for 15-20 mins before sample loading. HPTLC of FCF from 7th to 21st days was carried out using Linomat 5 applicator (CAMAG, Muttenz, Germany) using a 100 μ l Hamilton syringe. The TLC foils were developed in a solvent system of chloroform:ethanol (93:7). After running the foils were dried in an oven at 120°C for 5 mins and the developed plates were observed under a UV source at 254 and 366nm. The Rf value of bands observed was compared with the Rf value of the observed band of crystalline alternaric acid.

vi. In vivo bioassay: Tomato seeds were soaked in sterile water. The seeds were allowed to germinate in autoclaved Petri plates lined with Whatman No. 1 paper. After the seedlings reached two leaf stages, they were transferred

in pots. Tomato plants were grown for about 4 weeks and were used in *in vivo* bioassay. 0.5 ml of crystal solution along with water was taken in an injection syringe and this was injected in the petiole region of the plant. Sterile water was used in the control plants. The surface of the leaf was slightly pricked with sterilized syringe in order to enhance the rate of infection. The plants were monitored regularly for the development of visible symptoms.

Results

The crystals of alternaric acid were observed under 10X and 40X magnifications (Fig.1). The yield of alternaric acid obtained by this method is 0.05 g per 100 ml. This isolate produced maximum toxin from 18th day onwards and the Rf value was 0.5. (Fig. 2a). The toxins appear as blue fluorescing spots when placed under a short wavelength UV lamp (366nm) (Fig. 2b). The Rf value of crystalline alternaric acid and that of alternaric acid separated from crude FCF by HPTLC was 0.5. TLC foil of 10X10 dimensions was scanned under Scanner 3 at 254 and 366nm. A distinct peak of separated crystalline alternaric acid was observed at 366nm (Fig. 3). Symptoms appeared on the treated leaves after 24 hours from inoculation (Fig. 4). More than one peak was observed in the undiluted samples (Fig. 5a). By UV- spectrophotometric scanning the absorption maxima of the alternaric acid was 254 nm (Fig. 5b). Necrosis on the leaf was clearly visible on the Tomato plant treated with crystals whereas on the control plant there were no symptoms observed (Fig. 6).

Discussion

Early blight, caused by the deuteromycete fungus *A. solani* is a destructive disease of tomato world-wide. Alternaric acid, a phytotoxic metabolite of *A. solani*, (13) is a highly crystalline, colorless and an optically inactive unsaturated dibasic acid. It contains no methoxyl groups and

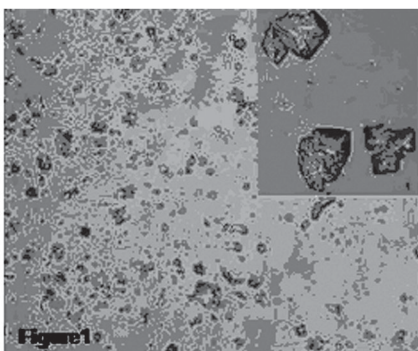


Fig. 1. Shows crystals of alternaric acid observed under 10X magnification and crystals observed under 40X magnification (inset)

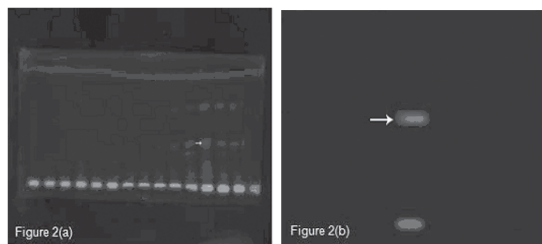


Fig. 2(a). Band of crude FCF (from 7th to 21st days) seen clearly at 366nm on 18th day on TLC foil (10X20) showing the presence of alternaric acid HPTLC analysis of purified alternaric acid and figure 2 (b) shows band of alternaric acid on TLC foil (10X10) observed at 366nm wavelength

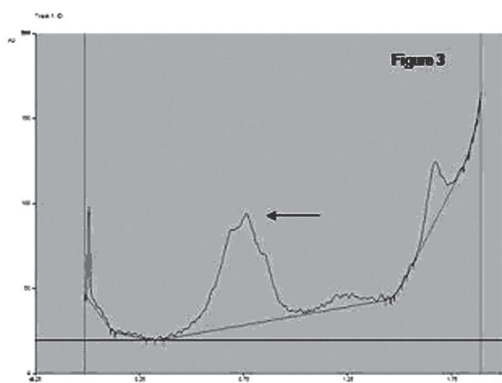


Fig. 3. Shows scanning of HPTLC foil in Scanner 3 at 366 nm

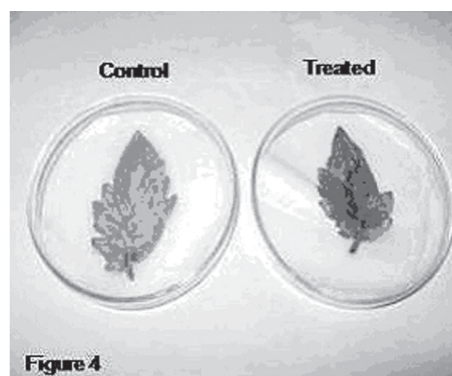


Fig. 4. Shows detached leaf bioassay

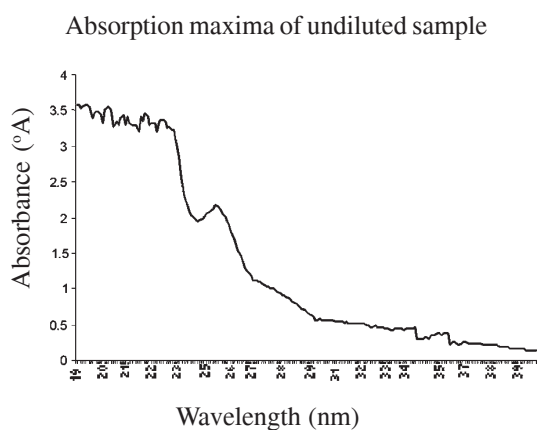


Fig. 5 (a). Shows UV-spectroscopic scan of undiluted alternaric acid from 190-400nm

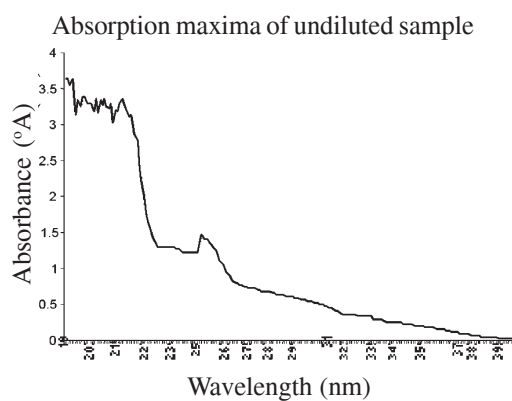


Fig. 5 (b). Shows UV-spectroscopic scan of diluted alternaric acid from 190-400nm

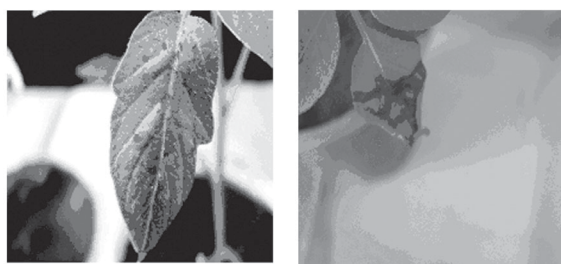


Fig. 6. Shows *in vivo* bioassay Treated

is shown to be 12-(5, 6-dihydro-4-hydroxy-6-methyl-2-oxopyran-3-yl)-4, 5-dihydroxy-3-methyl-9-methylene-12-oxododec-6-ene-5-carboxylic acid. (14).

Increase in alternaric acid yield was measured by weighing dried crystals of alternaric acid. The yield obtained was five times higher by this method than by the previous methods reported. The presence of colorless alternaric acid in crystalline form could be visualized microscopically under 10X and 40X magnifications and also through naked eyes. HPTLC is a fast and reliable technique. The advantage of HPTLC is that quantities of substances too small to be detected by chemical methods could be separated and thereafter their biological activity can be measured by performing bioassay. The presence of alternaric acid in crude FCF was confirmed by comparing both the R_f values of crude FCF and that of crystalline alternaric acid. Scanning of HPTLC foils showed a distinct peak which proves the presence and purity of alternaric acid.

The detached leaf assay is a simple method which allows controlled inoculation with specific isolates, without destroying the whole plant. The result of detached leaf bioassay showed similar symptoms as shown by the *A. solani* infected leaves in field. The symptoms appeared very fast and were distinct. Further virulence of crystals was checked and confirmed by *in vivo* bioassay. Thus the presence of alternaric acid

can be proved biologically. Spectrophotometric scanning of crystalline alternaric acid showed a distinct peak in diluted samples whereas; in undiluted sample many peaks were seen. Thus, the presence of alternaric acid was confirmed by this simple analytical technique.

Acknowledgements We are highly thankful to Dr. Subhash Patel, Anand Agricultural University, India for providing the *A. solani* isolate.

References

1. FAOSTATdata,2005..[http://faostat.fao.org/faostat/form?collection=Production.Crops.Primary & Domain=Production&servlet=1&hasbulk=&version=ext&language=EN](http://faostat.fao.org/faostat/form?collection=Production.Crops.Primary&Domain=Production&servlet=1&hasbulk=&version=ext&language=EN). Last updated February 2005.
2. Datar, V.V. and Mayee, C.D. (1972). Conidial dispersal of *Alternaria solani* in tomato. *Indian Phytopathology* 35: 68-70.
3. Basu, P.K. (1974). Measuring early blight, its progress and influence on fruit losses in nine tomato cultivars. *Can Plant Dis Surv.* 54: 45-51.
4. Jones, J.B., Jones, J.P., Stall, R.E. and Zitter, T.A. eds. (1993). *Compendium of Tomato Diseases*. St Paul, Minnesota, USA: American Phytopathological Society.
5. SheRf, A.F. and MacNab, A.A. (1986). *Vegetable Diseases and Their Control*. John Wiley & Sons, New York.
6. Montemurro, N. and Visconti, A. (1992). *Alternaria metabolites – chemical and biological data*. In: Chelkowski J, Visconti A (eds) *Alternaria biology, plant disease and metabolites*. Elsevier, Amsterdam, pp 449-558.
7. Brian, P.W., Elson, G.W., Hemming, H.G. and Wright, J.M. (1952). The phytotoxic properties of alternaric acid in relation to

- the etiology of plant diseases caused by *Alternaria solani* (Ell. & Mart.) Jones & Grout. *Appl. Biol.* 39: 308-321.
8. Pound, G.S. and Stahmann, M.A. (1951). The production of a toxic material by *Alternaria solani* and its relation to the early blight disease of tomato. *Phytopathology* 41: 1104-1114.
 9. Brian, P.W., Curtis, P.J., Hemming, H.G., Jeffreys, E.G., Unwin, C.H. and Wright, J.M. (1949). Alternaric acid, a biologically active metabolic product of the fungus *Alternaria solani*. *Nature* 164: 534.
 10. Stoessl, A. and Stothers, J.B. (1984). Alternaric acid. Proof of biosynthesis via condensation of two polyketide chains. *Can. J. Chem.* 62:549-553.
 11. Matern, U., Strobel, G. and Shepard, J. (1978). Reaction to phytotoxins in a potato population derived from mesophyll protoplasts. *Proc. Natl. Acad. Sci. USA.* 75: 4935-4939.
 12. Maiero, M., Bean, G.A. and Ng, T.J. (1991). Toxin production by *Alternaria solani* and its related phytotoxicity to Tomato Breeding lines. *Phytopathology* 81:1030-1033.
 13. Grove, J.F. (1952) Alternaric acid. Part I. Purification and characterization. *J. Chem. Soc.*, 50: 4056-4059.
 14. Bartels-Keith, J.R. (1960). Alternaric acid. Part II. Oxidation. *J. Chem. Soc.*, 7: 860-866.

***National Conference on
Emerging Trends in Biotechnology &
Annual Meeting of Society for Biotechnologists (India)
(September 24-26, 2011)***

***Organized jointly by
Society for Biotechnologists (India) & Department of Biotechnology
Acharya Nagarjuna University,
Nagarjuna Nagar – 522 510 Guntur, A.P., India***

Broad Areas of Focus

Cellular and Tissue Engineering , Bionanotechnology and Protein Engineering , Genetic Engineering , Plant & Animal Biotechnology, Immunotechnology, Industrial & Environmental Biotechnology, Pollution and Human Health, Regenerative Medicine, Genomics and Proteomics, Bioinformatics, Cancer Biology and Medical Biotechnology, Herbal Medicines, Molecular Neuroscience

For further details contact

Prof. K.R.S. Sambasiva Rao
Head, Department of Biotechnology
Acharya Nagarjuna University
Guntur, A.P., India – 522 510

Phone – 0863-2346355, Email – raokrss@yahoo.in

Tool development for Prediction of pIC_{50} values from the IC_{50} values - A pIC_{50} value calculator

Chandrabose Selvaraj, Sunil Kumar Tripathi, Karnati Konda Reddy and
Sanjeev Kumar Singh*

CADD and Molecular Modeling Laboratory,
Department of Bioinformatics, Alagappa University, Karaikudi, Tamilnadu, India

*For Correspondence - skysanjeev@gmail.com

Abstract

Half maximal inhibitory concentration (IC_{50}) value measures the effectiveness of compound inhibition towards biological or biochemical utility. Quantitative measure indicates the quantity required for particular inhibitor to inhibit a given biological process (i.e. an enzyme, cell, cell receptor or microorganism) by half. Occasionally, it is also converted to the pIC_{50} scale ($-\log IC_{50}$), in which higher values indicate exponentially greater potency. These are the experimental values which are predicted and coded in Nanomolar ($nM-10^{-9}$) and micromolar ($\mu M-10^{-6}$). These IC_{50} values differs in wide range of molecules. So, there are Varsity of ranges of applications in molecular modeling techniques especially 3D-QSAR, CoMFA, CoMSIA, Pharmacophore Mapping and many more applications. So, to predict the narrow value from the experimental value, the successful formula is described here to calculate the pIC_{50} value. As of now, no tool available as open source software to provide the value of pIC_{50} from IC_{50} values as pIC_{50} calculator. In this work we developed the tool for the prediction of pIC_{50} values from the IC_{50} in nanomolar and micromolar using the JavaScript programming language, which is available at the Sanjeevslab webpage: http://www.skysanjeev.110mb.com/index.php?p=1_7_Tools

Keywords: pIC_{50} , IC_{50} , QSAR, Nanomolar, Micromolar

Introduction

In a current scenario experimental and theoretical activity is very important in understanding the effectiveness of particular compounds while developing QSAR (Quantitative Structure Activity Relationship) model in computer aided drug designing methods. QSAR modeling has been conventionally applied as an evaluative approach, i.e., with the focus on developing retrospective and explanatory models of existing data (1, 2). Here, in this paper we have developed one tool for generating the pIC_{50} values from IC_{50} values. Half maximal (50%) inhibitory concentration of a substance (IC_{50}) commonly used for measuring the antagonist drug potency in pharmacological research. Synthesis of new molecules with bioassay of respective protein evaluates the inhibitory capacity of the particular molecule response towards the protein, in terms of micromolar and nanomolar called as IC_{50} values. The potential effectiveness of drug IC_{50} , in particular concentration of complex substance to provide 50% inhibition to certain reaction (3, 4) and is universally used to symbolize the inhibitory effect of compounds on competitive binding assays with functional antagonist assays and even though

the chemical assay is prepared and evaluated. Both nanomolar and micromolar describes the same value but different due to the power of conic (5). It exhibits how much of a meticulous substance/molecule is desirable to inhibit some biological progression by 50% (6), and also the quantitative measure indicate how much, a specific drug or other core is needed to hinder a given biological process (7). It is universally used to calculate a antagonist drug potency in pharmacological study (8). It is also converted to the pIC_{50} scale ($-\log IC_{50}$) (13), in which higher values indicate exponentially greater potency (9, 10). The IC_{50} values are having variant values, which differ from one ligand to another (11), it depends on minimum effective concentration of the drug towards the diseased protein (12). These values are broad in range, for molecular modeling and pharmacological field the IC_{50} values are converted in to pIC_{50} values (13). For this purpose there is formula to convert the IC_{50} value to pIC_{50} value with representing the logarithmic values.

$$pIC_{50} = \log 1/IC_{50} \quad (1)$$

$$pIC_{50} = -\log IC_{50} \quad (2)$$

The above formula can change the IC_{50} values into wide range to pIC_{50} narrow range. But the IC_{50} values are given in nanomolar and micromolar scale (14-15) so, again the nanomolar values also should included in the pIC_{50} . So the formula again changes according to nanomolar value, this is the formula for nanomolar conversion of IC_{50} values to pIC_{50} values (16).

$$pIC_{50} = -\log IC_{50} * 10^{-9} \quad (3)$$

These 1, 2 and 3 are basic formula for the conversion of the IC_{50} into pIC_{50} value in nanomolar. The bioassay values are interpreted as different numbers, which differ from one compound to another compound even in same

assay. pIC_{50} values is changing the IC_{50} values towards interpretation for all QSAR and Pharmacophore analysis. Till date there is no software or tool is available to convert IC_{50} to pIC_{50} values. Here we have generated the script and formula to create an algorithm for pIC_{50} as web based tool, for the molecular modeling and pharmacological calculation. As of now, this is first report on conversion of IC_{50} value to pIC_{50} value as a web tool. Possibilities of generating the range of pIC_{50} values playing the theoretical role, which distinguish this from IC_{50} values.

Materials and methods

JavaScript : JavaScript allows website designers with moderate programming skills to add capabilities to their web pages, including instant user feedback, advanced form processing, pop-up windows, advanced frame applications and much more. The basic elements of JavaScript language and several techniques to take web pages to the next level, reliable coding accuracy is required in WebPages. Here we code an algorithm based on JavaScript, which are embedded with functional values, and additionally this tool will work both online and offline. `<head> <body> <script> script algorithm place here </script> </body> </html>` (17, 18).

Algorithm Coding : The algorithm has been generated using the JavaScript, with mathematical functions, using 3 formulas as nanomolar (nM) function as describe above. According to this algorithm development the input value will be accepted in nanomolar and another for micromolar only.

Implementation of the Algorithm : The algorithm developed as base of JavaScript, the above mentioned formula is detail source for developing the tool for pIC_{50} calculator based on pro-

programming script. Here, the function `ctxt()` calls the starting of program and the function codes for `xslt` register all functions.

`ctxt`: the XPath context

Apart from that call for getting the element, the input box for the entering the IC_{50} values, and the document of web pages for getting the input element, are as follows.

```
document.getElementById('ic').value = "";
document.getElementById('pic').value = "";
```

If there is no element with the given id, this function will return null value. Note, that DOM implementation must have information that says about attribute of type ID. Attributes with the name 'id' are not type ID, unless defined in the document's DTD. The 'id' attribute is defined to be ID type in the common cases of XHTML, XUL, etc. Implementation do not know whether attributes are of type ID or not, are expected to return as null value. Simply creating an element and assigning an ID, which will not make the element accessible by 'getElementById'. One needs to insert the element first into the document tree with insert before or a similar method, probably into a hidden div. Here its getting input as a IC_{50} value and finally getting the output value from the programming end, i.e., pIC_{50} value. So the input is given by the user and the output is getting from the programming index.

As input and output environment is set down, to call for function for output, functions are first-class objects, that means they can be created dynamically and stored, passed and returned just like any other value, and declaring the mathematical function math, which corresponds to `a`, (i.e., equal to formula calculation.)

```
a = Math.log(a)/Math.log(10);
a = 9 - a;
```

It determines the mathematical functions logarithmic value, which is divided by the base 10 for checking the nanomolar value. The result of

'a' is again equal to 9-a, which explicit the value of nanomolar and closing the algorithm using the language JavaScript and HTML coding. For detail of algorithm development see Fig.1 which represents the flowchart for conversion of IC_{50} value to pIC_{50} value in nanomolar.

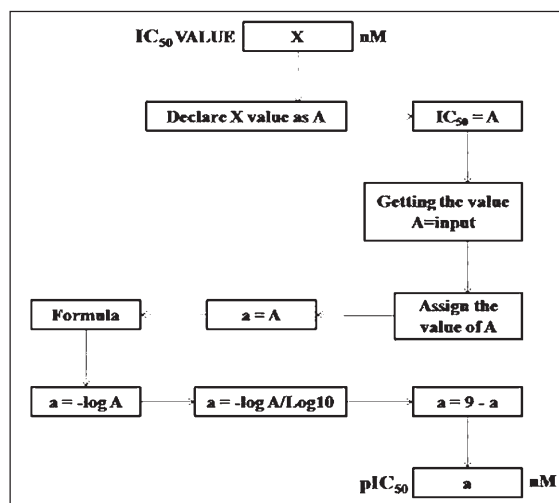


Fig.1. Representing the flowchart for conversion of IC_{50} value to pIC_{50} value in nanomolar.

Getting the value from user, the algorithm considers the values as X (unknown values in decimal event), then accessing the value of $X=A$, here the A is consider the decimal event IC_{50} . Backend of algorithm accessed with $(a=-\log A)$, here the conversion of A value to logarithmic value of decimal event take place with the base value of log10. The power of conic set with negative value of 9 for nanomolar and negative value of 6 for micromolar, so that power of conic, subtracted with value displayed as value of pIC_{50} . This algorithm is kept in web based 110mb server in Sanjeevslab domain namely and the webpage are constructed with the PHP coding.

Results and Discussion

At some stage in molecular modeling studies (e.g. ligand based drug design) there are

much use of IC_{50} to pIC_{50} value conversion. We can convert IC_{50} value to pIC_{50} value which is developed by using JavaScript and HTML, and is placed in website of Sanjeevslab. The script for the pIC_{50} calculator has been developed for prediction of pIC_{50} value with IC_{50} value units of nanomolar and micromolar. Here (Fig. 2) the background information of the program showing the mathematical calculation of pIC_{50} value. The IC_{50} value of compound staurosporine, which is known to have anti-fungal activity of 2.7nM (16), is given in pIC_{50} calculator. Here, the 2.7 as input value is get through the 'document.getElementById('ic').value = "";' declaring this input value as *var a* for the calculation of pIC_{50} value. During this calculation the log value of 2.7 to the base10 is calculated as 0.431363764, but the IC_{50} value is in nanomolar. There is again need of conversion with respect to the nanomolar, so it is subtracted with 9. Finally the logarithmic value is converted in nanomolar and finally the pIC_{50} value is calculated as 8.56863 (Fig. 2). In this algorithm development of pIC_{50} calculator with combined approach of JavaScript and HTML having a potential to find out accurate pIC_{50} value. This pIC_{50} value calculator will be helpful for quick validation of next generation drug discovery and development against drug target. The *in vitro*

pIC₅₀ Calculator
 Selvaraj.C, Sunil K.Tripathi, K.K.reddy, Sanjeev Kumar Singh*
 Department of Bioinformatics, Alagappa University, Karaikudi. 630003, India.

Conversion of IC₅₀ - pIC₅₀ Calculator: Nano molar

IC₅₀value :

pIC₅₀value :

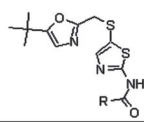
For Example : 1.2 (nM)

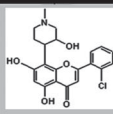
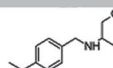
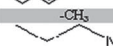




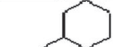


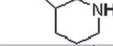




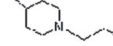

The pIC₅₀ value predicted is 8.920818753952375

Note: The IC₅₀ value you are entering it should be in Nanomolar (nM)

If you use this PIC₅₀ calculator Please Cite us.

Fig.2 Representing the output IC_{50} value to pIC_{50} values through pIC_{50} Calculator.



R-attachment	IC ₅₀ (nM)	pIC ₅₀ (Reference Value)	pIC ₅₀ (Calculator)
	330	6.4	6.481486060122113
	3	8.5	8.522878745280337
	5	8.3	8.301029995663981
	21	7.6	7.677780705266080
	3	8.5	8.522878745280337
	26	7.5	7.585026652029182
	50	7.3	7.301029995663981
	300	6.5	6.522878745280337
	50	7.3	7.301029995663981
	83	7.0	7.080921907623926
	11	7.9	7.958607314841775
	48	7.3	7.318758762624412
	43	7.3	7.366531544420414
	74	7.1	7.130768280269024
	18	7.7	7.744727494896694
	22	7.6	7.657577319177793
	150	6.8	6.823908740944319

biological activity data reported in form of IC_{50} value for inhibition of CDK2 by two series of aminothiazole derivatives was used for this validation. According to work by Singh *et al.*, (19) pIC_{50} values of Aminothiazole Derivatives from IC_{50} values was manually calculated and in this paper initial IC_{50} data obtained from the synthesized Aminothiazole Derivatives by Misra *et al.* (20) (Table 1. & Fig 3).

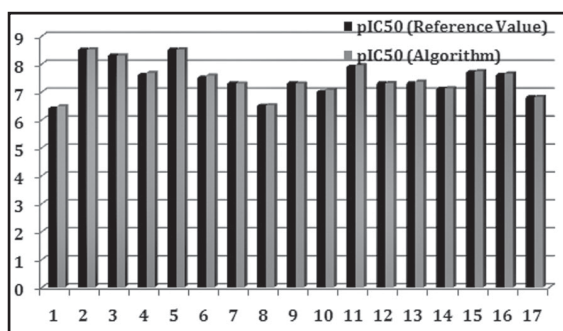


Fig. 3 Representing the resemblance of calculated pIC₅₀ value manually and with pIC₅₀ calculator

These values are analyzed for calculation and accuracy of the algorithm are tabulated. The values published as pIC₅₀ value are accurate and clear decimal values are obtained; both the values are differentiated in bar diagram, which shows that developed algorithm is accurate. (Table 1) and contains 17 synthesized ligand compound, represented in *Singh et al.* The bar diagram enclosed, represents the correctness and similarities in values which is predicted by the pIC₅₀ calculator and manually. Here the values are more accurate due to the programming algorithm and gives the value up to 10 decimal points. Bar diagram shows correlation with available values without much deviations, which shows predicted pIC₅₀ values are accurate and can be used further for other calculation and prediction in computer aided drug designing. Thus, the algorithm is much useful for drug designing community and user can minimize their time for calculations, especially those who are working with large data set related to pharmacoinformatics and chemoinformatics.

Acknowledgements

Authors are kindly acknowledging 110mb server for hosting the webpage and pIC₅₀ calculator and one author Chandrabose Selvaraj thankfully acknowledging Alagappa University for research fellowship.

References

1. Tropsha, A and Golbraikh, A., (2007) Predictive QSAR modeling workflow, model applicability domains, and virtual screening. *Curr Pharm Des.* 13:3494-504.
2. Dixon, S.L., Smondyrev, A.M., Knoll, E.H., Rao, S.N., Shaw, D.E and Friesner, R.A., (2006) PHASE: a new engine for pharmacophore perception, 3D QSAR model development, and 3D database screening: 1. Methodology and preliminary results. *J Comput Aided Mol Des.* 20:647-71.
3. Lyles, R. H., Poindexter, C., Evans, A., Brown, M. and Carlton R. Cooper. (2008). Nonlinear model-based estimates of IC₅₀ for studies involving continuous therapeutic dose-response data. *Contemporary Clinical Trials*, 29: 878-886.
4. Yung-Chi, C. and Prusoff, W. H. (1973). Relationship between the inhibition constant (KI) and the concentration of inhibitor which causes 50 per cent inhibition (I₅₀) of an enzymatic reaction. *Biochemical Pharmacology.* 22: 3098-3108.
5. Whitebread, S., Hamon J., Bojanic, D. and Urban, L. (2005). Keynote review: *In vitro* safety pharmacology profiling: an essential tool for successful drug development. *Drug Discovery Today*, 10: 1421-1433.
6. Joshi, K.A., Patil D.D. and Gejji S.P. (2009). Molecular electrostatic potentials in aromatic substituted 4-hydroxyquino-2-lones: Glycine/ NMDA receptor antagonists. *Journal of Molecular Modeling.* 15: 383-390.
7. Toutain, P-L. (2002). Pharmacokinetic/ pharmacodynamic integration in drug development and dosage-regimen optimization for veterinary medicine. *The AAPS Journal.* 4: 160-188.
8. Stahl, M., Guba, W. and Kansy, M. (2006). Integrating molecular design resources within

- modern drug discovery research: the Roche experience. *Drug Discovery Today*, 11:326-333.
9. Dessalew, N. and Singh S.K. (2008). 3D-QSAR CoMFA and CoMSIA study on Benzodipyrzoles as Cyclin Dependent Kinase 2 Inhibitors. *Medicinal Chemistry*. 4: 313-321.
 10. Lu, X.Y., Chen, Y.D., Sun, N.Y., Jiang, Y.J. and You, Q.D. (2010). Molecular-docking-guided 3D-QSAR studies of substituted isoquinoline-1,3-(2H,4H)-diones as cyclin-dependent kinase 4 (CDK4) inhibitors. *Journal of Molecular Modeling*. 16: 163-173.
 11. Herve, F., Caron, G., Duche, J-C., Gaillard, P., Abd Rahman, N., Tsantili-Kakoulidou, A., Carrupt, P.A., Dathis, P., Tillement, J.P. and Testa, B. (1998). Ligand Specificity of the Genetic Variants of Human α 1-Acid Glycoprotein: Generation of a Three-Dimensional Quantitative Structure-Activity Relationship Model for Drug Binding to the A Variant. *Molecular Pharmacology*. 54: 129-138.
 12. Gianazza, L., Eberini, I., Villa, P., Fratelli, M., Pinna, C., Wait, R., Gemeiner, M. and Miller, I. (2002). Monitoring the effects of drug treatment in rat models of disease by serum protein analysis. *Journal of Chromatography B: Analytical Technologies in the Biomedical and Life Sciences*, 771: 107-130.
 13. Singh, S.K., Dessalew, N and Bharatam, P.V. (2006). 3D-QSAR CoMFA study on indenopyrazole derivatives as cyclin dependent kinase 4 (CDK4) and cyclin dependent kinase 2 (CDK2) inhibitors. *European Journal of Medicinal Chemistry*, 41: 1310-1319.
 14. Kulkarni, R.G., Srivani, P., Achaiah G. and Sastry, G. N. (2007). Strategies to design pyrazolyl urea derivatives for p38 kinase inhibition: a molecular modeling study. *Journal of Computer-Aided Molecular Design*, 21(4): 155-166.
 15. Chung, J.Y., Chung, H. W., Cho, S. J., Hah, J.M. and Cho, A. E. (2010). QM/MM based 3D QSAR models for potent B-Raf inhibitors. *Journal of Computer-Aided Molecular Design*, 24(5): 385-397.
 16. Goodman, D., Morrison, M. (2004) *Java Script Bible* (6th edition), John Wiley, USA.
 17. Powell, T.A and Schneider, F. (2004) *JavaScript: the complete reference* (2nd edition), McGraw-Hill, USA.
 18. Tamaoki, T., Nomoto, H., Takahashi, I., Kato, Y., Morimoto, M. and Tomita, F. (1986). Staurosporine, a potent inhibitor of phospholipid/Ca⁺⁺dependent protein kinase. *Biochemical and Biophysical Research Communications*, 135: 397-402.
 19. Dessalew, N., Bharatam, P. and Singh, S.K. (2007), 3D-QSAR CoMFA Study on Aminothiazole Derivatives as Cyclin-Dependent Kinase 2 Inhibitors. *QSAR & Combinatorial Science*, 26: 85-91.
 20. Raj, N. Misra., Hai-yun. Xiao., Kyoung. S. Kim., Songfeng. Lu., Wen-Ching. Han., Stephanie. A. Barbosa., John. T. Hunt., David. B. Rawlins., Weifang. Shan., Syed. Z. Ahmed., Ligang. Qian., Bang-Chi. Chen., Rulin. Zhao., Mark. S. Bednarz., Kristen. A. Kellar., Janet. G. Mulheron., Roberta Batorsky., Urvashi. Roongta., Amrita. Kamath., Punit. Marathe., Sunanda. A. Ranadive., John. S. Sack., John. S. Tokarski., Nikola. P. Pavletich., Francis. Y. F. Lee., Kevin. R. Webster and S. David. Kimball. (2002). N-(Cycloalkylamino)acyl-2-aminothiazole Inhibitors of Cyclin-Dependent Kinase 2. N-[5-[[[5-(1,1-Dimethylethyl)-2-oxazolyl]methyl]thio]-2-thiazolyl]-4-piperidinecarboxamide (BMS-387032), a Highly Efficacious and Selective Antitumor Agent. *J. Med. Chem.* 47, 1719-1728.

Formulation, Characterization and Pharmacokinetic Studies of Carvedilol Nanoemulsions

Koteswari Poluri¹, Ramakrishna Sistla², Prabhakar Reddy Veerareddy^{*3},
Lakshmi M. Narasu⁴, Amol A Raje⁵ and Sunder M. Hebsiba⁵

¹S. N. Vanitha Pharmacy Maha Vidyalaya, Nampally Exhibition Grounds, Hyderabad, A.P, India

²Indian Institute of Chemical Technology, Tarnaka, Hyderabad, A.P, India

³St. Peter's Institute of Pharmaceutical Sciences, Hanamkonda, Warangal, A.P, India

⁴ Centre for Biotechnology, Jawaharlal Nehru Technological University, Hyderabad, A.P, India

⁵Vimta labs Ltd., 5, S.P.Biotech Park, Shameerpet, Hyderabad, A.P, India

*For Correspondence - vpreddyindia@yahoo.com

Abstract

The present study involves the formulation and evaluation of oral o/w nanoemulsions (NE) with two simple edible oils, avoiding the large quantities of surfactants and co-surfactants which were prepared by high energy emulsification technique. The particle size, polydispersity index (PDI), and zeta potential of prepared nano emulsions were determined by using zeta sizer and were found to be in the range of 33.4±3.9 nm, to 183.56±1.78nm, 0.051±0.04 to 0.38±0.06 and -2.87±0.65 to -14.2±0.72 mv respectively. Centrifugation, freeze-thaw cycling, storage at 4°C for 60days, X-ray diffraction (XRD) and Transmission electron microscopy (TEM) studies revealed the physical and chemical stability of the NEs. Entrapment efficiency and in-vitro release studies showed successful incorporation of carvedilol into NE with high drug loading efficiency and good stability. Comparative pharmacokinetic studies of NE and marketed dosage form in male SD rats revealed a significant increase in oral bio availability in NEs.

Key words: Nano emulsions, Sesame oil, Olive oil, Carvedilol, Sonication, LC-MS/MS

Introduction

Nano technology has emerged as one of the very promising fields of biomedical research in the last few decades. Nano technology based

health care products will expected to reach 2 trillion dollars target by the year 2015(1). Nano emulsion technology is one of the segments of nano technology market and can be defined as thermodynamically stable, transparent or translucent dispersions of oil and water having a size range of 50-200 nm (2).

Different types of oils and components can be used for the preparation of NEs to impart specific properties such as crossing different types of biological barriers like blood brain barrier upon administration (3). NEs can also be used as excellent vehicles in pharmaceutical field for the parenteral, oral and ocular or transdermal delivery of poorly permeable lipophilic drugs. Because of these unique properties, nano emulsions are gaining more importance as potential vehicles for the efficient delivery of lipophilic drug molecules (3, 4, 5).

Cardiovascular diseases including hypertension are one of the major causes of mortality in the world. Delivery of therapeutic agents to cardiac organelles has the potential to increase the efficiency of treatment protocols for heart failure. However, cardiac cells present special problems to the delivery of drugs, and the number of papers reported in this area is also a very few (6). Carvedilol was selected for the present study. It is a non selective beta adrenergic

blocking agent and widely used in the treatment of mild to moderate hypertension and angina pectoris. It has antioxidant and anti proliferative properties which makes it suitable to combat the deleterious effects of sympathetic nervous system activation in heart failure. It undergoes extensive first pass metabolism and its systemic bio availability is only 25 to 35% (7). As per Biopharmaceutical classification it belongs to class II compound and therefore it is insoluble in aqueous medium (8). Certain strategies such as fast dissolving tablets (9), muco adhesive drug delivery systems (10), self emulsifying drug delivery systems (11) and other controlled release systems (12, 13) were reported to improve the aqueous solubility, to overcome first pass metabolism and thereby increase the systemic bioavailability. But these technologies require unique production processes and also have certain disadvantages like limited formulation flexibility and complexity in manufacturing, high production costs, low stability, low drug loading and few choices of dosage forms.

The objectives of present study are to investigate the feasibility of development of o/w NEs loaded with carvedilol using sesame oil or olive oil by high energy homogenization technique, to study the effect of oil phase volume on the drug loading efficiency, particle size and zeta potential, to study the effect of concentration and type of surfactants on the globule size, zeta potential and in-vitro drug release characteristics and to carry out the comparative pharmacokinetic study of optimized nano emulsion with marketed tablet dosage-form in rats.

Materials and Methods

Materials: Carvedilol was a gift sample from Orchid Pharmaceuticals, India. Brij-97, Tween-80, dialysis tubing cellulose membrane (size: 43 mm × 27 mm) were purchased from Sigma

Aldrich, USA. Sesame oil was purchased from Thiagarajan Agro Products Pvt Ltd., Chennai, India. Olive oil was purchased from Figaro, Sri Roda Foods Pvt Ltd., New Delhi India. All other chemicals, water and solvents are of HPLC grade and purchased from S.D. Fine Chemicals, India.

Preparation of carvedilol nano emulsion : Various Carvedilol NEs were prepared by using high energy emulsification technique. Prior to emulsification the oil phase and aqueous phase were prepared separately.

A specified quantity of oil was taken in a beaker and 6.3 mg of drug was added and the total weight of the oil phase was determined. To this 200 µl of chloroform was added to dissolve the drug in oil. Then nitrogen gas was purged to evaporate the chloroform. This was confirmed by reweighing oil phase.

Aqueous phase was prepared by dissolving the non-ionic surfactant in HPLC grade water pH-6.8±0.2. A volume of this surfactant solution was added and a coarse emulsion was prepared by using a high shear stirrer (RQ-127A, Remi Motors, India) for 25 min at 6000 rpm. Then the coarse emulsion was subjected to high energy emulsification using a probe sonicator (Bandelin Sonoplus, Heinrichstrab 3-4 D-12207, Berlin, Germany) in a continuous mode at 37 to 40 HZ.

NEs were prepared using 100 µl of sesame oil and non-ionic surfactants Brij-97 or tween-80. Then various formulation parameters such as oil phase volume (100, 150 and 200 µl) and concentration of each surfactant (1.25, 1.5 and 1.75) were optimized for particle size, zeta potential and drug loading efficiency. The procedure was repeated for the preparation and optimization of carvedilol loaded olive oil nanoemulsions.

Preparation of Carvedilol tablet suspension :

The various pharmaco kinetic parameters of carvedilol NE formulation were compared with carvedilol extended release oral tablet (Cardivas, Sun Pharma, India) suspension in order to compare the oral bioavailability of carvedilol by NE formulation with tablet suspension. One tablet containing 10mg of carvedilol was taken and crushed into powder in a mortar and pestle. To this 19.2 ml of 1 % tween-80 solution was added and triturated to prepare a fine suspension with strength of about 0.52mg/ml.

Characterization of Nanoemulsions

Measurement of particle size and zeta potential:

The average particle size, poly dispersity index (PDI), and Zeta potential were measured by photon correlation spectroscopy (PCS) using a Malvern zeta sizer (Nano ZS Malvern Instruments Ltd., UK). The PDI represents the uniformity of the globule size and size distribution of the NE. The prepared formulations were diluted with HPLC grade water pH-6.8±0.2. The diluted NEs were kept in the cuvette with an attached dip cell. The cuvette was placed inside the instrument and the observations were recorded at 90° light scattering angle and temperature was maintained at 25 °C. During the measurement, average particle count rate was maintained between 50 to 500kcps. The zeta potential was also measured by using the same instrument with inbuilt software based on the electrophoretic mobility of globules and the Helmholtz-Smoluchowski equation (14, 15, and 16).

Helmholtz-Smoluchowski equation (Zeta potential (Z_p) = $6\pi\eta/\epsilon\chi$) Where Z_p is in volts, v = migration velocity cm/sec, η = viscosity of the medium in poise, ϵ = dielectric constant of the external medium, and χ = potential gradient in volts. Average size, poly dispersity index (PDI) and zeta potential were measured for all samples

using particle sizer Nano ZS (Malvern Instruments, UK).

HPLC analysis: A simple HPLC method was developed in the laboratory with a Phenomenex P/N0-00G-4274-EO C-18, Luna 5 μ , Size column on liquid chromatograph (Shimadzu-10ATVP) and a UV/visible detector (SPD-10ATVP). The mobile phase was Acetonitrile:0.01M phosphate buffer(pH-5.2±0.02) in the ratio of 69:31, at a flow rate of 1ml/min and the effluent was monitored at 242nm.

Solubility studies: Solubility studies of carvedilol were carried out in water, phosphate buffer saline pH 7.4 and Phosphate buffer saline containing 1% tween 80 in order to select the diffusion medium to perform *in-vitro* release studies. A volume of water or phosphate buffer saline pH 7.4 or Phosphate buffer saline containing 1% tween 80 was taken in to a conical flask. Excess quantity of carvedilol was added and shaken for 2 hrs on a mechanical shaker and kept aside for overnight. Then the solution was centrifuged. The supernatant liquid was taken, filtered, sonicated and appropriate dilutions were made and 20 μ l quantities were injected into HPLC.

Determination of carvedilol content in the formulations:

A volume of formulation was taken from the bulk and made up to 5ml with methanol. From this appropriate dilutions were made with phosphate buffer saline pH 7.4. Then filtered, degassed and 20 μ l was injected in to HPLC. The analysis was carried out by the above described HPLC method. The total drug content was calculated from the calibration curve $y = 83.106+0.9715(R^2 = 0.9993)$.

In vitro drug release studies: The in vitro drug release studies of carvedilol were carried out using dialysis bag diffusion technique (43mm x 27mm size, mol. wt. cutoff 12000 or greater, Sigma-Aldrich, USA). The bag containing 2ml of

NE was placed and immersed in a 50 ml beaker containing 25ml of phosphate buffer saline pH 7.4 containing 1% tween 80. The entire system was kept at $37^{\circ}\text{C}\pm 0.5^{\circ}\text{C}$ with continuous magnetic stirring. The samples were withdrawn at periodical time intervals (0min, 15min, 30min, 1, 2, 4, 6, 8 and 24 hrs) and replaced with equal volume of fresh medium to maintain sink conditions. The samples were filtered through $0.22\ \mu$ membrane filter, degassed in a bath sonicator (Spincotech, India) and injected in to HPLC column. HPLC analysis was carried out by the above mentioned method. All experiments were performed in triplicate (17).

X-ray diffraction: X-ray diffraction studies were carried out for the formulations that were stable in thermodynamic stability studies (C4, C7, C14 and C17) by using Siemens D-5000 (Germany). XRD studies performed on the samples by exposing them to $\text{CuK}\alpha$ radiation (40Kv, 30mA) and scanned from 10° to 80° , 2θ at a speed of 2° per minute.

Transmission electron microscopy (TEM): Transmission electron microscopic studies were conducted for the formulation C14. The globule size and morphology were observed with TEM analysis. The samples were placed on Formvar-coated copper grid. Then the samples were negatively stained with $50\ \mu\text{l}$ of 2% phospho tungstic acid for one minute and air dried. Excess liquid was blotted with whatman filter paper. Then the samples were observed under Philips TECNAI – FE12 Transmission Electron Microscope (120 kV) (18).

In-vivo Pharmacokinetic analysis: Based on physicochemical properties (Table 2) and *in-vitro* release studies (Fig 2A and 2B) C14 was selected and comparative pharmacokinetic studies were carried out with marketed carvedilol tablet (Cardivas, Sun Pharma, India). The experimental protocol was approved by Institutional Animal

Ethics Committee (Vimta Labs, Hyderabad). Study number: VLL/0510/NG/D017. Male Sprague Dawly rats of approximately 6-8 weeks of age weighing between 200 and 240gms were purchased from, National Institution of Nutrition (NIN), Hyderabad, India. The animals were acclimatized for a period of 5 days. All the rats had free access to reverse osmosis generated potable water and standard animal diet. Throughout the study period, room temperature and relative humidity were maintained at $20^{\circ}\text{C}\pm 2^{\circ}\text{C}$ and 30% to 70% RH respectively. Illumination was controlled to give 12 hrs dark cycles during the 24hrs period.

Overnight fasted rats were used for the study. Prior to the initiation of the study rats were weighed for the body weights. Twelve rats were randomized based on their body weights and distributed equally into 2 groups. One group of rats received carvedilol tablet suspension and another group of rats received carvedilol nano emulsion. Both the formulations were administered by oral gavage at the dose equivalent to 2.5mg/Kg of carvedilol. The dose volume administered was 4.8ml/kg body weight. Following oral administration approximately 0.3ml of blood samples were collected after anaesthetizing with isolorane from a group of 3 animals per time point from respective group at respective time intervals that is pre-dose (0), 5min, 0.25, 0.5, 1, 2, 4, 6, 8 and 24hrs post dosing from retro-orbital plexus in pre-labelled eppendorf tubes containing $20\ \mu\text{l}$ of 10% K2EDTA. The blood samples collected as pre-dose at (0) time were taken as control.

Analysis of blood samples: A volume of study sample and calibration curve samples and quality control samples were transferred to the pre-labeled ria vials, add $10\ \mu\text{l}$ of ISTD ($4\ \mu\text{g}/\text{ml}$ felodipine) and vortex, 2.5 ml of Tertiary Butyl Methyl Ether (TBME) was added to all the samples. These vials were placed on a shaker

for 10 minutes and centrifuged for 10 minutes at 4000 rpm at 20°C and supernatant was transferred in to pre-labeled ria vial and evaporated under a stream of nitrogen at 35°C until dryness, reconstituted the dried residue with 400µl of mobile phase and vortexed. Samples were loaded in to pre-labeled auto-injector vials and 10 µl of samples were injected onto LC-MS/MS system containing HPLC (AGILENT 1200 series (VLS-UTL/HPLC/01) and Mass spectrophotometer (AB MDS Sciex 4000, VLS-UTL/MASS/01) with a Column of Hypurity Advance, 100 X 4.6mm, 5µ. The column oven temperature was maintained at 40°C and the mobile phase was 0.1% Formic acid: Acetonitrile (25:75 v/v) with a flow rate of 0.6ml/min and an injection volume of 10µl. The separation was conducted under isocratic conditions, and the total run time was within 4minutes. The electron spray ionization was performed in the selected ion monitoring mode. The detection ions were at mass-to-charge ratios m/z of 407.3 amu (parent) to 222.1 amu (product) and 384.1 amu (parent) to 338.1 amu (product) for carvedilol and internal standard felodipine respectively. The chromatograms were evaluated by analyst 1.4.2 version software and the concentration of carvedilol was calculated. Then the pharmacokinetic parameters were calculated by non-compartmental analysis by winn online^(R) 5.2 software.

Statistical analysis: The pharmacokinetic parameters of the olive oil nano emulsion and marketed tablet suspension were compared by the student t-test. A p-value of less than 0.05 was considered as statistically significant.

Results

Nano emulsions loaded with carvedilol were successfully prepared by using high energy emulsification technique.

Optimization of oil phase volume and surfactant concentration: Based on literature survey and oil water partition coefficient studies sesame oil and olive oil were selected as sole lipid phase. To determine the optimum content of oil for the preparation of stable and high drug loaded NEs, different volumes of (100,150 and 200 µl) sesame or olive oil with 6.3 mg of carvedilol were taken. Brij 97 and Tween 80 were used as surfactants. In order to determine the optimum surfactant type and concentration NEs were prepared with 1, 1.25, 1.5 and 1.75% w/v of each surfactant. Globule size, ZP and PDI were measured for all the NEs as described above. The composition of all the NEs was given in the Table 1.

Characterization of carvedilol nano emulsions:

The physical properties such as globule size, PDI and zeta potential are essential parameters in predicting the physical stability of nano emulsions. The mean globule sizes of nano emulsions were in the range of 33.4±3.9 to 183.56±1.78nm and the PDI of nano emulsions were in the range of 0.07±0.08 to 0.35±0.026 which shows a narrow globule size range and size distribution in all formulations. All the carvedilol loaded nano emulsion formulations had zeta potentials between -2.87±0.65 to -14.18±0.72mv. These results were lower than the reported value of above 30 mV in stable parenteral emulsions, which suggests that the prepared formulations were more stable. All the characterization parameters were shown in the Table 2 and the effect of oil phase volume was shown in Fig.1.

Determination of drug content and In-vitro drug release studies:

Drug content was determined in the formulations which showed narrow particle size and polydispersity and found to be in the range of 43.81±2.68 to 98.93±1.31. *In - vitro* drug release studies were carried out in phosphate buffer saline pH 7.4 (PBS) containing

Table 1. Composition of Carvedilol loaded nano emulsions.

Code	Volume of oil phase (ml)		Quantity of surfactant (mg)		Volume of aqueous phase (ml)
	Sesame oil	Olive oil	Brij 97	Tween 80	
C1	100	-	150	-	10
C2	150	-	150	-	10
C3	200	-	150	-	10
C4	150	-	125	-	10
C5	150	-	175	-	10
C6	100	-	-	150	10
C7	150	-	-	150	10
C8	200	-	-	150	10
C9	150	-	-	125	10
C10	150	-	-	175	10
C11	-	100	150	-	10
C12	-	150	150	-	10
C13	-	200	150	-	10
C14	-	150	125	-	10
C15	-	150	175	-	10
C16	-	100	-	150	10
C17	-	150	-	150	10
C18	-	200	-	150	10
C19	-	150	-	125	10
C20	-	150	-	175	10

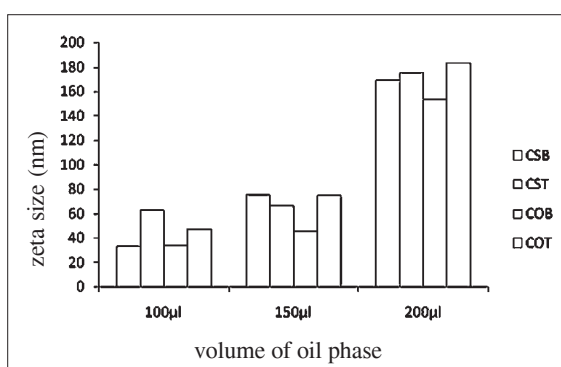


Fig.1. Effect of oil phase volume on particle size of nano emulsions ^a C, S, O, B and T represents the carvedilol, Sesame oil, Olive oil, Brij 97 and Tween 80 respectively.

1% tween 80 for the formulations (C14, C4, C7 and C17) that showed maximum drug loading and narrow globule size and narrow PDI . The *in-vitro* drug release profiles for the formulations C14, C4, C7 and C17 were shown in Fig-2A and 2B. The cumulative amount released was $63.68 \pm 0.8\%$, $31.8 \pm 3.0\%$, $27.56 \pm 9.2\%$, and $38.04 \pm 5.9\%$ in formulations C14, C4, C7 and C17 respectively. Plots of log % drug remaining against time were linear which indicates that the rate of drug release follows first order kinetics.

X-ray diffraction studies: X-ray diffraction studies were carried out to reveal the crystalline modification of the drug during preparation of nano

Table 2. Particle size, zeta potential, polydispersity index and % drug content measurements of optimized carvedilol nano emulsions.

Code	Particle size	Polydispersity (nm)	Zeta potential	%drug content (mv)
C1	33.4±3.9	0.248±0.05	-7.45±0.56	50.07±0.8
C2	75.74±0.92	0.07±0.08	-6.6±0.54	89.27±0.72
C3	169.63±1.4	0.285±0.04	-6.8±0.27	91.22±0.46
C4	97.77±0.9	0.116±0.07	-6.45±0.46	91.92±0.9
C5	67.75±1.58	0.37±0.02	-6.67±0.68	85.89±1.32
C6	63.09±1.19	0.176±0.02	-2.87±0.65	30.19±0.43
C7	66.58±1.54	0.188±0.06	-4.09±0.78	87.63±1.14
C8	175.29±6.9	0.31±0.029	-7.04±0.29	87.94±0.68
C9	69.45±9.42	0.28±0.063	-6.04±0.42	89.16±0.74
C10	75.54±1.07	0.051±0.04	-9.04±0.16	87.72±1.7
C11	34.45±1.167	0.31±0.01	-4.53±0.3	51.1±1.56
C12	45.49±0.73	0.326±0.04	-6.84±0.41	77.91±1.58
C13	153.76±2.72	0.33±0.02	-10.37±1.69	88.69±2.04
C14	54.18±0.37	0.12±0.04	-14.18±0.72	98.93±1.31
C15	38.81±1.32	0.36±0.03	-13.26±0.34	98.20±0.6
C16	47.38±1.61	0.26±0.02	-6.35±0.6	43.81±2.68
C17	75.21±1.8	0.38±0.06	-5.7±0.36	89.47±1.15
C18	183.56±1.78	0.35±0.026	-7.78±0.44	89.94±1.38
C19	61.47±4.21	0.31±0.025	-4.49±1.62	87.25±1.69
C20	60.73±0.54	0.251±0.04	-5.69±1.62	88.47±0.57

Data represents mean ± standard deviation (n=3)

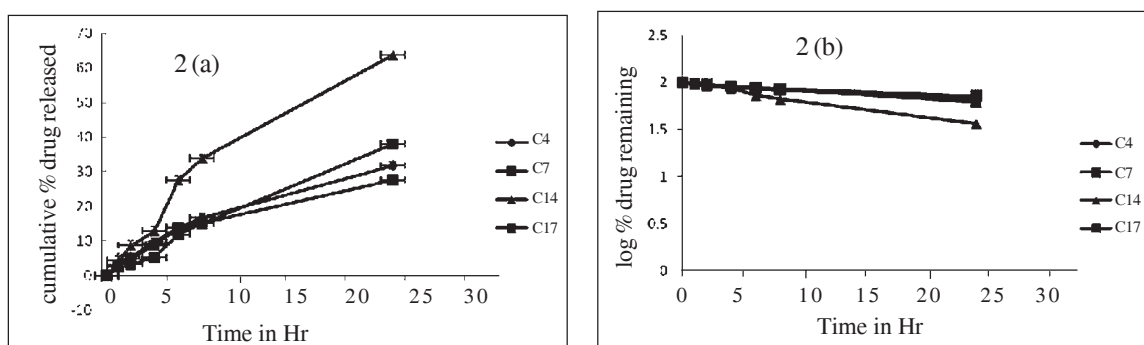


Fig. 2A and 2B. In-vitro drug release profiles

emulsions. The formulations C4, C14 and C17 did not show any kind of crystallinity which suggests that the drug molecules were in amorphous state. But in case of formulation C7 two peaks appeared in right angles. This may be due to the re-crystallization of the drug. The results were shown in Fig.3.

Transmission electron microscopy:

Transmission electron microscopic studies were carried out for the formulation C14 to observe the physical properties of NE droplets. Transmission electron micrographs revealed that the droplets were spherical, homogeneous and no signs of precipitation. The droplet size was correlated with the results from particle size analysis using zeta sizer. All these results were presented in Fig.4.

Pharmacokinetic studies: The plasma concentration vs time profiles of the carvedilol NE and carvedilol tablet suspension after administration of a single dose of 2.5mg/kg body weight were shown in Fig.5. The pharmacokinetic parameters were computed by non compartmental analysis using winN online software and the results were summarized in the Table 3. The NE was more effective in enhancing oral absorption and availability of carvedilol in the plasma. The average plasma concentrations of carvedilol were 70.07 ± 8.90 and 39.59 ± 5.78 after 1 hour following oral administration of NE and tablet suspension respectively. Plasma concentration of carvedilol when administered with the NE remained higher than with the tablet suspension for up to 6hrs. Significantly higher C_{max} , AUC and AUMC values were observed in case of NE compared to tablet suspension. MRT, T_{max} and $t_{1/2}$ values of carvedilol with NE were comparable with that of oral tablet suspension. Mean T_{max} values were 0.5 hours in case of NE and 0.67 ± 0.29 hours in case of tablet. There was no significant difference in $t_{1/2}$. All these results

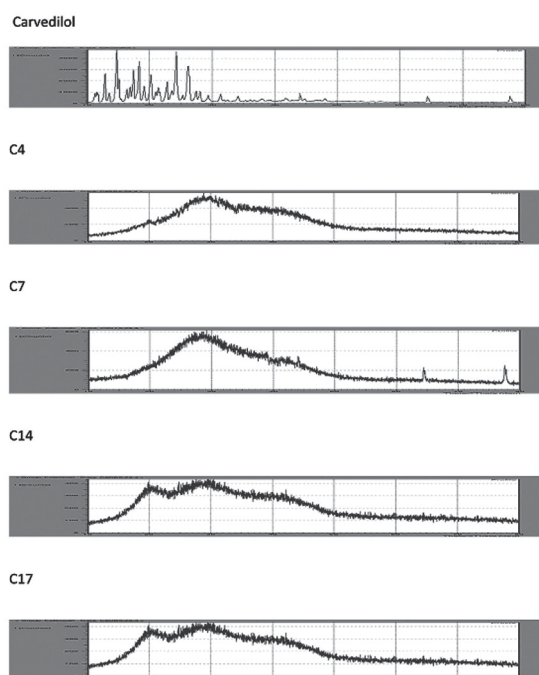


Fig.3. X-ray diffraction reports of standard drug Carvedilol and the nano emulsions (C4, C7, C14 and C17) loaded with carvedilol.

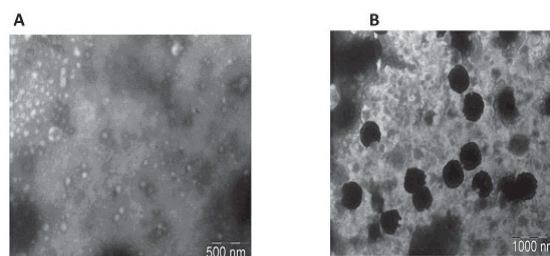


Fig.4. Transmission electron micrographs of the formulation C14 blank (A) and carvedilol loaded (B) nano emulsions. The scale bar represents a distance of 500nm in Picture (A), 1000 nm in picture (B).

revealed that the extent of oral absorption and bioavailability of carvedilol was significantly increased from oral nano emulsion compared with the tablets.

Discussion

Several drugs and dosage forms available for the treatment of hypertension, the mortality

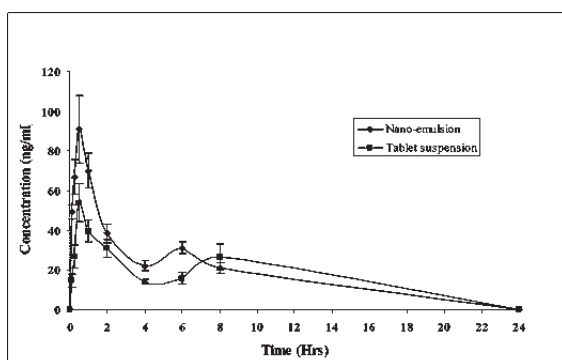


Fig. 5. Plasma concentration of carvedilol after oral administration of nano emulsion and oral tablet suspension (n=3).

rate is high in the world and over one million people per year suffer adverse reactions from doctor prescribed drugs. Carvedilol is a α_1 , β_1 and β_2 adrenergic receptor antagonist. It is indicated for the management of mild to moderate essential hypertension. In addition carvedilol is proven, with chronic treatment, to reduce cardiovascular mortality and improve survival in patients with systolic dysfunction after myocardial infarction. However, because of its poor aqueous solubility and extensive first pass metabolism many of the current dosage forms do not provide adequate drug concentration in the blood. As such there is a critical need to develop a novel drug delivery

Table 3. Pharmacokinetic parameters after oral administration of carvedilol nano emulsion (Formulation C14) and carvedilol oral tablet suspension

Parameter	Nano emulsion	Oral tablet suspension
	Mean±SEM	Mean±SEM
C max (ng/ml)	90.99±17.06	58.57±5.59
T max (hrs)	0.5±0.00	0.67±0.17
K e l (hrs)	0.17±0.02	0.11±0.05
T1/2 (hrs)	4.2±0.54	4.46±0
AUC0-t (ng*hr/ml)	291.76±18.99	190.13±9.07
AUMC	907.48±36.50	649.61±76.31
MRT	3.12±0.08	3.4±0.26

Each value represents mean±SD, n=3

system of carvedilol to enhance solubility, permeability and oral bioavailability. Lymphatic delivery is an alternate choice to avoid first pass metabolism in drug delivery and improves bio-availability, because intestinal lymph vessels drain directly into thoracic duct, further in to the venous blood, thus by passing the portal circulation. Main function of lymphatic system is to facilitate

absorption of long chain fatty acids via chylomicron formation. Lipid based formulations such as nano emulsion may enhance oral drug absorption by lymphatic transport via transcellular path way, by increasing gastrointestinal membrane permeability or transit time or by modifying the metabolism of drug. In this study the potential of oral carvedilol administration using oil in water nanoemulsion systems was examined.

In the present study the influence of oil type, quantity of oil, type and concentration of surfactant on particle size, zeta potential and loading efficiency were studied by using photon correlation spectroscopy, HPLC with UV detector. An essential component of the emulsion is the internal lipid core which constitutes the drug dissolved in oil and is surrounded by a thin layer of non-ionic surfactant. Sesame and olive oils are of vegetarian origin, bio-compatible and being used as edible oils from ancient times (19, 20). Moreover they are easily available and to our knowledge carvedilol loaded nano emulsions were not reported with these oils. Both the oils were stable at room temperature and they do not become rancid like other oils due to the presence of natural antioxidants. All these reasons motivate to select the sesame and olive oils for the present study. They have blood pressure reducing properties therefore their quantity was limited to 200 μ l (19). In all the formulations with 100 μ l of either sesame oil or olive oil the drug was deposited at the bottom of the beaker and the drug content was found to be less than 50%. This indicated that the volume of the oil was not sufficient to hold the entire drug inside. Hence the volume of oil was increased to 150 μ l. In this case no drug was seen at the bottom of beaker and the drug content was drastically increased to 98.93 \pm 1.31% which revealed that 150 μ l of oil was sufficient to hold 6.3mg of carvedilol. With increasing oil phase volume from 100 μ l to 200 μ l, a significant increase in globule size was observed in both the oils and the results were shown in Fig.1.

Surfactants play a major role in the preparation and stability of NEs. Surfactants form a monomolecular film around the dispersed droplets and there by reduces the interfacial tension and prevent the droplet coalescence. Brij-97 and tween-80 were used as surfactants for the present study. Though they are non-natural surfactants, they do not produce any toxic effects

when administered orally. The amount of surfactant is also important to form rigid film around dispersed globules. However use of excess amount of emulsifier can cause decrease in entrapment efficiency, burst release and formation of other colloidal species like liposomes and micelles and may even cause toxic effects (20). From the table it was evident that with increasing concentration of surfactant the globule size was decreased but the drug content was decreased and the optimum concentration of surfactant was found to be 1.25% in case of brij 97 and 1.5% in case of tween 80.

All the nanoemulsion compositions possess negative zeta potential, this may be due to the negative charge of fatty acids. The zeta potential is a measure of the surface charge and is important in keeping the droplets in dispersed state. The particle interactions are also controlled by the magnitude of the apparent surface charge of the dispersed globules. Torrey et al (2006) reported that, the ZP of particle formulations is a value of greater than +30mv or lower than -30mv for ensuring electrostatic stability. However, this suggested zeta potential cut off point is an experience based value and cannot be reliably used to predict the stability of NEs because a wide range of absolute zeta potential values (i.e., 1.5, 12.5, 45.5mv) have been reported for SNEDS and NEs (21,22). The zeta potential depends on the pH of the nanoemulsion. At lower PH values the zeta potential will be positive and at higher pH values it will be negative. The pH of all NEs was in the range of 6.5 \pm 0.03 to 6.8 \pm 0.03 and was also responsible for negative zeta potentials of NEs.

Carvedilol was a poorly soluble and poorly permeable drug and its Pka at pH 7.4 was 8.8. At this pH the degree of ionization will be almost 100% and it is assumed that the rate of solubility and hence the rate of drug release will be

enhanced. In-order to evaluate this parameter Phosphate buffer saline pH 7.4 was selected as the diffusion medium to carry out *in-vitro* drug release characteristics. The rate of drug release also depends on the solubility and partitioning characteristics of the drug in diffusion medium (23). The solubility studies of carvedilol revealed that the presence of tween 80 in PBS enhance its solubility in PBS. Therefore PBS containing 1% tween 80 was used as the diffusion medium. The *in-vitro* drug release follows first order kinetics. The rate and cumulative amount of drug release was highest in formulations C14 which contains olive oil as the lipid phase. This may be due to its high drug content, low surfactant concentration and narrow globule size. Drug release from the nano emulsions is also related to the partition coefficient of the drug in oil/ water system. More specifically for efficient transport of the drug from the formulation in to the systemic circulation, the drug must first pass from the lipid phase to the aqueous phase and then in to the gastro intestinal tract (GIT) lumen. The oil water partition coefficient studies of carvedilol revealed that the logP values of carvedilol in olive oil was higher than that in the sesame oil (23). This property of olive oil may cause the more amount of drug release from the nano emulsions (C14) in which olive oil was used as the oil phase. In X-ray diffraction studies formulation C7 showed two peaks at right angles. This may be due to the re-crystallization of the drug (13). Transmission electron micrographs revealed that the dispersed globules were spherical and show no signs of coalescence of the droplets and precipitation of the drug in oil phase or in continuous phase.

The *in-vivo* pharmacokinetic studies were performed for the formulation C14 which showed maximum *in-vitro* drug release. Pharmacokinetic parameters revealed that the extent of oral absorption and hence oral bioavailability of carvedilol was enhanced with

NE compared with that of marketed tablet suspension. AUC is expected as an indicator of the extent of absorption, where as Cmax and Tmax are considered as estimates of the absorption rate (24). This may be explained by the fact that the presence of omega-6 and omega-3 PUFA (poly unsaturated fatty acids) in olive oil which are essential fatty acids and are not produced by the human body may enhance the rate of oral absorption (25). The small droplet size, and hence the large surface area, lymphatic transport through the transcellular pathway (26) may also contribute to the increased bio availability.

Conclusion

Carvedilol loaded Nano emulsions were successfully prepared by high energy emulsification method using sesame oil or olive oil and non ionic-surfactants Brij 97 and and tween-80. The resultant Nano emulsions possess high drug loading efficiency. The *in-vitro* rate of drug release followed first order kinetics. In-vivo pharmaco kinetic studies revealed that the rate and extent of absorption of carvedilol was higher with oral NE compared with that of oral tablet suspension. Brij 97 was found to be effective non ionic surfactant for the preparation of stable NEs and co-surfactants are not required along with this.

Acknowledgement

The authors acknowledge Orchid Pharmaceuticals, Chennai, India for providing gratis sample of carvedilol. The authors also acknowledge the Vimta labs management for providing access for animal studies.

References

1. Shoib, A. (2007). Nanotechnology in Drug Delivery: Introduction and Recent Developments. The Internet Journal of Nanotechnology. 2.

2. Tadros, .T. (1983) In: P.Becher (Ed.), Encyclopedia of emulsion Technology, vol.1 Marcel Deckker, New york, , pp. 129-285.
3. Carsten, B., Androes, S., Adrian, F., Torsten, W. and Ralph, L. (2007). Novel poloxamer – based nano emulsions to enhance the intestinal absorption of active compounds. *Int.J. pharm.*, 329, 173-181.
4. Shah, P., Bhalodia, D. and Shelat, P. (2010). Nano emulsion: A pharmaceutical Review, *Sys Rev Pharm.* 1.
5. Lennart, L., Pia, S., Jan, W. and Ulf, O. (2007). Amorphous Drug Nano Suspension; Particle dissolution and crystal growth, *Langmuir*, 23, 9866-9874.
6. Lukyanenko, V. (2007). Delivery of nano-objects to functional sub-domains of healthy and failing cardiac myocytes. *Nano medicine*, 2, 831-46.
7. Ahmed, A., David, M., Duane, A., Natalie, D. and Michael, J. (2007) Population Pharmacokinetics of S(–)-Carvedilol in Healthy Volunteers After Administration of the Immediate-Release (IR) and the New Controlled-Release (CR) Dosage Forms of the Racemate, *The AAPS Journal*, 9.
8. Varsha, P., Abhishek, K., Vinod, V., Sheetal, D. and Leenata, M. (2009). Ternary complexation of carvedilol,? - cyclodextrin and citric acid for mouth-dissolving tablet formulation, *Acta Pharm.* 59, 121–132.
9. Vamshi, V., Chandrasekhar, K., Ramesh, G. and Madhusudan Rao, M. (2007). Development of Mucoadhesive Patches for Buccal Administration of Carvedilol, *Current Drug Delivery*, 4, 27-39.
10. Enas, A., Ehab, R. and Magdy, I. (2009). Preparation and Evaluation of Self-nanoemulsifying Tablets of Carvedilol, *AAPS PharmSciTech*, 10.
11. Ramesh, G., Vamshi, V., Kishan, V and Madhusudan Rao, Y. (2007). Studies on the influence of penetration enhancers on in vitro permeation of carvedilol across rat abdominal skin, *Current Trends in Biotechnology and Pharmacy*, 1 62-69.
12. Yuvaraj, S., Chetan Singh, T. and Anshu Sharma, C. (2007). Development and evaluation of carvedilol transdermal patches. *Acta Pharm*, 57, 151–159.
13. Akhayachatra, C., Praneet, t O., Tanasait, N., Natthan, C., Warisadasila, O. and Uracha, R. (2007). Physicochemical properties of lipid emulsions formulated with high-load all-trans-retinoic acid. *PDA J. Pharm. Sci. Technol.* 61, 461-471.
14. Endabetla, V., Kandadi, P. and Veerabrahma, K. (2009). Preparation, characterization and in vivo pharmacodynamic evaluation of Parenteral diclofenac submicron lipid emulsions, *PDA J. Pharm. Sci. Technol.*, 63,380-389.
15. Meyer, S., Berrut, S., Goodenough, T., Rajendram, V., Pinfield, V. and Povey, M. (2006). A comparative study of ultra sound and laser light diffraction techniques for particle size determination in dairy beverages. *Meas.Sci.Technolo.*, 17, 289-297.
16. Liberman, H., Rieger, M. and Banker, G. (1988). *Pharmaceutical dosageforms: Disperse systems*; Marcel Dekker: New York, Vol.1.
17. Jawahar, N., Nagasamy, D., Sureshkumar, R., Senthil, V., Ganesh, K., Vinoth, P., Sumeet, S. and Samantha, K. (2009). Development and characterization of

- PLGA-nanoparticles containing carvedilol, *J.Pharm. Sci & Res*, 3, 123-128.
18. Tushar, K., Aliasgar, S. and Mansoor, M. (2008). Improved bioavailability and brain Transport of Saquinavir upon Administration in Novel Nanoemulsion Formulations, *Int. J Pharma*. 347, 93-101.
 19. Sankar, D., Ramakrishna Rao, M., Sambandam, G. and Pugalendi, K. (2006). Effect of Sesame Oil on Diuretics or β -blockers in the Modulation of Blood Pressure, Anthropometry, Lipid Profile, and Redox status, *yale journal of biology and medicine* 79, 19-26.
 20. Manjunath, K., Reddy, J. and Venkateswarlu, V. (2005). Solid lipid nano particles as drug delivery systems, *Experimental clinical pharmacology*, 27, 127-144.
 21. Torrey, D., Michael, K. and Kevin, M. (2006). Optimizing silicone emulsion stability using zeta potential, *American Laboratory News*, June/July.
 22. Yi Z., Changguang, W., Albert, H., Chow, K., Tao, G., Zhirong, Z. and Ying, Z. (2010). Self nano emulsifying drug delivery system (SNEDDS) for oral delivery of Zedoary essential oil: Formulation and bioavailability studies, *Int J Pharm*. 383, 170-177.
 23. Esposito, Pierandrea, Coceani, Nicoletta, Del Curto, Maria Dorly, Carli and Fabio. (2004). Biphasic multicomponent pharmaceutical dosageforms containing substances able to modify the partitioning of drugs, *European Patent EP0917457*.
 24. Yun, L., Jingying, J., Gangyi, L., Chuan, L., Yanmei, L. and Chen, Y. (2009). Pharmacokinetics and Bioequivalence evaluation of two formulations of 10-mg amlodipine besylate: An open-label, healthy Chinese male volunteers, *Clinical Therapeutics*, 31, 777-783.
 25. Tiwari, S. and Amiji, M. (2006). Improved oral delivery paclitaxel following administration in nano emulsion formulations, *J nanosci NanoTechnolo*, 6, 3215-21.
 26. Hirunpanchi, V., Katagi, J., Sethabouppha, B. and Sato, H. (2005). Demonstration of docosahexanoic acid as a bioavailability enhancer for CYP3A substrates: In vitro and in vivo evidence using cyclosporine in rats, *Drug Metab Disp*, 34, 305-310.

Studies on Carrier State of *Chlamydophila abortus* in Naturally Infected Sheep

Rabia Abadía Elzlitne¹, Giuma Elaref Elhaffi², Vijayan R¹. and Sateesh Kumar^{1*}

¹Faculty of Vet. Medicine, Al Fateh University, Tripoli, Libya. ²Animal Health Center Tripoli, Libya

*For Correspondence - yeshjain@gmail.com

Abstract

The purpose of the study was to establish whether or not *C. abortus* is shed through the reproductive tract following infection under natural conditions. Two farms where enzootic abortion was endemic were investigated by sequential collection of vaginal secretions, faeces and serum samples from ewes which had chlamydial abortion six months earlier. PCR was used as a confirmatory tool after extracting DNA from faeces and vaginal secretions using primers specific to the MOMP gene. None of the samples tested were positive, suggesting that either there were no EBs of *C. abortus* in the samples or there were non infectious forms (RBs) which could not be detected by DNA amplification. Real-time PCR analysis of placental samples identified very few or no chlamydial genomes, which contrasted significantly with samples taken at the time of abortion. The *C. abortus* was detected by PCR for the first time in milk samples collected from ewes with EAE history using the IMS technique. The serum samples from these ewes showed significantly higher chlamydia-specific IgG titre during the period of peri-ovulation. In terms of flock management, the products of abortion should be considered the major and principal source of infection for transmission to naïve ewes.

Introduction

Ovine Enzootic Abortion (OEA) is one of the most common contagious disease affecting sheep and goats due to *Chlamydophila abortus* (*C. abortus*). Unlike other bacteria, the chlamydial development life cycle is characterized by two distinct developmental forms, elementary bodies (EBs) and reticulate bodies (RBs) respectively. The Elementary body is infectious, with rigid cell wall, which contains the major outer membrane protein (MOMP) and other proteins. The reticulate bodies are non-infectious, metabolically active forms of chlamydiae capable of synthesizing DNA, RNA and proteins. Enzootic abortion in sheep (EAE) causes a major financial loss worldwide and represents a significant zoonotic risk. It is clinically characterized by abortion and weak neonates in small ruminants. Pregnant sheep initially infected with *C. abortus* either abort late in gestation or give birth to weak or stillborn lambs as a result of placental pathology associated with infection (14). Using specific real-time PCR assay, few chlamydial genomes could be detected in vaginal swabs taken from post-abortion ewes at oestrus. Few genomes could also be detected from vaginal, cervical tissue samples and lymph nodes taken post-mortem (8).

Because parturition or abortion in *C. abortus* infected ewes is usually accompanied

by the passage of an infected placenta and or foetal tissues, the main concern of transmission of the infection to susceptible ewes in the periparturient period when the lambing environment may become contaminated with diseased tissues (18). Chlamydia-induced abortion in sheep was recognized to stimulate an immune response that protected against subsequent abortion (9). Ewes that experienced abortion as a result of experimental infection with *C. abortus* maintained an elevated systemic antibody response to the organism and this was associated with a chronic reproductive tract infection (13)

Since future fertility was apparently not compromised, ewes that aborted are usually retained and reintroduced to the flock. Identification of those carrier ewes could aid the development of a management strategy to eliminate continued disease outbreaks in flocks. The purpose of the present study was to establish whether or not *C. abortus* is shed through the reproductive tract following infection under natural conditions.

Material and Methods

Experimental design : Two sheep farms where enzootic abortion was endemic were selected to study the carrier state of *Chlamydophila abortus*. Fourteen ewes confirmed to have had aborted due to the natural infection of *C. abortus* six months earlier were randomly selected for the study and was investigated by sequential collection of vaginal secretions, faeces and serum samples.

Synchronization of oestrus cycle was carried out in all the fourteen ewes by inserting vaginal progesterone impregnated sponges and by parenteral administration of pregnant mare serum gonadotrophin (PMSG). Blood and faecal samples were collected on the day of sponge insertion. Thirteen days later the sponge was removed before injecting each ewe with PMSG.

Immediately Coagulated blood, faeces and vaginal samples were collected. Again 2 and 4 days later vaginal swabs were collected. The ewes were euthanized 33 days later and the fallopian tube, mid uterus, and vagina were used for chlamydial isolation. All samples were stored at -80°C until further use.

Collection of samples

Faecal samples: Fresh rectal faeces collected (0.1 to 25 g) were placed in transport medium mixed with a rotomixer and centrifuged at 1000 xg for 10 min. Twenty μl of the supernatant were then used to inoculate a monolayer of McCoy together with culture medium containing 200 $\mu\text{g}/\text{ml}$ of gentamycin (15).

Reproductive tract samples: The sections of the vagina distal, the mid region of the uterus and the oviduct were obtained under aseptic conditions and immersed into transport medium. The samples were cut up into smaller pieces with scissors and broken further with mortar and pestle. After centrifugation at 1000 g for 10 min, 100 μl of the supernatant were used to inoculate McCoy cells (12)

Vaginal swabs: Vaginal swabs for chlamydial isolation and PCR were collected after gently inserting sterile swabs into the vagina and rotating them in both directions. Immediately after sampling, the tip of the vaginal swab was immersed in transport medium, mixed with rotomixer and centrifuged at 1000 x g for 10 min. The supernatants were then used to inoculate McCoy cell monolayers and for DNA extraction. The samples were kept at -80°C until used.

Bacterial identification and isolation

McCoy cells, grown in 24-well plate monolayer were used for the isolation. Inoculated monolayers were examined for the presence of inclusion bodies after staining cover slips with Diff Quick stain at 48-72 hours post inoculation. Some

monolayers were frozen at -20 °C, then thawed at 37°C, and the inclusions were disrupted by shaking with glass beads for 1 min before centrifugation at 5000x g for 10 min at 4 °C. The supernatant was collected and the pellets were resuspended in sucrose phosphate glucose (SPG). The suspension was centrifuged again after brief sonication. The supernatant was pooled and centrifuged at 30,000 g for 30 min at 4°C (Sorvall instrument, Dupoint, USA). The pellet obtained after ultracentrifugation was used to inoculate fresh McCoy cell monolayers. After three inoculation cycles in fresh cells, the media and cell pellet were tested for chlamydia-specific lipopolysaccharide (LPS) by using the Clearview Chlamydiae test kit (Unipath, inc., Nepean, Ontario, Canada). Direct faecal samples smears were examined for the presence of MZN-positive elementary by Modified Zeihl Nelson (MZN) stain.

Immunological Technique

Enzyme linked immunosorbent assay (ELISA): The ELISA test was performed on serum samples collected before insertion of progesterone sponge insertion and 13 days later (sponge removal and PMSG injection).

Polymers Chain Reaction (PCR)

DNA extraction of vaginal and faecal swabs: The swabs collected in Chlamydia transport medium (CTM) were centrifuged at 2000 rpm for 10 minutes. About 400 µl of the supernatant was then pelleted by centrifugation for 10 minute at 1200xg. After resuspending the pellet in 180 µl of ATL solution (supplied in the QIAamp DNA mini kit) and adding 20 µl of proteinase K, the samples were incubated at 65°C overnight. The micro-centrifuge tube was centrifuged before adding 200 µl buffer AL to the sample, then vortex mixed for 15 sec and incubated at 70°C for 10 min. The tube was centrifuged and 200 µl of

ethanol (96-100%) was added and mixed. The mixture was then carefully poured in the QIAamp spin column. The cap was then closed and centrifuged at 6000 x g for 1 min. The QIAamp spin column was placed in a clean 2 ml collection tube and the other tube containing the filtrate discarded. 500 µl of buffer AW1 was added and centrifuged at 6000 x g for 1 min and the tube containing the filtrate was discarded. Then, 500 µl of Buffer AW2 was added and centrifuged at 20,000 x g for 3 minute and repeated as above. 200 µl of Buffer AE or distilled water was added. After incubation at room temperature for 1-5 min, the mixture was centrifuged at 6000 x g for 1 min and the DNA extract was stored at -20 °C until used.

DNA amplification: DNA was amplified as described by Creelan and McCullough (2000), using Clone 8 forward primer, 5' TGG TAT TCT TGC CGA TGAC 3'; and clone 8 reverse primer, 5' GAT CGT AAC TGC TTA ATA AAC CG 3' for the *omp* gene of *Chlamydomphila abortus*.. 3 µl of the DNA sample was added to 47 µl of a reaction mixture containing 1xPCR super mix (Life Technologies (20 mM Tris-HCl pH 8.4, 5 mM KCl, 1.5mM MgCl₂), 200 µM deoxynucleoside triphosphates, 2 Units *Taq* DNA polymerase and 1 mM of each primer. The reaction mixture was overlaid with 30 µl of mineral oil and initial denaturation at 95 °C for 5 minutes followed by 40 cycles of; 1 minute of at 94 °C, 1min of at 45 °C, 2 minutes at 72 °C and final 7 min extension at 72 °C.

The amplified product was analysed by subjecting 5 of PCR products to electrophoresis for 45 minute at 100 V on a 1 percent agarose gel. The gel was then stained with ethidium bromide and illuminated by ultraviolet light. Molecular weight markers X 174(Sigma) were included in every gel.

Statistical analysis

The antibody titres to *C. abortus* at two occasions of oestrus synchronization (day 0 and 13-days later) were compared by paired t test.

Results

Detection of chlamydiae: At various occasions of oestrus synchronization (Day 0 and 13-days later) *C. abortus* was not isolated or specific antigen was detected in the vaginal and faecal samples collected on the day of progesterone sponge insertion (Day 0) or on the day of sponge removal (day 13).

Detection of chlamydial LPS: Chlamydia-specific LPS were not detected by the Clearview test in the samples collected before insertion or in those obtained after sponge removal and PMSG injection. Samples continued to be negative after the third passage on McCoy cell tissue culture. PCR results using MOMP specific primers were also negative.

Systematic antibody response: Chlamydia-specific IgG antibodies were detected in the sera tested by ELISA. The mean IgG antibody titre of the serum samples obtained from the ewes on the day of sponge insertion was 2.05 (\log_{10}), and those obtained after the removal of the sponge was 2.93 \log_{10} (Table 1). The rise in antibody titre following treatment with progesterone was statistically significant ($p < 0.001$)

Discussion

In the present study the possibility of a carrier state following chlamydial abortion in two farms where enzootic abortion was endemic has been investigated by sequential collection of vaginal secretions, faeces and serum samples from ewes which had chlamydial abortion six months earlier. *C. abortus* was not isolated after three passages in any of the samples tested and chlamydial antigens were not detected by Clearview in the faecal samples and vaginal

Table 1. ELISA antibody titres (\log_{10}) of serum samples obtained before and after treatment with progesterone.

Animal No	Sponge insert-ion	Sponge removal
90	0.9	3.3
120	1.2	3.6
0163	1.2	3.6
114	2.4	3
113	2.7	3.6
119	1.8	3
17	2.4	3
18	2.4	2.1
19	2.7	2.4
116	3	3
23	1.5	2.1
111	2.4	3
115	2.1	2.4
Mean	2.05	2.93
P (<0.05)		

mucus obtained before or after insertion of the progesterone sponges. However, significant levels of antibodies were detected by ELISA in serum samples obtained before and after insertion of the sponges, with titres significantly rising after insertion.

In earlier studies, clinical, serological and immunological tests revealed that the lowest number of infected sheep was registered in animals younger than 18 and highest in animals aged 18 to 24 months. In sheep aged more than 3 years, titre of antibodies was significantly reduced. Furthermore, in sheep which aborted, the infection level was 2.5-fold higher as compared to sheep which didn't abort. The highest prevalence of chlamydia (66.7%) was registered in placentas of sheep which aborted (1). These results contradict those reported by Papp et al. (13), who detected LPS but not live chlamydiae, after the third passage of vaginal swabs obtained from chronically infected ewes. The specific serum antibodies to *Chlamydomphila abortus* was present

in 2,360 out of 20,878 sheep sera examined (11.7%), and in 85 out of 1,162 examined goats (7.7%) in slovak republic (2).

The lack of detection of chlamydial antigen by MZN or by culture is consistent with that reported by Clarkson and Philips, (3), who could not detect *C. abortus* in the faecal samples obtained from ewes in farms where enzootic abortion was endemic. However, other workers have reported that *C. abortus* is occasionally isolated from faeces (16). It appears that *C. abortus* is not excreted in the faeces of naturally aborting ewes but further studies are needed to examine flocks where enzootic abortion is present and for the possible role of faeces as source of infection, as some enteric isolates were reported to be capable of causing abortion in pregnant ewes after intravenous injection (15).

In the present study attempts to demonstrate chlamydial antigens by immunohistochemical staining of sections of the reproductive tract obtained from ewes six months after chlamydial-abortion were also unsuccessful. This is also in contradiction to the observations of Papp et al (11), who reported the demonstration of chlamydial antigens in vaginal and cervical samples obtained from chronically infected ewes using immunohistochemistry. However, their samples were obtained from ewes that had experienced *C. abortus* induced abortion 3 years earlier. Whereas in the present study the samples were obtained during the second oestrus cycle, six months after abortion due to *C. abortus*.

The Clearview Chlamydia test kit is reported to provide fast and easy-to-use method for the detection of chlamydiae. It has high sensitivity, which makes it a useful screening tool, but it is not species-specific as the LPS it detects are shared by other chlamydiae and possibly other bacteria.

It has been reported that *C. abortus* persists in subepithelial cells in the vagina, uterus, and oviduct of chronically infected ewes. Invasion of the chlamydiae beyond the mucosal epithelial cells provide opportunity for persistence. So it possible that viable *C. abortus* had not been excreted secretion during the period of collection.

The Polymerase Chain Reaction (PCR), which is easy, sensitive and quick method of detection, is now widely used for the detection of *C. abortus*. One advantage of using PCR for the detection of EAE is that viable EB do not have to be present, unlike the requirements for cell culture isolation. A PCR was used to detect the genome of *Chlamydomydia abortus* in samples of uterine tissue collected from 304 sheep. The total prevalence of the chlamydial genome was 30.9 per cent, with a significantly higher prevalence in the pregnant animals as 46.9 per cent. (10)

In the present study PCR was used as a confirmatory tool after extracting DNA from faeces and vaginal secretions' using primers specific to the MOMP gene as described by Creelan and McCullaugh (4). The use of ovine abortifacient strain-specific primers for the detection of DNA from placental tissues was reported to be a sensitive and specific. The specificity of clone 8 primers for *C. abortus* avoids the potential detection of *C. pecorum*, which is known to infect sheep (6). None of the samples tested were positive, suggesting that either there were no EBs of *C. abortus* in the samples or there were non infectious forms (RBs) which could not be detected by DNA amplification. It has been reported that chlamydiae can be detected at early stage by ribosomal RNA (rRNA).

A variety of sample preparation methods such as immunomagnetic separation (IMS) have successfully been applied to improve the

sensitivity of PCR assays (5). Real-time PCR analysis of placental samples identified very few or no chlamydial genomes, which contrasted significantly with samples taken at the time of abortion. The results suggested that the low levels of chlamydial DNA detected during the periovulation period and at lambing do not significantly impact on the epidemiology of EAE. In terms of flock management, the products of abortion should be considered the major and principal source of infection for transmission to naïve ewes. (8)

The *C. abortus* was detected by PCR for the first time in milk samples collected from ewes with EAE history using the IMS technique. However, the absence of a *C. abortus* using PCR and IMS in some animals with EAE history does not necessarily mean that they were free from the disease, as the possibility of excretion in milk is considered to be rather low (17). Chlamydiae may be present in low numbers in ewes and shed only intermittently or that other animals could act as reservoirs of infection (3). It is possible that the organism did not persist in the aborting ewes or the concentration of *C. abortus* DNA in the reproductive tract of persistently infected ewes so low, that it cannot be detected by PCR.

The peri-glandular region of basal zone of endometrium is an area where infiltrating macrophages reside (7). Infiltration of macrophages in peri glandular cells may help presentation of chlamydial antigen to be presented to MHC Class II and to stimulate the production of systemic antibodies. The serum samples from these ewes showed significantly higher chlamydia-specific IgG titre during the period of peri-ovulation. This finding is in close agreement with that of Papp et al. (11). There was also an increase in antibody reactivity during the periovulation period in 3 of the 8 sheep examined, with a slight increase in IgM and IgG antibodies.

Specific antichlamydial antibodies can neutralize chlamydial infectivity *in vitro* by preventing attachment to target cells or facilitating intracellular destruction. In terms of flock management, as suggested earlier by many researchers (8), the products of abortion should be considered the major and principal source of infection for transmission to naïve ewes

References

1. Bagdonas, J, Petkevicius, S, Russo, P, Pepin, M. and Salomskas, A. (2007). Prevalence and epidemiological features of ovine enzootic abortion in Lithuania. *Pol J Vet Sci.*, 10(4); 239-244.
2. Cisláková, L., Halánová, M., Kováčová, D and Stefancíková., A. (2007). Occurrence of antibodies against *Chlamydia abortus* in sheep and goats in the Slovak Republic. *Ann Agric Environ Med.*,14(2); 243-5.
3. Clarkson, M. J. and Philips., H. (1997). Isolation of faecal *Chlamydia* from sheep in Britain and their characterisation by cultural properties. *Veterinary Journal.* 153; 307-310.
4. Creelan, J. L. and Samuel J. McCullough. (2000). Evaluation of strain- specific primer sequences from an abortifacient strain of ovine *Chlamydia abortus* (*Chlamydia psittaci*) for the detection of EAE by PCR. *Infection and Immunity.* 1; 103-108.
5. Djonne, B., Jensen, M. R., Grant, I. R and Holstad, G (2003). Detection by immunomagnetic PCR of *Mycobacterium avium* subsp. *paratuberculosis* in milk from dairy goats in Norway. *Veterinary Microbiology* 92; 135-143.
6. Fukushi, H and Hirai, K. (1993). Restriction fragment length polymorphisms of rRNA as

- genetic markers to differentiate *Chlamydia* spp. *International Journal of Systematic Bacteriology*. 43(3); 613-617.
7. Lee, C. S., Gogolin-Ewens, K. and Brandon, M. R. (1988). Identification of a unique lymphocyte subpopulation in the sheep uterus. *Immunology* 63; 157-164
 8. Livingstone M, Wheelhouse N, Maley SW. and Longbottom D.(2009). Molecular detection of *Chlamydophila abortus* in post-abortion sheep at oestrus and subsequent lambing. *Vet Microbiol.*, 135(1-2); 134-141
 9. McEwen, A. D., Littlejohn, A. I. and Foggie, A.(1951). Enzootic abortion in ewes. Some aspects of infection and resistance. *Veterinary Record*. 63; 489-492.
 10. Michalopoulou, E, Leigh, A.J, and Cordoba, L.G. (2007). Detection of the genome of *Chlamydophila abortus* in samples taken from the uteri of 304 sheep at an abattoir. *Veterinary Record*. 161; 153-155
 11. Papp, J. R., Shewen, P.E. and Thorn, C.E. (1998). Immunocytological detection of *Chlamydia psittaci* from cervical and vaginal samples of chronically infected ewes. *Canadian Journal of Veterinary Research* 62; 72-74.
 12. Papp, J. R. A. and Shewen, P.E. (1996). Localization of chronic *Chlamydia psittaci* infection in the reproductive tract of sheep. *Journal of Infectious Diseases*. 174; 1296-1303
 13. Papp, J. R., Shewen, P.E., and Gartley, C.J. (1994). Abortion and subsequent excretion of chlamydiae from the reproductive tract of sheep during estrus. *Infection and Immunity*. 62; 3786-3792.
 14. Philips, H.L. and Clarkson, M.J. (2002). Investigation of Pre-natal *Chlamydophila abortus* (*Chlamydia psittaci*) Exposure of Female Lambs and the Outcome of their First Pregnancy . *The Veterinary Journal*, 163; 329-330.
 15. Philips, H (1993). Enreic chlamydia and enzootic abortion of ewes. Ph.D thesis, University of Liverpool, UK.
 16. Rodolakis, A., Salinas, J. and Papp, J. (1998). Recent advances on ovine chlamydial abortion. *Veterinary Record*, 29(,3-4); 275-288.
 17. Thomas, R., Davison, H.C. and Wilsmore, A.J. (1990). Use of the IDEIA ELISA to detect *Chlamydia psittaci* (ovis) in material from aborted fetal membranes and milk from ewes affected by enzootic abortion. *British Veterinary Journal*. 146; 364-367.

Automated Synchronization of *P. falciparum* using a Temperature Cycling Incubator

Alejandro Almanza,^{1, 2} Lorena Coronado,¹ Nicole Tayler,¹ Liuris Herrera^{1, 2} and Carmenza Spadafora^{1, 2*}

¹Centro de Biología Celular y Molecular de las Enfermedades (CBCME), Instituto de Investigaciones Científicas y Servicios de Alta Tecnología (INDICASAT AIP), Panama.

²International Cooperative Biodiversity Groups (ICBG), Smithsonian Tropical Research Institute (STRI), Panama.

*For Correspondence - cspadafora@indicat.org.pa

Abstract

As malaria keeps affecting millions of lives every year, research based in culture of *Plasmodium falciparum* *in vitro* needs to be efficient and accurate. The development of better techniques and methodologies for the growth and maintenance of the parasites can save money, time, and lead to more trustable results. It has been observed, first in patients and then in the laboratory, that the malaria *falciparum* parasites growth is affected by high temperatures. This trait can be used with laboratory cultures to synchronize and maintain the parasites in the same stage of their cell cycle. This harmony of stages is very desirable for the purpose of conducting metabolomic, proteomic and transcriptome analysis as well as for drug screening. Most scientists in the field of malaria use chemicals (usually sorbitol) that kill certain stages of the parasite to obtain synchronization, but this latter method does not last long and the parasites thus treated should not be used for assays immediately after the treatment, due to the toxic effects that might have been infringed in the culture. A temperature cycling incubator (TCI) was acquired in our laboratory and it was used to test the synchronization of the multidrug resistant W2 and chloroquine resistant 7G8 strains, commonly used in our bioassays where they and their synchronization constitute essential tools for our

drug discovery program. We followed the protocol designed by Haynes and Moch in 2002 and we made a comparison of the effectiveness of each of the two methods, chemical and temperature based. Our results show W2 synchronization by temperature cycling, with the help of an initial use of 0.3 M alanine, to last more than two months while a tight synchronization with the use of 5% sorbitol was lost as rapidly as in one week. Sorbitol could also be used with the TCI for synchronization with good results. However, 7G8 could not be efficiently synchronized with temperature cycling using the same program as that of W2.

Key Words: *P. falciparum*, Culture, Synchronization, High temperature, TCI.

Introduction

It has been described that *in vitro* growth of *Plasmodium falciparum* is inhibited by high temperatures (1-5) and there have been relationships drawn from these findings on how fever in malaria patients may influence parasite growth, coordination of cyclic stages, and parasitemia.

In 2002, Haynes and Moch published a method for using these observations to synchronize *P. falciparum* cultures for laboratory

use (6). For almost every *in vitro* experiment with this parasite there is a need for a synchronized culture. Traditionally, a chemical like sorbitol has been used to kill the mid to late stages of *P. falciparum*, leaving only rings alive and thus synchronizing the culture. The method optimized by Haynes and Moch saved the parasite from constant exposure to a foreign chemical and made maintenance of culture more amenable to the labor hours of technicians and scientists. The method used an exact cycle of 48 hours for the completion of the cell cycle. They used the FVO, Dd2, and 3D7 strains to test their system and gave suggestions on other strains that could be synchronized through temperature (FCR-3, CAMP, and FCB-2). We incorporated their temperature cycling methodology to try to synchronize the 7G8 (7) strain and the chloroquine resistant strain, W2 (8) used in our bioassays for drug screens; here we report the conditions used and the outcome of our test.

Material and Methods

Culture: We cultured strains 7G8 and W2 using the conventional method of Trager & Jensen (9) with some modifications, that include the use of RPMI 1640 medium modified (Sigma-Aldrich), 25 mM HEPES, 15 μ M hypoxanthine, 50 mg/mL gentamicine sulfate, and 200 mM L-Glutamine, supplemented with 10% human serum, 2% sodium bicarbonate and a balanced mix of gases (90% N₂, 5% O₂ and 5% CO₂). Cultures were checked every day for optimal development and health by making thin film slides stained with Giemsa and having their parasitemia assessed by light microscopy for up to 70 days.

Synchronization of parasites: Cultures of 7G8 and W2 were incubated in parallel in a temperature cycling incubator (TCI) (Cooled Incubator, Sanyo, Model MIR-154) and a static temperature incubator set at 37°C (Lab-Line Instruments Inc. Imperial III Incubator). The TCI temperature

fluctuations and their exposition times are as following: (19:30), 22°C (2:22), 37°C (13:42), 39.8°C (9:30), 37.2°C (21:26), 38.2°C (1:00) (same as Haynes' conditions for FVO); making the parasite cycle last exactly 48 hours. We used 0.3 M alanine (Sigma-Aldrich) as first treatment for synchronization of cultures in TCI (5) and 5% sorbitol for cultures in a 37°C incubator, as described (10). We made a comparison between the collected data from the W₂ and 7G8 strain culture of *P. falciparum* exposed to the febrile temperatures of the TCI and those set at 37°C in a normal incubator.

Results and Discussion

The TCI method synchronized our culture obtaining values between 85% and 100% synchrony during a 70 day period (Figure 1). At this point we stopped counting. It is worth noting that with this method we can also obtain high parasitemias if needed. In the cultures kept at 37°C and treated with sorbitol, as used to maintain

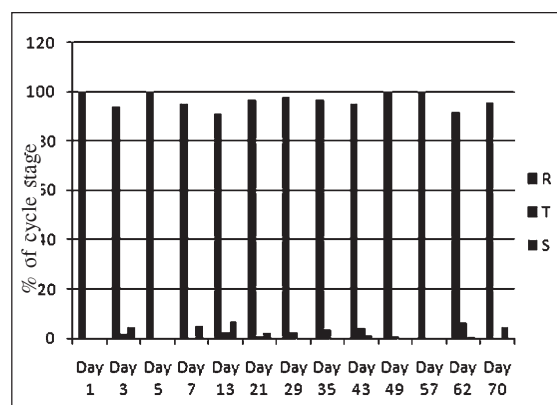


Fig. 1. Synchronization of *P. falciparum* by alanine and incubation in a TCI. To assess synchronization the percentage of each of the stages of the cell cycle of the parasite was determined in Giemsa stained smears taken from the culture on the days depicted in the graph. Parasites were treated one time with 0.3M alanine at the beginning of the culture and then they were placed on a temperature cycling incubator (TCI). R (rings), T (trophozoites), S (schizonts).

our parasites, we only got synchronization for a little over a week (Figure 2), and almost never observed 100% synchronization. While at the first day after treatment there were 93.8% of rings, by day 9 there was already a mix of 43.3% rings, 36.7% trophozoites, and 20% schizonts.

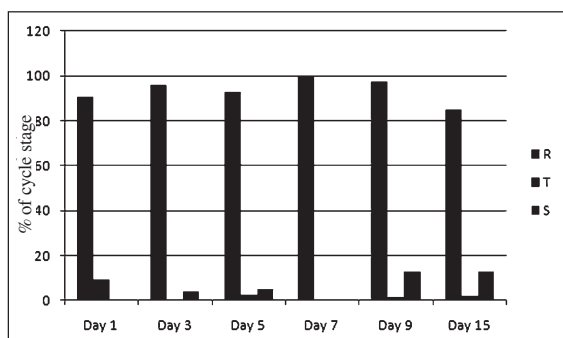


Fig. 2. Synchronization of *P. falciparum* by sorbitol and use of a 37°C incubator. To assess synchronization the percentage of each of the stages of the cell cycle of the parasite was determined in Giemsa stained smears taken from the culture on the days depicted in the graph. Parasites were treated one time with 5% sorbitol at the beginning of the culture and then they were placed on a 37°C constant temperature incubator. R (rings), T (trophozoites), S (schizonts).

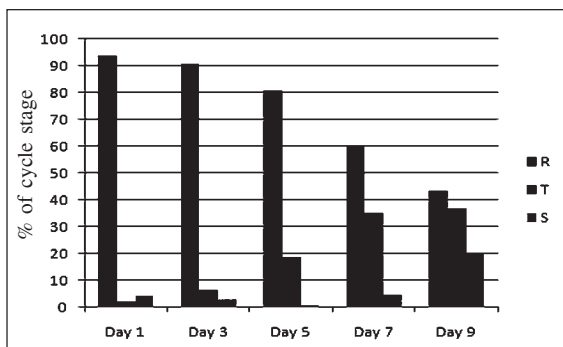


Fig. 3. Synchronization of *P. falciparum* by sorbitol and use of a TCI. To assess synchronization the percentage of each of the stages of the cell cycle of the parasite was determined in Giemsa stained smears taken from the culture on the days depicted in the graph. Parasites were treated one time with 5% sorbitol at the beginning of the culture and then they were placed on a temperature cycling incubator (TCI). R (rings), T (trophozoites), S (schizonts).

For the purpose of comparing if the choice of chemical used at the beginning of the synchronization period was responsible for the success of the method, we placed a culture synchronized with sorbitol into the TCI. Although alanine proved to be slightly superior, excellent synchronization results were again obtained with sorbitol, which points out to the great advantage of using a TCI over a 37°C incubator, and that this is the major factor responsible for the good outcome of synchronization numbers. One thing to note, though, is that at constant 37°C we always got higher parasitemias than in the TCI incubator, but the culture was less synchronized.

As for the 7G8 strain, with the alanine treatment and incubation in the TCI, we could not obtain the synchronization last for more than a week with the temperature program we used for the W2 strain (data not shown). After their publication in 2002 where they reported problems synchronizing 7G8 with their TCI method, Moch and Haynes have been able to put 7G8 in synchrony using this methodology, with a different temperature program (personal communication). For a malaria research laboratory, if it is possible to acquire more than one temperature cycling incubator, it is worth the investment. Together with the alanine treatment which seems to be less toxic on the parasites than the sorbitol one (11), the time shifts of technicians are perfectly adjusted to when they receive samples for the bioassays, making the method highly efficient and work amenable.

Conclusions

The repetitive automated synchronization cycle achieved with TCI makes availability of parasites within work hour schedules, at the same time that it helps satisfying specific aims of our research that require high synchronization. Through adjustments in programming of the TCI, different strains of *P. falciparum* can be highly synchronized, considering that each one has

different cycles of temperatures and times of exposure. In our case, the W2, a highly valuable strain for drug screening, can be satisfactorily synchronized with this methodology while retaining great viability and making the results of bioassays more accurate.

Acknowledgements

The authors would like to thank Kathy Moch from the Walter Reed Army Institute of Research, Maryland, USA, for teaching the methodology of TCI to AA. This work was possible through a NIH (Fogarty International Center) ICBG grant (TW006634) and a SENACYT infrastructure grant (INF09-37).

References

1. Aunpad, R., Somsri, S., Na-Bangchang, K., Udomsangpetch, R., Mungthin, M., Adisakwattana, P. and Chaijaroenkul, W. (1998). The effect of mimicking febrile temperature and drug stress on malarial development. *Annals of Clinical Microbiology and Antimicrobials*, 8: 19.
2. Long, H.Y., Lell, B., Dietz, K. and Kremsner, P.G. (2001). *Plasmodium falciparum*: *in vitro* growth inhibition by febrile temperatures. *Parasitol Res*, 87 (7): 553-555.
3. Kwiatkowski, D. (1989). Febrile temperatures can synchronize the growth of *Plasmodium falciparum in vitro*. *J Exp Med*, 169 (1): 357-61.
4. Gravenor, M.B. and Kwiatkowski, D. (1998). An analysis of the temperature effects of fever on the intra-host population dynamics of *Plasmodium falciparum*. *Parasitology*, 117 (Pt 2): 97-105.
5. Pavithra, S.R., Banumathy, G. and Joy, O., Singh, V., Tatu, U. (2004). Recurrent fever promotes *Plasmodium falciparum* development in human erythrocytes. *J Biol Chem*, 279 (45): 46692-46699.
6. Haynes, J.D. and Moch, J.K. (2002). Automated Synchronization of *Plasmodium falciparum* Parasites by Culture in a Temperature-Cycling Incubator. *Methods in Molecular Medicine*, 72: 489-497. Humana Press, Inc., Totowa, NJ
7. Bhattacharjee, AK., Kyle, DE. and Vennerstrom, JL. (2001). Structural Analysis of Chloroquine Resistance Reversal by Imipramine Analogs. *Antimicrobial Agents and Chemotherapy*, 45: 2655-2657
8. Burkot, T.R., Williams, J.L. and Schneider, I. (1984). Infectivity to mosquitoes of *Plasmodium falciparum* clones grown *in vitro* from the same isolate. *Trans R Soc Trop Med Hyg*, 78:339-341.
9. Trager, W. and Jensen, J.B. (1976). Human malaria parasites in Continuous culture. *Science*, 193: 673-675.
10. Lambers, C. and Vanderberg, J. (1979). Synchronization of *Plasmodium falciparum* erythrocytic stages in culture. *J Parasitol*, 65 (3): 418-420.
11. Dagan, A., Efron, L., Gaidukov, L., Mor, A. and Ginsburg, H. (2002). In Vitro Antiplasmodium Effects of Dermaseptin S4 Derivatives. *Antimicrobial Agents and Chemotherapy*, 46: 1059-1066.

Genome Analysis of Selected Foodborne Pathogens for Identification of Drug Targets

Sushil Kumar Shakyawar, Arun Goyal and Vikash Kumar Dubey*

Department of Biotechnology, Indian Institute of Technology Guwahati,
Guwahati-781 039, Assam, India

*For Correspondence - vdubey@iitg.ernet.in

Abstract

As the bacterial pathogens are showing growing resistance against existing antibiotics, there is an urgent requirement of pharmaceutical companies for designing new and effective drugs against these pathogens causing common foodborne diseases. We have performed *in-silico* genomic analysis of two virulent foodborne pathogens *Listeria monocytogenes* and *Bacillus cereus* for identification of potential drug targets for novel drug discovery. Our prediction found small number of genes of each pathogen to be targeted for drug designing. The gene products are found to be involved in various important regulatory proteins, membrane proteins and hypothetical proteins of unknown function of bacterial species. Further using KEGG pathway prediction various enzyme proteins were found which have active role in biosynthetic and metabolic pathways. The primary goal of this study was to provide a valuable resource of drug targets to the scientific community. The current data is included in “Drug Targets Protein Database” developed by our group.

Key word: Antimicrobial drugs; Essential proteins; Drug targets.

Introduction

Burden of microbial diseases and simultaneously more antibiotic resistance shown

by bacteria on existing antibiotic drugs needs a different approach to find drug targets for destroying bacteria more effectively. The development of effective antimicrobial drugs is the major challenge in field of pharmacogenomics. Growing number of microbial genome sequencing projects have generated large number of sequences. Recently, a number of computational tools have been developed for *in silico* analysis of gene sequence information (1). The genome information is also useful to identify potential and essential candidate of the microbial systems (2). A good target is a gene essential for bacteria to survive, yet cannot be found in the mammalian host (3). An ideal drug target should provide adequate selectivity yielding a drug which is specific or highly elective against the pathogen with respect to the human host. Moreover, the target should be involved in viability, growth and other essential metabolic processes of the pathogen at least under the condition of infection (4). Most of the previous research is revealed with identification of essential gene on the basis of experimental data acquired from gene disruption and systematic mutagenesis studies on the bacterium (5). There is huge chance of lethal action on bacteria by inactivation of essential genes. Targeting non human homologous genes are much important to avoid possibilities of unacceptable crossreactivity that might causes

side effect to the host (6). We have performed *in-silico* genomic analysis of virulent foodborne pathogens *Listeria monocytogenes* and *Bacillus cereus* for identification of potential drug targets for novel drug discovery. *Listeria monocytogenes* causes Listeriosis a virulent foodborne clinical infection. Similarly, *Bacillus cereus* a, Gram-positive, rod-shaped, beta hemolytic bacterium causing causing severe nausea, vomiting and diarrhoea. These data could be used for the identification of conserved protein sequences which are essential for bacterial survival (7). These conserved proteins are very important in finding drug targets in pathogens, ideal antimicrobial targets should be highly conserved among as well as essential for the pathogenic bacteria (8).

Methods

The BLAST executable of protein sequences for these two bacterial species were downloaded from NCBI By using CD-HIT paralog sequences at 60% identity were excluded from further study as earlier described (9, 10). The essential gene sequences were taken form from the Database of Essential Gene (DEG). Non human homologous sequences were identified by BLASTP analysis of non redundant sequences at E-value cut-off of 10^{-3} against human protein sequences (9, 10). Non human homologous sequences were aligned with sequences downloaded from DEG database using BLASTP at an E-value cut-off of 10^{-10} and 30% identity. The resultant protein sequences were considered as essential drug target proteins. Further using

KEGG (<http://www.genome.jp/kegg.html>.) pathway prediction these essential drug target proteins were analyzed whether these are active role in various metabolic and cellular pathways.

Results and Discussion

Bacteria are the greatest threat to food safety and may cause food poisoning. *Listeria monocytogenes* is a causative agent of Listeriosis, a most virulent foodborne clinical infection and leading cause of death among foodborne bacterial pathogens (11). The majority of human listeriosis cases occur in neonates, immunosuppressed, pregnant women and old people. This is a major threat to human health (12). The recent study describes the way *Listeria* grabs onto molecular handles on cells in the small intestine and then switches on those cells' own uptake systems to hitch a ride inside (13). Similarly, *Bacillus cereus* is a, Gram-positive, rod-shaped, beta hemolytic bacterium causing nausea, vomiting and diarrhea. Generally speaking, *Bacillus* foodborne illnesses occur due to survival of the bacterial endospores when food is improperly cooked.

The computational analysis of full genome sequences for identification of probable antimicrobial drug targets has become a new trend in pharmacogenomics. Two bacterial pathogens causing foodborn human disease (Table1) were covered for genome analysis and summary of the results are listed in Table 1. The current study has been included in our database (14).

List of all drug targets for each pathogen is listed in Tables 2 & 3. We got adequate number

Table 1. Summary of genome analysis of selected bacterial species

Species	Disease caused	Total No. of protein coding sequence	Non-paralogs	Non human homologous proteins	Number of proteins with matches in DEG (Essential proteins)
<i>Bacillus cereus</i>	<i>B. cereus</i> food poisoning	5754	5486	4256	99
<i>Listeria monocytogenes</i>	Listeriosis, perinatal septicemia, meningitis, encephalitis, intrauterine infections	2846	2814	1973	82

Table 2. List of potential drug targets in *Bacillus cereus*

S. No.	Gene ID	Query gene name	Similar Essential Gene in Essential Gene Databank	Gene name (DEG)	Functions
1.	217956718	DNA polymerase III, beta subunit	DEG10010002; GI:16077070; <i>Bacillus subtilis</i> 168	dnaN	DNA polymerase III (βsubunit)
2.	217956751	IS3-family transposase, OriB	DEG10050630; GI:30995473; <i>Haemophilus influenzae</i> Rd KW20	HII721	transposase
3.	217956824	DNA-binding protein HU 1	DEG10010160; GI:16079336; <i>Bacillus subtilis</i> 168	hbs	nonspecific DNA-binding protein HBSu
4.	217956846	Transcriptional activator, ArcC family	DEG10040261; GI:90111290; <i>Escherichia coli</i> MG1655	marA	Multiple antibiotic resistance protein marA
5.	217956849	N-acetylmuramoyl-L-alanine amidase	DEG10100610; GI:57117169; <i>Mycobacterium tuberculosis</i>	cwlM	H37Rv PROBABLE HYDROLASE
6.	217956852	Transposition helper protein, IS21 family	DEG10100541; GI:15610563; <i>Mycobacterium tuberculosis</i> H37Rv	Rv347c	POSSIBLE TRANSPOSASE
7.	217956859	Transcription regulator, Cro/CI family-related protein	DEG10120204; GI:118497481; <i>Francisella novicida</i> U112	FTN_0889	transcriptional regulator, cro/CI-type HTH domain
8.	217956883	Bifunctional glutamate-cysteine ligase/glutathione synthetase	DEG10120083; GI:118496889; <i>Francisella novicida</i> U112	gshA	Glutamate-cysteine ligase
9.	217956894	DNA-binding response regulator	DEG10070064; GI:15901089; <i>Streptococcus pneumoniae</i>	SP_1227	DNA-binding response regulator
10.	217956895	Sensor histidine kinase	DEG10010262; GI:16081092; <i>Bacillus subtilis</i> 168	yyeG	two-component sensor histidine kinase
11.	217956900	Site-specific tyrosine recombinase XerS	DEG10040560; GI:16131663; <i>Escherichia coli</i> MG1655	xerC	Integrase/recombinase
12.	217956960	NlpC/P60 family domain protein	DEG1005047; GI:16273226; <i>Haemophilus influenzae</i> Rd KW20	nlpC	lipoprotein
13.	217322984	hypothetical protein BCAA1187_B0006	DEG10010000; GI:16077070; <i>Bacillus subtilis</i> 168	dnaN	DNA polymerase III beta subunit
14.	217957585	DNA replication and repair protein RecF	DEG1002000; GI:15925709; <i>Staphylococcus aureus</i> N315	recF	Recombinational DNA repair ATPase (RecF pathway)
15.	217957600	Conserved hypothetical protein TIGR00103	DEG10020027; GI:15926156; <i>Staphylococcus aureus</i> N315	SA0437	conserved hypothetical protein
16.	217957606	Thymidylate kinase	DEG10010008; GI:16077096; <i>Bacillus subtilis</i> 168	mk/tdk	thymidylate kinase
17.	217957610	Hypothetical protein BCAA1187_A0043	DEG10080302; GI:15646113; <i>Helicobacter pylori</i> 26695	HP1504	hypothetical protein
18.	217957612	Tetrapyrrole methylase family protein	DEG10020030; GI:15926166; <i>Staphylococcus aureus</i> N315	SA0447	conserved hypothetical protein
19.	217957616	Primase-related protein	DEG10070228; GI:15903846; <i>Streptococcus pneumoniae</i>	spr1804	conserved hypothetical protein
20.	217957621	4-diphosphocytidyl-2C-methyl-D-erythritol kinase	DEG10010011; GI:16077114; <i>Bacillus subtilis</i> 168	ispE	4-diphosphocytidyl-2-C-methyl-D-erythritol kinase

21.	217957632	tetrapyrrole methylase family protein/MazG family protein	DEG10050133;GI:16272408; <i>Haemophilus influenzae Rd KW20</i>	mazG	Nucleoside triphosphate pyrophosphohydrolyase
22.	217957633	S4 domain protein	DEG10020036;GI:15926183; <i>Staphylococcus aureus N315</i>	SA0464	conserved hypothetical protein
23.	217957636	cell division protein DivIC	DEG10010015;GI:16077130; <i>Bacillus subtilis 168</i>	divIC	cell-division initiation protein (septum formation)
24.	217957639	(RNA(Ile)-)lysine synthetase	DEG10010016;GI:16077135; <i>Bacillus subtilis 168</i>	yacA	conserved protein
25.	217957643	chaperonin, 33 kDa	DEG10050293;GI:16272751; <i>Haemophilus influenzae Rd KW20</i>	hsO	Hsp33-like chaperonin
26.	217957645	para-aminobenzoate synthase, component I	DEG10130045;GI:50083571; <i>Acinetobacter baylyi ADP1</i>	tpE	anthranilate synthase component I
27.	217957647	4-amino-4-deoxychorismate lyase PabC	DEG10130099;GI:50083832; <i>Acinetobacter baylyi ADP1</i>	ilvE	chain amino acid transferase
28.	217957648	dihydropteroate synthase	DEG10130341;GI:50085894; <i>Acinetobacter baylyi ADP1</i>	folP	7,8-dihydropteroate synthase
29.	217957649	dihydroneopterin aldolase	DEG10070128;GI:15902313; <i>Streptococcus pneumoniae</i>	sufD	Aldolase-pyrophosphokinase
30.	217957650	2-amino-4-hydroxy-6-hydroxymethylidihydropteridine pyrophosphokinase	DEG10040033;GI:16128135; <i>Escherichia coli MG1655</i>	folK	2-amino-4-hydroxy-6-hydroxymethylidihydropteridine pyrophosphokinase
31.	217957662	2C-methyl-D-erythritol 2,4-cyclodiphosphate synthase	DEG10010020;GI:16077159; <i>Bacillus subtilis 168</i>	yacN/ispF	2-C-methyl-D-erythritol 2,4-cyclodiphosphate synthase
32.	217957664	Serine O-acetyltransferase	DEG10040539;GI:16131478; <i>Escherichia coli MG1655</i>	cysE	Serine acetyltransferase
33.	217957671	Transcription antitermination protein NusG	DEG10040702;GI:16131812; <i>Escherichia coli MG1655</i>	nusG	transcription termination factor
34.	217957673	Ribosomal protein L1	DEG10010025;GI:16077171; <i>Bacillus subtilis 168</i>	rpIA	ribosomal protein L1 (BL1)
35.	217957674	Ribosomal protein L10	DEG10010026;GI:16077172; <i>Bacillus subtilis 168</i>	rpJ	Ribosomal protein L10 (BL5)
36.	217957675	Ribosomal protein L7/L12	DEG10010027;GI:16077173; <i>Bacillus subtilis 168</i>	rpLL	Ribosomal protein L12 (BL9)
37.	217957687	Ribosomal protein L23	DEG10010037;GI:16077186; <i>Bacillus subtilis 168</i>	rpW	Ribosomal protein L23
38.	217957693	Ribosomal protein L29	DEG10010043;GI:16077192; <i>Bacillus subtilis 168</i>	rpmC	Osomal protein L29
39.	217957694	Ribosomal protein S17	DEG10010044;GI:16077193; <i>Bacillus subtilis 168</i>	rpmQ	Ribosomal protein S17 (BS16)
40.	217957701	Ribosomal protein L18	DEG10010051;GI:16077200; <i>Bacillus subtilis 168</i>	rpIR	Ribosomal protein L18
41.	217957703	Ribosomal protein L30	DEG10010053;GI:16077202; <i>Bacillus subtilis 168</i>	rpmD	Ribosomal protein L30 (BL27)
42.	217957708	Translation initiation factor IF-1	DEG10010058;GI:16077207; <i>Bacillus subtilis 168</i>	infA	Initiation factor IF-1

43.	217957712	DNA-directed RNA polymerase, alpha subunit	DEG10010062;GI:1607721; <i>Bacillus subtilis</i> 168	rpoA	RNA polymerase (α subunit)
44.	217957716	cobalt transport protein	DEG10020249;GI:15927800; <i>Staphylococcus aureus</i> N315	SA2019	Conserved hypothetical protein
45.	217957727	glycerate kinase	DEG10050042;GI:16272065; <i>Haemophilus influenzae</i> Rd KW20	gixK	Hypothetical protein
46.	217957729	conserved hypothetical protein TIGR00159	DEG10070191;GI:15903462; <i>Streptococcus pneumoniae</i>	spr1419	Conserved hypothetical protein
47.	217957730	hypothetical protein BCAA187_A0200	DEG10020245;GI:15927743; <i>Staphylococcus aureus</i> N315	SA1966	Conserved hypothetical protein
48.	217957736	gluconate permease	DEG10110157; GI:16766219; <i>Salmonella typhimurium</i> LT	STM2913	H ⁺ /gluconate symporter
49.	217957748	putative ABC transporter, substrate-binding protein	DEG10020076;GI:15926499; <i>Staphylococcus aureus</i> N315	SA0771	Conserved hypothetical protein
50.	217957751	oxidoreductase, FAD-binding	DEG10100593; GI:15610926; <i>Mycobacterium tuberculosis</i> H37Rv	Rv3790	Probable oxidoreductase
51.	217957756	oligopeptide ABC transporter, permease protein	DEG10140154;GI:15828881; <i>Mycoplasma pulmonis</i> UAB CTIP	oppB	Ligopeptide ABC transporter, permease protein
52.	217957757	oligopeptide ABC transporter, permease protein	DEG10080053;GI:15644928; <i>Helicobacter pylori</i> 26695	dppC	Peptide ABC transporter, permease protein (dppC)
53.	217957760	oligopeptide ABC transporter, oligopeptide-binding protein	DEG10080052;GI:15644926; <i>Helicobacter pylori</i> 26695	dppA	Dipeptide ABC transporter, periplasmic dipeptide-binding protein (dppA)
54.	217957763	putative oligopeptide ABC transporter, oligopeptide-binding protein	DEG10080052; GI:15644926; <i>Helicobacter pylori</i> 26695	dppA	Dipeptide ABC transporter, periplasmic dipeptide-binding protein (dppA)
55.	217957769	molybdenum ABC transporter, permease protein	DEG10100383;GI:15609536; <i>Mycobacterium tuberculosis</i> H37Rv	cysT	Probable sulfate Transport Integral Protein ABC transporter
56.	217957773	transcriptional regulator, LysR family	DEG10130120;GI:50083964; <i>Acinetobacter baylyi</i> ADP1	ACIAD0746	Putative transcriptional regulator (LysR family)
57.	217957778	sugar-binding transcriptional regulator, LacI family	DEG10050595;GI:16273524; <i>Haemophilus influenzae</i> Rd KW20	purR	Purine nucleotide synthesis repressor
58.	217957792	extracellular solute-binding protein family 5	DEG10080052;GI:15644926; <i>Helicobacter pylori</i> 26695	dppA	Dipeptide ABC transporter, periplasmic dipeptide-binding protein (dppA)
59.	217957793	oligopeptide ABC transporter, permease protein	DEG10060059; GI:12044929; <i>Mycoplasma genitalium</i> G37	oppB	Oligopeptide ABC transporter, permease protein (OppB)
60.	217957794	oligopeptide ABC transporter, permease protein	DEG10080053; GI:15644928; <i>Helicobacter pylori</i> 26695	dppC	Peptide ABC transporter, permease protein (dppC)
61.	217957797	hydrolase, haloacid dehalogenase-like family	DEG10020241;GI:15927733; <i>Staphylococcus aureus</i> N315	SA1957	conserved hypothetical protein
62.	217957806	UDP-N-acetylmuramoyl-tripeptide--D-alanyl-D-alanine ligase	DEG10010070;GI:16077524; <i>Bacillus subtilis</i> 168	murf	UDP-N-acetylmuramoyl-D-glutanyl-2, 6-diaminopimelate-D-alanyl-D-alanine ligase

63.	217957810	holo-(acyl)-carrier-protein) synthase	DEG10010071;GI:16077529; <i>Bacillus subtilis</i> 168	acpS	holo-acyl carrier protein synthase
64.	217957812	alanine racemase	DEG10010072;GI:16077531; <i>Bacillus subtilis</i> 168	alr	D-alanine racemase
65.	217957817	conserved hypothetical protein TIGR00150	DEG10010073;GI:16077658; <i>Bacillus subtilis</i> 168	ydiB	Conserved protein
66.	217957818	hypothetical protein BCAA187_A0309	DEG10010074;GI:16077659; <i>Bacillus subtilis</i> 168	ydiC	Probable protease
67.	217957828	xanthine/uracil permease family protein	DEG10110218;GI:16767518; <i>Salmonella typhimurium</i> LT2	ycd	permease with ATP/GTP-binding site
68.	217957830	sensor histidine kinase	DEG10010262; GI:16081092; <i>Bacillus subtilis</i> 168	ycyG	two-component sensor histidine kinase
69.	217957841	proline dehydrogenase	DEG10100174;GI:15608328; <i>Mycobacterium tuberculosis</i> H37Rv	Rv1188	Probable proline dehydrogenase
70.	217957845	transposase in <i>Marmococcus halophilus</i>	DEG10050630; GI:30995473; <i>Haemophilus influenzae</i> Rd KW20	HI1721	Transposase
71.	217957848	Phosphoribosylaminoimidazole carboxylase, ATPase subunit	DEG10050583;GI:16273506; <i>Haemophilus influenzae</i> Rd KW20	purK	Phosphoribosylaminoimidazole carboxylase ATPase subunit
72.	217957863	ATP-dependent DNA helicase PerA	DEG10010080;GI:16077729; <i>Bacillus subtilis</i> 168	perA	ATP-dependent DNA helicase
73.	217957866	hypothetical protein BCAA187_A0380	DEG10050093; GI:16272162; <i>Haemophilus influenzae</i> Rd KW20	HI0198	hypothetical protein
74.	217957872	putative ABC transporter, substrate-binding protein	DEG10020025; GI:15926141; <i>Staphylococcus aureus</i> N315	SA0422	Hypothetical protein
75.	217957878	glutamyl-tRNA(Gln) amidotransferase, C subunit	DEG10010082; GI:16077735; <i>Bacillus subtilis</i> 168	gatC	glutamyl-tRNA(Gln) amidotransferase (subunit C)
76.	217957888	aminopeptidase AmpS	DEG10020212;GI:15927453; <i>Staphylococcus aureus</i> N315	ampS	aminopeptidase ampS
77.	217957912	Transposase	DEG10050630; GI:30995473; <i>Haemophilus influenzae</i> Rd KW20	HI1721	transposase
78.	217957915	hypothetical protein BCAA187_A0431	DEG10120176; GI:118497344; <i>Francisella novicida</i> U112	FTN_0749	predicted metal-dependent hydrolase
79.	217957919	Na ⁺ /H ⁺ antiporter NhaC	DEG10050402;GI:16273033; <i>Haemophilus influenzae</i> Rd KW20	nhaC	Na ⁺ /H ⁺ antiporter
80.	217957929	iron compound ABC transporter, permease protein	DEG10050541;GI:16273375; <i>Haemophilus influenzae</i> Rd KW20	HI1471	iron chelatin ABC transporter permease protein
81.	217957930	iron compound ABC transporter, permease protein	DEG10050541; GI:16273375; <i>Haemophilus influenzae</i> Rd KW20	HI1471	iron chelatin ABC transporter permease protein
82.	217957932	pyrimidine nucleoside-disulfide oxidoreductase family protein	DEG10010230; GI:16080264; <i>Bacillus subtilis</i> 168	yumC	imiliar to thioredoxin reductase

83.	217957949	glutamine ABC transporter, permease/substrate-binding protein	DEG10040134; GI:16128778; <i>Escherichia coli</i> MG1655	glnP	Glutamine transport system permease protein glnP
84.	217957954	PTS system, IIBC component	DEG10020290; GI:15928117; <i>Staphylococcus aureus</i> N315	ptsG	PTS system, glucose-specific IIBC component
85.	217957969	Thiamine-phosphate pyrophosphorylase	DEG10050143; GI:16272366; <i>Haemophilus influenzae</i> Rd KW20	thtE	thiamine-phosphate pyrophosphorylase
86.	217957972	Methyl-accepting chemotaxis protein	DEG10040244; GI:16129380; <i>Escherichia coli</i> MG1655	trg	Methyl-accepting chemotaxis protein III
87.	217957974	putative ABC transporter, permease protein	DEG10050126; GI:16272305; <i>Haemophilus influenzae</i> Rd KW20	H0355	ABC transporter permease protein
88.	217957986	DNA-binding protein	DEG10150055; GI:116052113; <i>Pseudomonas aeruginosa</i> UCBPP-PA14	PA14_11150	putative transcriptional regulator
89.	217957994	putative tellurium resistance protein	DEG10130239; GI:50085095; <i>Acinetobacter baumannii</i> ADP1	terD	tellurium resistance protein
90.	217957995	tellurium resistance protein	DEG10130239; GI:50085095; <i>Acinetobacter baumannii</i> ADP1	terD	tellurium resistance protein
91.	217957997	putative tellurium resistance protein	DEG10110108; GI:16765169; <i>Salmonella typhimurium</i> LT2	yoaE	hypothetical protein containing CBS domain
92.	217958038	pts system, N-acetylglucosamine-specific iibc component	DEG10020290; GI:15928117; <i>Staphylococcus aureus</i> N315	ptsG	PTS system, glucose-specific IIBC component
93.	217958046	formate acetyltransferase	DEG10050082; GI:16272145; <i>Haemophilus influenzae</i> Rd KW20	pfmB	formate acetyltransferase 1-like protein
94.	217958047	Pyruvate formate-lyase-activating enzyme	DEG10050081; GI:16272144; <i>Haemophilus influenzae</i> Rd KW20	pfmA	pyruvate formate lyase-activating enzyme 1
95.	217958064	hypothetical protein BCAA187_A0583	DEG10140062; GI:15828648; <i>Mycoplasma pulmonis</i> UAB CTIP	cysS	Cysteine-lyase synthetase
96.	217958067	putative glutamate synthase, large subunit	DEG10130453; GI:50086330; <i>Acinetobacter baumannii</i> ADP1	gltB	glutamate synthase large chain precursor
97.	217958078	penicillin-binding domain protein	DEG10050632; GI:16273611; <i>Haemophilus influenzae</i> Rd KW20	mrcB/pomB	penicillin-binding protein 1B
98.	217958084	sensory box/GGDEF family protein	DEG10130392; GI:50086105; <i>Acinetobacter baumannii</i> ADP1	ACIAD3099	conserved hypothetical protein; putative membrane protein
99.	217958097	replicative DNA helicase	DEG10010264; GI:16081096; <i>Bacillus subtilis</i> 168	dnaC	replicative DNA helicase

Table 3. List of potential drug targets in *Bacillus cereus*

S.No.	Gene ID	Query gene name	Similar Essential Gene in Essential Gene Databank (DEG)	Gene name	Functions
1.	16802049	chromosomal replication initiation protein	DEG10010001:G116077069; <i>Bacillus subtilis</i> 168	dnaA	initiation of chromosome replication
2.	16802050	DNA polymerase III subunit β	DEG10010002:G116077070; <i>Bacillus subtilis</i> 168	dnaN	DNA polymerase III (beta subunit)
3.	16802053	recombination protein F	DEG10020002:G115925709; <i>Staphylococcus aureus</i> N315	recF	Recombinational DNA repair ATPase (RecF pathway)
4.	16802056	hypothetical protein lmo0008	DEG101402526:G115829136; <i>Mycoplasma pulmonis</i> UAB CTIP	cls	Cardiolipin Synthetase
5.	16802070	hypothetical protein lmo0022	DEG10040470:G190111546; <i>Escherichia coli</i> MG1655	agaV	PTS system, N-acetylgalactosamine-specific IIB component 2
6.	16802075	hypothetical protein lmo0027	DEG10020290:G115928117; <i>Staphylococcus aureus</i> N315	ptsG	PTS system, glucose-specific IIBC component
7.	16802078	hypothetical protein lmo0030	DEG10060221:G112045121; <i>Mycoplasma genitalium</i> G37	MG_265	Cof-like hydrolase
8.	16802079	LacI family transcription Regulator	DEG10050595:G116273524; <i>Haemophilus influenzae</i> Rd KW20	purR	purine nucleotide synthesis repressor
9.	16802087	carbamate kinase	DEG10040907:G116128505; <i>Escherichia coli</i> MG1655	arcC/abcF	Carbamate kinase
10.	16802090	hypothetical protein lmo0042	DEG10040465:G116130990; <i>Escherichia coli</i> MG1655	yjiA	Hypothetical protein
11.	16802092	30S ribosomal protein S6	DEG10010269:G116081143; <i>Bacillus subtilis</i> 168	rpsF	ribosomal protein S6 (BS9)
12.	16802100	hypothetical protein lmo0052	DEG10140198:G115828988; <i>Mycoplasma pulmonis</i> UAB CTIP	MYPU_5170	Conserved hypothetical protein
13.	16802101	50S ribosomal protein L9	DEG10010265:G116081102; <i>Bacillus subtilis</i> 168	rplI	ribosomal protein L9
14.	16802102	replicative DNA helicase	DEG10010264:G116081096; <i>Bacillus subtilis</i> 168	dnaC	replicative DNA helicase
15.	16802105	hypothetical protein lmo0057	DEG10020016:G115925985; <i>Staphylococcus aureus</i> N315	SA0272	similar to transmembrane protein Tmp7
16.	16802109	hypothetical protein lmo0061	DEG10100024:G115607425; <i>Mycobacterium tuberculosis</i> H37Rv	Rv0284	Possible conserved member Protein
17.	16802144	hypothetical protein lmo0096	DEG10040470:G190111546; <i>Escherichia coli</i> MG1655	agaV	PTS system, N-acetylgalactosamine-specific IIB component 2
18.	16802179	hypothetical protein lmo0131	DEG10130392:G150086105; <i>Acinetobacter baumannii</i> ADP1	ACIAD3099	conserved hypothetical protein; putative membrane protein
19.	16802183	hypothetical protein lmo0135	DEG10110050:G116764211; <i>Salmonella typhimurium</i> LT2	yjiB	ABC-type/oligopeptide/nickel transport system
20.	16802184	hypothetical protein lmo0136	DEG10140104:G115828754; <i>Mycoplasma pulmonis</i> UAB CTIP	oppB	Oligopeptide ABC transporter, permease protein (OppB)

21.	16802185	hypothetical protein lmo0137	DEG10080053;GI 15644928; <i>Helicobacter pylori</i> Z6695	dppC	dipeptide ABC transporter, permease protein (dppC)
22.	16802200	hypothetical protein lmo0152	DEG10110050;GI 16764211; <i>Salmonella typhimurium</i> LT2	yjIB	ABC-type/oligopeptide/nickel transport system
23.	16802201	hypothetical protein lmo0153	DEG10070158;GI 15902950; <i>Streptococcus pneumoniae</i>	lmb	Lipoprotein
24.	16802206	hypothetical protein lmo0158	DEG10140208;GI 15829020; <i>Mycoplasma pulmonis</i> UAB C71P	MYPU_5490	COF family HAD hydrolase protein
25.	16802210	DNA polymerase III subunit delta	DEG10010009;GI 16077099; <i>Bacillus subtilis</i> 168	holB	DNA polymerase III (delta subunit)
26.	16802214	GIY-YIG nuclease superfamily protein	DEG10020029;GI 15926165; <i>Staphylococcus aureus</i> N315	SA0446	Conserved hypothetical protein
27.	16802215	hypothetical protein lmo0167	DEG10020030;GI 15926166; <i>Staphylococcus aureus</i> N315	SA0447	conserved hypothetical protein
28.	16802225	hypothetical protein lmo0179	DEG10070115;GI 15902125; <i>Streptococcus pneumoniae</i>	ABC-MSP	ABC transporter membrane-spanning permease - sugar transport
29.	16802226	hypothetical protein lmo0180	DEG10060158;GI 108885091; <i>Mycoplasma genitalium</i> G37	MG_189	ABC transporter, permease protein
30.	16802227	hypothetical protein lmo0181	DEG10100311;GI 15609178; <i>Mycobacterium tuberculosis</i> H37Rv	Rv2041c	Probable sugar-binding lipoprotein
31.	16802233	hypothetical protein lmo0187	DEG10070228;GI 15903846; <i>Streptococcus pneumoniae</i>	spr1804	Conserved hypothetical protein
32.	16802236	4-diphosphocytidylyl-2-C-methyl-D-erythritol kinase	DEG10010011;GI 16077114; <i>Bacillus subtilis</i> 168	ispE	4-diphosphocytidylyl-2-C-methyl-D-erythritol kinase
33.	16802254	hypothetical protein lmo0208	DEG10040140;GI 16128834; <i>Escherichia coli</i> MG1655	yjQ	Hypothetical protein
34.	16802261	hypothetical protein lmo0215	DEG10070074;GI 15901374; <i>Streptococcus pneumoniae</i>	SP_1529	polysaccharide biosynthesis protein, putative
35.	16802262	hypothetical protein lmo0216	DEG10020036;GI 15926183; <i>Staphylococcus aureus</i> N315	SA0464	conserved hypothetical protein
36.	16802268	hypothetical protein lmo0222	DEG10050293;GI 16272751; <i>Haemophilus influenzae</i> Rd KW20	hsO	Hsp33-like chaperonin
37.	16802270	hypothetical protein lmo0224	DEG10050637;GI 16273369; <i>Haemophilus influenzae</i> Rd KW20	folP-B /folP-2	Dihydropterolate synthase
38.	16802271	hypothetical protein lmo0225	DEG10100566;GI 57117133; <i>Mycobacterium tuberculosis</i> H37Rv	folX/foIB	Probable Dihydroneopterin Aldolase Folb (DHNA)
39.	16802272	hypothetical protein lmo0226	DEG10040033;GI 16128135; <i>Escherichia coli</i> MG1655	folK	2-amino-4-hydroxy-6-hydroxymethylidihydropteridine pyrophosphokinase
40.	16802282	2-C-methyl-D-erythritol 2,4-cyclodiphosphate synthase	DEG10010020;GI 16077159; <i>Bacillus subtilis</i> 168	yacN/ispF	2-C-methyl-D-erythritol 2,4-cyclodiphosphate synthase
41.	16802284	hypothetical protein lmo0238	DEG10040639;GI 16131478; <i>Escherichia coli</i> MG1655	cysE	Serine acetyltransferase
42.	16802292	transcription antitermination protein	DEG10040702;GI 16131812; <i>Escherichia coli</i> MG1655	nusG	Transcription termination

	NusG			factor
43.	50S ribosomal protein L10	DEG10010026;GI 16077172; <i>Bacillus subtilis</i> 168	rplJ	Ribosomal protein L10 (BL5)
44.	hypothetical protein lmo0272	DEG10140085;GI 15828715; <i>Mycoplasma pulmonis</i> UAB CTIP	MYPU_2440	COF family HAD hydrolase protein, conserved
45.	hypothetical protein lmo0275	DEG10050028;GI 16272035; <i>Haemophilus influenzae</i> Rd KW20	rec2	Recombination protein
46.	hypothetical protein lmo0276	DEG10060221;GI 12045121; <i>Mycoplasma genitalium</i> G37	MG_265	CoI-like hydrolase
47.	putative lipoprotein	DEG10020076;GI 15926499; <i>Staphylococcus aureus</i> N315	SA0771	Conserved hypothetical protein
48.	hypothetical protein lmo0287	DEG10010263;GI 16081093; <i>Bacillus subtilis</i> 168	ycyF	Two-component response regulator
49.	hypothetical protein lmo0288	DEG10010262;GI 16081092; <i>Bacillus subtilis</i> 168	ycyG	Two-component sensor histidine kinase
50.	hypothetical protein lmo0291	DEG10020008;GI 15925727; <i>Staphylococcus aureus</i> N315	SA0021	Conserved hypothetical protein
51.	SPOUT methyltransferase superfamily protein	DEG10040111;GI 16128619; <i>Escherichia coli</i> MG1655	ybeA	Hypothetical protein
52.	hypothetical protein lmo0318	DEG10050143;GI 16272366; <i>Haemophilus influenzae</i> Rd KW20	thiE	Thiamine-phosphate pyrophosphorylase
53.	hypothetical protein lmo0345	DEG10060327;GI 12045258; <i>Mycoplasma genitalium</i> G37	rpiB	ribose 5-phosphate isomerase B
54.	hypothetical protein lmo0352	DEG10050198;GI 16272557; <i>Haemophilus influenzae</i> Rd KW20	fucR	L-fucose operon activator
55.	hypothetical protein lmo0357	DEG10020060;GI 15926377; <i>Staphylococcus aureus</i> N315	fruA	fructose specific permease
56.	hypothetical protein lmo0358	DEG10020060;GI 15926377; <i>Staphylococcus aureus</i> N315	fruA	fructose specific permease
57.	hypothetical protein lmo0359	DEG10010257;GI 16080765; <i>Bacillus subtilis</i> 168	fbaA	fructose-1,6-bisphosphate aldolase
58.	hypothetical protein lmo0360	DEG10050198;GI 16272557; <i>Haemophilus influenzae</i> Rd KW20	fucR	L-fucose operon activator
59.	hypothetical protein lmo0361	DEG10080188;GI 15645675; <i>Helicobacter pylori</i> 26695	HP1061	hypothetical protein
60.	hypothetical protein lmo0370	DEG10150009;GI 116053849; <i>Pseudomonas aeruginosa</i> UCBBP-PA14	PA14_01560	hypothetical protein
61.	hypothetical protein lmo0371	DEG10040547;GI 16131552; <i>Escherichia coli</i> MG1655	yidP	Hypothetical transcriptional regulator yidP
62.	hypothetical protein lmo0374	DEG10040298;GI 16129692; <i>Escherichia coli</i> MG1655	celA/cbbB	PTS system, cellobiose-specific IIB component
63.	hypothetical protein lmo0382	DEG10050198;GI 16272557; <i>Haemophilus influenzae</i> Rd KW20	fucR	L-fucose operon activator

64.	I6802445	hypothetical protein lmo0400	DEG10020295;GI 15928227; <i>Staphylococcus aureus</i> N315	SA2434	fructose phosphotransferase system enzyme fruA homolog
65.	I6802460	hypothetical protein lmo0416	DEG10150055;GI 11605213; <i>Pseudomonas aeruginosa</i> UCBBP-PA14	PA14_11150	putative transcriptional regulator
66.	I6802470	hypothetical protein lmo0426	DEG10020060;GI 15926377; <i>Staphylococcus aureus</i> N315	fruA	fructose specific permease
67.	I6802471	hypothetical protein lmo0427	DEG10020060;GI 15926377; <i>Staphylococcus aureus</i> N315	fruA	fructose specific permease
68.	I6802472	hypothetical protein lmo0428	DEG10020295;GI 15928227; <i>Staphylococcus aureus</i> N315	SA2434	fructose phosphotransferase system enzyme fruA homolog
69.	I6802474	hypothetical protein lmo0430	DEG10130303;GI 50085591; <i>Acinetobacter baylyi</i> ADP1	ACIAD2511	putative transcriptional regulator (LysR family)
70.	I6802485	hypothetical protein lmo0441	DEG10040110;GI 16128618; <i>Escherichia coli</i> MG1655	mrdA	Penicillin-binding protein 2
71.	I6802498	hypothetical protein lmo0454	DEG10100250;GI 57116872; <i>Mycobacterium tuberculosis</i> H37Rv	moxR/moxR1	Probable Transcriptional Regulator Protein MOXR1
72.	I6802531	hypothetical protein lmo0488	DEG10130120;GI 50083964; <i>Acinetobacter baylyi</i> ADP1	ACIAD0746	putative transcriptional regulator (LysR family)
73.	I6802535	hypothetical protein lmo0492	DEG10050429;GI 16273646; <i>Haemophilus influenzae</i> Rd KW20	geVA	Transcription activator
74.	I6802536	hypothetical protein lmo0493	DEG10100180;GI 15608355; <i>Mycobacterium tuberculosis</i> H37Rv	Rv1215c	hypothetical protein
75.	I6802541	hypothetical protein lmo0498	DEG10080091;GI 15645199; <i>Helicobacter pylori</i> 26695	lacA/rpi	ribose-5-phosphate isomerase B
76.	I6802554	hypothetical protein lmo0511	DEG10150194;GI 116049679; <i>Pseudomonas aeruginosa</i> UCBBP-PA14	PA14_42180	hypothetical protein
77.	I6802562	hypothetical protein lmo0519	DEG10050322;GI 16272835; <i>Haemophilus influenzae</i> Rd KW20	enuB	multidrug resistance protein B
78.	I6802578	hypothetical protein lmo0535	DEG10050595;GI 16273524; <i>Haemophilus influenzae</i> Rd KW20	purR	purine nucleotide synthesis repressor
79.	I6802581	hypothetical protein lmo0538	DEG10010094;GI 16078483; <i>Bacillus subtilis</i> 168	ykuR	similar to deacetylases
80.	I6802605	phosphoribosyl-AMP cyclohydrolase	DEG10100264;GI 57116892; <i>Mycobacterium tuberculosis</i> H37Rv	hisI2/hisI	phosphoribosyl-AMP cyclohydrolase
81.	I6802606	imidazole glycerol phosphate synthase subunit HisF	DEG10130468;GI 50086378; <i>Acinetobacter baylyi</i> ADP1	hisF	imidazole glycerol phosphate synthase, cyclase subunit

Table 4. List of proteins (mainly enzymes) having active role in biosynthetic and metabolic pathways of *Bacillus cereus*

S.No.	Gene ID	Protein name	Role	EC number
1.	217956718	DNA polymerase III subunit beta	Purine metabolism; Pyrimidine metabolism DNA replication; Mismatch repair Homologous recombination	EC:2.7.7.7
2.	217956883	glutamate-cysteine ligase/glutathione synthetase	Glutathione metabolism; Metabolic pathways	EC:6.3.2.2
3.	217957585	recombination protein F	Homologous recombination	
4.	217957645	para-aminobenzoate synthase, component	Folate biosynthesis	EC:2.6.1.85
5.	217957727	glycerate kinase	Glycine, serine and threonine metabolism; Glycerolipid metabolism; Glyoxylate and dicarboxylate metabolism Methane metabolism; Metabolic pathways Microbial metabolism in diverse environments	EC:2.7.1.31
6.	217957757	oligopeptide ABC transporter, permease protein	ABC transporters	
7.	217957760	oligopeptide ABC transporter, oligopeptide-binding protein	ABC transporters	
8.	217957806	UDP-N-acetylmuramoyl-tripeptide--D-alanyl-D-alanine ligase	Lysine biosynthesis; Peptidoglycan biosynthesis Metabolic pathways	EC:6.3.2.10
9.	217957812	alanine racemase	D-Alanine metabolism; Metabolic pathways	EC:5.1.1.1
10.	217957828	guanine-hypoxanthine permease, xanthine/uracil permease family protein	putative MFS transporter, AGZA family, xanthine/uracil permease	
11.	217957830	sensor histidine kinase	two-component sensor histidine kinase	EC:2.7.13.3
12.	217957841	proline dehydrogenase	Arginine and proline metabolism; Metabolic pathways; Biosynthesis of secondary metabolites	EC:1.5.99.8
13.	217957848	phosphoribosylaminoimidazole carboxylase ATPase subunit	Purine metabolism; Metabolic pathways; Biosynthesis of secondary metabolites	EC:4.1.1.21
14.	217957863	ATP-dependent DNA helicase PerA	Nucleotide excision repair; Mismatch repair	EC:3.6.1.-
15.	217957919	Na ⁺ /H ⁺ antiporter NhaC	Methane metabolism	
16.	217957932	probable thioredoxin reductase	Pyrimidine metabolism	EC:1.8.1.9
17.	217957954	protein-N(pi)-phosphohistidine-sugar phosphotransferase (enzyme II of the phosphotransferase system) (PTS system glucose-specific IIBC component)	Glycolysis / Gluconeogenesis; Amino sugar and nucleotide sugar metabolism; Phosphotransferase system	EC:2.7.1.69
18.	217957972	methyl-accepting chemotaxis protein	Two-component system; Bacterial chemotaxis	
19.	217958046	formate acetyltransferase	Pyruvate metabolism; Propanoate metabolism Butanoate metabolism; Metabolic pathways	EC:2.3.1.54
20.	217958067	putative glutamate synthase	Alanine, aspartate and glutamate metabolism Nitrogen metabolism; Metabolic pathways Biosynthesis of secondary metabolites Microbial metabolism in diverse environments	EC:1.4.1.13

Table 5. List of proteins (mainly enzymes) having active role in biosynthetic and metabolic pathways of *Bacillus cereus*

S.No.	Gene ID	Protein name	Role	EC Number
1.				
2.	16802049	chromosomal replication initiation protein	Two-component system	
3.	16802050	DNA polymerase III subunit beta	Purine metabolism Pyrimidine metabolism Metabolic pathways DNA replication Mismatch repair Homologous recombination	EC:2.7.7.7
4.	16802056	hypothetical protein	Glycerophospholipid metabolism Metabolic pathways	EC:2.7.8.-
5.	16802075	hypothetical protein	Phosphotransferase system (PTS)	
6.	16802102	replicative DNA helicase	DNA replication	EC:3.6.1.-
7.	16802183	oligopeptide ABC transport system substrate-binding proteins	ABC transporters	
8.	16802200	hypothetical protein	ABC transporters	
9.	16802334	hypothetical protein	Two-component system	
10.	16802403	hypothetical protein	Fructose and mannose metabolism Metabolic pathways Phosphotransferase system (PT)	

of promising drug target protein in each species. Finally 82 genes in *Listeria monocytogenes* and 99 genes in *Bacillus cereus* were found which can be used as promising drug targets. The targets genes identified are involved in regulator protein, membrane proteins and hypothetical proteins of unknown function of bacterial species. No similar protein is functional in human. Further KEGG pathway prediction shows that 20 proteins in *Bacillus cereus* and 9 proteins in *Listeria monocytogenes* were found to have active role in biosynthetic and metabolic pathways (Table 4 and Table 5). The data for total number of gene sequence following non human homologous sequences and essential genes are shown in Table 1.

Recent publication of genome sequences of many organisms and several new bioinformatics tools have facilitated identification of antimicrobial drug targets in pharmacogenomics. In recent study, RecA was found an important factor in DNA repair and the activator of the SOS response that contributes to the resistance against acid and bile and to the ability of *L. monocytogenes* to adhere and invade human intestine epithelial cells (15). Present study reveals

with *in silico* analysis of essential genes as a preliminary step to screen through genome of these pathogens. We found some enzyme proteins actively involved in various processes like DNA replication, recombination, repairing etc. thus these enzyme/proteins can be used to deactivate RecA to inhibit further growth of *L. monocytogenes*. On average very less number of genes was annotated as essential genes so to allow for experimental analysis, leading to a systematic strategy in designing novel antimicrobial active compounds. These genes are of interest for further characterization to understand role of these gene in survival of species, as multi-drug target as they are involved in regulator protein, membrane proteins involved in biosynthetic and metabolic pathways and hypothetical proteins of unknown function of bacterial species. The compounds active on these genes are expected to be more effective for lethal action on bacteria without affecting host body. The long term goal of the study is to analyse several pathogens genome and prepare an extensive database of essential drug target proteins database as scientific resource.

Acknowledgment

Infrastructural facilities provided by Indian Institute of Technology Guwahati and Financial support by Department of Biotechnology, Government of India are acknowledged.

References

1. Kaminski, N. (2000). Bioinformatics. A user's perspective. *Am. J. Respir. Cell Mol. Biol.*, 23: 705-711.
2. Sakharkar, K.R., Sakharkar, M.K. and Chow, V.T. (2004). A novel genomics approach for the identification of drug targets in pathogens, with special reference to *Pseudomonas aeruginosa*. In *Silico Biol.*, 4: 355-360.
3. Allsop, A.E. (1998). New antibiotic discovery, novel screens, novel targets and impact of microbial genomics. *Curr. Opin. Microbiol.*, 1: 530-534.
4. Sakharkar, K.R., Sakharkar, M.K. and Chow, V.T.K. (2004) A novel genomics approach for the identification of drug targets in pathogens, with special reference to *Pseudomonas aeruginosa*. In *Silico Biol.*, 4: 0028.
5. Judson, N. and Mekalanos, J.J. (2000). TnAraOut, A transposon-based approach to identify and characterize essential bacterial genes. *Nat. Biotechnol.*, 18: 740-745.
6. Frtiz, B. and Raczniak, G.A. (2002) Bacterial genomics: potential for antimicrobial drug discovery. *BioDrugs.*, 16:331.
7. Miesel, L., Greene, J. and Black, T.A. (2003). Genetic strategies for antibacterial drug discovery. *Nat. Rev. Genet.*, 4: 442-456.
8. Rosamond, J. and Allsop, A. (2000). Harnessing the Power of the Genome in the Search for New Antibiotics. *Science*, 5460: 1973 – 1976
9. Ramaswamy, V., Cresence, V.M., Rejitha, J.S., Lekshmi, M.U., Dharsana, K.S., Prasad, S.P. and Vijila, H.M. (2007). *Listeria*—review of epidemiology and pathogenesis. *J Microbiol Immunol Infect.*, 40: 4-13.
10. Li, W., Jaroszewski, L. and Godzik, A. (2001). Clustering of highly homologous sequences to reduce the size of large protein databases. *Bioinformatics*, 17: 282-283.
11. Suthar, N., Goyal, A. and Dubey, V.K. (2009). Identification of potential drug targets of *Leishmania infantum* by in-silico genome analysis. *Letters in Drug Design and Discovery*, 6: 620-622.
12. Salihu, M. D., Junaidu, A. U., Manga, S. B., Gulumbe, M. L., Magaji, A. A., Ahmed A., Adamu, A.Y., Shittu, A. and Balarabe, I. (2008). Occurrence of *Listeria monocytogenes* in smoked fish in Sokoto, Nigeria. *African Journal of Biotechnology*, 7: 3082-3084.
13. Pentecost, M., Kumaran, J., Ghosh, P. and Amieva, M.R. (2010) *Listeria monocytogenes* Internalin B Activates Junctional Endocytosis to Accelerate Intestinal Invasion. *PLoS Pathogens*, DOI: 10.1371/journal.ppat.1000900
14. Shakyawar, S.K., Goyal, A. and Dubey, V.K. (2011). Database of *in silico* Predicted Potential Drug Target Proteins in Common Bacterial Human Pathogens. *American Journal of Drug Discovery and Development*, 1: 70-74.

15. Van der Veen, S. and Abee, T. (2011). Contribution of *Listeria monocytogenes* RecA to acid and bile survival and invasion of human intestinal Caco-2 cells. Int J Med Microbiol <http://dx.doi.org/10.1016/j.ijmm.2010.11.006>

Targeted Integration of *Bacillus thuringiensis* δ -Endotoxin *cryIFa1* in Brinjal (*Solanum melongena* L.)

Dipty Shrivastava,¹ Monika Dalal,^{1§} Vikrant Nain,^{1#} P. C. Sharma,² P. Ananda Kumar*¹

¹National Research Centre on Plant Biotechnology, IARI, New Delhi -110012, India.

²School of Biotechnology, GGS Indraprastha University, Sector -16C Dwarka Delhi, India.

Present addresses - #School of Biotechnology, Gautam Buddha University, Greater Noida-201308, India

[§]National Research Centre for Sorghum, Rajendra Nagar, Hyderabad-500 030, India

*For Correspondence - kumarpa@nrpcb.org

Abstract

Gene integration in plants by homologous recombination eliminates variation in transgene expression and gives a predictable plant phenotype. Present study demonstrates homologous recombination-mediated integration of *Bacillus thuringiensis cryIFa1* gene at *Flavonoid-3-glucosyltransferase* (anthocyanin biosynthesis pathway) locus in Brinjal (*Solanum melongena* L.), for introduction of resistance against its major insect pest 'Brinjal Fruit and Shoot Borer' (BFSB) (*Leucinodes orbonalis*). The transgenic lines showed complete protection against BFSB. These results provide a novel perspective on development of genetically modified crops with stable and predictable transgene expression, and the possibility of the utilization of such promising technology in future crop improvement programmes.

Key words: Anthocyanin, *Bt* transgenic, Gene targeting, Homologous recombination, *cryIF*, *Leucinodes orbonalis*.

Introduction

Technological developments in the field of plant molecular biology and biotechnology have revolutionized crop improvement (1). Available gene pool of all the living organisms makes it possible to introduce beneficial genes from any

species to the desired crop varieties (2). Standard plant genetic transformation techniques are *Agrobacterium*-mediated transformation and particle bombardment (3). In both of these approaches random transgene integration by illegitimate recombination in the genome results in considerable variation in transgene expression across different integration events and variation in transgene copy number (4). In addition, random T-DNA integration induces undesirable mutations in the host genome with unpredictable phenotypes (5). Gene targeting is a potential technology that can be used for making transgenic plants with predictable transgene expression and changes in host plant genome (6). It is based on homologous recombination, which allows the integration of DNA at predetermined positions, and therefore facilitates precision genome manipulation (7, 8).

Gene targeting has been efficiently applied to modify the genomes of bacteria (9), fungi (10) and eukaryotes (11), especially mammals where the targeting frequencies of 10^{-2} have been reported (12, 13). In plants a gene targeting frequency of only 10^{-6} to 10^{-3} have been reported. (14, 15,16,). Different strategies that include extending the homology length in targeting vectors (17) and using strong positive-negative selection to enrich the targeted events had been tested (18, 19). Shukla *et al.* (21) and Townsend *et al.* (20)

described modification of maize gene *IPKI* and tobacco gene *SuRB* gene respectively (20, 21). Shukla et al. (21) introduced an herbicide resistance gene into the *IPKI* locus and found that 3-20 percent of the resistant samples had *IPKI* targeted integration. Townsend et al. (20) used homologous recombination to target small change in the *SuRB* gene that resulted in achieving gene-targeting rates of four percent.

Since the first report on transgene integration by HR in plants (22), with the exception of a recent report by Shukla et al. (21), all attempts were limited to the demonstration of either integration of an exogenous gene at a predefined locus with increased frequency or screening rare HR events from random integration events (23). The present study was carried out to harness the benefit of gene targeting by developing insect resistant *Bt* transgenic brinjal (*Solanum melongena*).

Brinjal (*Solanum melongena* L), an important vegetable crop is severely infested by Brinjal Fruit and Shoot Borer (BFSB) (*Leucinodes orbonalis*) (Lepidoptera: Pyralidae) (24). The *B. thuringensis cryIF* gene has been found to be very effective against BFSB (Kumar et al. unpublished) and hence was selected for introduction in brinjal. For screening out the random T-DNA integration events at early stages of transgenic plant development, *GUS* reporter gene was used as a negative screening marker. Two targeted gene integration events were recovered out of 954 random gene integration events. The present study successfully demonstrated genetic modification of a crop plant for insect resistance by gene targeting.

Materials and Methods

Vector construction for homologous recombination : Brinjal cv. Pusa Purple Long was used as the host plant for carrying out the gene

targeting experiments. *Flavonoid-3-glucosyltransferase (F3G)* gene from anthocyanin synthesis pathway, which catalyzes the conversion of flavonoids into glycosides, was selected as a target locus. The target gene *F3G* was PCR amplified from brinjal genomic DNA using gene specific primers based on the published sequence (GenBank accession no. E12713). The PCR amplicon (1.3 kb) was cloned into pGEMTeasy vector (Promega) and referred as pF3G-TA. To develop HR mediated gene integration vector, *F3G* gene from pF3G-TA vector was sub-cloned in pCAMBIA1304 using *XbaI* (vector)-*XhoI* (insert) blunt at 5' end and *SalI* site at 3' end. pBI121Δ*GUS* vector was generated by deleting *GUS* gene from pBI121 vector. In the next step, *nptII* expression cassette and CaMV35S promoter with NOS terminator from pBI121Δ*GUS* were excised out with *EcoRI* and *PmeI*, end-filled and cloned at end-filled *BamHI* site (640 bp) of *F3G* and the construct was referred as pF3GT (Fig. 1). The synthetic codon modified *cryIF* gene was cloned in *XbaI*-*BamHI* sites present between CaMV35S promoter and NOS terminator, downstream to *nptII* expression cassette. This final construct named as pF3GT-F, was used as the gene targeting construct.

Genetic transformation of brinjal : Binary vector pF3GT-F was mobilized in *Agrobacterium tumefaciens* strain EHA-105 by freeze-thaw method (25). Brinjal was genetically transformed by using cotyledon leaf explants (26). The rooted kanamycin resistant plants were transplanted to pots, acclimatized and maintained in a glass house.

Histochemical GUS assay : Third leaf from putative transformants was analyzed for *GUS* activity (27), for screening the T-DNA integration events. Leaf tissues were immersed in 0.5 ml *GUS* assay buffer (0.5M EDTA, Triton X-100, 0.1M Sodium phosphate buffer

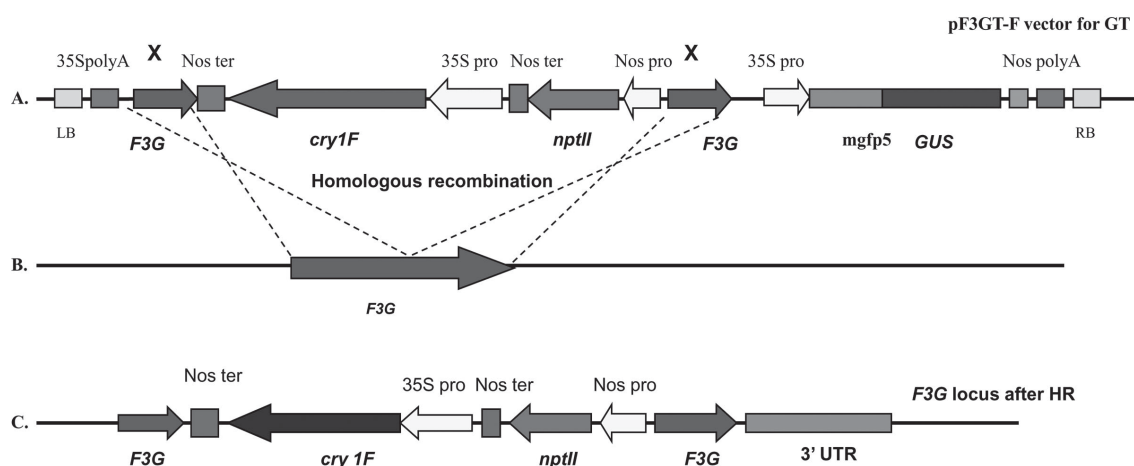


Fig. 1 Strategy of gene targeting through homologous recombination in brinjal (*S. melongena* L.). A. Vector construct (pF3GT-F) for targeted integration of *nptII* and *cry1F* gene at *F3G* locus by homologous recombination, *GUS* expression cassette lies out of homologous recombination cassette (region between two X), B. showing homologous recombination between T-DNA and *F3G* locus in brinjal genome, homologous recombination events will not have *GUS* gene integration in plant genome, C. *F3G* locus after homologous recombination mediated integration of *nptII* and *cry1F* genes.

(pH 8) and X-Gluc (52.0 gm/ml) in 24 well plates and incubated overnight at 37°C, followed by incubation in 70% ethanol for four hours to remove chlorophyll.

Molecular Analysis : Plant genomic DNA was isolated from T-0 plants (28), and screened for *GUS*, *nptII* and *cry1F* gene using a modified PCR protocol for testing Agrobacterium contaminated transgenic plants (29). Following gene specific primer sequences were used - *nptII* forward primer (5'-CAA TCG GCT CTG ATG CCG-3') reverse primer (5'-AGG CGA TAG AAG GCG ATG CGC-3'), *GUS* forward primer (5'-GAC TGT AAC CAC GCG TCT GTT GAC-3') reverse primer (5'-AGC CAT GCA CAC TGA TAC TCT TCAC-3'), *cry1F* forward primer (5'-GGA GTG GGA GTG GCG TTT GGC CTG-3') reverse primer (5'-CCA GTT TGT TGG AAG GCA ACT CCC-3'). These primer sets were designed for the amplification of 0.74 kb, 1.2 kb and 1.0 kb fragments of *nptII*, *GUS* and *cry1F* genes, respectively. The PCR conditions were

as follows: Initial denaturation at 94°C for 4 min; followed by 33 cycles of 94°C (1 min), 55°C (1 min), and 72°C (1 min) and final extension at 72°C for 5 min.

Results and Discussion

Target site selection : Large variations in expression and stability among different random integration events of transgenic plants developed by T-DNA integration are caused by genomic context in which the transgenes have integrated (6). Genes integrated in heterochromatin generally get silenced due to methylation of promoter region or packing of DNA into chromatin (6), making the promoter inaccessible to RNA polymerases and transcription factors. Targeted gene integration at a predetermined location in the plant genome by homologous recombination provides a mechanism to develop transgenics with predictable expression. However, expression of the transgene depends on the selection of targeting site used for HR based heterologous gene

integration. To develop transgenic brinjal for insect resistance, *Bt* gene driven by strong CaMV35S promoter must express in leaf, young stem and fruits at considerably higher level. It is possible only when the gene locus selected for targeted integration of *Bt* gene is under favorable chromatin structure or context for transcription in all the target tissues.

In the present study, *F3G* gene, a key enzyme in anthocyanin biosynthesis pathway was selected as a locus for gene targeting. Anthocyanin pigment is present in leaf vein, young stem, flower and fruit (Fig. 2A-B). RT-PCR analysis also confirmed that *F3G* gene is expressed

in leaves, young stems, flowers (petal) and fruit epidermis (Fig. 2C). So, *F3G* locus can be a suitable genomic context for expression of *cryIF* gene, driven by a constitutive promoter. *F3G* is encoded by an intron-less gene of 1.3 kb length and there are 3 copies of *F3G* in *S. melongena* genome (Fig. 2D). Hence, disruption of single copy of *F3G* gene may not have pleiotropic effects on the plant. The active transcription of *F3G* in all the desired tissues was presumed to provide a favorable genomic context for expression of *cryIF* gene and presence of two functional *F3G* copies after loss of one copy of *F3G* by targeted gene integration may not have any significant effect on anthocyanin synthesis. This strategy

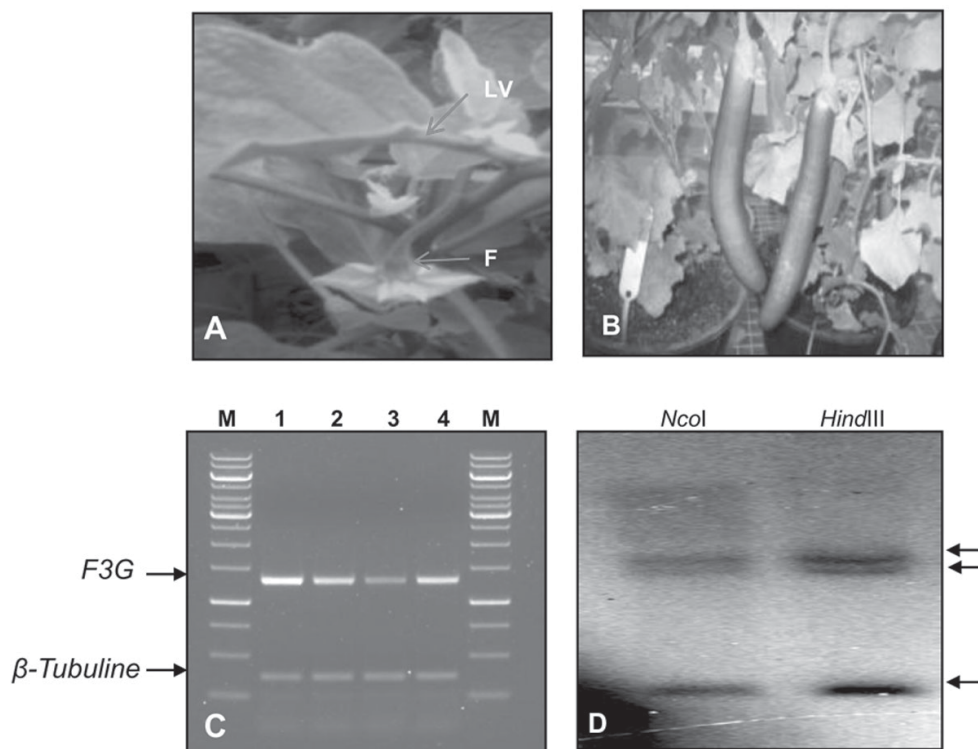


Fig. 2 Analysis of *F3G* expression and gene copy number in brinjal. A-B. anthocyanin pigmentation in leaf vein (LV), flower (F) and B. fruits, C. RT PCR for *F3G* transcript in 1. leaf, 2-3. stem and fruit epidermal tissues and 4. petal, showing expression of *F3G* gene in these tissues, D. Southern analysis indicating three copies of *F3G* gene in brinjal genome.

may overcome two limitations of current transgenic technology i.e., unpredictable transgene expression and effect of the mutation induced by transgene integration. Selection of multiple copy gene as targeted site for HR based integration may result in multicopy transgenics. However, this is a rare possibility, when chances of getting one HR event is in an order of 10^{-4} chances of getting two integration events in a single cell will be in an order of 10^{-8} .

Identification of gene targeted events

Low frequency of homologous recombination in comparison to random T-DNA integration is a major limitation to find a rare gene-targeted transgenic event. Earlier Terada et al., has used a positive-negative selection for identification of six gene targeting events in rice (30). However, use of negative selection such as diphtheria toxin (DT) has a disadvantage because the presence of even single toxin molecule produced by transient expression is sufficient to kill a cell. Losing any cell having gene integration by HR, because of transiently expressed DT will be counterproductive when GT frequency is in an order of 10^{-4} . To overcome this problem a negative screening strategy in combination with

a positive selection marker *nptII* was employed in the present study. The T-DNA carries *GUS* gene expression cassette, which is placed out of *F3F* gene sequence used for homologous recombination (Fig. 1). Thus the random integration transgenic events will have a functional *GUS* expression cassette while transgenic developed by homologous recombination will be devoid of *GUS* gene (Fig. 1, 3). Random integration events were screened out by *GUS* assay at an early stage of plant regeneration. However, with this approach non-transgenic and partial T-DNA integration (without *GUS*) events also show *GUS*-negative results. Hence, putative transgenic plants need further molecular analysis. This limitation was overcome by employing a PCR screening method earlier developed in our laboratory (29) that overcomes the limitation of false positive amplification arising from contaminating *Agrobacterium*. Combination of negative screening with modified PCR protocol greatly simplified the identification of rare HR events. Use of negative screening methodology may prove useful in plants that have long callus phase during regeneration. Random integration events can be screened out during early callus phase.

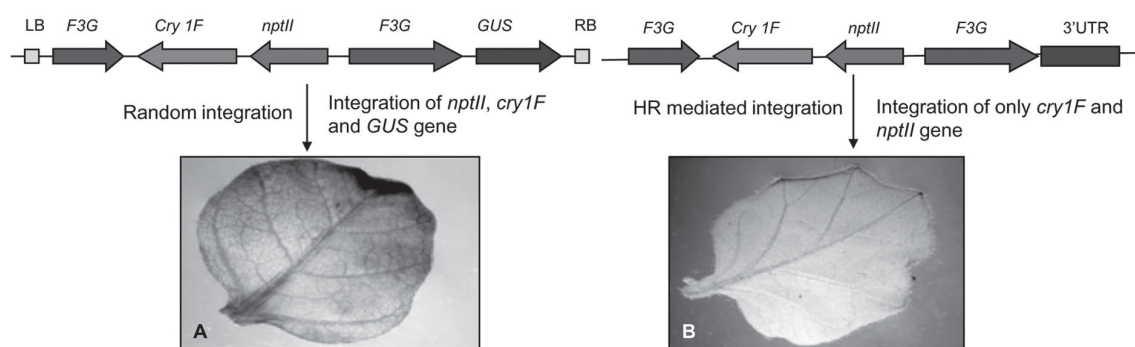


Fig. 3 GUS assay of leaf from putative transgenic brinjal plants. A. Transgenic plants developed through random T-DNA integration (GUS positive), B. Transgenic plants developed through targeted gene integration (GUS negative).

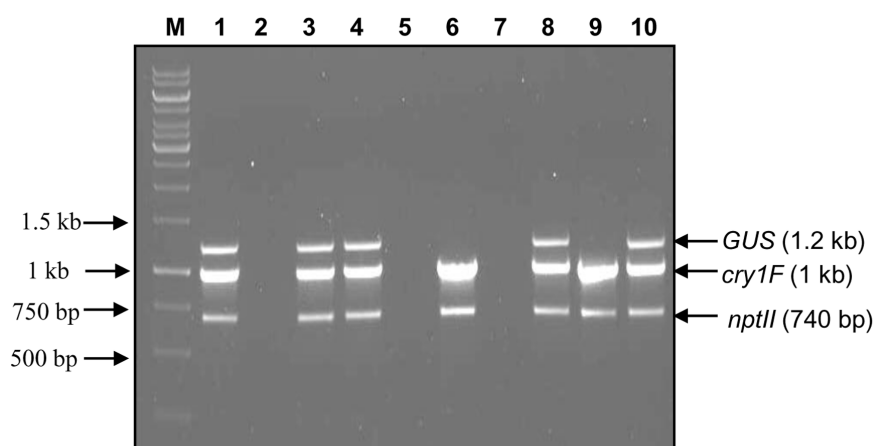


Fig. 4: PCR amplification of *cry1F*, *nptII* and *GUS* gene for confirmation of putative transgenic brinjal for homologous recombination mediated gene integration. M. Marker 1 kb DNA ladder, Lane 1, 3, 4, 8 and 10 putative transgenic brinjal obtained through random integration, lane 6 and 9 putative GT events and lane 2, 5 and 7 escapes.

At the first step of screening, out of 956 kanamycin resistant shoots obtained through *Agrobacterium*-mediated genetic transformation, 189 were found *GUS* negative. The *GUS* positive shoots were eliminated from the study and *GUS* negative shoots were further analyzed for HR based gene targeting events. At the second step of screening, integration of *nptII* and *cry1F* without *GUS* gene was confirmed by PCR (Fig. 3). Out of the 189 shoots screened by PCR, 75 shoots showed integration of all the three genes (possibly low expressing lines) while 112 shoots showed integration of none or only *nptII* (possible escapes or truncated T-DNA integration). Two transgenic lines were found positive for *nptII* and *cry1F* integration but without *GUS* gene (putative GT events) (Fig. 4).

HR based gene targeting in plants has been used only to demonstrate either induction of mutation or replacement of endogenous DNA fragment (23). Development of GT rice cell lines tolerant to the acetolactate synthase (*ALS*) inhibiting herbicide bipyribac (BS) have been

reported (31). Terada et al. (2007) Improved GT procedure to obtain nine independent transformed calli in rice having Alcohol dehydrogenase2 (*Adh2*) gene modified with the frequency of 2% per surviving callus. Shukla et al. (2009) used ZFNs to modify endogenous loci in maize. Insertional disruption of one target locus, *IPK1*, resulted in both herbicide tolerance and the expected alteration of the inositol phosphate profile in developing seeds. Herbicide-resistance mutations were introduced into *SuR* loci by ZFN-mediated gene targeting at frequencies exceeding 2% of transformed cells for mutations as far as 1.3 kilobases from the ZFN cleavage site. More than 40% of recombinant plants had modifications in multiple *SuR* alleles (20, 21)

In this report, an important vegetable crop has been transformed by targeted gene integration and the heterologous gene introduced (synthetic *cry1F*) to provides protection against its major insect pest BFB (*L. orbonalis*). The present study provides initial leads in the development

of *Bt* transgenic lines by gene targeting using a short length (643 bp) homologous sequences and without help of any recombinase genes. This will prove useful for application of HR based gene targeting in other crop species for genetic improvement as well as in functional genomics.

Acknowledgement:

This research work was supported by research grant from department of biotechnology, Ministry of Science and Technology, Government of India.

References

1. Moose, S.P. and Mumm, R.H. (2008). Molecular plant breeding as the foundation for 21st century crop improvement. *Plant Physiology*, 147: 969-977.
2. Kumar, P.A., Malik, V.S. and Sharma, R. P. (1996). Insecticidal proteins of *Bacillus thuringiensis*. *Advances in Applied Microbiology*, 42:1-43.
3. Christou, P. (1996). Transformation technology. *Trends Plant Science*, 1: 423-431.
4. Gelvin, S. B. and Kim, S. I. (2007). Effect of chromatin upon *Agrobacterium* T-DNA integration and transgene expression. *Biochemical Biophysical Acta*, 1769: 410-421.
5. Deineko, E.V., Zagorskaya, A. A. and Shumny, V.K. (2007). T-DNA-induced mutations in transgenic plants. *Russian Journal of Genetics*, 43: 1-11.
6. Puchta, H. and Hohn, B. (2005). Green light for gene targeting in plants. *Proceedings of the National Academy of Science USA*, 102: 11961-11962.
7. Reiss, B. (2003). Homologous recombination and gene targeting in plant cells. *International Review of Cytology*, 228: 85-139.
8. Hanin, M. and Paszkowski, J. (2003). Plant genome modification by homologous recombination. *Current Option in Plant Biology*, 6: 157-62.
9. Weller, G.R., Kysela, B., Roy, R., Tonkin, L.M., Scanlan, E. and Della, M. (2002). Identification of a DNA non homologous end-joining complex in bacteria. *Science*, 297: 1686-1689.
10. Pafiques, F. and Haber, J.E. (1999). Multiple pathways of recombination induced by double-strand breaks in *Saccharomyces cerevisia*. *Microbiology and Molecular Biology Reviews*, 63: 349-404.
11. Offringa, R., Franke-van Dijk, M.E., DeGroot, M.J., van-den Elzen, P.J. and Hooykaas, P.J. (1993). Nonreciprocal homologous recombination between *Agrobacterium* transferred DNA and a plant chromosomal locus. *Proceedings of National Academy of Science USA*, 90: 7346-7350.
12. Doetschman, T., Gregg, R. G., Maeda, N., Hooper, M. L., Melton, D.W., Thompson, S. and Smithies, O. (1987). Targeted correction of a mutant HPRT gene in mouse embryonic stem cells. *Nature*, 330: 576-578.
13. Thomas, K.R. and Capecchi, M.R. (1987). Site-directed mutagenesis by gene targeting in mouse embryo-derived stem cells. *Cell*, 51: 503-512.
14. Lee, K.Y., Lund, P., Lowe, K. and Dunsmuir, P. (1990). Homologous recombination in plant cells after *Agrobacterium*-mediated transformation. *Plant Cell*, 2: 415-425.
15. Miao, Z.H. and Lam, E. (1995). Targeted disruption of the TGA3 locus in *Arabidopsis thaliana*. *Plant Journal*, 7: 359-365.

16. Terada, R., Urawa, H., Inagaki, V., Tsugane, K. and Iida, S. (2002). Efficient gene targeting by homologous recombination in rice. *Nature Biotechnology*, 20: 1030–1034.
17. Thykjaer, T., Finnemann, J., Schauser, L., Christensen, L., Poulsen, C. and Stougaard, J. (1997). Gene targeting approaches using positive-negative selection and large flanking regions. *Plant Molecular Biology*, 35: 523–530.
18. Gallego, M. E., Sirand, P. and White, C. I. (1999). Positive negative selection and T-DNA stability in Arabidopsis transformation. *Plant Molecular Biology*, 39: 83-93.
19. Terada, R., Assao, H. and Iida, S. (2004). A large Agrobacterium mediated transformation procedure with a strong positive negative selection for gene targeting in rice (*Oryza sativa* L.). *Plant Cell Reports*, 22: 653–659.
20. Townsend, J.A., Wright, D.A., Winfrey, R.J., Fu, F., Maeder, M.L., Joung, J.K. and Voytas, D.F. (2009). High frequency modification of plant genes using engineered zinc finger nucleases. *Nature*, 459: 442-5.
21. Shukla, V.K., Doyon, Y., Miller, J.C., DeKelver, R.C., Moehle, E.A., Worden, S.E., Mitchell, J.C., Arnold, N.L., Gopalan, S., Meng, X., Choi, V.M., Rock, J.M., Wu, Y.Y., Katibah, G.E., Zhifang, G., McCaskill, D., Simpson, M.A., Blakeslee, B., Greenwalt, S.A., Butler, H.J., Hinkley, S.J., Zhang, L., Rebar, E.J., Gregory, P.D. and Urnov, F.D. (2009). Precise genome modification in the crop species *Zea mays* using zinc-finger nucleases. *Nature*, 459: 437- 441.
22. Paszkowski, J., Baur, M., Bogucki, A. and Potrykus, I. (1988). Gene targeting in plants. *EMBO Journal*, 7: 4021–4026.
23. Iida, S. and Terada, R. (2005). Modification of endogenous natural genes by gene targeting in rice and other higher plants. *Plant Molecular Biology*, 59: 205–219.
24. Atwal, A.S. (1976). *Agricultural Pests of India and South East Asia*, Kalyani Publishers, New Delhi.
25. Hofgen, R. and Willmtzer, L. (1988). Storage of competent cells of Agrobacterium transformation. *Nucleic Acids Research*, 16: 9877.
26. Kumar, P.A., Mandaokar, A., Sreenivasu, K., Chakrabarti, S.K., Bisaria, S., Sharma, S.R., Kaur, S. and Sharma, R.P. (1998). Insect-resistant transgenic brinjal plants. *Molecular Breeding*, 4: 33-37.
27. Jefferson, R.A., Kavanagh, T.A. and Bevan, M.W. (1987). GUS fusions: β -glucuronidase as a sensitive and versatile gene fusion marker in higher plants. *EMBO Journal*, 6: 3901-3907.
28. Doyle, J. J. and Doyle, J. L. (1990). Isolation of plant DNA from fresh tissue. *Focus*, 12: 13-15.
29. Nain, V., Jaiswal, R., Dalal, M., Ramesh, B. and Kumar, P.A. (2005). Polymerase chain reaction analysis of transgenic plants contaminated by Agrobacterium. *Plant Molecular Biology Reports*, 23: 59-65.
30. Terada, R., Hisatomi, Y.J., Saitoh, M., Asao, H. and Iida, S. (2007). Gene targeting by homologous recombination as a biotechnological tool for rice functional genomics. *Plant Physiology*, 144: 846–856.
31. Endo, M., Osakabe, K., Ono, K., Handa, H., Shimizu, T. and Toki, S. (2007). Molecular breeding of novel herbicide-tolerant rice by gene targeting. *Plant Journal*, 52: 157-166.

Effect of Dietary Alpha Glycine on Cocoon Production in the Silk Worm *Bombyx mori*

Biswaranjan Paital* and Kalyani Bohidar

Entomology Wing, P. G. Department of Zoology, Utkal University
Bhubaneswar, India, 751 004.

*For Correspondence - biswaranjanpaital@gmail.com

Abstract

The effect of dietary L-glycine (gly) on the growth and production of pupa and cocoon of the Nistari variety of silk worm *Bombyx mori* was investigated. Different treatment schedules (2% and 3% gly smeared on the mulberry leaves with once and twice supplementation from 1st and 2nd day of Vth instar larvae) were performed with suitable controls. The growth of the larvae and silk gland weight were significantly increased with gly supplementation. L-gly supplementation also enhanced the cocoon and pupa production. However, gly was found to have specific effects on the growth and production of pupa and cocoon of *Bombyx mori*.

Key words: L-glycine, Larvae, Dietary management, Silk gland, Growth, *Bombyx mori*.

Introduction

Nutrient supplements have been studied over decades to improve the production of economically important species of insects. In case of arthropods, especially in lepidoptera, many reports are there regarding improvement of their growth and production of pupa and cocoon of *Bombyx mori* and reproduction with better dietary supplement (1; 2; 3). Etebari *et al.* (4) reported that glutamic acid and urea supplementation to silk worm *Bombyx mori*, has

a remarkable effect on its larval growth and body glucose level. Therefore, improving the quality of mulberry leaves by supplying bacterial and fungal biofertilizers with an aim to produce better quality and quantity cocoons has been studied (5). Hydrolyzed soybean protein, P-soyatoses which contains high amount of leucine has also been used to get an augmentation of silk proteins in silk glands (6). Further, the dose dependant vitamin supplementation with both positive and negative impact on the growth of *B. mori* larvae has been reported. However, Ito (7) described that carbohydrate, protein and other nutritional supplementation with artificial feeds can positively influence the larval growth, survival and cocoon production in silk worm *B. mori*. Nutrient supplementation also has multifarious effects including increase in hemolymph protein concentration (8, 9) and weight of body, silk gland and cocoon weight (10, 11) in silk worms. But nutritional over supplement may create the disease epizootics which finally may reduce silk production.

Apart from sericulture values, Hu *et al.* (12) reported that amino acids from silk worm pupa have medicinal values as it increases intracellular reactive oxygen species in human hepatoma cells and acts as carcinostatic agent by inducing apoptosis. Improved and qualitative

silk worm pupa has also human nutritional values (13, 14). In this regard, Babu *et al.* (2) tried to enhance spinning rate in Mysore and NB₄D₂ varieties of silk worm *B. Mori*. However, information on the effect of dietary gly supplementation on cocoon and pupa production is seldom available. It is note worthy to mention here that glycine has the principal function as a precursor to proteins. Synthesis of the central C₂N subunit of all purines needs glycine as precursor. D-aminolevulinic acid, the key precursor of porphyrins, is biosynthesized from glycine and succinyl-CoA in higher eukaryotes. This amino acid is also acts as a building block to numerous natural products. On the other hand, gly supplementation found to have organ specific roles in animals (15, 16). The organ specific role of dietary gly is also found to be functionally related with age or different life stages of the animals. Kanafi *et al.* (17) summarized that additional dietary supplementation of vitamins and other biological nutrients influence the growth of the silk worms. They found that the dietary supplementations of the above nutrients cause better cocoon production in the silk worms as a function of weather, larval condition, variety of worms etc. Therefore, it was hypothesized that dietary L-glycine may have specific role on the silk gland growth and cocoon production in *B. mori*. To answer this hypothesis, this study was intended to find out the role of dietary alpha gly supplementation on pupa and cocoon production of the Nistari variety of the silk moth *Bombyx mori*. Additionally, the effect was also checked with larvae and silk gland growth of the worm.

Materials and Methods

Chemicals and feeds: Fresh mulberry leaves were supplied by Department of Sericulture, Sikharchandi Mulberry Centre, Bhubaneswar, India. Double distilled (DW) water was used for all treatment purposes. Nistari variety of *B. mori*

seeds were collected from Eri Seed Station, Khurda of Odisha, India. L- gly was procured from Sigma chemicals, USA.

Experimental protocol: The eggs were maintained in the laboratory condition and allowed to hatch on sterilized plastic trays. The larvae were then transferred carefully with fine brush onto the tender mulberry leaves kept on sterilized bamboo baskets which were covered with mosquito net (1 mm pore size). Larvae were supplied with tender leaves twice a day. No treatment was imposed up to IVth instar. The larvae from the above stock were divided into nine groups with 25 healthy, equal weighed (0.2 ± 0.02 g) larvae in each. The treatment schedule is given in Table 1.

In each basket, three equal weighed fresh mulberry leaves (~12.5 g) were smeared with 2.5 ml of 2% or 3% gly solution (dissolved in DW) in both dorsal and ventral surfaces of the leaves and dried under shade to remove moisture and then fed to the larvae. In control groups, 2.5

Table 1. Treatment schedule for the experiment. Group name symbol- percent (0, 1, 2) of gly (G) once (1) or twice (2) treatment from the 1st (I) or 2nd (II) day of Vth instar.

SN	Group name	Glycine (%)	No. of feeding/day	Starting day of treatment
1	0G1I	0	once	1 st
2	0G2I	0	twice	1 st
3	0G2II	0	twice	2 nd
4	2G1I	2	once	1 st
5	2G2I	2	twice	1 st
6	2G1II	2	once	2 nd
7	2G2II	2	twice	2 nd
8	3G1I	3	once	1 st
9	3G2I	3	twice	1 st
10	3G1II	3	once	2 nd
11	3G2II	3	twice	2 nd

ml of only distilled water was smeared on the leaves. For once a day treatment group, first feed in morning was preferred and in twice a day treatment group two consecutive feeds were preferred only to ensure that the whole treated leaves are consumed by the worms. Rest of the feedings was given with untreated leaves (each of 9.5 ± 0.50 g) leaves each time. All groups were fed four times per day up to spinning started by the worms. Before spinning 10 larvae were sacrificed and their silk glands were excised and weighted. Out of the rest larvae, another 10 larvae were used to measure mature larval weight, cocoon weight (after 72 hr of cocoon formation) and shell weight (after the insect emerged out). Weighing was performed with the help of an electronic balance (Afcoset, India, model - ER-200 A) with 0.1 mg resolution.

Statistical analysis: All results were expressed as mean \pm SD of 10 samples. Statistical significance was evaluated within the groups by

two way ANOVA analysis followed by Duncan's new multiple range test. Mean values between two groups were considered as significance at $P = 0.05$ levels.

Results

The present study clearly indicated that gly supplementation with the diets has a remarkable effect on the metabolism of silk worm *B. mori*. Both 2% and 3% gly supplementation was found to enhance the growth of the worm having highest in 3% gly once treated group and was lowest in 2% gly once a day group. It was further noticed that growth of the worms increases from gly treatment in the order of $C < 2\%$ once a day $< 2\%$ twice a day $< 3\%$ once a day $< 3\%$ twice a day group irrespective of the treatment started from 1st day or 2nd day of Vth instar (Table 2).

Growth of the silk gland has also been found to be influenced by dietary gly

Table 2. Effect of gly on the larval, silk gland and pupal growth and cocoon production of the silk worm *Bombyx mori*.

Group	Mature larval wt. (g)	Mature silk gland wt. (g)	Cocoon wt. (g)	Shell wt. (g)	Shell ratio
0G1I	1.68 ± 0.26	0.18 ± 0.03	0.49 ± 0.09	0.09 ± 0.03	0.19 ± 0.06
0G2I	1.7 ± 0.26	0.17 ± 0.02	0.48 ± 0.04	0.09 ± 0.01	0.19 ± 0.03
0G2II	1.62 ± 0.15	0.16 ± 0.02	0.46 ± 0.02	0.09 ± 0.01	0.20 ± 0.03
2G1I	1.99 ± 0.16	0.18 ± 0.01	0.71 ± 0.07	0.14 ± 0.01	0.20 ± 0.02
2G2I	2.08 ± 0.23	0.33 ± 0.02	0.42 ± 0.12	0.15 ± 0.12	0.21 ± 0.04
2G1II	1.97 ± 0.30	0.25 ± 0.07	0.66 ± 0.06	0.15 ± 0.02	0.22 ± 0.03
2G2II	2.01 ± 0.23	0.35 ± 0.02	0.35 ± 0.02	0.51 ± 0.07	0.29 ± 0.03
3G1I	2.09 ± 0.21	0.29 ± 0.02	0.63 ± 0.04	0.16 ± 0.02	0.25 ± 0.02
3G2I	2.41 ± 0.02	0.33 ± 0.02	0.63 ± 0.03	0.17 ± 0.01	0.26 ± 0.03
3G1II	2.21 ± 0.19	0.29 ± 0.02	0.66 ± 0.06	0.17 ± 0.01	0.25 ± 0.03
3G2II	2.407 ± 0.15	0.30 ± 0.02	0.62 ± 0.05	0.19 ± 0.03	0.31 ± 0.03

supplementation in the worms in all treated groups with respect to controls except 2% gly treatment from the 1st day group. Maximum silk gland weight was observed in 2% gly twice a day treatment from the 2nd day of 5th instar group in comparison to other groups. The order of increased silk gland growth was 0G1I = 0G2I = 0G2II = 2G1I < 2G1II < 3G1I = 3G1II < 3G2II < 3G2I < 2G2I < 2G2II.

Like growth parameters, cocoon weight was also increased in almost all treated groups except 2G2I group in which it decreased from the control group. The order of the cocoon weight remained as 2G2I < 0G1I = 0G2I = 0G2II < 2G2II < 3G2II ~ 3G2I ~ 3G1I < 2G1II ~ 3G1II < 2G1I.

The shell weight have shown a different pattern than the above three parameters. 3% gly was found to have magnificent role on increased shell production than 2% gly treatment. However, 2% gly had enhanced cocoon weight in comparison to control group. The order of shell weight was 0G1I = 0G2I = 0G2II < 2G1I < 2G1II < 2G2I ~ 2G2II < 3G1I < 3G2I < 3G1II < 3G 2II (Table 2).

The statistical differences between the groups are given in Table 3.

Discussion

Diet management in silk worms can improve their trait which has application not only in sericulture but also in nutritional and medicinal values for human beings (12, 17). One of the important fields in this context is supplementation of amino acids via the mulberry leaves to the silk worm larvae. Results of the present study indicate that supplementation of L- gly via the smeared mulberry leaves improves the growth of the larvae, silk gland as well as cocoon of Nistari variety of *Bombyx mori*. Our results are in good agreement with Babu *et al.* (2) who observed enhanced growth and spinning in the Mysore and NB₄D₂ variety of *Bombyx mori* with 3% gly supplementation.

The present results indicate that 3% gly treatment once or twice a day from the 1st day of Vth instar larvae has the highest effect on the augmentation of growth rate than 2% treatments. It indicates the growth enhancing effects of more supplementation of gly in the larvae which is in good agreement with Babu *et al.* (2). Therefore, 2% gly treatment irrespective of the starting day of treatment with the leaves was not sufficient to enhance the growth of the larvae. But the matured gland weight does not corresponded with the

Table 3. Statistical significance between the groups. Only one control group was taken into account as the mean values of all three controls groups were almost same. PR-parameters, LW- larval weight, GW- gland weight, CW-cocoon weight, SW-shell weight and SR- shell ratio. A-2 % Gly once from 1st day, B-2 % Gly twice from 1st day, C-2 % Gly once from 2nd day, D-2 % Gly twice from 2nd day, E-3 % Gly once from 1st day, F-3 % Gly twice from 1st day, G-3 % Gly once from 2nd day, H-3 % Gly twice from 2nd day and I-Control. Two letters in the 1st row (except PR) indicate the group names between which the P values of the parameters were given below the group names. P is taken as statistically significant = 0.05. P < 0.05 (e), P=0.05 (a), P=0.01 (b), P=0.001 (c), P=0.0001 (d).

PR	AB	AC	AD	AE	AF	AG	AH	AI	BC	BD	BE	BF	BG	BH	BI	CD	CE	CF	CG	CH	CI	DE	DF	DG	DH	DI	EF	EG	EH	EI	FG	FH	FI	GH	GI	HI
LW	e	e	e	e	c	a	c	b	e	e	e	b	e	b	b	e	e	d	a	c	b	e	c	e	c	b	b	e	b	c	a	e	d	e	d	d
GW	d	c	d	d	d	d	e	d	e	b	e	b	c	d	d	a	d	a	e	d	d	e	d	d	d	b	e	a	d	b	d	d	a	d	d	
CW	e	e	d	a	a	e	a	d	e	d	a	a	e	a	d	d	e	e	e	e	d	c	c	d	c	e	e	e	e	d	e	e	d	e	d	d
SW	e	e	e	a	b	b	d	c	e	e	e	a	e	d	d	e	e	a	e	d	d	e	a	e	d	d	e	e	c	d	e	b	d	b	d	d
SR	e	e	d	c	d	b	d	e	e	d	a	b	a	d	e	d	a	b	e	d	e	a	e	a	e	d	e	e	c	c	e	b	c	c	c	d

growth of the larvae. 2% gly twice a day treatment started from the 2nd day of Vth instar larvae has found to have maximum silk gland growth. On the other hand, high growth of the larvae was found to have higher cocoon weight as found in case of 2% gly once a day treatment from the 1st day treatment of the Vth instar larvae. However, the higher silk gland growth with 2% gly twice a day has found to have maximum shell weight. Therefore, it contributes to the low pupa growth. In contrast, maximum pupa growth was observed with minimal larvae and gland growth with 2% gly once a day treatment of the 1st day of Vth instars larvae. But in such case maximum cocoon weight was noticed. Therefore, it is clear that silk gland and larval growth has not positive relation with pupa weight and shell weight. It is here to mention that both the pupa and shell on the raw products of the sericulture have different applications. Therefore, the exact biochemical or physiological role for the L-gly supplementation with different concentrations from the day 1 or 2 of the Vth instar of *B. mori* larvae is a matter of future investigation.

Conclusion

It can be concluded from the present study that the maximum silk gland protein or cocoon or shell production with 2% gly smeared mulberry leaves with twice a day supplementation from the 2nd day or 2% gly once a day or 2% gly twice a day from the 2nd day of the Vth instar, respectively, are required. The above phenomenon clearly indicates that gly have specific effect on the growth of the larvae, gland, pupa and cocoon production in the Nistari variety of the silk worm *B. Mori*.

Acknowledgements

This study was a project work under taken by BRP for the partial fulfillment of MSc in Zoology at Utkal University. BRP is extremely grateful to the University Grants Commission,

New Delhi for providing a fellowship under RFSMS scheme (F.4-3/2006 (XI plan/BSR/7-173/2007(BSR)). The authors are highly thankful to the Head, Department of Zoology for providing the laboratory facilities.

References

1. Davis G. R. F. (1978). Growth response of larvae of *Tenebrio molitor* to concentrations of dietary amino acids. *Journal of Stored Products Research*, 14:69-71.
2. Babu, V. P., Gowda, B. L. V., Govindan, R. and Gowda, M. (1999). Effect of L-Glycine on Growth of Silkworm *Bombyx mori* L. *Entomon*, 25:335-339.
3. Eid, M. A. A., El-Nakkady, A. N. and Salem, M. A. (1988). Effects of supplementary amino acids on silk secretion by larvae of *Philosamia ricini* (Boisd.). *Indian Journal of Sericulture*, 28: 224-232.
4. Etebari, K., Ebadi, R. and Matindoost, L. (2007). Physiological Changes of Silkworm (*Bombyx mori* L.) Larvae Fed on Mulberry Laves Supplemented with Nitrogenous Compounds. *Journal of the Entomological Research Society*, 9:1-15.
5. Rao, D. M. R., Kodandaramaiah, J., Reddy, M. P., Katiyar, R. S. and Rahmathulla, V. K. (2007). Effect of VAM fungi and bacterial biofertilizers on mulberry leaf quality and silkworm cocoon characters under semiarid conditions. *Caspian Journal of Environmental Science*, 5:111-117.
6. Raman, C., Manohar, S. L., Xavier, N. and Krishnan, M. (2007). Expression of silk gene in response to P-soyatose (hydrolyzed soy bean protein) supplementation in the fifth instar male larvae of *Bombyx mori*. *Journal of Cell Molecular Biology*, 6:163-174.

7. Ito, T. (1967). Nutritional Requirements of the Silkworm, *Bombyx mori* L. Proceeding Japan Academy, 43:57-61.
8. Nagata, M. and Kobayashi, J. (1990). Effect of nutrition on storage protein concentration in the larval hemolymph of the silkworm, *Bombyx mori*. The Journal of Sericulture Science of Japan, 59:469-474.
9. Kishnan, M., Subburathinam, K. M. and Janarthanan, S. (1995). Effects of hydrolyzed soy protein (P-soyatoase) on hemolymph protein profile, larval and pupal characters of silkworm, *B. mori* L. (Lepidoptera: Bombycidae). Sericologia, 32:227-235.
10. Sarker, A. A., Haque, M. R., Rab, M. A. and Absa, N. (1995). Effect of feeding mulberry (*Morus* sp.) leaves supplemented with different nutrients to silk worm (*Bombyx mori* L.). Current Science, 69:185-188.
11. Vanisree, V., Nirmala, X. and Krishnan, M. (1996). Response of five different races of silkworm, *Bombyx mori* L. (Lepidoptera: Bombycidae), to hydrolyzed soy protein supplementation. Sericologia, 36:691-698.
12. Hu, D., Liu, Q., Cui, H., Wang, H., Han, D. and Xu, H. (2005). Effects of amino acids from selenium-rich silkworm pupas on human hepatoma cells. Life Sciences, 77:2098-2110.
13. Katayama, N., Ishikawa, Y., Takaoki, M., Yamashita, M., Nakayama, S., Kiguchi, K., Kok, R., Wada, H., Mitsushashi, J. and Space Agriculture Task Force. (2008). Entomophagy: A key to space agriculture. Advance Space Research, 41:701-705.
14. Mitsushashi, J. (1997). People who eat insects, Heibon-Sha, Tokyo.
15. Bosquet, G. (1976). Glycine incorporation during starvation in *Bombyx mori*. Relation to respiratory metabolism. Journal of Insect Physiology, 22:541-545.
16. Froh, M., Thurman, R. G. and Wheeler, M. D. (2002). Molecular evidence for a glycine-gated chloride channel in macrophages and leukocytes. American Journal of Physiology and Gastrointestinal Liver Physiology, 283:G856-G863.
17. Kanafi, R. R., Ebadi, R., Mirhosseini, S. Z., Seidavi, A. R., Zolfaghari, M., Etebari, K. (2007). A review on nutritive effect of mulberry leaves enrichment with vitamins on economic traits and biological parameters of silkworm *Bombyx mori* L. Invertebrate Survival Journal, 4:86-91.

Molecular Identification and Development of Nuclear DNA ITS Sequence Based Marker to Distinguish *Coscinium fenestratum* Gaertn. (Menispermaceae) from its Adulterants

S. P. Balasubramani and Padma Venkatasubramanian*

Centre for Pharmacognosy, Pharmaceutics & Pharmacology
Institute of Ayurveda & Integrative Medicine (I-AIM)
Foundation for Revitalisation of Local Health Traditions (FRLHT)
Bangalore-560106, India.

*For Correspondence - padma.venkat@frlht.org

Abstract

Coscinium fenestratum Gaertn. (Menispermaceae), commonly known as 'tree turmeric', is an endangered plant species used in Traditional Systems of Medicine in Asia to treat diabetes, hypercholesterolemia, tetany etc. Market survey in India indicates *Berberis aristata*, *B. asiatica*, *B. lycium* of family Berberidaceae and *Morinda umbellata* (Rubiaceae) are traded as substitutes or adulterants of *C. fenestratum*. To strengthen the pharmacognosy parameters, molecular identification of *C. fenestratum* was performed based on the nuclear DNA ITS (internal transcribed spacer) sequence. Subsequently, a species-specific DNA marker was developed for easy identification of *C. fenestratum*. The marker developed can be used as a molecular pharmacognosy tool in quality control of herbal raw drugs.

Key words: *Coscinium fenestratum*, ITS sequence, Adulterants, DNA marker, Pharmacognosy, Quality Control

Introduction

Coscinium fenestratum (Gaertn.) is a seed propagated dioecious, large, woody climber with

cylindrical stem. It is commonly called as 'Tree Turmeric' and belongs to the family Menispermaceae. This plant is indigenous to the Indo-Malayan region. In India, it is restricted to Western Ghats at 500 – 750 m altitude (1). IUCN Red list of threatened plants indicates that *C. fenestratum* as endangered in India, vulnerable in Vietnam, rare in Singapore and intermediate in Sri Lanka (2).

For centuries the stems of *Coscinium fenestratum* is used in the Traditional System of Medicine in Asia. It is called as 'Kaliyaka' in Ayurveda and is used for treating diabetes (3), in Sri Lanka as an anti-dote for tetanus (4, 5). *C. fenestratum* is called 'Hamm' in Thai language, the stem is very popularly used for balancing blood pressure, being a detoxifying and anti-diabetic agent and for treatment of hypercholesterolemia (6).

Pharmacological studies have shown that *C. fenestratum* has anti-fungal, anti-yeast, anti-bacterial, hypotensive and antiproliferative activities (1). The major components in wood and root of *C. fenestratum* are isoquinoline alkaloids such as berberine, palmatine, tetrahydropalmatine, crebanine and jatrorrhizine, while berberine is found

to be the major and active constituent. It has been shown to bind to DNA and inhibit its cleavage (7). Antibacterial, antileishmanial, antiplatelet, anti-diarrhoeal, anti-protozoan, cardioprotective, anti-cancer, anti-inflammatory, anti-hepatotoxic, immunostimulatory and anti HIV properties have been reported with berberine (7).

In India, market survey indicates that *Berberis aristata* DC, *B. asiatica* Roxb., *B. lycium* Royle, and *Morinda umbellata* L. are traded as adulterants or substitutes of *C. fenestratum* (1, 8). The annual trade combining all the five species is estimated to be 500 – 1000 MT (8). Morphologically intact *C. fenestratum* stems can be distinguished from the other 'Tree Turmeric' candidates using the radical array in the transverse section (3). However, when traded as chips or in powder form it is not distinguishable.

Biotechnology-driven applications play an important role in modern pharmacognosy analysis for herbal drug development and discovery. Current focus on chemotype-driven fingerprinting and related techniques requires integration with genotype-driven molecular techniques so that an optimal characterization of botanical materials is possible (9). Chinese researchers have applied DNA markers extensively for characterization of botanicals from the Chinese materia medica. These markers have shown remarkable utility in quality control of commercially important botanicals like Ginseng, Echinacea, *Atractylodes* etc (10).

DNA markers to distinguish some of the authentic and the adulterant medicinal plants used in Indian System of medicine have also been reported from our lab (11 – 13). ITS (Internal Transcribed Spacer) sequences have been shown to be a valuable source of evidence to resolve phylogenetic relationships in many angiosperm groups (14). ITS1 separates 18S and 5.8S, while ITS2 separates 5.8S and 26S rRNA genes.

Because of their different rates of evolution, ITS regions have become the favored markers in evolutionary studies at different taxonomic levels (15). In recent times, these sequence variations are used to develop species-specific markers for identification and authentication of raw drugs and herbal formulations (16 – 18).

The objective of the present study was to identify *C. fenestratum* at molecular level and to develop a species-specific marker based on ITS region to distinguish from its adulterants.

Materials and Methods

Plant material: Field and market samples of *Berberis aristata*, *Berberis asiatica*, *Berberis lycium*, *Coscinium fenestratum* and *Morinda umbellata*, were collected from different geographical locations of India. The authenticity of the samples was confirmed by Dr. K. Ravikumar, botanist at FRLHT, Bangalore. Each sample was assigned with a specific laboratory identification number as indicated in Table 1. Voucher specimens were deposited in the Herbarium and Raw Drug Repository (FRLH), Bangalore, India.

Chemicals: Tris-HCl, EDTA, NaCl, CTAB (Cethyltrimethylammonium bromide), LiCl, PVP (Polyvinyl pyrrolidone), Beta mercaptoethanol, isopropanol, agarose, boric acid and ethanol were purchased from Sigma Chemicals (USA). Enzymes (Taq Polymerase and RNase A), buffer, MgCl₂ and dNTP's for PCR amplification were purchased from Bangalore Genei (Bangalore, India).

Genomic DNA Extraction: Dried stem samples of *C. fenestratum*, *B. aristata*, *B. asiatica*, *B. lycium* and *M. umbellata* were surface sterilized and cut in small pieces. The pieces were ground into coarse powder in a domestic blender. The protocol described by Milligan (19) was used for DNA extraction with modifications. Approximately, 100 mg of the coarse powder was

ground with liquid nitrogen to fine powder. Extraction buffer containing CTAB 2% (w/v), NaCl 1.4 M, EDTA 20mM, Tris-HCl (pH 8) 100mM, PVP 1% (w/v) and beta mercaptoethanol 0.2% (v/v) (pH 7.5 to 8.0) was added to the powder. The slurry was incubated at 60°C in a water bath for 60 – 90 min followed by extraction using chloroform: isoamyl alcohol (24:1) (v/v) and centrifuged at 9000 rpm for 10 min at 4°C. The chloroform: isoamyl alcohol extraction was repeated twice with the aqueous phase. Finally, the aqueous phase was separated and DNA was precipitated with ice cold ethanol. Nucleic acid was recovered by centrifugation at 8,000 rpm for 15 min at 4°C and the pellet was dissolved in TE buffer (Tris-HCl 10 mM, EDTA 1mM; pH 8). The contaminating RNA was removed by treating with RNase A (20 µg/µL) for 30 min at 37°C. The quantity and purity of DNA was checked using UV spectrophotometer by calculating the A_{260}/A_{280} ratio (20) (Shimadzu, Tokyo, Japan). The DNA stock was maintained at a concentration of 30 – 50 ng / µL.

Amplification of *C. fenestratum* ITS region: ITS1 and ITS2 regions of *C. fenestratum* were amplified using the universal primers (21). Details of the primers and the region amplified are given in Table 2. PCR reaction contained approximately 60 ng genomic DNA, 2.5 µL 10X Taq buffer, 1.5 mM MgCl₂, 0.4 mM dNTP mixture, 30 pM of each primer, 1U Taq DNA polymerase and made up to 25 µL with sterile distilled water. Amplification reaction was optimized at 95°C for 3 min followed by 35 cycles of 95°C for 35sec, 60°C for 30 sec, 72°C for 45sec with a final extension step at 72°C for 3min. PCR products were resolved in 1.2% agarose, 0.5X TBE gels prestained with ethidium bromide (0.5 µg/ml). Simultaneously, 100 bp DNA ladder or Lambda DNA EcoRI/HindIII double digest (Fermentas, Burlington, Canada) was loaded to confirm the size of the amplicon. The gel was visualized under

UV radiation on a transilluminator (Reprostar, CAMAG, Muttenz, Switzerland) and digital photographed (Canon, Tokyo, Japan). Each experiment was repeated at least three times with all available accessions of each species to confirm its reproducibility and repeatability.

Direct sequencing of *C. fenestratum* ITS1 and ITS2 region: PCR product of *C. fenestratum* ITS1 and ITS2 amplification was purified from agarose gel using QIAquick gel extraction kit (Qiagen, Hilden, Germany) following manufacturer's instruction. Sequencing was performed in an automated ABI 3100 Genetic Analyser (Applied Biosystems, CF, USA) by Bangalore Genei (Bangalore, India). Forward and reverse sequencing were done individually with primers ITS1 and ITS2 respectively. Sequence results were submitted to GenBank, National Centre for Biotechnology Information (NCBI), Bethesda MD, USA

Homology analysis: Sequence of ITS1 and ITS2 region for *B. aristata*, *B. asiatica*, *B. lycium* and *M. umbellata* was adopted from NCBI nucleotide sequence database, GenBank (<http://www.ncbi.nlm.nih.gov/nucleotide/>). The details of the accession numbers used in this study are given in the Table 3. Homology analysis was performed by employing CLUSTALW (www.ebi.ac.uk/clustalw/). The homology percentage in the ITS regions of *C. fenestratum* with its substitute species was calculated.

Development of species-specific marker for *C. fenestratum*: Variation in the ITS1 and ITS2 sequences of *C. fenestratum*, *B. aristata*, *B. asiatica*, *B. lycium*, and *M. umbellata* was used for developing species-specific marker for *C. fenestratum*. DNA primers capable of giving specific amplification with *C. fenestratum* ITS1 region was developed using NCBI primer blast tool (<http://www.ncbi.nlm.nih.gov/tools/primer-blast/>). The oligonucleotides were custom-

synthesized by Bioserve biotechnologies (Hyderabad, India). PCR reaction with the species specific primer set (CF1F and CF1R) contained 30 ng of genomic DNA, 2.5 µl of 10x assay buffer, 1.5 mM MgCl₂, 0.3mM dNTP mix, 30pM of each primer, 1U of Taq DNA polymerase (Bangalore Genei, India) and the volume was made up to 25 µl with sterile distilled water. PCR programme conditions optimized for the species-specific primer set was as follows: 94°C for 4 min, followed by 35 cycles of 30 sec at 94°C, 30 sec at 60°C and 40 sec at 72°C with a final extension step for 2 min at 72°C.

Results

DNA extraction and Quality checking: The protocol described in the Materials and Methods yielded a good quality and quantity of high molecular weight genomic DNA from dried stem samples of the test species studied. The yield was about 400-600 ng of DNA per 100 mg of tissue. An absorbance (A_{260}/A_{280}) ratio of 1.6-1.8 indicated insignificant levels of contaminating proteins and polysaccharides.

Amplification and Sequencing of *C. fenestratum* ITS1 and ITS2 region: Primers ITS1 and ITS2 amplified a 245 bp (Figure 1) sequence of the ITS1 region while a 386 bp ITS2 region (Figure 2) was amplified with the primers ITS3 and ITS4 for the *C. fenestratum* samples (Table 2). Homology searches were performed within GenBank's non-redundant database using the BLAST (Basic Local Alignment Search Tool) algorithm at <http://www.ncbi.nlm.nih.gov/BLAST/> of the National Center for Biotechnology Information (NCBI), with the program BLASTN. BLAST results revealed that the sequence did not show complete similarity with any known nucleotide sequences. The sequences were submitted to GenBank (Accession numbers: GQ496588 for ITS1 and GQ496589 for ITS2) (Figure 3).

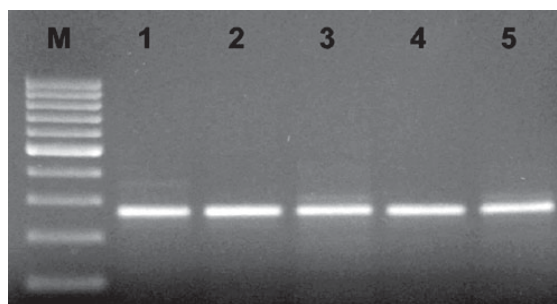


Fig. 1. PCR amplification of the *C. fenestratum* ITS1 sequence (245 bp) Lane M- 100 bp ladder; Lanes 1 to 5- different *C. fenestratum* accessions used in this study

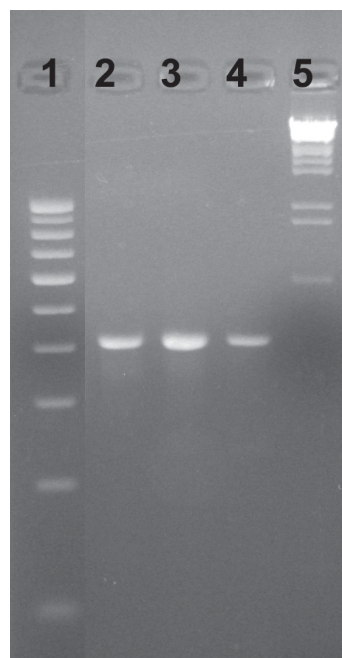


Fig. 2. PCR amplification of *C. fenestratum* ITS2 sequence (386 bp) Lane 1 – 100 bp ladder; Lane 2 – *C. fenestratum* L/06/09/031; Lane 3 – *C. fenestratum* L/07/02/033; Lane 4 – *C. fenestratum* L/07/08/010; Lane 5 – Lambda DNA EcoRI/HindIII double digest

Sequence analysis : Homology analysis of the *C. fenestratum* ITS1 and ITS2 regions was performed with the corresponding regions of the substitute plant species *B. aristata*, *B. asiatica*, *B. lycium* and *M. umbellata*. Details of the ITS sequence employed for each adulterant species

a)

```

1 cctcaccgatg ttttgtcgag cctgcacagc agagagaccc tcgcgaaccg tctcgaagaa
                                CF1F
61 catccccggc atcgtgccgc cgcggccgcc ggcgaccggg aggcccgcca gtctcggcgg
121 aacaacaaac ccccggcgcg gctcgcgcca aggaataatc gaaacagacg gtgcgctccg
181 cgcgtcccgt atcctcgaac gactctcggc aacggatatac tcggctctcg catagataaa
                                CF1R
241 aaacg
    
```

b)

```

1 gctcgtatg gaaggcttgc ggaggaagca ttgaataactt atgatcatcg agtctttgaa
61 cgcaagttgc gcccgaggcc accaggccga gggcacgtct gcctggggct cacgcaacgc
121 gccgctccca cccccaaag ggggggggga agcgaaggtt ggctccccg gggggctggt
181 tcacgggtggg ttgaaaccgc ggcccccccg ccgccaaga acccaatcat ggggggtcga
241 caaacctccc cctcaccgga atggaaagag ccgctcaaag ggccgcccgc aagggggcaa
301 agggaccccc gcggtggtta acccgagccg acccctggtc agggggggccc ccccgttgat
361 tttaacatta taattaaccg gagggg
    
```

Fig. 3. a) GQ496588. *Coscinium fenestratum* internal transcribed spacer 1, complete sequence; and 5.8S ribosomal RNA gene, partial sequence b) GQ496589. *Coscinium fenestratum* 5.8S ribosomal RNA gene, partial sequence; and internal transcribed spacer 2, complete sequence

and their homology percentage with the respective ITS region of *C. fenestratum* is given in the Table 3. Variations in the ITS sequences was observed among the different species studied.

Development and Validation of Species-specific marker for *C. fenestratum*: NCBI primer blast tool was used to develop and validate the species-specific markers for *C. fenestratum*. On *in silico* analysis, a primer set (CF1F and CF1R) indicated a high specificity for amplification of 196 bp only from the ITS1 sequence of *C. fenestratum* (Table 4). The synthesized oligos were incorporated in a PCR

reaction individually with the genomic DNA of *C. fenestratum* and its adulterant species. Electrophoretic separation of the amplicon indicated 196 bp product only with the *C. fenestratum* samples and it did not give any non-specific amplification with the other test species under study (Figure 4).

Discussion

Herbal medicinal products may vary in composition and properties, unlike conventional pharmaceutical products prepared from synthetic, chemically pure materials by means of

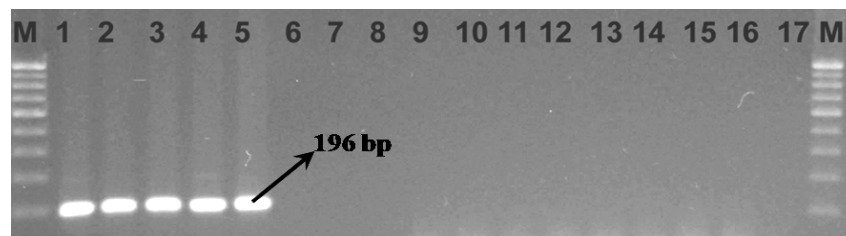


Fig. 4. PCR amplification with CF1F and CF1R using the genomic DNA of *C. fenestratum* and its adulterant species Lane M – 100 bp ladder; 1 to 5 – *C. fenestratum* accessions; Lane 6 to 8 – *B. aristata*; Lane 9 to 11 – *B. asiatica*; Lane 12 to 14 – *B. lycium*; Lane 15 to 17 – *M. umbellata*

Table 1. Details of the plant samples used in the study.

S No.	Name of the species	Place of collection	Accession No.
1	<i>C. fenestratum</i>	Bangalore market, KA	L/06/09/031
2		Kanyakumari, TN	L/06/12/015
3		Pune, MH	L/07/02/033
4		Bangalore market, KA	L/07/04/015
5		Nadavayal forest, Wayanad, KL	L/07/08/010
6	<i>B. aristata</i>	Potter's hill, Shimla, HP	L/08/09/012
7		Shillaru, Shimla, HP	L/08/10/008
8		Potter's Hills, Shimla, HP	L/08/10/011
9	<i>B. asiatica</i>	Mulshi, Mussoorie, HP	L/07/12/001
10		Saharan-Nahar Road, HP	L/08/09/013
11		Saharan-Nahar road, HP	L/08/09/016
12	<i>B. lycium</i>	Karol, Manikaran, HP	L/06/06/037
13		Shillaru, Kangra, HP	L/08/10/009
14		Chail, Solan, HP	L/08/10/010
15	<i>M. umbellata</i>	Kannimarsholai, Tiruchi, TN	L/07/04/001
16		Sirumalai hills, Dindigul, TN	L/07/07/053
17		Mavanatham, Erode, TN	L/09/03/009

Table 2. Details of the primers used for amplifying the ITS1 and ITS2 regions of *C. fenestratum*

Primer details					
Region	Direction	Name of the primer	Primer sequence (5' 3')	Size of the amplicon	GenBank accession No.
ITS1	Forward	ITS 1	TCCGTAGGTGAACCTGCGG	245 bp	GQ496588
	Reverse	ITS 2	GCTGCGTTCCTTCATCGATGC		
ITS2	Forward	ITS 3	GCATCGATGAAGAACGCAGC	386 bp	GQ496589
	Reverse	ITS 4	TCCTCCGCTTATTGATATGC		

Table 3. The homology score in the ITS regions of *C. fenestratum* with its adulterant species

Adulterant Species	GenBank accession no.	Homology %	
		ITS1	ITS2
<i>B. aristata</i>	GQ259132	43.87	37.03
<i>B. asiatica</i>	GQ259133	52.55	34.44
<i>B. lycium</i>	GQ259134	51.53	35.18
<i>M. umbellata</i>	AY514063	52.04	56.66

Table 4. Details of the *C. fenestratum* species-specific markers designed using the ITS1 sequence.

Plant species	Name of the marker	Sequence of the DNA marker (5' - 3')	Product size
<i>C. fenestratum</i>	CF1F CF1R	AGCCTGCACAGCAGAGAGAC CGTTGCCGAGAGTCGTTTC	196 bp

reproducible manufacturing techniques and procedures. Correct identification and quality assurance of the starting material is an essential prerequisite to ensure reproducible quality of herbal medicine, which contributes to its safety and efficacy. According to WHO general guidelines for methodologies on research and evaluation of traditional medicines, first step in assuring quality, safety and efficacy of traditional medicines is correct identification (22).

Most of the cases of accidental herbal medicine misuse start with wrong identification of a medicinal plant prescribed (23). Many of the traditional systems have records where one common vernacular name is applied to two or more entirely different species or genus. For eg., Ginseng has almost become a generic name with 13 different species traded in the world market (23). For example Chinese or Asiatic ginseng (*Panax ginseng*), American ginseng (*Panax quinquefolius*), Siberian ginseng (*Eleutherococcus senticosus*), Ayurvedic ginseng (*Withania somnifera*) and Russian ginseng (*Acanthopanax senticosus*), to name a few. Such names could create confusion over prescription, which may eventually lead to serious consequences.

WHO has developed several guidelines for carrying out standardization procedures of raw herbal products, which basically include pharmacognostical, physico-chemical, pharmacological and toxicological methods (22).

Microscopic and macroscopic standards could be drawn out, where a plant can be differentiated from another entirely different plant which may look similar in external appearance. Currently, genetic fingerprinting and the use of analytical quality-control equipments like HPLC and HPTLC are performed on a large scale for standardization and identification of herbal drugs. Each technique has its limitations (14). DNA level identification is gaining popularity as an effective, reliable and simple pharmacognostic tool to resolve the confusion in taxonomic identification of herbal raw drugs. Because genetic composition is unique for each species irrespective of the physical form and is less affected by age, physiological condition, environmental factors, harvest, storage and processing. DNA extracted from leaves, stems or roots of an herb all carry the same genetic information and extracted DNA can be stored for longer duration as they are stable (10).

Panax (ginseng) is a representative genus of medicinal herbs which was subjected to several methods of DNA analysis by Chinese including PCR-RFLP, AFLP, RAPD, SSR, sequencing of rDNA-ITS region and DNA barcoding (10, 24). Universal PCR primers designed from highly conserved regions flanking the ITS region, relatively small size (600–700 bp) of the ITS region and high copy number (>100 per cell) enable easy amplification of the ITS region (10, 14). ITS sequence has reduced variability within the species (25). These advantages have made ITS region and ribosomal RNA gene sequence

as preferred choice for molecular typing. RFLP fingerprints based on 18S rRNA and ITS sequence to distinguish *C. fenestratum* from its adulterants *Arcangelisia flava* and *Fibruarea tinctoria* in the Thai herbal market (26).

DNA information may not be directly correlated with the amounts of the active ingredients. However, genetic data has its own advantages over other methods of authentication. Molecular markers are least affected by age, environmental factors and physiological conditions of the plant samples they are not tissue specific and thus can be detected at any stage of development, with a small amount of sample, in any physical form (14). DNA based methods have been successfully used to even authenticate herbal constituents in commercial herbal preparations in which the components have been ground, boiled, concentrated, dried and blended (10). DNA markers can increase industrial application of the molecular techniques (27).

The DNA markers described in this study will be useful in quality control of herbal raw drugs and also in selecting genuine *C. fenestratum* for research. However, DNA markers together with the chemical fingerprint would improve quality of herbal medicines.

Acknowledgement

Financial support for this study was provided by Ministry of Environment and Forests, Government of India as "Centre of Excellence" grant. Authors wish to thank Dr. K. Ravikumar, Dr. Jawahar and Mr. R. Murugan, for collection of authentic plant samples and useful discussion. Thanks are due to Prof. K.V. Krishnamurthy for his suggestions in preparing this manuscript.

References

1. Tushar K.V., George S., Remashree A.B. and Balachandran I. (2008). *Coscinium fenestratum* (Gaertn.) Colebr.-A review on this rare, critically endangered and highly-traded medicinal species. *J Plant Sci.*, 3: 133-145.

2. Walter, K.S and Gillett, J.H. (1998). 1997-IUCN Red List of Threatened Plants. Cambridge-International Union for Conservation of Nature (IUCN), World Conservation Union.
3. Anonymous. (2006). The Ayurvedic Pharmacopoeia of India, Part I, Vol V. Government of India, Ministry of Health and Family Welfare, Department of Indian Systems of Medicine & Homoeopathy, New Delhi, pp. 60-62
4. Warriar, P.K., Nambiar, V.P.K. and Ramankutty, C.. (1994). Indian Medicinal Plants, a Compendium of 500 species. Orient Longman Limited, Madras, pp. 191-193.
5. Shirwaikar, A., Rajendran, K. and Punitha I.S.R.. (2005). Antidiabetic activity of alcoholic stem extract of *Coscinium fenestratum* in streptozotocin-nicotinamide induced type 2 diabetic rats. *J Ethnopharmacol*, 97: 369-374.
6. Rojsanga P, Gritsanapan W and Suntornsuk L. (2006). Determination of berberine content in the stem extracts of *Coscinium fenestratum* by TLC densitometry. *Med Princ Pract.*, 15: 373-378.
7. Wongbutdee J. (2009). Physiological effects of Berberine. *Thai Pharm Health Sci J.*, 4: 78 - 83
8. Ved DK and Goraya GS. (2008). Demand and supply of medicinal plants in India. Bishen Singh Mahendra Pal Singh, Dehra Dun.

9. Joshi K, Chavan P, Warude D and Patwardhan B. (2004). Molecular markers in herbal drug technology. *Current science*, 87: 159 – 165
10. Yip PY, Chau CF, Mak CY and Kwan HS. (2007). DNA methods for identification of Chinese medicinal materials. *Chinese Medicine*, 2:9
11. Devaiah KM and Venkatasubramanian P. (2008). Genetic characterization and authentication of *Embelia ribes* using RAPD-PCR and SCAR marker. *Planta Med*, 74: 194 – 196.
12. Devaiah KM and Venkatasubramanian P. (2008). Development of SCAR marker for authentication of *Pueraria tuberosa* (Roxb. Ex. Willd.) DC. *Current Science*, 94: 1306- 1308
13. Devaiah KM, Balasubramani SP and Venkatasubramanian P. (2010). Development of Randomly Amplified Polymorphic DNA based SCAR marker for identification of *Ipomoea mauritiana* Jacq (Convolvulaceae). *eCAM*, doi: 10.1093/ecam/neq023 (In press)
14. Yan-Bo Z, Pang-Chui S, Cho-Wing S, Zheng-Tao W and Yao T. (2007). Molecular Authentication of Chinese Herbal Materials. *J Food Drug Anal*, 15:1- 9
15. Onarici SG, Sancak C, Sumer S, Ozcan S. (2009). Phylogenetic relationship of some wild wheat species based on the internal transcribed spacer sequences of nrDNA. *Current Science*, 96: 794 - 800
16. Xie H, Hue K-K, Chao Z and Pan S-L. (2009). Identification of crude drugs from Chinese Medicinal Plants of the genus *Bupleurum* using ribosomal DNA ITS sequences. *Planta Medica*, 75: 89 - 93
17. Howard C, Bremner PD, Fowler MR, Isodo B, Scott NW and Slater A. (2009). Molecular identification of *Hypericum perforatum* by PCR amplification of the ITS and 5.8S rDNA region. *Planta Medica*, 75: 854 – 869
18. Balasubramani SP, Murugan R, Ravikumar K and Venkatasubramanian P. (2010). Development of ITS sequence based molecular marker to distinguish, *Tribulus terrestris* L. (Zygophyllaceae) from its adulterants. *Fitoterapia*, 81: 503-508
19. Milligan BG. (1998). DNA isolation. In: Hoelzel AR, editor. *Molecular genetic analysis of populations*. IRL Press, Oxford, pp. 263.
20. Fai FC and Ngan FN. (2002). Quantification of DNA. In: Shaw PC, Wang J, But H-PP. *Authentication of Chinese medicinal materials by DNA technology*. World Scientific, Singapore, pp. 25 - 42
21. White TJ, Bruns T, Lee S and Taylor J. (1990). Amplification and direct sequencing of fungal ribosomal RNA genes for phylogenetics. In: Innis MA, Gelfand DH, Sninsky JJ and Thomas J, editors. *PCR protocols: a guide to methods and applications*. Academic Press, San Diego, pp. 315
22. Anonymous. (2000). WHO general guidelines for methodologies on research and evaluation of traditional medicine. Available at: http://whqlibdoc.who.int/hq/2000/WHO_EDM_TRM_2000.1.pdf.
23. Kumar CD. (2007). Pharmacognosy can help minimize accidental misuse of herbal Medicine. *Current Science*, 93: 1356 – 1358
24. Song J, Yao H, Li Y, Li X, Lin Y, Liu C, Han J, Xie C and Chen S. (2009). Authentication

- of the family Polygonaceae in Chinese pharmacopoeia by DNA barcoding technique. *J Ethnopharmacol.*, 124: 434-439.
25. Kress WJ, Wurdack KJ, Zimmer EA, Weigt LA and Janzen DH. (2005). Use of DNA barcodes to identify flowering plants. *PNAS*, 102: 8369 - 8374
26. Watthanachaiyingcharoen R, Komatsu K, Zhu S, Vajragupta O and Leelamanit W. (2010). Authentication of *Coscinium fenestratum* among the other menispermaceae plants prescribed in Thai folk medicines. *Biol Pharm Bull.*, 33:91-94
27. Dyaneshwar W, Preethi C, Kalpana J and Bhushan P. (2006). Development and Application of RAPD-SCAR Marker for Identification of *Phyllanthus emblica* LINN. *Biol Pharm Bull.*, 29: 2313-2316.

Development of Matrix Type Transdermal Patches of Lacidipine: Evaluation of Physicochemical, *in vitro*, *ex vivo* and Mechanical Properties

Ramesh Gannu, Adukondalu Devandla, Madhav Burra and Madhusudan Rao
Yamsani*

National Facilities in Engineering and Technology with Industrial Collaboration (NAFETIC), University College of
Pharmaceutical Sciences, Kakatiya University, Warangal-506 009 (A.P), India

*For correspondence - ymrao123@yahoo.com

Abstract

Transdermal patches were developed for a low oral bioavailable drug, lacidipine (LCDP) employing ethyl cellulose/Eudragit RL100 and polyvinyl pyrrolidone (PVP) as polymeric matrices. The effect of binary mixtures of polymers on physicochemical properties such as thickness, moisture absorption and moisture content; *in vitro* release, *ex vivo* permeation and mechanical properties was evaluated. *Ex vivo* permeation studies across rat abdominal skin were conducted using Franz diffusion cells. Binary mixture of polymer, ethyl cellulose-PVP and Eudragit RL100-PVP at 2.5:7.5 (LE4) and 5:5 (LP3) showed maximum amount of drug release and *ex vivo* permeation (LE4, 2282.3 μg ; LP3, 2765.7 μg). Different kinetic models used to interpret the release kinetics and mechanism indicated that release from all formulations followed zero order release kinetics with fickian diffusion pattern. The flux of LE4 and LP3 formulations showed a flux of 17 and 21.1 $\mu\text{g cm}^{-2} \text{h}^{-1}$, which could meet the target flux. The tensile strength of LE4 and LP3 were found to be 0.6 and 1.1 Kg mm^{-2} . Matrix type transdermal patches having suitable mechanical properties for LCDP were developed and evaluated.

Keywords: Lacidipine, Transdermal, Drug release, Skin permeation, Matrix patches, Mechanical properties

Introduction

The transdermal route of administration is recognized as one of the potential route for the local and systemic delivery of drugs. This route offers many advantages over the oral dosage form, such as improving patient compliance in long-term therapy, bypassing first-pass metabolism, sustaining drug delivery, maintaining a constant and prolonged drug level in plasma, minimizing inter- and intra-patient variability, and making it possible to interrupt or terminate treatment when necessary (1). However, the highly organized structure of stratum corneum forms an effective barrier to the permeation of drugs, which must be modified if poorly penetrating drugs are to be administered. The use of chemical penetration enhancers would significantly increase the number of drug molecules suitable for transdermal delivery (2).

LCDP is a calcium channel blocker used in the treatment of hypertension and atherosclerosis cardiovascular disorders. It also possess antioxidant effect and is one of the most vascular selective drugs of the dihydropyridines (3, 4). LCDP undergoes extensive first-pass hepatic metabolism and has a mean absolute bioavailability of about 10 % (4–52 %). LCDP is completely metabolized in the liver by cytochrome P450 3A4 to pharmacologically inactive metabolites (4). The low oral bioavailability restricts its use, therefore

alternative mode of delivery system is desirable, to deliver the drug at effective concentrations to treat hypertension. LCDP was selected as a model drug because; its oral dose is low (2-8 mg), low molecular mass 455.5 g mol^{-1} and low oral bioavailability.

The system designs for transdermal patches include matrix, microreservoir, reservoir, adhesive and membrane moderated matrix hybrid. Matrix type transdermal patches remain the most popular as they are easy to manufacture (5). Microemulsion based reservoir system was developed with the enhancement of bioavailability from our laboratory (6). The developed system suffers from poor mechanical properties. Transdermal system with suitable mechanical properties would be desired to withstand during wear and tear. Therefore a matrix type system for prolonged release of LCDP having suitable mechanical properties to withstand wear and tear is developed.

The present paper describes the development of matrix type patches for LCDP. The developed patches were also evaluated for physicochemical, *in vitro*, *ex vivo* and mechanical properties.

Materials and Methods

Materials: Lacidipine, Eudragit RL100, ethyl cellulose and poly vinyl pyrrolidone 30 K were obtained as gift samples from Dr Reddy's Laboratories, Hyderabad, India. All other chemicals and solvents used were of analytical reagent grade.

Preparation of patches: Matrix type transdermal patches containing LCDP were prepared by film casting technique using different ratios of ethyl cellulose/Eudragit RL 100 and poly vinyl pyrrolidone (Table 1). Weighed quantity of polymers was dissolved in 20 mL of solvent mixture consisting of 1:1 ratio of dichloromethane

and methanol. Weighed quantity of LCDP was dissolved in 5 mL of solvent system. The polymeric solution is kept for swelling for 6 hr. Then drug solution, d-limonene as permeation enhancer and dibutyl phthalate as plasticizer are added to the polymeric solution and vortexed for 5 min then transferred into Anumbra petri plate. Drying of these patches is carried out at room temperature for overnight and then in vacuum oven at room temperature for 8 to 12 hrs. The prepared patches were removed, cut to size each having 3.56 cm^2 and stored in desiccator.

Weight and thickness variation test: Each formulated film was prepared in triplicate and ten circular films having an area of 3.56 cm^2 were cut from each plate. Their weight was measured using digital balance (Shimadzu, Japan). The thickness of films was measured using digital screw gauge (Digimatic micrometer, Mitutoyo, Japan).

Estimation of LCDP in polymeric films: The formulated polymeric films were assayed for drug content. Three patches from each formulation series were taken, cut into small pieces and was allowed to dissolve in a 100 mL of 0.5% of w/v Tween 80 solution. The solution was diluted suitably filtered through membrane filter (0.45μ) and LCDP content was measured using HPLC (7).

In vitro release studies: Drug release from the transdermal patch was studied using dissolution apparatus (Disso 2000, Labindia, India) equipped with an auto sampler and fraction collector for collection and replenishment of samples and dissolution medium respectively. Water impermeable back up membrane was placed on one side of the patch and further was adhered to USP-V (Paddle over disc). It was placed in dissolution vessel containing 500 mL of 0.5 % w/v Tween 80 solution as *in vitro* release medium. The study was conducted at 50 rpm as stirring

speed and temperature of 32° C. Samples were collected at preset time intervals and analyzed using UV-Vis spectrophotometer (Elico, India) at 282 nm.

Release kinetics and mechanisms of drug release: Different kinetic models, zero order, first order (8), Higuchi and Korsmeyer expressions (8, 9) were applied to interpret the drug release kinetics to know the mechanism of drug release from these matrix systems with the help of equations 1-4.

$$M_t = M_0 + K_0 t \text{-----(1)}$$

$$\ln M_t = \ln M_0 + K_1 t \text{-----(2)}$$

$$M_t = K_H t^{1/2} \text{-----(3)}$$

$$M_t/M_\infty = K_k t^n \text{-----(4)}$$

M_t cumulative amount of drug release at time t ; M_0 , is the initial amount of drug K_0, K_1, K_H and K_k are rate constants for zero order, first order, Higuchi and Korsmeyer model respectively; M_t/M_∞ is the fraction of drug release at time t n , release exponent indicative of the operating release mechanism. The correlation coefficient values (r^2) presented in table 2

Moisture absorption studies: The films were weighed accurately and placed in a desiccator containing 100 mL of saturated solution of aluminium chloride (79.5 % RH). After 3 days, the films were taken out and weighed, the percentage of moisture uptake was calculated as the difference between final and initial weight with respect to initial weight (10).

Moisture content: The patches were weighed and kept in a desiccator containing calcium chloride at 40° C for 24 hr. The final weight was noted when there was no further change in the weight of patch. The percentage of moisture content was calculated as a difference between initial and final weight with respect to initial weight (11).

Measurement of mechanical properties: Mechanical properties, elongation at break (E.B) and tensile strength (T.S) of the films were evaluated using a microprocessor based advanced force gauge equipped with a motorized test stand (Ultra Test, Mecmesin, West Sussex, UK), equipped with 25 kg load cell. Film strip (60x10

Table 1. Composition of LCDP transdermal patches

Formulation	Ingredient (mg)			
	LCDP	EC20	ERL100	PVP
LE1 (10:0)	90	-	2500	-
LE2 (7.5:2.5)	90	-	1875	625
LE3 (5.0:5.0)	90	-	1250	1250
LE4 (2.5:7.5)	90	-	625	1875
LP1 (10:0)	90	2500	-	-
LP2 (7.5:2.5)	90	1875	-	625
LP3 (5.0:5.0)	90	1250	-	1250
LP4 (2.5:7.5)	90	625	-	1875

LCDP, Lacidipine; EC20, Ethyl cellulose 20, ERL 100, Eudrgait RL 100; PVP, Polyvinyl pyrrolidone
 Solvent system used is 25 mL of 50:50 of dichloromethane and methanol
 Plasticizer 20 % w/v of dibutylphthalate
 d-limonene 8 % w/v was incorporated

Table 2. Physicochemical, *in vitro* release, *ex vivo* permeation parameters and mechanical properties of LCDP transdermal patches

Formulation	Weight (mg)	Thickness (μm)	Assay (%)	Q_{24}^R (μg)	Q_{24}^P (μg)	Flux ($\frac{\mu\text{g}}{\text{cm}^2\text{h}^{-1}}$)	$K \times 10^{-3}$ (cm^{-1})	Lag time (h)	T.S (kg mm^{-2})	E.B ($\% \text{ mm}^{-2}$)
LE1	152.3 \pm 5.2	201.3 \pm 12.5	98.6 \pm 6.1	3012.4 \pm 95.8	1608.3 \pm 107.4	15.9	1.99	4.53	2.8 \pm 0.33	15.4 \pm 1.41
LE2	155.6 \pm 3.5	205.6 \pm 10.4	97.1 \pm 5.2	3981.7 \pm 271.2	1984.8 \pm 214.2	17.7	2.21	3.58	1.8 \pm 0.21	28.6 \pm 2.80
LE3	157.1 \pm 2.8	207.2 \pm 8.7	97.6 \pm 3.2	5312.7 \pm 206.6	2110.2 \pm 203.6	17.2	2.15	2.81	1.1 \pm 0.18	67.1 \pm 7.17
LE4	160.4 \pm 6.1	210.4 \pm 11.4	100.1 \pm 1.9	6892.1 \pm 214.2	2282.3 \pm 173.4	17.0	2.12	2.13	0.6 \pm 0.03	86.2 \pm 10.14
LP1	150.2 \pm 3.8	185.6 \pm 14.3	98.3 \pm 4.6	3210.2 \pm 216.0	1376.3 \pm 124.3	10.5	1.31	5.83	0.3 \pm 0.01	18.2 \pm 2.71
LP2	151.5 \pm 4.6	186.9 \pm 13.6	97.8 \pm 4.1	6331.3 \pm 271.2	2050.8 \pm 113.1	16.7	2.09	5.83	0.5 \pm 0.11	30.1 \pm 3.04
LP3	153.2 \pm 5.9	190.3 \pm 15.1	101.5 \pm 3.4	8014.6 \pm 201.4	2765.7 \pm 148.7	21.1	2.63	4.25	1.1 \pm 0.23	72.8 \pm 6.85
LP4	156.3 \pm 3.4	193.2 \pm 10.2	100.1 \pm 1.4	7891.2 \pm 214.2	2609.9 \pm 211.4	16.9	2.11	4.11	1.4 \pm 0.17	95.6 \pm 8.26

Q_{24}^R , cumulative amount of LCDP released in 24 h; Q_{24}^P , cumulative amount of LCDP permeated in 24 h; K, permeation coefficient.

mm) free from air bubbles or physical imperfections, was held between two clamps positioned at a distance of 3 cm. A card board was attached on the surface of the clamp to prevent the film from being cut by the grooves of the clamp. During measurement, the top clamp at a rate of 2 mm s^{-1} pulled the strips to a distance till the film broke. The force and elongation were measured when the films were broken. Results from film samples, which were broken at end were not included in observations. The mechanical properties are calculated using equation 5 and 6.

$$\text{T.S. (Kg mm}^{-2}\text{)} = [\text{Force at break (Kg)} / \text{Initial cross sectional area of the patch (mm}^{-2}\text{)}] \dots \dots \dots (5)$$

$$\text{E.B (}\% \text{mm}^{-2}\text{)} = [\text{Increase in length (mm)} / \text{Original length} \times 100 / \text{Cross sectional area (mm}^{-2}\text{)}] \dots \dots \dots (6)$$

Preparation of rat abdominal skin: The animal study was conducted in accordance with the approval of the animal ethical committee, Kakatiya University, India. Wistar rats weighing 150–200 g were sacrificed using anaesthetic ether. The hair of test animals was carefully trimmed with electrical clippers and the full thickness skin was removed from the abdominal region. The epidermis was prepared surgically by heat separation technique (12), which involved soaking the entire abdominal skin in water at 60°C for 45 s, followed by careful removal of the epidermis. The epidermis was washed with water and used for *ex vivo* permeability studies.

Ex vivo permeation studies: Franz diffusion cell with a surface area of 3.56 cm^2 was used for *ex vivo* permeation studies. The rat skin was mounted between donor and receptor compartments of the diffusion cell with stratum corneum facing the donor compartment. The transdermal patch was placed over the skin and a dialysis membrane (Hi-Media, Mumbai, India) was placed over the patch so as to secure the patch tightly from getting dislodged from the skin (the transdermal patch was sandwiched between the skin and dialysis membrane). The receiver

compartment of the diffusion cell was filled with 12 mL of phosphate buffer pH 7.4 containing 40 % v/v polyethylene glycol (PEG) 400 and the setup was placed over a magnetic stirrer with temperature maintained at 37°C . PEG 400 was incorporated to maintain sink conditions and the contents of receptor compartment were agitated at 400 rpm and was placed over a multi-magnetic stirrer (Cintex, Mumbai, India). The study was conducted at 37°C and samples of 1 mL were collected at preset time points and replenished with PBS (pH 7.4) containing 40 % v/v PEG 400. The cumulative amount of LCDP permeated was determined using HPLC (7) and concentration was corrected for sampling effects according to the equation 7 (13).

$$C_n^1 = C_n [V_T / V_T - V_s] [C_{n-1}^1 / C_{n-1}] \dots \dots (7)$$

where C_n^1 is the corrected concentration of the n^{th} sample, C_n is the measured concentration of LCDP in the n^{th} sample, C_{n-1}^1 is the corrected concentration in the $(n-1)^{\text{th}}$ sample. C_{n-1} is the measured concentration of LCDP in the $(n-1)^{\text{th}}$ sample, V_T is the total volume of the receiver fluid and V_s is the volume of the sample drawn.

The steady state flux was calculated from the slope of steady state portion of the line in the plot of drug amount permeated Vs time. Permeability coefficient (Kp) was calculated by dividing the flux with dose. The lag time was calculated from the intercept on the time axis in the plot of cumulative amount permeated Vs time. The target flux was calculated using equation 8.

$$\text{Target flux} = (C_{SS} \times \text{CLt} \times \text{BW}) / A \dots \dots \dots (8)$$

C_{SS} , the LCDP concentration at therapeutic level ($8.6 \mu\text{g L}^{-1}$) and CLt the total body clearance, 83.9 mL h^{-1} (calculated from volume of distribution, 2300 mL kg^{-1} and half life 19 h) (14), BW the standard human body weight of 60 kg, A represents the surface area of the diffusion cell

(i.e. 3.56 cm²). The calculated target flux value for LCDP was 12.16 µg cm⁻² h⁻¹.

FTIR studies: LCDP, ethyl cellulose, Eudragit RL100, PVP, polymer mixture and physical mixture of polymers and LCDP were placed in clear glass containers and exposed to 40°C/75 % RH for 4 weeks. After 4 weeks, the samples were subjected to FTIR studies by making pellets with KBr.

Stability studies: The stability study for optimized formulations (LE4 and LP3) was conducted according to the International Conference on Harmonisation (ICH) guidelines (15). Sufficient samples of the formulations were wrapped in aluminium foil and stored in a petri dish at a temperature of 40 ± 2° C/75 ± 5 % R.H (Skylab Instruments & Engineering Pvt Ltd, Thane, India) for 6 months. Samples were withdrawn at intervals of 1, 2, 3, and 6 months and analyzed for drug content using the HPLC (7).

Statistical analysis: Statistical comparisons were made using Student's t-test using Sigmatat software (Jandel Corp., CA, USA). Results were considered significant at 95 % confidence interval (p < 0.05) and results were expressed as mean ± SD.

Results and Discussion

Formulation of transdermal patches of LCDP: Polymer films were formulated with varying concentrations of ethyl cellulose or ERL 100 and PVP. The experiment was initiated by taking 2 gm of polymer and 90 mg of drug. As the polymer concentration increased the films could accommodate more amount of LCDP. Precipitation of the drug was noticed with 2 g of polymer and when the polymer was increased, the precipitation was decreased. No precipitation was observed with 2.5 g and above of the polymer. Therefore the amount of polymer selected was 2.5 gm and in order to improve drug release PVP

at different ratios was incorporated. The physical appearance of the films was transparent suggesting that the drug was completely solubilized in the polymeric matrix. Based on preliminary experiments, d-limonene at a concentration of 8 % v/w (showed maximum permeation of LCDP across rat skin) was incorporated as penetration enhancer.

The results of weight variation test for various transdermal films are shown in Table 2. Results of weight variation test indicated uniformity in weight of the patches, as evidenced by RSD values, which were less than 6.

Thickness of films varied from 201.3 (LE1) to 210.4 µm (LE4); 185.6 (LP1) to 193.2 µm (LP4) in respective series. The results (Table 2) suggest that the change in polymer composition did not produce any significant effect (p>0.05) on the thickness. The thickness was found to be uniform as it was evidenced from RSD values, which were less than 6.

The results of content uniformity are shown in table 1 and indicate good uniformity in drug content. The drug content was from 97.1 to 101.5 % in formulation LE2 and LP3 respectively.

In vitro drug release studies: The release profiles of LCDP from transdermal patches were

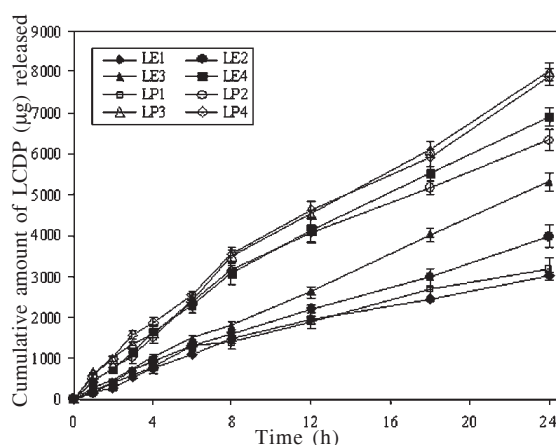


Fig 1. In vitro release profiles of LCDP transdermal patches

shown in Fig 1. Formulations LE4 (6892.1 μg) and LP3 (8014.6 μg) showed maximum amount of release among their series with zero order ($r^2 > 0.9$) release kinetics as it was evidenced from correlation coefficients. It was apparent from the release profiles of formulations, that the drug release was governed by polymer composition. As the concentration of hydrophilic polymer (PVP) increased in the formulations, the drug release rate increased substantially. There appeared a significant difference ($p < 0.05$) in the final amount of drug release, which might be due to the fact that the amount of water soluble polymer influences the drug release from the patches. For all formulations the first order, zero order and Higuchi correlation coefficients were calculated and shown in Table 3. All formulations followed Fickian model of release pattern as it was evidenced from release exponent ($0.16 \leq n \leq 0.39$), indicating that the release mechanism was diffusion mediated.

Moisture absorption and moisture content:

Moisture absorption and moisture content studies provide information regarding stability of the formulation (5). The moisture absorption in the formulations ranged from 0.03 to 1.71 % and 0.24 to 2.5 % in LE and LP series respectively. The moisture content in the patches ranged from 0.02 to 0.39 % and 0.05 to 0.39 % in LE and LP series

respectively (Fig 2). The results revealed that the moisture absorption and moisture content was found to increase with increasing concentration of hydrophilic polymer (PVP). The small moisture content in the formulations helps them to remain stable and from becoming a completely dried and brittle film (16) and low moisture absorption protects material from microbial contamination and bulkiness of the films (17). The rank order of moisture absorption and moisture content respectively were $LE1 < LE2 < LE3 < LE4$ and $LP1 < LP2 < LP3 < LP4$; $LE1 < LE2 < LE3 < LE4$ and $LP1 < LP2 < LP3 < LP4$.

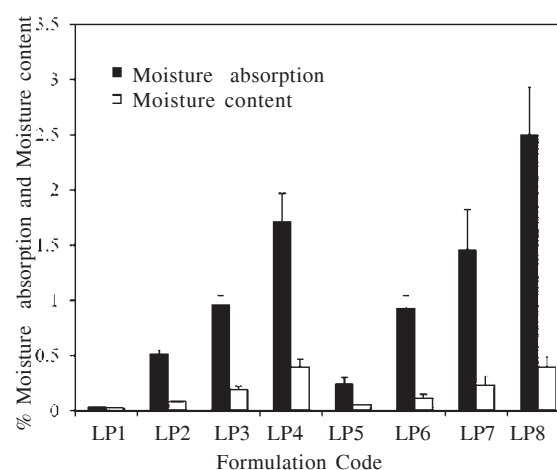


Fig 2. Moisture absorption and moisture content of LCDP transdermal patches

Table 3. *In vitro* release kinetics of LCDP transdermal patches

Formulation	Zero order		First order		Higuchi		Peppas-Korsmeyer
	r^2	K	r^2	K	r^2	K	n
LE1	0.974	56.6	0.633	0.069	0.981	822.7	0.38
LE2	0.964	63.2	0.604	0.062	0.975	879.0	0.37
LE3	0.958	61.4	0.581	0.054	0.961	1052.0	0.33
LE4	0.941	60.7	0.559	0.045	0.979	1684.4	0.33
LP1	0.940	37.4	0.536	0.043	0.981	761.2	0.16
LP2	0.937	59.5	0.575	0.050	0.981	1704.6	0.35
LP3	0.937	75.2	0.565	0.046	0.974	1799.3	0.39
LP4	0.904	60.3	0.537	0.338	0.899	1206.3	0.37

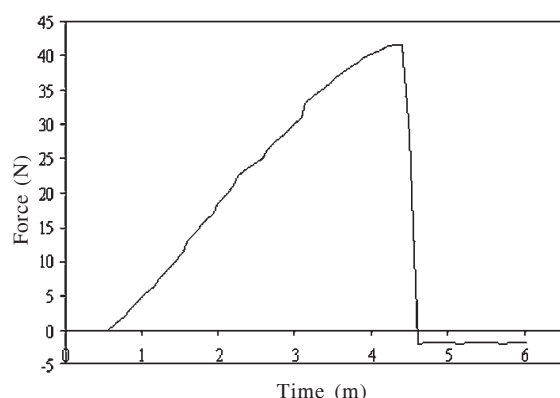


Fig 3. Tensile strength properties measurement of LCDP transdermal patches

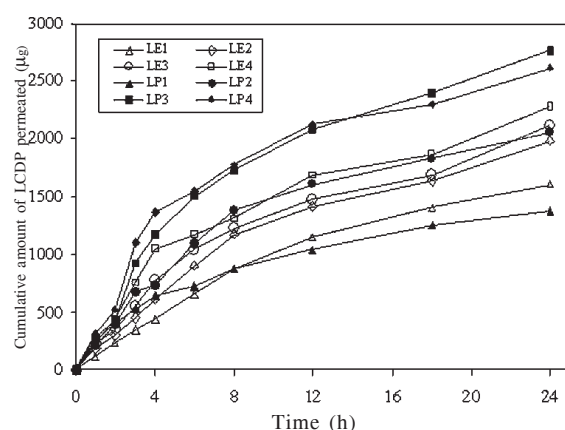


Fig 4. *Ex vivo* permeation profiles of LCDP transdermal patches

Mechanical properties of films: The tensile testing gives an indication of the strength and elasticity of the film, reflected by the parameters, TS and E/B. A soft and weak polymer is characterized by a low TS and E/B; a hard and brittle polymer is defined by a moderate TS and low E/B; a soft and tough polymer is characterized by a moderate TS and high E/B; where as a hard and tough polymer is characterized by a high TS and E/B (18). Hence, it is suggested that a suitable transdermal film should have a relatively high TS and E/B.

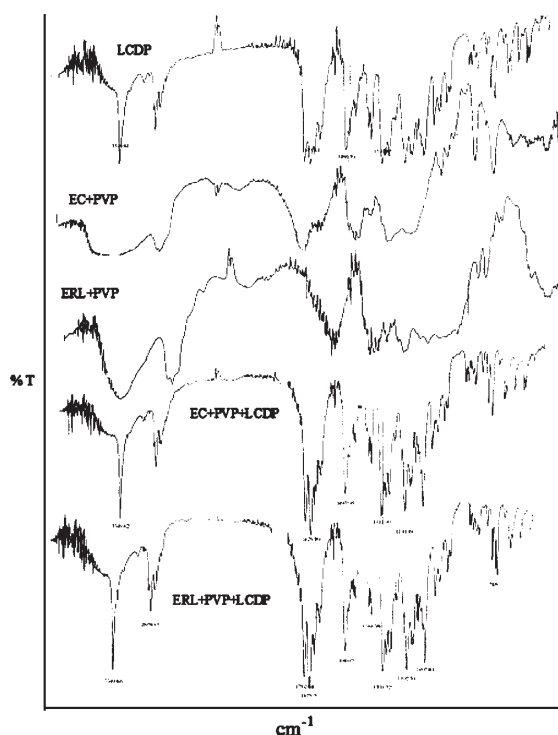


Fig 5. FTIR spectra of LCDP, polymer mixtures and LCDP with polymer mixtures

The results of mechanical properties are shown in Table 2 and Fig 3. Formulation LE1 and LP4 exhibited greater values of TS (2.75 kg mm⁻² and 1.42 kg mm⁻² for LE1 and LP4 respectively). Formulation LE4 (15.4 mm⁻²) and LP4 (95.6 mm⁻²) showed greater values of elongation at break in their respective series. The results revealed that as the concentration of PVP increased in LE series, the tensile strength was found to decrease and vice versa seen in elongation at break. Both TS and E/B were found to be increased with increasing concentration of PVP in LP series. These observations indicate that formulation LE4 and LP3 patches were found to be strong, not brittle and flexible.

***Ex vivo* permeation of LCDP from transdermal patches:** The results of drug permeation from transdermal patches of LCDP through rat skin are presented in Table 2 and

Fig 4. Formulations LE4 and LP3 showed maximum drug permeation among their series. The patches LE1, LE2, LE3, LE4 LP2, LP3 and LP4 could meet the target flux ($12.16 \mu\text{g cm}^{-2} \text{h}^{-1}$). However, the formulations showed higher lag times except formulation LE4. Therefore the patches LE4 (2282.3 μg) and LP3 (2765.7 μg) were considered to be optimum formulations. In *ex vivo* permeation studies, the permeation pattern is similar to *in vitro* release pattern. The results revealed that LCDP was released from the formulation and permeated through rat abdominal skin and hence could possibly permeate through the human skin. The permeation profiles were found follow Higuchi kinetics as it was evidenced from correlation coefficients (0.976-0.996)

FTIR studies: The FTIR spectral analysis of LCDP alone showed that the principal peaks were observed at wave numbers of 3349.8, 2974.9, 1702, 1675.4, 1496.4 and 1310.8. In the spectra of the physical mixture of LCDP, ERL and PVP were 3349.7, 2979.5, 1702.6, 1675.7, 1498, and 1311.3; 3349.4, 2974.5, 1675.8, 1497.9 and 1311.3 wave numbers were observed for the mixture of LCDP, ethyl cellulose and PVP. However, some additional peaks were observed with physical mixtures, which could be due to the presence of polymers. These results suggest that there is no interaction between the drug and polymers used in the study. The polymers used are in controlled/sustained release matrix type patches because of their compatibility with a number of drugs (19).

Stability study: The stability of the optimized formulations (LE4 and LP5) was investigated as per ICH guidelines. On storing the TDDS at a temperature of $40 \pm 2^\circ\text{C}/75 \pm 5\% \text{RH}$ for 6 months, 1.52 % (LE4) and 1.89 % (LP3) degradation was observed. As the degradation is less than 5 % in the formulation, a shelf life of 2 years could be assigned.

Conclusions

Matrix type transdermal therapeutic systems of lacidipine could be prepared with the required flux having suitable mechanical properties. Further work is recommended in support of its efficacy claims by long term pharmacokinetic and pharmacodynamic studies in human beings.

Acknowledgements

One of the authors (Ramesh Gannu) thank AICTE, New Delhi, India for providing financial assistance in the form of National Doctoral Fellowship (NDF).

References

1. Chien, Y. W. (1987). Transdermal Therapeutic System. In *Controlled Drug Delivery Fundamentals and Applications*, 2nd ed.; Robinson, J R., Lee, V H, Eds.; New York: Marcel Dekker, 1987; pp 524–552.
2. Kanikannan, N., Andega, S., Burton, S., Babu, R.J. and Singh, M. (2004). Formulation and in vitro evaluation of transdermal patches of melatonin. *Drug Dev. Ind. Pharm.* 30: 205-212.
3. Lee, C.R and Bryson, H.M. (1994). Lacidipine: a review of its pharmacodynamic and pharmacokinetic properties and therapeutic potential in the treatment of hypertension. *Drugs* 48: 274-296
4. Mc Cormack, P.L and Wagstaff, A.J. (2003). Lacidipine a review of its use in the management of hypertension, *Drugs* 63: 2327-2356
5. Mukherjee B, Mahapatra S, Gupta R, Patra B, Tiwari A and Arora P. (2005). A comparison between povidone-ethyl cellulose and povidone-eudragit transdermal dexamethasone matrix patches based on in

- vitro skin permeation. *Eu J Pharm Biopharm* 59: 475-483.
6. Ramesh, G., Chinna, R.P., Vamshi, V.Y., Shravan, K.Y and Madhusudan, R.Y. (2010). Enhanced bioavailability of lacidipine via microemulsion based transdermal gels: formulation optimization, ex vivo and in vivo characterization. *Int J Pharm* 388: 231-241
 7. Ramesh, G., Vamshi, V.Y., Chinna, R.P., Shravan, K.Y and Madhusudan, R.Y. (2009). Development of high performance liquid chromatography method for lacidipine in rabbit serum: application to pharmacokinetic study. *Anal Chim Acta* 632: 278-283
 8. Costa, P. and Lobo, S.J.M. (2001). Modeling and comparison of dissolution profiles. *Eur J Pharm Sci* 13:123-133
 9. Kusum, D.V., Saisivam, S., Maria, G.R and Deepti, P.U. (2003). Design and evaluation of matrix diffusion controlled transdermal patches of verapamil hydrochloride. *Drug Dev. Ind. Pharm.* 29: 495-503
 10. Korsmeyer, R.W., Gurny, R., Doelker, E., Buri, P. and Peppas, N. A. (1983). Mechanism of solute release from porous hydro-matrices and other factors may be responsible. *Int. J. Pharm.* 15: 25-35
 11. Gupta, R. and Mukarjee, B. (2003). Development and invitro evaluation of diltiazem hydrochloride transdermal patches based on povidone-ethyl cellulose matrices. *Drug Dev. Ind. Pharm* 29 (1): 1-7
 12. Levang, A.K., Zhao, K and Singh, J. (1999). Effect of ethanol/propylene glycol on the in vitro percutaneous absorption of aspirin, biophysical changes and macroscopic barrier properties of the skin. *Int J Pharm.* 181: 255-263
 13. Hayton, W.L and Chen, T. (1982). Correction of perfusate concentration for sample removal. *J Pharm Sci.* 71: 820-821
 14. Clarke's Analysis of Drugs and Poisons (2007) www.medicinescomplete.com.
 15. ICH stability guidelines (No. QIA) (R2). Federal Register 2003, 68 (225), 65717.
 16. Mutalic, S and Udupa, N. (2004). Glibenclamide transdermal patches: physicochemical, pharmacodynamic and Pharmacokinetic evaluation. *J. Pharm. Sci.* 93(6): 1577-1594.
 17. Arora, P. and Mukherjee, B. (2002). Design, development, physicochemical, *in vitro* and *in vivo* evaluation of transdermal patches containing diclofenac diethyl ammonium salt. *J Pharm Sci*, 91: 2076-2089.
 18. Aulton, M.E., Abdul-Razzak, M.H. and Hogan, J.E. (1981). The mechanical properties of hydroxypropyl methylcellulose films derived from aqueous systems: the influence of solid inclusions. *Drug Dev. Ind. Pharm.* 7: 649-668.
 19. Raymond, CR., Paul, JS and Marian, EQ. (2009). Hand book of pharmaceutical excipients. Washinton, DC: Pharmaceutical Press and American Pharmacists Association., 262-267, 525-533 and 581-585

Amplified Fragment Length Polymorphisms Reveals High Intraspecific Variability in Field Isolates of *Leishmania panamensis*

Carlos M. Restrepo¹, Efraín Pérez Lao¹, Carolina De La Guardia¹, Octavio E. Sousa², José E. Calzada³ and Ricardo Leonart^{1*}

¹Instituto de Investigaciones Científicas y Servicios de Alta Tecnología (INDICASAT-AIP), Panamá

²Centro de Investigaciones y Diagnóstico de Enfermedades Parasitarias (CIDEP), Facultad de Medicina, Universidad de Panamá, Panamá

³Instituto Conmemorativo GORGAS de Estudios de la Salud, Panamá

*For Correspondence - rleonart@indicat.org.pa

Abstract

Leishmania parasites cause leishmaniasis, a potentially deadly re-emergent disease that affects millions throughout the world. In Panama, the disease is showing an increasing trend, with estimates of thousands of new cases every year. The main manifestations are the cutaneous and mucocutaneous forms. Genetic variability studies in *Leishmania* are extremely important to define key elements of the eco-epidemiology of the disease. However, few studies have addressed this issue in Panama, and these have been based mainly on kinetoplastid DNA RFLP. The amplified fragment length polymorphisms (AFLP) is a very efficient technique for rapid detection of genetic variability, particularly useful on organisms without sequenced genomes. Although this technique has been used successfully on many species, including several protozoa, its use for studying genetic variability in *Leishmania* parasites is just in its beginnings. We have optimized and used AFLP to address genetic diversity in *Leishmania panamensis*, a poorly studied member of the *Viannia* subgenus. We have found that this technique is able to generate high numbers of peaks when low selective EcoRI and MseI primers were used (+0, +1, +2 series).

Additionally, we have found that an important proportion of those alleles, up to 57% for some primer combinations, are polymorphic. Some of these alleles are potentially useful to rapidly distinguish *L. panamensis* and *L. guyanensis*, the two most genetically similar species of the subgenus. The AFLP was an efficient technique to screen the *Leishmania panamensis* genome for polymorphisms, allowing the rapid detection of hundreds of polymorphic alleles.

Keywords: AFLP, *Leishmania*, Genetic Variability, Polymorphisms

Introduction

Leishmania parasites (Kinetoplastida: Trypanosomatidae) are the cause of the neglected disease leishmaniasis, accounting for significant morbidity and lethality at more than 88 countries around the world. This disease is zoonotic, caused by several species of parasites and transmitted by sand flies (Diptera: Psychodidae). Estimates from the World Health Organization (WHO) point to several million people infected and more than 350 million at risk. The global incidence of leishmaniasis is on the rise, and has been classified as importance level I by the WHO, meaning that the disease is re-emergent, uncontrolled and

expanding. The fact that there are many asymptomatic cases and systematic under-reporting further complicates the possibilities of disease control (1, 2).

In Panama, although the main manifestation are the cutaneous and mucocutaneous forms, the disease is considered a major health problem, accounting for about 3000 new cases every year and a possible under report of about 50% (3). Although several *Leishmania* species have been sporadically reported in Panama, including the potentially pathogens for humans *Leishmania mexicana*, *Leishmania amazonensis*, and *Leishmania colombiensis*, the most common is *Leishmania (Viannia) panamensis*, being the major causative agent of cutaneous and mucocutaneous leishmaniasis in the country (3, 4, 5, 6). The mucocutaneous form accounts for about 5% of the patients and has the worst prognosis, frequently producing deforming lesions. Recently, the application of molecular detection methods has allowed some evidence of previously unreported species for the country, *Leishmania naiffi*, in *Lutzomyia* vectors in the Panama Canal area (7).

The study of the genetic variability of *Leishmania* parasites is considered a topic of high relevance to many aspects of the natural history, ecology and epidemiology of the organism. The current methods for exploring the genetic diversity in *Leishmania* have included the use of multilocus enzyme electrophoresis [8, 9], PCR-RFLPs [10], RAPDs (11), multilocus DNA sequencing (12) and microsatellites (13).

The Amplified Fragment Length Polymorphisms (AFLP) is a technique developed to explore genetic diversity of organisms when no DNA sequence information is available (14). This technique has been extremely useful to assess the degree of genetic variability of many biological groups, showing high reproducibility and

robustness. Several authors have successfully tested AFLP to assess genetic diversity in protozoa species such as *Plasmodium chabaudi* (15), *Plasmodium falciparum* (16), *Trypanosoma brucei* (17, 18) and *Eimeria tenella* (19). Although the AFLP is a technique widely employed for that purpose in many other taxa, its use for studying *Leishmania* parasites is scarce. Here we optimize experimental conditions for the application of AFLP to *Leishmania panamensis* parasites and show that this technique has a great potential for examining both inter and intraspecific genetic variability.

Materials and Methods

Strains Culture Conditions and DNA extractions : Several field isolates of *Leishmania panamensis* were obtained from the Institute of Scientific Research and High Technology Services of Panama (INDICASAT-AIP), Instituto Conmemorativo Gorgas de Estudios de la Salud (ICGES) and Center for Research and Diagnosis of Parasitic Diseases, CIDEP, Faculty of Medicine, University of Panama. All strains used (indicated here as P2, P5, P6, P7, P8 and P9) were isolated from patients of cutaneous leishmaniasis from endemic areas in central Panama, and were previously characterized using multilocus isoenzyme typing or kinetoplast PCR-RFLP DNA typing [20]. Additionally, a reference strain of *Leishmania guyanensis* (MHOM/BR/1975/M4147) was included for comparison. Promastigotes were cultured at 25°C, in tissue culture flasks (Nunc, USA), using Schneider medium (Sigma, USA) with 0.4 g/L de NaHCO_3 , 20% FCS (Invitrogen, USA) and 50 µg/ml gentamycin (Invitrogen, USA). After reaching high density, 5 ml cultures were centrifuged at 3000 rpm for 5 min, pellets washed in same volume of PBS 1X, and DNA immediately extracted using a commercial kit (Wizard® Genomic DNA purification kit, Promega, USA). DNA quality, concentration and digestibility were

checked by agarose gel electrophoresis.

Strain typing: Identity of the strains used were confirmed using the hsp70 gene PCR-RFLP as previously described (21, 22). Briefly, hsp70 amplicons (approximately 500 ng) were digested either with HaeIII or BccI in final volume of 20 μ l, then loaded in 1.5% agarose gel and visualized with ethidium bromide staining using standard procedures (23). Restriction fragments patterns were compared to previously published results (21, 22).

AFLP reactions and data analysis: Fluorescent AFLP kits (Applied Biosystems, USA) were used for the whole procedure, which include EcoRI +3 and MseI +3 selective primers (Regular Plant Genomes kit, P/N 4303050), EcoRI+2 and MseI+3 selective primers (Small Plant Genomes kit, P/N 4303051), and EcoRI+0+1+2 and MseI+0+1+2 selective primers (AFLP Microbial Fingerprinting Kit, P/N 402948). Restriction – digestion reactions were performed as recommended by the manufacturer. Briefly, 50 ng of DNA were incubated in 11 μ l reaction containing 1X T4 DNA ligase buffer containing ATP, 50 mM NaCl, 45 μ g/ml acetylated BSA, 1 μ l MseI adaptor, 1 μ l EcoRI adaptor, 5 u EcoRI (BioLabs, USA), 5 u Tru9I (Promega, USA), and 64 u T4 DNA Ligase (BioLabs, USA), for 2 h at 37°C. After incubation, these reactions were diluted with 189 μ l of 20 mM Tris-HCl, 0.1 mM EDTA, pH 8.0. Preselective amplifications were performed combining 4 μ l of diluted restriction – ligation reaction with 1 μ l preselective primers and 15 μ l amplification core mix (P/N 402005, Applied Biosystems, USA). Thermal cycling was 72°C x 2 min, 30 cycles of (94°C x 20 sec, 56°C x 30 sec, 72°C x 2 min), 60°C x 30 min, and hold at 4°C. Ten microliters of this reaction were diluted with 190 μ l of TE as above. Selective amplifications reactions were prepared with 3 μ l of diluted preselective reaction, 1 μ l selective MseI primer (5 μ M), 1 μ l selective EcoRI primer

(1 μ l) and 15 μ l amplification core mix. A touchdown thermal cycling protocol was followed according to the manufacturer, with the exception that the number of extension cycles at 72°C was increased to 40. All reactions were loaded in a Genetic Analyzer 3130xl using GeneScan 500 (ROX) as internal size standard. Detection and sizing of peaks were conducted with GeneMarker v. 1.91 software (Softgenetics, USA) using the standard AFLP procedure recommended by the manufacturer (24).

Results and Discussion

To assess the identity of the biological material, all the *Leishmania* strains used for the experiments were genotyped using PCR – RFLP of heat-shock protein 70 gene. All the strains analyzed show HaeIII and BccI patterns consistent with previous typing results (see Fig. 1 for a representative agarose electrophoresis result).

The strategy followed to assess the usefulness of AFLP on *Leishmania panamensis*

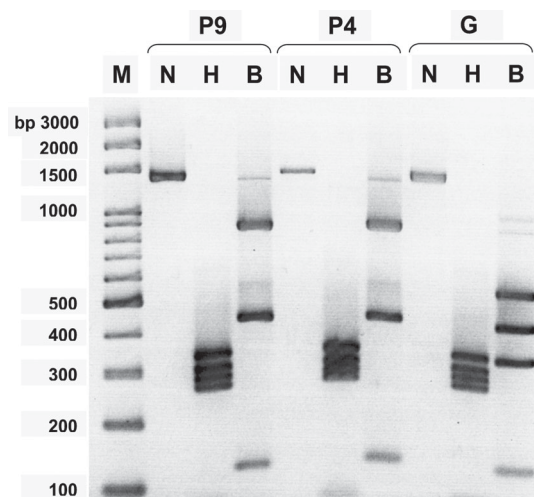


Fig. 1. Representative image of agarose gel electrophoresis of HaeIII and BccI digests of hsp70 amplicon for the *Leishmania* species used at this study. M: size standards; bp: base pairs; P9 and P4: *L. panamensis* isolates; G: *L. guyanensis* reference strain; N: undigested hsp70 amplicon; H: HaeIII digestion products; B: BccI digestion products.

isolates involved the following steps, a) testing protocols for extraction and purification of high molecular weight DNA from promastigotes, b) testing integrity and digestibility of the high molecular weight DNA, c) testing the best experimental conditions for AFLP reactions (number of cycles at pre selective and selective PCR), and d) selecting the best primer combinations for selective PCR with a small number of isolates. These initial optimization experiments were done with *L. panamensis* strain P2. After testing several variations (data not shown), the best conditions found for the AFLP were 1) high molecular weight DNA extraction and purification using a commercial salting-out based kit (Wizard Genomic DNA Purification kit, Promega, USA), and 2) changing the AFLP

protocol by raising the number of preselective cycles to 30, and the number of selective cycles to 40.

As commercial AFLP kits were used (Applied Biosystems, USA), tests for the number of cycles were done for both the control bacterial DNA and the *L. panamensis* strain P2. The increase in the number of cycles at both the pre-selective and the selective PCR steps allowed the reproducible detection of more peaks passing the threshold of 100 fluorescence intensity units, without increasing the noise at the baseline of the electropherograms (Figure 2). When several DNA extractions were repeatedly subjected to the whole procedure a good reproducibility was observed on the electropherograms (data not shown).

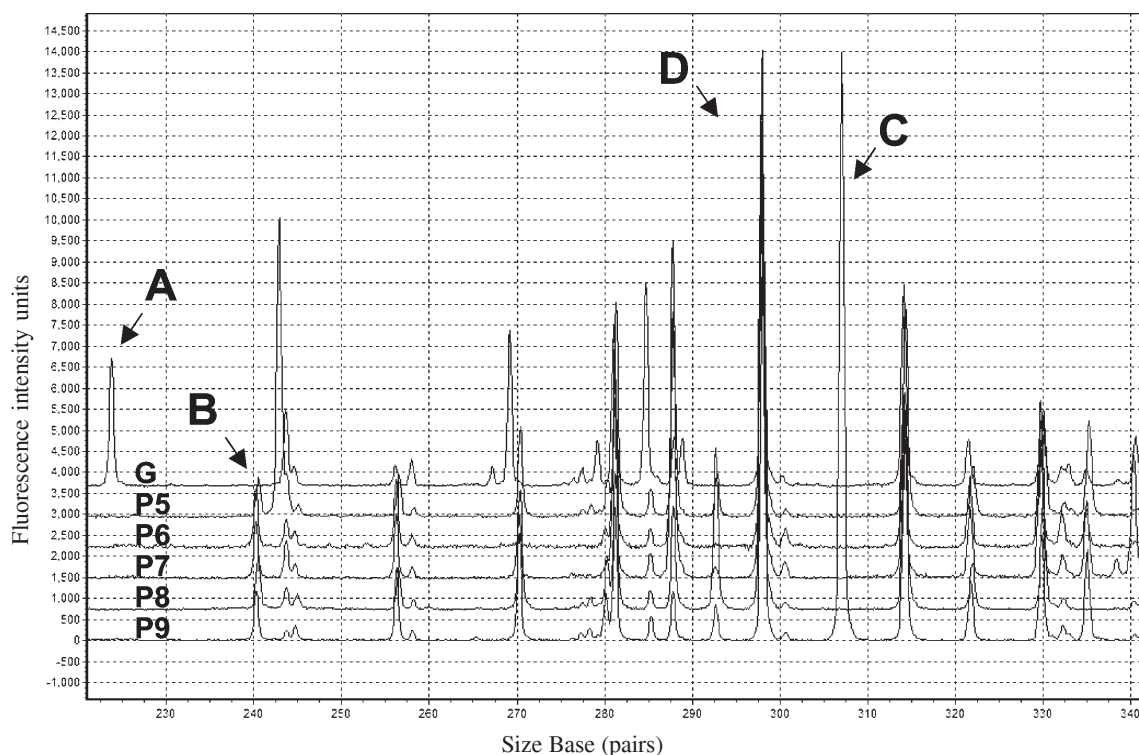


Fig. 2. Representative electropherogram of fluorescently labeled AFLP fragments, generated by the selective primers EcoRI-0-MseI-CA. G: *L. guyanensis*; P5-P9: *L. panamensis* isolates. Arrows indicate A) possible *L. guyanensis* specific alleles; B) possible *L. panamensis* specific alleles; C) *L. panamensis* polymorphic peaks; D) alleles common to all strains analyzed.

Digestions of *Leishmania* genomic DNA with EcoRI and Tru9I (data not shown) showed that most of the digested DNA was at sizes higher than the useful range described for AFLP (50-500 base pairs). These higher than expected sizes were anticipated due to the high GC content of the *Leishmania* genome and the fact that the recognition sites for these enzymes are AT rich sequences. We proceeded to AFLP reactions optimizations by doing the selective primers screening with one of the *L. panamensis* isolates to cover all the possible combinations of available EcoRI and MseI primers. The +3 and +2 combinations (corresponding to the Regular Plant Genomes and Small Plant Genomes AFLP kits) generally yielded low numbers of peaks (Table 1), consistent with the results of the restriction analysis of genomic DNA and the characteristics

of the *Leishmania* genome. Thus, further analysis included several *L. panamensis* isolates (P5, P6, P7, P8 and P9) and one reference *L. guyanensis* strain, and were only done with the +2, +1 and +0 corresponding to the Microbial Fingerprinting AFLP kit. Although this kit contained 81 possible selective primer combinations, we used only the 67 producing more than ten (10) clear peaks (Table 2).

The primer combinations producing the highest numbers of bands on *L. panamensis* were EcoRI-0-MseI-A, EcoRI-0-MseI-T, EcoRI-0-MseI-G, and EcoRI-C-MseI-0 (Table 3). Unexpectedly, some primer combinations rendered too few or no bands at all. The primer combinations yielding the highest cumulative number of bands were EcoRI-G-MseI-0, EcoRI-

Table 1. Number of peaks detected for each combination of selective (- 3) primers on *Leishmania panamensis*.

EcoRI selective primer	MseI selective primer							
	CAA	CAC	CAG	CAT	CTA	CTC	CTG	CTT
TT	1	0	1	3	2	3	4	2
TA	4	3	7	1	4	4	6	8
TG	5	8	6	5	6	9	6	8
AT	5	9	7	2	8	6	12	2
AG	11	11	11	4	4	9	6	11
TC	4	9	5	3	5	12	12	3
AA	4	8	13	7	5	3	6	7
AC	15	8	12	4	10	12	4	18
AAC	19	11	9	4	8	6	8	12
AAG	8	3	18	8	7	10	10	7
ACA	12	8	8	7	5	11	14	17
ACC	7	7	7	4	9	12	3	8
ACG	5	7	16	3	10	11	6	8
ACT	14	5	6	4	9	7	15	5
AGC	7	6	11	5	4	3	10	7
AGG	6	11	9	4	14	7	5	8

AFLP analysis of *Leishmania panamensis*.

Table 2. Number of peaks detected for each combination of selective Mse (+0, =1, +2) primers on *Leishmania panamensis*.

EcoRI	MseI selective primer								
selective primer	0	A	C	G	T	CA	CT	CC	CG
0	0	60	41	53	59	29	30	24	44
A	36	29	0	48	29	31	15	22	21
C	50	19	41	19	33	12	19	12	18
G	18	40	23	26	25	20	14	18	20
T	44	10	25	14	24	19	8	11	11
AA	23	13	17	16	13	17	7	5	5
AC	40	15	30	20	0	15	0	9	20
AG	12	16	18	16	11	9	10	6	11
AT	19	17	19	15	11	10	7	9	0

0-MseI-A, and EcoRI-0-MseI-C, with a range from 7 to 164 peaks (Table 3). The analysis of several isolates allowed us to look at variations among *L. panamensis* isolates and between *L. panamensis* and reference *L. guyanensis*. These comparisons revealed that an important proportion of the peaks were reproducibly polymorphic. The combinations showing the highest percentages of polymorphic peaks for these *L. panamensis* isolates were EcoRI-AA-MseI-T, EcoRI-T-MseI-0, and EcoRI-0-MseI-T, ranging from 7% to 57% (Table 3). The primer combinations tested showed many peaks with the potential to clearly differentiate between both species. This possibility would require, however, the analysis of a higher number of isolates from both species.

These results are not in agreement with those reported by Kumar et al. (25) for *Leishmania donovani*, where they found much higher proportions of polymorphic peaks and higher number of alleles when selective +3 primers were used. Those results, however, are not directly

comparable, as these authors explored different species and did not give details about the allele scoring process. Here we have applied a rather conservative approach by considering only peaks exceeding 100 fluorescence intensity units to assure reproducibility of electropherograms, even at the expense of losing potentially useful peaks. In our hands, this procedure gave us good allele calling reproducibility.

Although a limited number of isolates was analyzed, our results support the idea that there is substantial genetic diversity among *L. panamensis* isolates. As far as we know, this is the first report on the evaluation of AFLP to characterize genetic diversity of *Leishmania panamensis*. Another species of the *Viannia* subgenus, *Leishmania peruviana*, has shown very low genetic variability when analyzed using other markers, (26).

Polymorphisms observed at AFLP peaks may be the result of mutations at any of the

Table 3. Primer combinations from the Mse (+0, +1, +2) series giving the highest numbers of peaks at the *Leishmania* isolates tested.

Most common alleles (number of peaks) ¹	Most alleles on <i>L. guyanensis</i> only (number of peaks) ²	Most alleles on <i>L. panamensis</i> only (number of peaks) ³	Most cumulative number of alleles on <i>L. panamensis</i> (number of peaks) ⁴	Most polymorphic alleles on <i>L. panamensis</i> (number of peaks) ⁵	Higher percentage of polymorphic peaks (percentage) ⁶
EcoRI-T-MseI-CC (96)	EcoRI-A-MseI-0 (16)	EcoRI-0-MseI-A (36)	EcoRI-G-MseI-0 (164)	EcoRI-G-MseI-0 (80)	EcoRI-AA-MseI-T (57)
EcoRI-G-MseI-G (74)	EcoRI-0-MseI-A (13)	EcoRI-A-MseI-0 (24)	EcoRI-0-MseI-A (158)	EcoRI-0-MseI-T (76)	EcoRI-T-MseI-0 (54)
EcoRI-C-MseI-0 (69)	EcoRI-0-MseI-CG (13)	EcoRI-0-MseI-CG (19)	EcoRI-0-MseI-C (154)	EcoRI-0-MseI-G (68)	EcoRI-0-MseI-T (52)
EcoRI-0-MseI-C (65)	EcoRI-AC-MseI-0 (13)	EcoRI-A-MseI-A (13)	EcoRI-A-MseI-0 (153)	EcoRI-0-MseI-C (65)	EcoRI-0-MseI-G (52)
EcoRI-G-MseI-0 (54)	EcoRI-0-MseI-T (11)	EcoRI-A-MseI-T (13)	EcoRI-0-MseI-T (145)	EcoRI-A-MseI-0 (61)	EcoRI-C-MseI-G (51)
EcoRI-G-MseI-A (49)	EcoRI-A-MseI-A (11)	EcoRI-G-MseI-0 (13)	EcoRI-C-MseI-0 (136)	EcoRI-C-MseI-0 (55)	EcoRI-T-MseI-T (51)
EcoRI-A-MseI-0 (45)	EcoRI-0-MseI-C (8)	EcoRI-0-MseI-G (12)	EcoRI-0-MseI-G (129)	EcoRI-0-MseI-CG (54)	EcoRI-AT-MseI-G (49)
EcoRI-C-MseI-C (43)	EcoRI-AC-MseI-A (8)	EcoRI-0-MseI-T (11)	EcoRI-T-MseI-CC (129)	EcoRI-T-MseI-0 (49)	EcoRI-G-MseI-0 (48)

(¹) Primer combinations producing the highest number of alleles common to all tested *L. guyanensis* and *L. panamensis*.
 (²) Primer combinations producing the highest number of alleles present only in *L. guyanensis*, absent at all tested *L. panamensis*.
 (³) Primer combinations producing the highest number of alleles common to all tested *L. panamensis*, and absent at reference *L. guyanensis*.
 (⁴) Primer combinations producing the highest cumulative number of alleles on all tested *L. panamensis*.
 (⁵) Primer combinations producing the highest number of polymorphic alleles at all tested *L. panamensis*.
 (⁶) Primer combinations giving the highest percentage of polymorphic alleles at all tested *L. panamensis*.

restriction sites and/or changes in the size of the restriction fragments due to insertions, deletions or other rearrangements at the original sequence. It has been shown that rearrangements of repeated sequences are a common process leading to protozoan genome variability (27, 28). It is possible that the inherently variable nature of repetitive sequences accounts for an important part of the observed AFLP polymorphisms. That might be especially possible for *L. panamensis*, a not very well studied member of the subgenus *Viannia*. Full genome sequencing of another member of the subgenus, *L. braziliensis*, has shown higher amino acid and sequence divergence as well as a higher number of repetitive sequences than that of the other sequenced members of the *Leishmania* subgenus, *L. major* and *L. infantum* (29).

Conclusions

When AFLP low selectivity EcoRI and MseI primers were used (+0, +1 and +2) on *Leishmania panamensis*, the patterns obtained revealed large numbers of usable alleles and a significant proportion of polymorphic bands. Additionally, many of those bands showed the potential to distinguish between *L. panamensis* and *L. guyanensis*. Thus, AFLP is a molecular fingerprinting technique showing promising potential to explore genetic diversity at *Leishmania panamensis*, both at intraspecific and interspecific levels. Its application will allow researchers to look deeper into new polymorphisms and possibly correlate them to eco-epidemiologically relevant traits and other important aspects of the biology of the parasite. The high efficiency of AFLP to detect many polymorphisms simultaneously in this parasite makes the technique very attractive to address epidemiological relevant issues as drug resistance, variations in clinical symptoms, and micro-evolutionary patterns, among many others.

Acknowledgements

Authors are very grateful to Dr. Patricia Llanes for strains supply and Mrs. Laura Pineda for technical assistance on parasite cultures. This study was funded by the National Secretary of Science, Technology and Innovation of Panama (SENACYT), grant No. FID08-104.

References

1. Desjeux, P. (2004). Leishmaniasis: current situation and new perspectives. *Comp Immunol Microbiol Infect Dis*, 27: 305–318.
2. Reithinger, R., Dujardin, J.C., Louzir, H., Pirmez, C., Alexander, B., Brooker, S. (2007). Cutaneous leishmaniasis. *Lancet Infect Dis*, 7: 581–596.
3. Vásquez, A., Paz, H., Alvar, J., Perez, D. and Hernandez, C. (1998). Informe Final: Estudios Sobre la Epidemiología de la Leishmaniasis en la parte Occidental de la República de Panamá. Instituto Conmemorativo Gorgas de Estudio de la Salud, Ministerio de Salud Pública, Panamá.
4. Christensen, H.A., Herrer, A. and Telford, S.R. Jr (1972). Enzootic cutaneous leishmaniasis in eastern Panama. II. Entomological investigations. *Ann Trop Med Parasitol*, 66: 55–66.
5. Christensen, H.A., Fairchild, G.B., Herrer, A., Johnson, C.M., Young, D.G. and de Vásquez, A.M. (1983). The ecology of cutaneous leishmaniasis in the Republic of Panama. *J Med Entomol*, 20: 463–484.
6. Christensen, H.A., de Vasquez, A.M. and Petersen, J.L. (1999). Short report: epidemiologic studies on cutaneous leishmaniasis in eastern Panama. *Am J Trop Med Hyg*, 60: 54–57.

7. Azpurua, J., De La Cruz, D., Valderama, A. and Windsor, D. (2010). *Lutzomyia* Sand Fly Diversity and Rates of Infection by *Wolbachia* and an Exotic *Leishmania* Species on Barro Colorado Island, Panama. *PLoS Negl Trop Dis*, 4(3): e627.
8. Rioux, J.A., Lanotte, G., Serres, E., Pratlong, F., Bastien, P. and Perieres, J. (1990). Taxonomy of *Leishmania*. Use of isoenzymes. Suggestion for a new classification. *Ann Parasitol Hum Comp*, 65: 111–125.
9. Miles, M.A., Pova, M.M., de Souza, A.A., Lainson, R. and Shaw, J.J. (1980). Some methods for the enzymic characterization of Latin-American *Leishmania* with particular reference to *Leishmania mexicana amazonensis* and subspecies of *Leishmania hertigi*. *Transactions of the Royal Society of Tropical Medicine and Hygiene*, 74: 243–252.
10. Victoir, K., Bañuls, A.L., Arevalo, J., Llanos-Cuentas, A., Hamers, R., Noel, S., De Doncker, S., Le Ray, D., Tibayrenc, M. and Dujardin, J.C. (1998). The gp63 gene locus, a target for genetic characterization of *Leishmania* belonging to subgenus *Viannia*. *Parasitology*, 117: 1–13.
11. Hide, M., Bañuls, A.L. and Tibayrenc, M. (2001). Genetic heterogeneity and phylogenetic status of *Leishmania (Leishmania) infantum* zymodeme MON-1: epidemiological implications. *Parasitology*, 123: 425–432.
12. Mauricio, I.L., Yeo, M., Baghaei, M., Doto, D., Pratlong, F., Zemanova, E., Dedet, J.P., Lukes, J. and Miles, M.A. (2006). Towards multilocus sequence typing of the *Leishmania donovani* complex: resolving genotypes and haplotypes for five polymorphic metabolic enzymes (ASAT, GPI, NH1, NH2, PGD). *International Journal for Parasitology*, 36: 757–769.
13. Bulle, B., Millon, L., Bart, J.M., Gallego, M., Gambarelli, F., Portus, M., Schnur, L., Jaffe, C.L., Fernandez-Barredo, S., Alunda, J.M. and Piarroux, R. (2002). Practical approach for typing strains of *Leishmania infantum* by microsatellite analysis. *Journal of Clinical Microbiology*, 40: 3391–3397.
14. Vos, P., Hogers, R., Bleeker, M., Reijans, M., van de Lee, T., Hornes, M., Frijters, A., Pot, J., Peleman, J. and Kuiper, M. (1995). AFLP: a new technique for DNA fingerprinting. *Nucleic Acids Res*, 23(21): 4407–4414.
15. Grech, K., Martinelli, A., Pathirana, S., Walliker, D., Hunt, P. and Carter, R. (2002). Numerous, robust genetic markers for *Plasmodium chabaudi* by the method of amplified fragment length polymorphism. *Molecular & Biochemical Parasitology*, 123: 95–104.
16. Rubio, J.M., Berzosa, P.J. and Benito, A. (2001). Amplified fragment length polymorphism (AFLP) protocol for genotyping the malarial parasite *Plasmodium falciparum*. *Parasitology*, 123: 331–6.
17. Masiga, D.K., Tait, A. and Turner, C.M. (2000). Amplified fragment length polymorphism in parasite genetics. *Parasitol Today*, 16: 350–3.
18. Tait, A., Masiga, D., Ouma, J., MacLeod, A., Sasse, J., Melville, S., Lindegard, G., McIntosh, A. and Turner, M. (2002). Genetic analysis of phenotype in *Trypanosoma brucei*: a classical approach to potentially complex traits. *Phil Trans R Soc Lond B*, 357: 89–99.

19. Shirley, M.W. and Harvey, D.A. (2000). A genetic linkage map of the apicomplexan protozoan parasite *Eimeria tenella*. *Genome Res*, 10: 1587-93.
20. Miranda, A., Carrasco, R., Paz, H., Pascale, J.M., Samudio, F., Saldaña, A., Santamaría, G., Mendoza, Y. and Calzada, J.E. (2009). Molecular Epidemiology of American Tegumentary Leishmaniasis in Panama. *Am J Trop Med Hyg*, 81(4): 565-571.
21. Montalvo, A.M., Fraga, J., Montano, I., Monzote, L., Marin, M., Van Der Auwera, G., Dujardin, J.C., Velez, I.D. and Muskus, C. (2010). Differentiation of *Leishmania (Viannia) panamensis* and *Leishmania (V.) guyanensis* using BccI for hsp70 PCR-RFLP. *Transactions of the Royal Society of Tropical Medicine and Hygiene*, 104: 364-367.
22. Montalvo, A.M., Fraga, J., Monzote, L., Montano, I., De Doncker, S., Dujardin, J.C. and Van der Auwera, G. (2010). Heat-shock protein 70 PCR-RFLP: a universal simple tool for *Leishmania* species discrimination in the New and Old World. *Parasitology*, 137(8): 1159-68.
23. Sambrook, J., Fritsch, E.F. and Maniatis, T. (1989). *Molecular Cloning: A Laboratory Manual*. Cold Spring Harbor Laboratory, Cold Spring Harbor, NY; 1989.
24. Riley, M., Sheng, C. and Liu, J. (2010). Application Note: Software for Amplified Fragment Length Polymorphism (AFLP). SoftGenetics, LLC, www.softgenetics.com Last accessed November 2010.
25. Kumar, A., Boggula, V.R., Sundar, S., Shasany, A.K. and Dube, A. (2009). Identification of genetic markers in Sodium Antimony Gluconate (SAG) sensitive and resistant Indian clinical isolates of *Leishmania donovani* through amplified fragment length polymorphism (AFLP). *Acta Tropica*, 110: 80-85.
26. Bañuls, A.L., Dujardin, J.C., Guerrini, F., De Doncker, S., Jacquet, D., Arevalo, J., Noel, S., Le Ray, D. and Tibayrenc, M. (2000). Is *Leishmania (Viannia) peruviana* a distinct species? A MLEE/RAPD evolutionary genetics answer. *Journal of Eukaryotic Microbiology*, 47: 197-207.
27. Lanzer, M., de Bruin, D., Wertheimer, S.P. and Ravetch, J.V. (1994). Organisation of chromosomes in *Plasmodium falciparum*: a model for generating karyotypic diversity. *Parasitol Today*, 10:114-7.
28. Kebede, A., De Doncker, S., Arevalo, J., Le Ray, D. and Dujardin, J.C. (1999). Size-polymorphism of mini-exon gene-bearing chromosomes among natural populations of *Leishmania*, subgenus *Viannia*. *International Journal for Parasitology*, 29: 549-557.
29. Peacock, C.S., Seeger, K., Harris, D., Murphy, L., Ruiz, J.C., Quail, M.A., Peters, N., Adlem, E., Tivey, A., Aslett, M., Kerhornou, A., Ivens, A., Fraser, A., Rajandream, M.A., Carver, T., Norbertczak, H., Chillingworth, T., Hance, Z., Jagels, K., Moule, S., Ormond, D., Rutter, S., Squares, R., Whitehead, S., Rabbinowitsch, E., Arrowsmith, C., White, B., Thurston, S., Bringaud, F., Baldauf, S.L., Faulconbridge, A., Jeffares, D., Depledge, D.P., Oyola, S.O., Hilley, J.D., Brito, L.O., Tosi, L.R.O., Barrell, B., Cruz, A.K., Mottram, J.C., Smith, D.F. and Berriman, M. (2007). Comparative genomic analysis of three *Leishmania* species that cause diverse human disease. *Nat Genet*, 39: 839-847.

Calcium Addition Potentially Reverses Lead and Manganese Induced Enzymatic and Behavioral Alterations in Rats

M. Ram Kumar, K. Praveen Kumar, V. Kavitha and G. Rajarami Reddy*

Department of Zoology, Sri Venkateswara University, Tirupati – 517502, India

*For Correspondence - gottipolu2002@yahoo.com

Abstract

Chronic exposure to lead (Pb) or manganese (Mn) is known to alter variety of neurological and behavioral functions. In this study, we have examined the neuro-behavioral perturbations in rats exposed to both Pb and Mn, and the protective effect of calcium supplement. Rats (3 months old) were exposed to Pb (0.2% through drinking water) and Mn (intraperitoneally daily at a concentration of 2.5 mg/kg body wt) for a period of 3 weeks.

A separate batch of animals received calcium (0.02%) in drinking water together with Pb and exposed to Mn. Following exposures, the neurochemical alterations were assessed by determining the activity changes in synaptosomal acetyl cholinesterase (AChE) and mitochondrial ATPases in different brain regions (cortex, hippocampus and cerebellum). Behavioral studies included both cognitive (water maze tasks) and non-cognitive (open field, exploratory and locomotor tasks). Combined exposure to Pb and Mn resulted in behavioral dysfunctions (decrease in latency, swim distance, swim speed in water maze task and decrease in open field behavior and locomotor activity). Similar to the changes observed in motor and cognitive behavior, decrease in the activity of both AChE and ATPases were also observed in the brain regions

of Pb+Mn exposed rats. However, the animals which received calcium together with Pb+Mn showed reversal effect in behavioral as well as the activity of the enzymes suggesting protective role of calcium supplementation against the Pb and Mn induced neurotoxicity. The results of this study support our earlier findings on the protective role of calcium and zinc against Pb and Mn induced neurotoxicity.

Keywords: Behavioral perturbations, Water maze, Lead, Manganese, Locomotor activity, cholinergic system, Calcium protection.

Introduction

The nervous system is the primary target for the low levels of Pb-exposure and the developing brain appears to be especially vulnerable to Pb/Mn-neurotoxicity (1-6). Pb-exposure at very low doses produces serious adverse effects on the central nervous system of children and infants, and these effects last for several years (7). Perinatal exposure to low levels of Pb has been shown to exert behavioral and neurochemical alterations in both suckling and adult rats (8). Pb is known to exert its neurotoxic effects by competing with calcium for calcium receptors coupled with second messenger functions (9) and in some cases, to inhibit the actions of Ca^{2+} as a regulator of cell function (9).

Manganese (Mn) is an essential trace metal that is present in all tissues of mammals. This element can act both as a nutrient and a toxicant to the brain (10). The higher intake of Mn, either through the air or the diet, may result in severe pathologies, particularly in the central nervous system (CNS) leading to manganism, a Parkinson-like disorder (11). The toxic effects of Mn have been widely studied using animal models, notably concerning the accumulation of Mn in tissues and interactions with various other elements (e.g., iron [Fe], zinc [Zn] copper [Cu]) after subchronic or chronic administration (12).

The adverse effects of Mn on the nervous system probably result from the failure of protective enzymes capable to detoxify critical amounts of Mn or to alter its oxidation potential. A multifactor hypothesis is more likely, and could involve iron-induced oxidative stress and the direct interaction of Mn with dopaminergic terminal mitochondria, leading to selective mitochondrial dysfunction and subsequent excitotoxicity (13,14). In this study, we have examined the alterations in brain enzymes and behavioral perturbations in rats exposed to both lead and manganese since both metals coexist in environment originating from different exposure sources. We have also studied the protective effects of calcium against the alterations caused by Pb+Mn.

Materials and Methods

Procurement and maintenance of experimental animals: Young albino rats (Wistar) of 3 months age were purchased from IISc, Bangalore and maintained in the animal house of Dept. of Zoology, S.V. University. The animals were housed in clear plastic cages with hardwood bedding in a room maintained at $28^{\circ} \pm 2^{\circ}$ C and relative humidity $60 \pm 10\%$ with a 12 hour light/day cycle. The animals were fed with standard pellet diet supplied by Sri Venkateswara Traders, Bangalore and water *ad libitum*.

Animal exposure to Pb and Mn: Animals were exposed to 0.2% lead acetate (Sigma) by adding Pb- acetate to de-ionized drinking water and Mn (2.5 mg/kg) (Sigma) intraperitoneally daily for a period of 21 days. Control rats received only deionized water without Pb, intraperitoneally saline (0.9%) injections daily up to 21 days.

Calcium (Ca^{2+}) was supplemented as 0.02% in 0.2% Pb- water. The behavioral tasks in control, Pb+Mn-exposed and calcium supplemented 3 months old rats were observed in the open-field, water maze, exploratory behavior chamber and locomotory activity recorder. The brain regions (cerebral cortex, cerebellum and hippocampus) of control, Pb+Mn-exposed, and Ca^{2+} supplemented rats were collected and used for biochemical assays.

Behavioural Studies

Open-Field Behavior: The open field test has been widely used to assess emotional reactivity/anxiety. It provides measures of locomotor activity. The horizontally directed activity (or locomotion) is measured by the number of line crossings, and vertically directed activity (or exploration) is measured by the frequency of rearings (15). The open-field behaviour of three months age rats was assessed in a wooden box measuring 90 x 90 x 30 cm high. The floor of the arena was divided into 36 equal squares by black lines. Immediately after a rat was placed in the centre of the open field, the movement of the animal was scored. The number of squares crossed with all paws (crossings), the standings on the hind legs (rearings), placing the nose against wall or floor (sniffing), wiping, licking, combing or scratching of any part of the body (grooming) were counted in all sessions. All the activities measured were combined together to assess the mean total behaviour in each session. Testing was carried out on five consecutive days in five minute sessions in control, Pb-exposed and supplemented animals.

Locomotor Activity: Locomotor activity of the rat was studied with Opto-Varimex mini (Columbus Instruments, USA). The data was taken as total duration 30 minutes to each animal during the 5 minutes session interval.

Exploratory Behaviour: Exploratory behaviour was evaluated in the hole board. The apparatus was an open-field arena with four equally spaced holes (3 cm in diameter) in the floor. Each rat was placed individually in the centre of the arena for 5 min, during which we recorded head-dip count and head-dipping duration, in seconds. A head dip was scored if both eyes disappeared into the hole. Head-dipping duration data are expressed as total duration during the 5-min session. The results for head dip are expressed as number of counts, and for head-dipping duration in seconds.

Morris water maze: Spatial discrimination learning not only involves place learning, which is learning a position in space which in this case is the position of the hidden platform in the Morris water escape task, but also involves non-spatial components like procedural learning (such as learning to search for an escape platform) and visual or other sensorimotor processes together with possible motivational/emotional processes necessary for executing the task. After acquisition of the spatial water escape task, a probe trial can reveal whether the rats have actually learned the position of the platform. Furthermore, a spatial discrimination reversal task after the acquisition of the spatial task, measures mainly place learning because the rats are already familiar with the procedural component.

The water maze is a circular water tank measuring 1.85 m in diameter and 0.7 m deep constructed according to a basic design similar to that of Morris (16). Four points along the circumference of the water tank were designated arbitrarily North (N), South (S), East (E), and West

(W), thus dividing the maze into four quadrants. The pool was filled to a depth of 30 cm with water made opaque with white, non toxic water-based paint. A circular submerged platform (diameter 12.5 cm) remained below the surface of water. All parameters involving time and distance are measured in seconds. Testing was carried out on five consecutive days. Control, Pb+Mn treated and Ca²⁺ supplemented rats were subjected to water maze learning tasks.

Biochemical Studies

Preparation of mitochondrial fraction: Mitochondrial fractions were prepared by following the method of Lai and Clark (17) by homogenizing in 5 volumes (w/v) of Sucrose-EDTA-Tris buffer (SET) buffer (0.25 M sucrose, 10 mM Tris-HCl, and 1 mM EDTA, pH 7.4). The homogenate was first centrifuged at 800 g for 10 min at 4°C, and then the supernatant was centrifuged at 10,000g for 20 min. Then the pellet of mitochondrial fraction was suspended in SET buffer.

Estimation of AChE: The specific activity of AChE was determined as described by Ellman et al., (18). The reaction mixture contained 3.0 ml of 0.1M phosphate buffer (pH 8.0), 20 µl of 0.075 M acetylthiocholine iodide and 100 µl of 0.01 M 5, 5-dithiobis 2-nitrobenzoic acid. The reaction was initiated with the addition of 100 µl of crude homogenate. The contents were incubated for 30min at room temperature and the color absorbance was measured at 412nm in spectrophotometer (Hitachi, Model U-2000). The enzyme activity was expressed as µ moles of ACh hydrolyzed /mg protein/h.

Estimation of Adenosine Triphosphatase (ATPase) activity: Na⁺K⁺ and Mg²⁺ATPase activities in the tissues were estimated following the method of Tirri et al., (19). Briefly, 1% homogenates of the tissues were prepared in 0.25 M ice cold sucrose solution. Homogenates were

divided into two parts. One part was centrifuged at 1400g and the supernatant thus obtained was used as an enzyme source for Mg^{2+} ATPase, while the other part of the homogenate was used for the estimation of the total ATPase.

Mg^{2+} ATPase: The reaction mixture for Mg^{2+} ATPase assay contained 0.5 ml of tris buffer (0.13 M; pH 7.4), 0.4 ml of substrate ATP, 0.5 ml of Magnesium chloride (0.05 M $MgCl_2$) and 0.2 ml of mitochondrial fraction (enzyme source). The contents were incubated at 37° C for 15 minutes and the reaction was stopped by the addition of 10% TCA. Zero time controls were maintained by adding TCA prior to the addition of homogenate/mitochondrial fraction. The contents were centrifuged at 1000g for 15 minutes and the inorganic phosphate was estimated in the supernatant fraction following the method of Fiske and Subbarow (20).

Na^+K^+ ATPase: 1% (W/V) homogenate already set apart was used for the total ATPase assay. The reaction mixture in a final volume of 2.6 ml contained, 0.5 ml of Tris buffer (0.13 M; pH 7.4), 0.4 ml of substrate ATP, 0.5 ml $MgCl_2$ (0.05 M), 0.5 ml potassium chloride (KCl, 0.05 M), 0.5 ml of sodium chloride (NaCl, 0.05 M) and 0.2 ml of crude homogenate/ mitochondrial fraction (enzyme source). The contents were incubated at 37° C for 15 minutes and the reaction was arrested by the addition of 1.5 ml of 10% TCA prior to the addition of homogenate. The contents were centrifuged and the inorganic phosphate was estimated in the supernatant fraction (Na^+K^+ ATPase = Total ATPase - Mg^{2+} ATPase).

Estimation of protein content: Protein content of the tissues was estimated by the method of Lowry et al. (21).

Analysis of Data: The data was subjected to statistical analysis (ANOVA and t-test as applicable) using standard statistical procedures.

Results

Open field behavior: The results presented in Fig.1 show decreased locomotor behavior in all responses (crossings, rearings, sniffings, groomings) of the open-field in Pb+Mn exposed rats compared to controls. The control rats showed higher locomotor activity (111.6 crossings, 14.2 rearings, 19.2 sniffings, 19.2 groomings) compared to Pb+Mn treated rats (31.7 crossings, 3.1 rearings, 3.7 sniffings, 4.3 groomings). However, the addition of calcium to Pb+Mn, showed a marginal reversal in the alterations observed in the locomotor behavior (46.88 crossings, 4.33 rearings, 6.77 sniffings, 7.33 groomings) of Pb+Mn treated rats.

Locomotor activity: The results of locomotor activity (Fig.2) showed a decrease in the total number of movements in the Pb+Mn treated rats than the control rats. The administration of calcium along with the Pb+Mn, showed increase in the locomotory activity than Pb+Mn exposed rats.

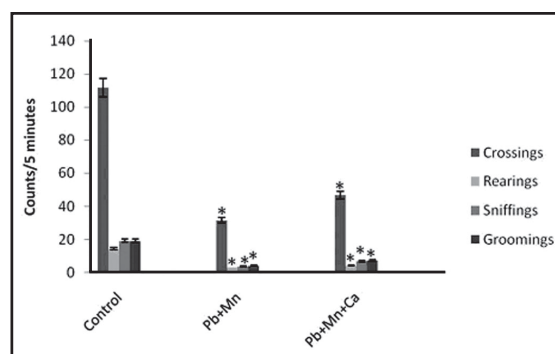


Fig.1. Open-field behavior of control, Pb+Mn exposed and Ca^{2+} supplemented rats. Rats were exposed to 0.2% lead acetate through drinking water and Mn (2.5 mg/kg) intraperitoneally daily for a period of 21 days. Calcium (0.02%) was added in 0.2% Pb water. Each bar represents mean \pm SD (n = 6). The values marked with asterisk (*) are significantly different from controls at $p < 0.05$ – $p < 0.001$.

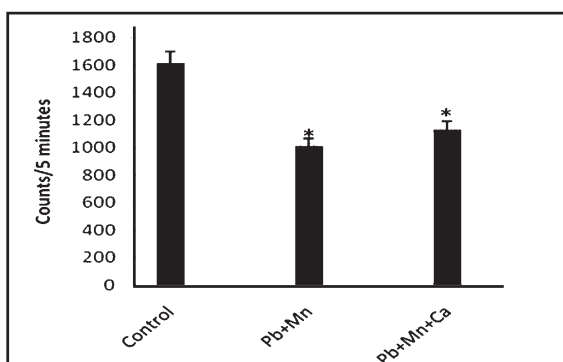


Fig.2. Total locomotor activity of control, Pb+Mn exposed and Ca²⁺ supplemented rats. Rats were exposed to 0.2% lead acetate through drinking water and Mn (2.5 mg/kg) intraperitoneally daily for a period of 21 days. Calcium (0.02%) was added in 0.2% Pb water. Each bar represents mean ± SD (n = 6). The values marked with asterisk (*) are significant at p<0.001

Exploratory behavior: From the figure 3, it is evident that Pb+Mn treated rats showed a decrease in head dip duration (3.52 sec/5 min) and number of head dippings (1.91 times/ 5 min)

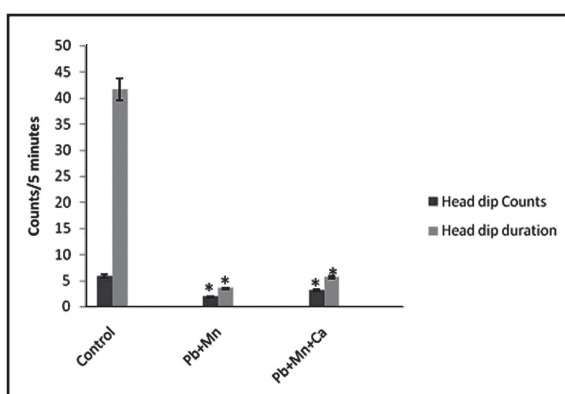


Fig.3. Exploratory behavior of control, Pb+Mn exposed and Ca²⁺ supplemented rats. Rats were exposed to 0.2% lead acetate through drinking water and Mn (2.5 mg/kg) intraperitoneally daily for a period of 21 days. Calcium (0.02%) was added in 0.2% Pb water. Each bar represents mean ± SD (n = 6). The values marked with asterisk (*) are significant at p<0.001

than the control rats (head dip duration: 41.625 sec/5min and the number of head dippings: 5.875 times/5min). However, the administration of calcium showed a marginal increase in both head dip duration (5.66 sec/ 5 min) and number of head dippings (3.166 times/5 min) than the Pb+Mn alone treated rats.

Water maze learning: Behavioral assessments on water maze confirmed the impairment in performance of the water maze acquisition, reversal and working memory tasks in Pb+Mn exposed rats (Figs 4 to 6). All the rats easily learned to find the submerged platform except for the first day of training when all subjects performed at chance level. The Pb+Mn exposed rats took significantly longer time than control animals to find the hidden platform.

Acquisition phase : From the Fig. 4, it evident that Pb+Mn exposure significantly impaired the water maze acquisition performance. In the first day of training session, no specific alterations were

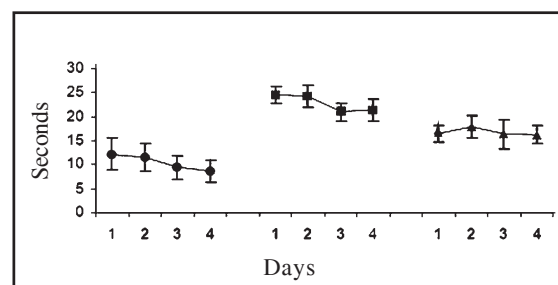


Fig.4. Average escape latency (time in seconds) of control, Pb+Mn exposed and Ca²⁺ supplemented rats to find the hidden platform during the acquisition phase (the platform remained in the same position). Rats were exposed to 0.2% lead acetate through drinking water and Mn (2.5 mg/kg) intraperitoneally daily for a period of 21 days. Calcium (0.02%) was added in 0.2% Pb water. Each bar represents mean ± SD (n = 6). The changes are significant at P<0.05-0.001.

- Control animals,
- Lead and manganese exposed animals,
- ▲ Calcium Supplemented Animals

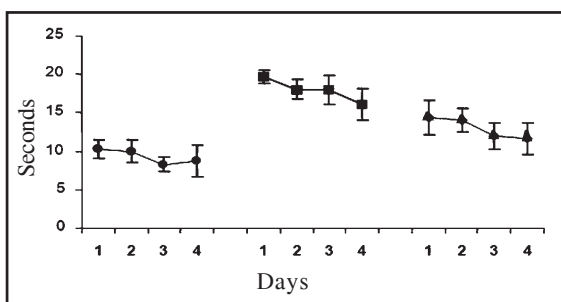


Fig.5. Average escape latency (time in seconds) of control, Pb+Mn exposed and Ca supplemented rats to find the hidden platform during the reversal phase (the platform was changed to opposite quadrant). Rats were exposed to 0.2% lead acetate through drinking water and Mn (2.5 mg/kg) intraperitoneally daily for a period of 21 days. Calcium (0.02%) was added in 0.2% Pb water. Each bar represents mean \pm SD (n = 6). The changes are significant at $P < 0.05$ -0.001. ●: Control Animals, ■: Lead and Manganese Exposed Animals, ▲: Calcium supplemented animals

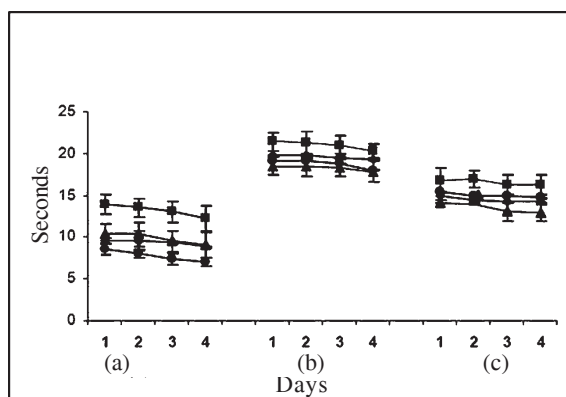


Fig.6. Average escape latency (time in seconds) of control, Pb+Mn exposed and Ca^{2+} supplemented rats to find the hidden platform during the working memory phase (the platform was kept in four different quadrant). Rats were exposed to 0.2% lead acetate through drinking water and Mn (2.5 mg/kg) intraperitoneally daily for a period of 21 days. Calcium (0.02%) was added in 0.2% Pb water. Each bar represents mean \pm SD (n = 6). The changes are significant at $P < 0.005$ -0.01.

(a): Control animals, (b): Pb+Mn exposed animals and (c): Ca^{2+} supplemented animals : Escape stand hidden in south side and rats were allowed from north, east and west : Escape stand hidden in east side and rats were allowed from west, south and north : Escape stand hidden in west side and rats were allowed from east, south and north

found between control and treated rats. Later, control rats quickly proceeded to the north quadrant where the platform is located and identified the hidden platform, whereas Pb+Mn treated rats took longer time to reach the hidden platform. Pb+Mn-exposed rats exhibited the tendency of peripheral swimming, thereby took longer time to reach the platform. The mean escape latency of controls was 12.17 ± 3 on 1st day, 11.62 ± 2.9 on 2nd day, 9.42 ± 2.4 on 3rd day and 8.67 ± 2.2 on 4th day. The Pb+Mn treated young rats exhibited increase in the escape latencies (24.56 ± 1.2 on 1st day, 24.2 ± 1.8 on 2nd day, 21.02 ± 2.2 on 3rd day and 21.3 ± 1.9 on 4th day). The escape latency however greatly reduced in Pb+Mn-exposed rats supplemented with Ca^{2+} (16.54 ± 2.3 on 1st day, 17.86 ± 1.7 on 2nd day, 16.32 ± 2.3 on 3rd day and 16.2 ± 3.1 on 4th day).

Reversal phase: During the spatial discrimination of reversal task, the submerged platform was shifted to south quadrant. All the groups initially spent more time in north quadrant and then reached to the south quadrant. In the first session, there was not much difference in all treated and control groups. From the Fig. 5, it is evident that the control rats showed mean latencies of 10.29 ± 1.2 on 1st day, 10.01 ± 1.5 on 2nd day, 8.27 ± 0.9 on 3rd day and 8.72 ± 0.9 on 4th day. The Pb+Mn-treated young rats exhibited increase in the escape latencies (19.7 ± 1.3 on 1st day, 18.02 ± 1.9 on 2nd day, 18.01 ± 2.1 on 3rd day and 16.09 ± 2.2 on 4th day). The escape latency however greatly reduced in Pb+Mn-exposed rats supplemented with Ca^{2+} (14.408 ± 1.5 on 1st day, 14.02 ± 1.7 on 2nd day, 12.02 ± 1.9 on 3rd day and 11.62 ± 2.2 on 4th day).

Working memory: As the platform is changed to different quadrants in working memory, the escape latencies were greater than acquisition and reversal phases. However, all the control as well as Pb+Mn-exposed rats took lesser time to

locate the hidden platform kept in north quadrant from all the three directions suggesting the retention of earlier acquisition (Fig. 6). As in the case of acquisition and reversal phases, Pb+Mn-exposure exhibited greater impairments in working memory also.

Acetylcholinesterase: Among the different brain regions studied, the specific activity of synaptosomal AChE in control rats was recorded highest in hippocampus, followed by cerebral cortex and cerebellum. In case of Pb+Mn treated animals, a decrease in the activity of AChE was observed in all the three brain regions i.e., hippocampus followed by cerebral cortex and cerebellum. The animals which received calcium together with Pb+Mn indicated significant recovery in AChE activity in all the three brain regions (Fig. 7).

Adenosine triphosphatases: The specific activity of Na⁺K⁺ ATPase was recorded highest in cerebral cortex (0.282), followed by hippocampus (0.217) and cerebellum (0.146) in the control rats. In case of Pb+Mn treated rats, a decrease in the Na⁺K⁺ ATPase activity was recorded in all the brain regions, i.e., cerebral cortex (0.211) followed by hippocampus (0.172) and cerebellum (0.101). However, calcium supplementation to Pb+Mn, reversed the inhibitory effect of Pb+Mn in all the brain regions; i.e., cerebral cortex (0.256) followed by hippocampus (0.198) and cerebellum (0.124) (Fig.8).

In the control rats, the activity of Mg²⁺ ATPase was recorded highest in hippocampus (0.894) followed by cerebral cortex (0.783) and cerebellum (0.624). Pb+Mn treated rats exhibit significant decrease in Mg²⁺ ATPase activity in all the three brain regions. i.e., hippocampus (0.717) followed by cerebral cortex (0.712) and then cerebellum (0.526). Calcium supplementation to Pb+Mn, however, reversed this effect producing a marginal increase in the Mg²⁺ ATPase

activity, i.e., hippocampus (0.768) followed by cerebral cortex (0.754) and cerebellum (0.601) (Fig.9).

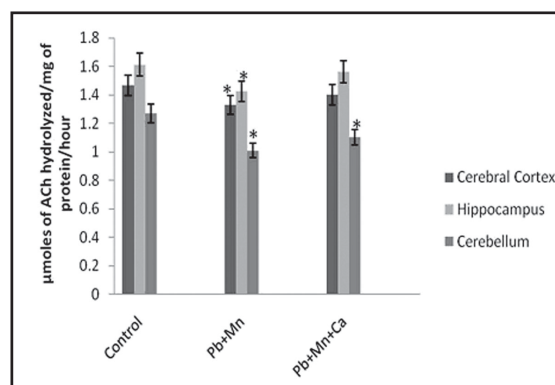


Fig.7. Effect of Pb+Mn exposure on AChE activity in cerebral cortex, hippocampus and cerebellum. Rats were exposed to 0.2% lead acetate through drinking water and Mn (2.5 mg/kg) intraperitoneally daily for a period of 21 days. Calcium (0.02%) was added in 0.2% Pb water. Each bar represents mean ± SD (n = 6). The changes (values marked with asterisk *) are significant at p<0.001.

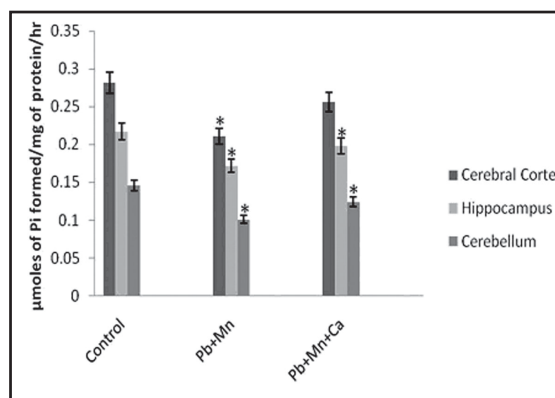


Fig.8. Effect of Pb+Mn exposure on Na⁺K⁺ ATPase activity in cerebral cortex, hippocampus and cerebellum. Rats were exposed to 0.2% lead acetate through drinking water and Mn (2.5 mg/kg) intraperitoneally daily for a period of 21 days. Calcium (0.02%) was added in 0.2% Pb water. Each bar represents mean ± SD (n = 6). The changes (values marked with asterisk *) are significant at p<0.001.

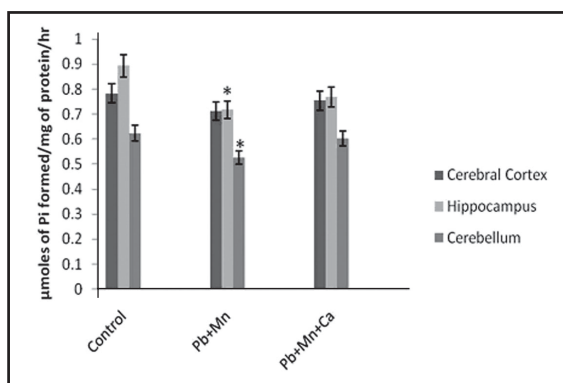


Fig.9. Effect of Pb+Mn exposure on Mg^{2+} ATPase activity in cerebral cortex, hippocampus and cerebellum. Rats were exposed to 0.2% lead acetate through drinking water and Mn (2.5 mg/kg) intraperitoneally daily for a period of 21 days. Calcium (0.02%) was added in 0.2% Pb water. Each bar represents mean \pm SD (n = 6). All values marked with asterisk (*) are significantly ($p < 0.01$) different from control.

Discussion

Our recent work (22, 23) has shown inhibitory effect of Pb on AChE activity in the developing nervous system and reversal effect with calcium supplementation. Keeping in view of these findings, the present study was aimed at examining the combined effect of Pb and Mn-exposure on the activity of AChE and ATPases as well as locomotor and cognitive behaviour, and the protective effect of calcium supplementation.

Control animals showed higher frequency of all the open field responses (crossings, rearings, sniffings and grooming) where as significant decrease was observed in open field responses of Pb+Mn-exposed rats compared to controls. The open field test has been widely used to assess emotional reactivity/anxiety. It provides measures of locomotor activity (15). The memory of habituation in the open field is processed by the hippocampus, which is believed to be a target for metal neurotoxicity.

In the present study, the cognitive deficits in Pb+Mn-exposed rats were examined by water maze swim tasks. As the platform is changed to different quadrants in working memory, the escape latencies in working memory were greater than acquisition and reversal phases. However, all the control as well as Pb+Mn-exposed rats took lesser time to locate the hidden platform kept in north quadrant from all the three directions suggesting the retention of earlier acquisition.

The impaired performance in water maze swim tasks of Pb+Mn exposed rats can be attributed to motor impairments because there were significant differences between swim latencies in control and Pb+Mn exposed groups. These results demonstrate that chronic exposure to Pb+Mn, causes learning impairment by way of deficits in both working memory and reference memory. Thus, the results of our behavioral studies indicate that the ability needed to solve a complex task is more affected by the combined exposure of Pb and Mn. However Ca^{2+} supplementation significantly reversed the Pb+Mn induced behavioral impairments.

The nervous system is the primary target for the Pb-exposure and the developing brain appears to be especially vulnerable to Pb neurotoxicity (3-5). Pb has high affinity for the free sulfhydryl groups in enzymes and proteins and its binding can alter their correct function in numerous processes (24, 25). This may be the reason for the observed inhibition of AChE activity. The alteration in the motor activity is one of the most studied effect of the intoxication, but learning impairments, in particular, caused by Pb has been described at very low doses and included a decrease in the intelligence quotient as well as memory (26). Therefore, a significant decrease in open field behavior and cognitive behavior in Morris water maze were observed with combined exposure to Pb+Mn.

A generalised reduction in brain cholinergic function has been reported in Pb-treated rats. Exposure to Pb resulted in a decrease in the AChE activity in cerebellum and hippocampus at various post natal time points (22). Neonatal exposure to Pb altered the muscarinic receptor density (27) which account for the deficits in central cholinergic functions (28). The results of our present study are in agreement with these findings.

The alterations in AChE activity during early postnatal development could be related with the fact that Pb crosses the blood brain barrier quite readily (29). The inhibitory effect of Pb on AChE activity also reflected in alterations in the motor activity (30, 5). The results of the present study showed maximum alterations in AChE content in hippocampus of Pb-treated rats. The cholinergic synapses are more in hippocampus as compared to cerebral cortex and cerebellum (31). AChE inhibition in this area leads to cognitive and non cognitive alterations as this is the principle area for memory and cognition. The fact that the hippocampus develops late (32) and sequester, Pb, primarily in the mossy fibre pathway (33) would put this structure at particular risk for damage following early Pb-exposure.

Since the cholinergic system is responsible for the behavioral manifestations, any alteration in the cholinergic system would be reflected in the behavior. In the present study, the observed alterations in cholinergic system have greatly influenced the open field behavior of rats exposed to Mn and Pb. The memory and spatial discrimination tasks in Morris water maze also decreased suggesting the hippocampal damage due to Pb+Mn exposure.

Supplementation with Ca^{2+} reversed the Pb and Mn induced inhibition in AChE activity. The reversal of inhibition in the activity of AChE by supplementation with Ca^{2+} may be due to competition of these metals for similar binding

sites and reducing the availability of binding sites for Pb or Mn.

Ca^{2+} is a divalent cation just like Pb. Because the same transport mechanism is operative for absorption of Pb and Ca^{2+} from the gastrointestinal tract there is resulting competitive interaction between Pb and Ca^{2+} (34). Studies have shown that Pb has an inhibitory effect on the peripheral nervous system through stimulus coupled or Ca^{2+} dependent release of acetylcholine (35) and this inhibitory effect of Pb at the neuromuscular junction and the ganglion was similar to the effect of reducing the concentration of Ca^{2+} in bathing media of neural preparations; so it is not surprising that this inhibitory effect of Pb can be overcome by the addition of Ca^{2+} . Absorption of Pb by gastrointestinal tract is inversely related to the amount of Ca^{2+} present (36, 37). Furthermore Ca^{2+} supplements had a protective effect by significantly reducing blood Pb levels in pregnant women whose diets were deficient in Ca^{2+} (38, 39). Ziegler *et al.*, (40) observed an inverse relationship between dietary Ca^{2+} and Pb retention and absorption in young infants.

Pb+Mn-exposure exerted inhibitory action on the activity of enzymes Mg^{2+} , and Na^+K^+ ATPases in the developing brain. Heavy metals such as Pb can bind to a number of sites on proteins including imidazole, histodyl, carbonyl and especially sulfhydryl side chains (41). Heavy metals have great affinity for ATPase system and they interact with enzyme molecule resulting in the inhibition (42). Pb has been reported to inhibit Na^+K^+ ATPase of mammalian tissues (43, 44) and also interferes with mitochondrial function and blocks the O_2 uptake. Bhaumik and Raychudhari (45) reported that the inhibition of Na^+K^+ ATPase may be due to the flow of the $Na^+ K^+$ ions from the tissues to the blood. The decrease in the Mg^{2+} ATPase activity might be due to low operation of oxidative pathway, resulting in

decreased formation of free energy and altered cellular energy metabolism (46).

The combination of Pb^{2+} and Mn^{2+} produced a pronounced decrease in the activity of $Na^+ K^+$ -ATPase, but the magnitude of the change was the sum of the individual metal effects. (47). It is known that brain derived Na^+K^+ ATPase is among the enzymes particularly affected by Pb (48-50). The decrease of Na^+K^+ ATPase activity can change the gradients of Na^+ and K^+ across the cell membrane and can be the cause of the disturbances in neurotransmitters levels (50).

The observed high activity of ATPase in the cortex, cerebellum and hippocampus regions of the brain suggests the involvement of these regions in different behavioral functions. It is known that the level of ATPase parallels the metabolic demands of different regions of rat brain and the differential sensitivity to Pb+Mn neurotoxicity in these brain regions is not due to a preferential metal accumulation, but is possibly due to alteration of biochemical or cellular processes that are uniquely associated with, or greatly enhanced in a particular region (51, 8). Regional variations in AChE and ATPases activity levels observed in different brain regions could be due to structural and functional differences in brain regions. Addition of Ca^{2+} reduced the effects of Pb+Mn on the activities of AChE and ATPases in brain regions. The supplemented Ca^{2+} may compete for similar binding sites as that of Pb and Mn. Supplementation with Ca^{2+} decreases Pb gastrointestinal absorption and decreases tissue accumulation (52). Thus Ca^{2+} replaces Pb and Mn in the body reducing the Pb+Mn-burden in the body.

Thus, from the present study, it is evident that exposure to a combination of Pb and Mn inhibited the activities of both Mg^{2+} ATPase and Na^+K^+ ATPase enzymes as well as AChE leading

to decrease in motor and cognitive functions. Calcium supplementation significantly reversed these alterations in enzyme activities as well as behavioral functions suggesting therapeutic role of calcium for Pb+Mn induced neurotoxicity.

Acknowledgements

The authors acknowledge the financial support from CSIR Grant No. 37(1349)/08/EMR-II and DST Grant No.SR/SO/AS-72/2008.

References

1. Kuhlmann, A.C., Mc Glothan, J. L. and Guilarte, T. R. (1997). Developmental lead exposure causes spatial learning deficits in adult rats. *Neurosci. Lett.* 233: 101-104.
2. Zawia, N. H., Sharan, R., Brydie, M., Uyama, T. and Crumpton, T. (1998). SP1 as a target site for metal-induced perturbations of transcriptional regulation of developmental brain gene expression. *Dev. Brain Res.* 107: 291-298.
3. Reddy, G. R. and Zawia, N. H. (2000). Lead exposure alters Egr-1 DNA binding in the neonatal rat brain. *Int. J. Dev. Neurosci.* 18: 791-795.
4. Chetty, C. S., Reddy, G. R., Murthy, K. S., Johnson, J., Sajwan K. and Desai D. (2001). Prenatal lead exposure alters the expression of neuronal nitric oxide synthase in rat brain. *Int. J. Toxicol.* 20: 113-120.
5. Basha, M. R., Wei, W., Brydie, M., Razmiafshari M. and Zawia, N. H. (2003). Lead induced developmental perturbations in hippocampal Sp1 DNA-binding are prevented by zinc supplementation. *Int. J. Dev. Neurosci.* 21: 1-12.
6. Devi, C. B., Reddy, G. H., Prasanthi, R. P. J., Chetty, C. S. and Reddy, G. R. (2005). Developmental lead exposure alters mitochondrial monoamine oxidase and

- synaptosomal catecholamine levels in rat brain. *Int. J. Dev. Neurosci.* 23(4): 375- 381.
7. Needleman, H. L., Schell, A., Bellinger, D., Leviton, A. and Allred, B. (1990). The long-term effects of exposure to low doses of lead in childhood: An 11-year follow up report. *N. Engl. J. Med.* 322: 83-88.
 8. Moreira, E. G., Rosa, G. J. M., Barros, S. B. M., Vassilieff, V. S. and Vassilieff, I. (2001). Antioxidant defense in rat brain regions after developmental lead exposure. *Toxicology* 169: 145-151.
 9. Bressler, J. P. and Goldstein, G.W. (1991). Mechanisms of lead neurotoxicity. [Review]. *Biochem. Pharmacol.* 41: 479-484.
 10. Oskarsson, A., Palminger, H. I. and Sundberg, J. (1995). Exposure to Toxic Elements via Breast Milk. *Analyst* 120(3): pp. 765-770.
 11. Rabinowitz, M., Leviton, A. and Needleman, H. (1985). Lead in Milk and Infant Blood: A Dose-response Model. *Archives of Environmental Health* 40(5): pp. 283-286.
 12. Missy, P., Marie-Claire, L., Cunat, L., Joyeux, M. and Burnel, D. (2000). Effects of Subchronic Exposure to Manganese Chloride on Tissue Distribution of Three Essential Elements in Rats. *International journal of Toxicology.* 19(5): 313-321.
 13. Albers, D. S. and Beal M. F. (2000). Mitochondrial dysfunction and oxidative stress in aging and neurodegenerative disease. *J. Neural. Transm. Suppl.* 59: 133-154.
 14. Albrecht, J., Sonnewald U., Waagepetersen, H. S. and A. Schousboe. (2007). Glutamine in the central nervous system: Function and dysfunction. *Front. Biosci.* 12: 332-343.
 15. Prickaerts, J., Vente, J. D., Ittersum, M. M. V. and Steinbusch, H. W. M. (1998). Behavioral, neurochemical and neuroanatomical effects of chronic postnatal N-nitro-L-arginine methyl ester treatment in neonatal and adult rats. *Neuroscience.* 87: 181-195.
 16. Morris, R. G. M. (1984). Developments of water maze procedure for studying spatial learning in the rat. *J. Neurosci. Meth.*, 11: 47-60.
 17. Lai, J. C. and Clark, J. B. (1979). Preparation of synaptic and nonsynaptic mitochondria from mammalian brain. *Methods. Enzymol.* 55: 51-60.
 18. Ellman, G. L., Courtney, K. D., Andres, V. R. M. and Featherstone, R. M. (1961). A new and rapid colometric determination of acetylcholinesterase activity. *Biochem. Pharmacol.* 7: 88-95.
 19. Tirri, R., Lagerspetz, K. Y. H. and Kohnen, J. (1973). Temperature dependence of the ATPase activities in brain homogenates during the postnatal development of the rat. *Comp. Biochem. Physiol.* 44B: 473.
 20. Fiske, C. H. and Subba Row, Y. (1925). The calorimetric determination of phosphates. *J. Biol. Chem.* 66: 375-400.
 21. Lowry, O. H., Rosenbrough, N. J., Farr, A. L. and Randal, R. J. (1951). Protein measurement with Folin phenol reagent. *J. Biol. Chem.* 193: 265-275.
 22. Reddy, G. R., Riyaz Basha, Md., Devi, C. B., Suresh, A., Baker, J. L., Shafeek, A., Heinz, J. and Chetty, C. S. (2003). Lead induced effects on acetylcholinesterase activity in cerebellum and hippocampus of developing rat. *Int. J. Dev. Neurosci.* 21: 347-352.

23. Reddy, G. R., Bhuvanewari, C. Devi. and Chellu, S. Chetty. (2007). Developmental Lead Neurotoxicity: Alterations in Brain cholinergic system. *NeuroToxicology* 28:402-407.
24. Chetty, C. S., Rajanna, S., Hall, E., Fail, S. and Rao, Y.P. (1996). In vitro and *in vivo* effects of lead, methylmercury and mercury on inositol 1, 4, 5-triphosphate and 1, 3, 4, 5-tetra bis phosphate receptor bindings in rat brain. *Toxicol. Lett.* 87: 11-17.
25. Bagchi, D., Vuchetich, P. J., Bagchi, M., et al., (1997). Induction of oxidative stress by chronic administration of sodium dichromate (chromium VI) and cadmium chloride (cadmium II) to rats. *Free Radic. Biol. Med.* 22(3): 471-478.
26. Cory-Slechta, D. A. (1995). Bridging human and experimental animal studies of lead neurotoxicity: moving beyond IQ. *Neurotoxicol. Teratol.* 17(3): 219-21; discussion 249-51.
27. Rossouw, J., Offermeier, J. and van Rooyen, J. M. (1987). Apparent central neurotransmitter receptor changes induced by low-level lead exposure during different developmental phases in the rat. *Toxicol Appl Pharmacol.* 91(1): 132-139.
28. Govoni, S., Memo, M., Lucchi, L., Spano, P.F. and Trabucchi, M. (1980). Brain neurotransmitter systems and chronic lead intoxication. *Pharmacol. Res. Commun.* 12, 447-460.
29. King, L. M., Banks, W. A. and George, W.J. (2000). Differential zinc transport into testis and brain of cadmium sensitive and resistant murine strains. *J. Androl.* 21(5): 656-663.
30. Correa, M., Miquel, M. and Aragon, C. M. (2000). Lead acetate potentiates brain catalase activity and enhances ethanol-induced locomotion in mice. *Pharmacol Biochem Behav.* 66(1): 137-42.
31. Ehlert, F. J., Dumont, Y., Roeske, W. R. and Yamamura, H. I. (1980). Muscarinic receptor binding in rat brain using the agonist, [3H] cis methylidioxolane. *Life Sci.* 24;26(12): 961-967.
32. Duffy, C. J. and Teyler, T. J. (1978). Development of potentiation in the dentate gyrus of rat: physiology and anatomy. *Brain Res Bull.* 3(5): 425-30.
33. Fjordingstad, E. J., Danscher, G. and Fjordingstad, E., (1974). Hippocampus. Selective concentration of lead in the normal rat brain. *Brain. Res.* 80(2): 350-354.
34. Mushak, P. and Crocetti, A. F. (1991). Methods for reducing lead exposure in young children and other risk groups: an integrated summary of a report to the U.S. Congress on childhood lead poisoning. *Environ Health Perspect.* 89: 125-135.
35. Rubin, R. P. (1970). The role of calcium in the release of neurotransmitter substances and hormones. *Pharmacol. Rev.* 22(3): 389-428.
36. Mahaffey, K. R., Haseman, J. D. and Goyer, R. A. (1973). Dose response to lead ingested in rat fed low dietary calcium. *J. Lab. Clin. Med.* 82: 92-101.
37. Goyer, R. A. (1995). Chelation of toxic metals: current interests. *Environ. Health. Perspect.* 103(11): 988-9.
38. Farias, P., Borja-Aburto, V. H., Rios, C., Hertz-Picciotto, I., Rojas-Lopez, M. and Chavez-Ayala, R. (1996). Blood lead levels in pregnant women of high and low socioeconomic status in Mexico City. *Environ. Health Perspect.* 104(10): 1070-4.

39. Hernandez-Avila, M., Gonzalez-Cossio, T., Palazuelos, E., Romieu, I., Aro, A., Fishbein, E., Peterson, K. E. and Hu, H. (1996). Dietary and environmental determinants of blood and bone lead levels in lactating postpartum women living in Mexico City. *Environ. Health. Perspect.* 104(10): 1076-1082.
40. Ziegler, E. E., Edwards, B. B., Tensen, R. L., Mahaffey, K. R. and Forman, S. I. (1978). Absorption and retention of lead by infants. *Pediatr. Res.* 12, 29-34.
41. Kench, J. K. (1972). *Trans. Roy. Bio. Afr.* 40: 209.
42. Walton, G. M. and Gill, G. N. (1973). Adenosine 3', 5'-monophosphate and protein kinase dependent phosphorylation of ribosomal protein. *Biochemistry.* 3;12(14): 2604-2611.
43. Cross, R. L., Cross, B.A. and Wang, J. H. (1970). Detection of a phosphorylated intermediate in mitochondrial oxidative phosphorylation. *Biochem. Biophys. Res. Commun.* 10;40(5): 1155-61.
44. Cardone, E., Lessler, M. A. and Brierley, G. P. (1971). Mitochondrial oxidative phosphorylation interaction of lead and inorganic phosphate. *Proc. Soc. Exp. Biol. Med.* 136: 300.
45. Bhaumik, Raychudhari. (1976), *Ind. J. Physiol. Allied. Sci.* 29(4): 111.
46. Boyer, P. (1977). In: *The Enzymes*, Academic press, NY. 3rd Edn. Vol. 13.
47. Hussain, T., Ali, M. M. and Chandra, S. V. (1987). The combined effect of Pb²⁺ and Mn²⁺ on monoamine uptake and Na⁺, K⁺-ATPase in striatal synaptosomes. *J Appl Toxicol.* 7(4):277-80.
48. Siegel, G. J., Fogt, S. K. and Hurley, M.J. (1977). Lead action on sodium plus potassium activated adenosine triphosphatase from electroplax, rat brain and rat kidney. In: Eds, Shamoo, M. W. and A.E., *Membrane Toxicity*. Plenum press, New York. 465-493.
49. Fox, D. A., Rubinstein, S. D. and Hsu, P. (1991). Developmental lead exposure inhibits adult rat retinal, but not kidney, Na⁺ K⁺ ATPase. *Toxicol. Appl. Pharmacol.* 109: 482-493.
50. Fox, D. A., Rubinstein, S. D. and Hsu, P. (1991). Developmental lead exposure inhibits adult rat retinal, but not kidney, Na⁺ K⁺ ATPase. *Toxicol. Appl. Pharmacol.* 109: 482-493.
51. Widzowski, D. V. and Cory-Slechta, D. A. (1994). Homogeneity of regional brain lead concentrations. *Neurotoxicology* 15(2): 295-307.
52. Peraza, M. A., Fierro, F., Barber, D. S., Casarez, E. and Rael, L. T. (1998). Effects of micronutrients on metal toxicity. *Environ. Hlth. Perspect.* 106(1), 203-216.

NEWS

Indian Government will universalise secondary education: President of India Pratibha Patil recently emphasized on Right to Education for primary schooling and government committed to universalize the secondary education through Rashtriya Madhyamik Shiksha Abhiyan. Further announced in budget session that Girls' hostels are being set up in 3,500 educationally backward blocks in the country to bring secondary education to all.

Moment of immense tragedy for Japan: Prime Minister of India Dr. Manmohan Singh said, "This is a moment of immense and grave tragedy for Japan". Dr. Singh expressed heart-felt condolences to Japan and said India stands in full solidarity with the people of that country. He said in Parliament that "I am confident that this House will join me in reiterating the heartfelt condolences of people of India to the friendly people of Japan and extending our prayers and thoughts to them during this most horrific disaster".

Peace needed for development: President Pratibha Devisingh Patil underscored the need for peace to usher in development so that people can devote their energy to cultural, educational, social and economical development. Addressing the public at the Naga Heritage Village, Kisama, on her maiden visit to the state, the President made a fervent appeal to the people of Nagaland to ensure an atmosphere of peace and tranquility. She asserted, people must work together as one unit, whatever tribe they are from, whatever region they may come from, and whatever community they may belong to in order to add to the overall progress of the nation. Asserting that our nation is moving ahead to be counted as one of the major economies of the world, she said our objective remains to have a high economic growth rate and to have an inclusive growth process.

Bacterial Computers: Genetically Engineered Bacteria have Potential to Solve Complicated Mathematical Problems

A research team at Missouri Western State University in Missouri and Davidson College in North Carolina, USA engineered the DNA of *E.coli*, creating

bacterial computers capable of solving a classic mathematical problem known as the Hamiltonian Path Problem. The Hamiltonian Path Problem asks whether there is a route in a network from a beginning node to an ending node, visiting each node exactly once. The genetic circuitry of the bacteria was modified to enable them to find a Hamiltonian path in a three-node graph. Bacteria that successfully solved the problem reported their success by fluorescing both red and green, resulting in yellow colonies. The findings of the research demonstrate that computing in living cells is feasible, opening the door to a number of applications. The second-generation bacterial computers illustrate the feasibility of extending the approach to other computationally challenging math problems.

Anshul Sarvate

Microwave Pre-Cooking of French Fries Reduces Cancer Chemicals

Microwaving the French fries before frying them reduces the levels of a cancer-causing substance. The discovery of acrylamide - a possible carcinogenic in humans — has led to much research being done to investigate the benefits of alternative cooking methods. Acrylamide forms during processes such as frying, baking and roasting where high-temperature and low-moisture conditions exist. Microwave application prior to frying resulted in a marked reduction of the acrylamide level in the surface region. When the potato strips were subjected to frying after a microwave pre-cooking step, acrylamide content in the whole potato strip was reduced by 36%, 41% and 60% for frying at 150, 170 and 190°C respectively. Microwaving French fries before cooking takes little time and in fact, microwave pre-cooked samples fried to the same degree of cooking appeared to have a more acceptable colour, probably due to the more gentle heat treatment they experienced during frying.

Pavithra V

Found: The Apple Gene for Red

CSIRO researchers have located the gene that controls the colour of apples — a discovery that may

lead to bright new apple varieties. The leader of the CSIRO Plant Industry research team, Dr Mandy Walker said that red colour in apple skin is the result of anthocyanins, the natural plant compounds responsible for blue and red colours in many flowers and fruits. Using the latest molecular technology, how much particular genes were activated, or expressed, in apple skin as the fruit ripened and coloured was measured. The gene requires light for activation. By identifying master genes that were activated by light, the gene that controls the formation of anthocyanins in red apples was expressed, and it was found that in green apples this gene is not expressed as much as in red apples. In collaboration with apple breeders at the Department of Agriculture and Food in Western Australia (DAFWA), the scientists were able to show that fruit colour can be predicted even in seedling apple plants by measuring the form of this gene that is present.

Deblina Dey

EDUCATION

PhD/Post Doctoral Programs

Post-doctoral/ Research Scholar/Research Associate/Research technicians: Positions are available immediately in Nanomedicine Research Center, University of South Florida in the laboratory of Dr. Narasaiah Kolliputi to investigate the cellular and molecular mechanisms of oxidant mediated lung injury and pro-inflammatory effects in the lungs with special emphasis on inflammasome, redox signaling and microRNA regulation. The successful candidates will join a vibrant team in studying the oxidative stress, inflammasome regulation, microRNA and pro-inflammatory gene regulation in cell culture and animal models. Expertise in cell culture, biochemical and molecular biology techniques and animal work (mouse) is desirable. For Research Associate/Postdoc positions, PhD or MD/PhD in Life Sciences is required. For Research technician MS or BS with research experience is required. Please send a cover letter and CV by email to: Narasaiah Kolliputi, PhD, Assistant Professor, Nanomedicine Research Center, Division of Allergy and Immunology, Internal Medicine, College of Medicine, University of South Florida, 12901 Bruce B. Downs Blvd, Tampa, FL 33612, Phone: 813-974-5419, Fax: 813-974-8575, Email: nkollipu@health.usf.edu

Post Doctoral Positions: Opportunities are available with Dr Raman Garg, Chief Mentor, Rukmini Devi Group of Institutions which are run under the aegis of Seth Pokhar Mal Educational Society (www.spmes.org). Interested candidates can contact Prof (Dr) Raman Garg, Chief Mentor & Research Head, Rukmini Devi Group of Institutions. C/o Seth Pokhar Mal Educational Society (SPMES), info@rdcecn.org, www.spmes.org.

Post-Doctoral Positions: Two post-doctoral positions are immediately available for highly motivated researchers to study molecular mechanisms of skeletal muscle growth and wasting. Research involves the use of genetic mouse models, immunohistochemistry, and cell culture techniques. Strong background in molecular biology and biochemistry techniques are must. Prior experience with micro RNAs, epigenetic, promoter analysis, flow cytometry, and/or metabolism studies will be a plus. Interested candidates should submit their curriculum vitae along with contact information for 2-3 references to: Ashok Kumar, Ph.D., Anatomical Sciences and Neurobiology, University of Louisville School of Medicine, Louisville, KY 40202. Email: ashok.kumar@louisville.edu.

OPPORTUNITIES

Centre for Research in Nanoscience and Nanotechnology, University of Calcutta, Kolkata, India- 700 019. Applications are invited from eligible candidates to work as Project Fellows under supervision of Principal Investigators in Department of Biochemistry, Botany, Chemical Technology, Zoology & Radio Physics & Electronics. Essential Qualifications are M. Tech or M. Sc or Post-B. Sc., B. Tech in the relevant discipline. GATE/NET qualification is desirable. Candidates with Ph.D. degree may also be considered. Resumes can be sent to Prof D. J. Chattopadhyaya, Director of Centre for Research in Nanoscience and Nanotechnology on or before 28th May 2011. Date and Time of Walk-in-Interview: 3rd June, 2010. on 02:00 PM. Venue: 2nd Floor, Seminar Room, Department of Chemical Technology, 92, A. P. C. Road, Kolkata – 700009. *Emoluments:* Commensurate with the selected candidate's qualification and experience as per university norms. The candidates are requested to bring their original certificates (or provisional postgraduate certificate) along with a set of attested copies.

National Institute of Immunology (NII) (an autonomous research institute), Aruna Asaf Ali Marg, New Delhi, India –110067. Applications are invited from eligible candidates for the post of Staff Scientist-II in the Pay Band (PB-3) of Rs 15600-39100 with Grade Pay of Rs 5400 plus allowances as per GOI rules. Essential Qualifications Ph.D with 1 year Post Doctoral experience in relevant field. Preference will be given to candidates with authorships in National/International Patents. Last date for applications is 12 April 2011. Age limit: The upper age limit is 35 years relaxable for SC/ST/OBC & PH candidates in accordance with GOI rules. Interested candidates may submit their applications duly completed to the Senior Manager on a plain paper in the prescribed format which can be downloaded from the website, along with attested copies of certificates of academic & professional qualifications, present position and past experience, Caste/PH certificate (if applicable), a recent photograph and a Demand Draft of Rs 1001- (SC I STI PH and women candidates are exempted from payment of fees) drawn on any Bank, payable at Delhi NII New Delhi in favour of Director, National Institute of Immunology latest by 12/04/2011. Information can also be obtained from Nil URL: www.nii.res.in.

SEMINARS/WORKSHOPS/CONFERENCES

Hands-on Workshop on Molecular Biotechnology and Bioinformatics: A workshop on Molecular Biotechnology and Bioinformatics was going to held on May 16-20, 2011 at International Institute of Information Technology (IIIT), Pune, India organized by School of Biotechnology, International Institute of Information Technology, P-14, Rajiv Gandhi Info Tech Park, Hinjewadi, Phase - I, Pune-411 057, India. Deadline for abstracts/proposals: 2 May 2011. Registration Fee- Rs. 6000/- (includes tea and food for 5 days). On-campus accommodation charges extra @ Rs. 400/- per day per person. Register online at the following website - <http://www.isquareit.ac.in/biotechworkshop>. For further details contact: Prof. Dr. Sheo Mohan Singh, Msc (UK), PhD (Germany), PDF (UK, USA), School of Biotechnology, International Institute of Information Technology, P-14, Rajiv Gandhi

Info Tech Park, Hinjewadi, Phase - I, Pune, India-411 057. Phone – 095450 89202. Email – sheos@isquareit.ac.in.

4th International Congress of Environmental Research:

An International conference on Environmental Research will be held during December 15-17, 2011 at Sardar Vallabhbhai National Institute of Technology (SVNIT), Ichchhanath, Surat, Gujarat, India organized jointly by Journal of Environmental Research and Development (JERAD) A-6, Comfort Garden, Janki Nagar, Chuna Bhatti, Bhopal – 462016 (India) and Sardar Vallabhbhai National Institute of Technology (SVNIT), Ichchhanath, Surat, Gujarat (India). Deadline for abstracts/proposals: 16 June 2011. Abstract can be submitted online through E-mail: icer2011@gmail.com. For further information contact: Professor Subhash C. Pandey, Editor-In-Chief, Journal of Environmental Research And Development, Director, International Congress of Environmental Research, A-6, Comfort Garden, Janki Nagar, Chuna Bhatti, Bhopal (INDIA). PIN – 462016. Phone : +91-755-4222030. Mobile: +91 9825138685, +91 9426185768, +230 947 5319, +66-89206-9970. E-mail: icer2011@gmail.com.

2nd International Conference on Stem Cells and Cancer (ICSCC-2011):

An International conference on Stem Cells and Cancer will be held during October 15-18, 2011 at International Institute of Information Technology (I²IT), Pune, India organized by School of Biotechnology, International Institute of Information Technology, P-14, Rajiv Gandhi Info Tech Park, Hinjewadi, Phase - I, Pune-411 057, India. Deadline for abstracts/proposals: 31 July 2011. The online registration is now open at <http://www.eregnow.com/icccc2011> where you can register, upload the abstract and pay online by credit/debit/net banking facility. For further details contact: Prof. Dr. Sheo Mohan Singh, Msc (UK), PhD (Germany), PDF (UK, USA), School of Biotechnology, International Institute of Information Technology, P-14, Rajiv Gandhi Info Tech Park, Hinjewadi, Phase - I, Pune, India-411 057. Phone –095450 89202. Email – icccc2011@gmail.com, icccc2011@isquareit.ac.in.

**International Symposium on
Innovations in Free Radical Research and
Experimental Therapeutics
&
5th Annual Convention of Association of
Biotechnology and Pharmacy**

(December 7-9, 2011)

**Venue: Karunya University, Karunya Nagar,
Coimbatore – 641 114, Tamilnadu, India**

Broad Areas of Focus

Oxidative stress, Free radicals and Antioxidants
Free Radical and Cancer
Life style diseases
Herbal Drugs, Nutraceuticals in
experimental therapy
Immunomodulators and Radioprotectors
Immunopharmacology
Toxicology
Translation Research
Pharmaceutical Biology
Drug Metabolism and Drug Interactions
Complementary and Alternative Medicines

Contact for further details

Dr. Guruvayoorappan Chandrasekaran
Organizing Secretary
Department of Biotechnology, Karunya University
Coimbatore – 641 114, Tamilnadu, India
Email - gurukarunya@gmail.com

Registered with Registrar of News Papers for India
Regn. No. APENG/2008/28877

Association of Biotechnology and Pharmacy

(Regn. No. 28OF 2007)

Executive Council

Hon. President

Prof. B. Suresh

President, Pharmacy Council of India
New Delhi

President Elect

Prof. K. Chinnaswamy

Chairman, IPA Education Division and
EC Member Pharmacy Council of India
New Delhi

Vice-Presidents

Prof. M. Vijayalakshmi

Guntur

Prof. T. K. Ravi

Coimbatore

General Secretary

Prof. K. R. S. Sambasiva Rao

Guntur

Regional Secretary, Southern Region

Prof. T. V. Narayana

Bangalore

Treasurer

Dr. P. Sudhakar

Guntur

Advisory Board

Prof. C. K. Kokate, Belgaum

Prof. B. K. Gupta, Kolkata

Prof. Y. Madhusudhana Rao, Warangal

Prof. M. D. Karwekar, Bangalore

Prof. K. P. R. Chowdary, Vizag

Dr. V. S.V. Rao Vadlamudi, Hyderabad

Executive Members

Prof. V. Ravichandran, Chennai

Prof. Gabhe, Mumbai

Prof. Unnikrishna Phanicker, Trivandrum

Prof. R. Nagaraju, Tirupathi

Prof. S. Jaipal Reddy, Hyderabad

Prof. C. S. V. Ramachandra Rao, Vijayawada

Dr. C. Gopala Krishna, Guntur

Dr. K. Ammani, Guntur

J. Ramesh Babu, Guntur

Prof. G. Vidyasagar, Kutch

Prof. T. Somasekhar, Bangalore

Prof. S. Vidyadhara, Guntur

Prof. K. S. R. G. Prasad, Tirupathi

Prof. G. Devala Rao, Vijayawada

Prof. B. Jayakar, Salem

Prof. S. C. Marihal, Goa

M. B. R. Prasad, Vijayawada

Dr. M. Subba Rao, Nuzividu

Prof. Y. Rajendra Prasad, Vizag

Prof. P. M. Gaikwad, Ahmednagar

Printed, Published and owned by Association of Bio-Technology and Pharmacy # 6-69-64 : 6/19, Brodipet, Guntur - 522 002, Andhra Pradesh, India. Printed at : Don Bosco Tech. School Press, Ring Road, Guntur - 522 007. A.P., India Published at : Association of Bio-Technology and Pharmacy # 6-69-64 : 6/19, Brodipet, Guntur - 522 002, Andhra Pradesh, India. Editors : Prof. K.R.S. Sambasiva Rao, Prof. Karnam S. Murthy